Mutant Huntingtin toxicity modifiers revealed by a spatiotemporal proteomic profiling

Sara Gutiérrez Ángel

München 2018

Mutant Huntingtin toxicity modifiers revealed by a spatiotemporal proteomic profiling

Sara Gutiérrez Ángel

Dissertation

an der Fakultät für Biologie
der Ludwig–Maximilians–Universität München

vorgelegt von
Sara Gutiérrez Ángel

München, den 18 Oktober 2018

Die wissenschaftliche Arbeit, die dieser Dissertation zugrunde liegt, wurde im Labor von Prof. Dr. Rüdiger Klein, Department Moleküle-Signale-Entwicklung, am Max-Planck-Institut für Neurobiologie, Martinsried, Deutschland durchgeführt.

Dissertation eingereicht am:
Erstgutachter: Prof. Dr. Rüdiger Klein
Zweitgutachter: Prof. Dr. Angelika Böttger

Tag der Einreichung: 18 Oktober 2018
Tag der mündlichen Prüfung: 13 März 2019

Erklärung

Ich versichere hiermit an Eides Statt, dass die vorgelegte Dissertation von mir selbständig und ohne unerlaubte Hilfe angefertigt ist.

München, den 18 Oktober 2018

Sara Gutiérrez Ángel

Eidesstattliche erklärung

Hiermit erkläre ich, dass die Dissertation nicht ganz oder in wesentlichen Teilen einer anderen Prüfungskommission vorgelegt worden ist und ich mich anderweitig einer Doktorprüfung ohne Erfolg nicht unterzogen habe.

München, den 18 Oktober 2018

Sara Gutiérrez Ángel

"There is not a discovery in science, however revolutionary, however sparkling with insight, that does not arise out of what went before. 'If I have seen further than other men,' said Isaac Newton, 'it is because I have stood on the shoulders of giants."

Isaac Asimov

"If we knew what it was we were doing, it would not be called research, would it?"

Albert Einstein

CONTENTS

LIST OF FIGURES

LIST OF TABLES

LIST OF ABBREVIATIONS

°C	Celsius degree
µ	mu
AD	Alzheimer's disease
ALS	Amyotrophic lateral sclerosis
ASO	Antisense oligonucleotide
ATP	Adenosine triphosphate
BDNF	Brain-derived neurotrophic factor
BSA	Bovine serum albumin
CCDs	Coiled-coiled domains
cDNA	complementary DNA
CE	Cerebellum
CNS	Central nervous system
CNTF	Ciliary neurotrophic factor
CO	Cortex
Crmp	Collapsin response mediator protein
Cryo-EM	Cryogenic-electron microscopy
CSF	Cerebrospinal fluid
CU	University of Cambridge
DAPI	4', 6-diamidino-2-phenylindole
DMEM	Dulbecco's Modified Eagle's Medium
DNA	Deoxyribonucleic acid
DS	Donkey serum
DUSOM	Duke University School of Medicine
E	Embrionic day
ECM	Extracellular matrix

EDTA	Ethylenediaminetetraacetic acid
ER	Endoplasmatic reticulum
FBS	Fetal bovine serum
FGF	Fibroblast growth factor
FHS	Fetal horse serum
GABA	Gamma-aminobutyric acid
GCND	German Center for Neurodegenerative Diseases
GDNF	Glial cell-line derived neurotrophic factor
GPe	External globus pallidus
GPi	Internal globus pallidus
h	hour
HATH	Homologous to the amino terminus of HDGF
HBSS	Hank's Balanced Salt Solution
HC	Hippocampus
HDGF	Hepatoma-derived growth factor
HEK	Human embryonic kidney
HMG-1L2	High mobility group protein 1-like 2
HRPs	HDGF-related proteins
HTT	Huntingtin
HttEx1	Huntingtin exon 1
IB	Inclusion body
iBAQ	Intensity-based absolute quantification
IF	Immunostaining
IHC	Immunohistochemistry
IL-6	Interleukin-6
iPCs	Induced pluripotent stem cells
KI	knock-in
KO	Knock-out
LB	Luria-Bertani
LC-MS/MS	Liquid chromatography-tandem mass spectrometry
LCRs	Low complexity regions
LDH	lactate dehydrogenase
LEDGF	Lens epithelium-derived growth factor
LIF	Leukemia inhibitory factor
mHTT	mutant Huntingtin
min	minute
MPIB	Max Planck Institute of Biochemistry

MPIN	Max Planck Institute of Neurobiology
MRI	Magnetic resonance imaging
MS	Mass-Spectometry
MSNs	Medium spiny neurons
MTT	methylthiazolyldiphenyl-tetrazolium bromide
MW	Molecular weight
N2a	Neuro2a cell line
NDDs	Neurodegenerative diseases
NEAA	Non-essential aminoacids
NES	Nuclear export signal
NF	Neurotrophic factor
NGF	Nerve growth factor
NHMFL	National High Magnetic Field Laboratory
NLS	Nuclear localization signal
OE	Overexpression
OSU	Ohio State University
p75NTR	p75 neurotrophin receptor
PAGE	Polyacrylamide gel electrophoresis
PBS	Phosphate buffered saline
PCA	Principal Component Analysis
PCH	Pericentric constitutive heterochromatin
PCR	Polymerase Chain Reaction
PD	Parkinson's disease
PFA	Paraformaldehyde
PNS	Peripheral nervous system
PolyQ	Polyglutamine
PRD	Proline rich domain
PVDF	Polyvinylidene difluoride
RNA	Ribonucleic acid
rpm	revolutions per minute
RT	Room temperature
s	second
SA	Sodium azide
SDS	Sodium dodecyl sulfate
siRNA	Small interfering RNA
SNPs	Single nucleotide polymorphisms
SOD	Superoxide dismutase

ST	Striatum
STN	Subthlamic nucleus
TAE	TRIS-acetate buffer
TBS	Tris buffered saline
Thal	Thalamus
TrK	Tropomyosin receptor kinase
V	volts
WB	Western Blot
YSM	Yale School of Medicine

ABSTRACT

Huntington's disease (HD) is a genetic hereditary disorder characterized by aggregation of polyQ-expanded mutant Huntingtin (mHTT) protein and progressive neurodegeneration within different brain regions, but specially in cortex and striatum. The pathology is associated with motor, cognitive and psychiatric symptoms. A hallmark of HD is the aggregation of polyglutamine-expanded (polyQ) huntingtin from soluble oligomers to inclusion bodies. Still nowadays, the character of these aggregates and the transition to the neuronal functional disorder, is poorly understood.

In this thesis, the progression of the disease was assessed in a spatiotemporal manner in the R6/2 mice, a HD model, in order to find molecular signatures that could lead first, to a more detailed description of the disorder and second, to the elucidation of possible protein candidates that eventually have the ability of modify HD-related toxicity. Initially, it was approached by mass spectrometry-based quantitative proteomics to break down the spatiotemporal mechanisms of degeneration in HD. The formation of insoluble inclusion bodies throughout the disease progression correlated with the profound remodeling of the soluble proteome. The complexity in protein numbers of the aggregates was detailed through a quantitative characterization. This deep analysis unraveled the dependency of the aggregates' protein sequestration on specific biophysical features and sequence domains.

Based on the proteomic data and applying different criteria, a follow-up study of some proteins was carried out. Overexpression of a selected group of the sequestered proteins improved the cellular viability in a cell line model of HD and reduced in most cases the inclusion body size. The effect of most of those proteins was specific to a mHTT-toxicity induced context. These results suggest that widespread loss of function contributes to

aggregate-mediated toxicity.

The strong effect of one of the protein candidates in the viability assays, Hepatome-derived grow factor (HDGF), lead to a closer examination. The effect of the protein was confirmed in primary neurons, in both transient transfection and in long-term viral transduction. Overexpression of HDGF in the striatum of R6/2 mice significantly rescued their exploratory behavior and ameliorated their clasping phenotype.

In summary, the thesis represents a multi-disciplinary study in the R6/2 mouse model, spanning from proteomics to *in vivo* overexpression of a validated sequestered protein, which appears to be a potential therapeutic mHTT-toxicity modifier. Collectively, the study provides an integrative approach to solve HD molecular mechanisms and contributes to fill in the gap between identification of disease-associated pathways and their corresponding phenotypes.

CHAPTER 1

INTRODUCTION

1.1 Neurodegenerative diseases

Neurodegeneration is the term that defines the progressive demise of neuronal structure and function, including their death. Among the hundreds of different neurodegenerative diseases (NDDs), the main focus has been given mainly to a few of them, including Alzheimer's disease (AD), Parkinson's disease (PD), HD, and amyotrophic lateral sclerosis (ALS). Other less common NDDs, though no less devastating, are also an important challenge. At a subcellular level, they appear to be connected by many similarities. Uncovering these analogies could be translated into therapeutic advances that may ameliorate many diseases simultaneously. Among these common features we can find atypical protein interaction networks, protein misfolding [49], as well as induced cell death [146, 27]. NDDs diverge from each other in the different proteins that are mutated which aggregate, in the states they adopt, in the aggregate location (extracellular or intracellular; cytoplasmatic or nuclear), as well as in the affected neuronal populations. Many NDDs are caused by genetic mutations which are, mostly, located in completely unrelated genes. They, however, lead to protein misfolding, aggregation and neurodegeneration as common traits. These molecular defects in turn lead to alterations at the cellular, circuit and behavioral levels.

One of the most challenging questions for personalized medicine today is, in fact, the translation of genetic information into functional mechanisms that are applicable to disease pathogenesis. In particular, in NDDs it is essential to address this issue. While disease-causing mutations have been identified for most NDDs, the mechanistic details of the pathology remain elusive for most of them. The progress of effective therapies has

been limited by the restrictions of our knowledge regarding the causes and the mechanisms by which neurons die in NDDs. Despite that, several neurobiological breakthroughs have brought closer the possibility of effective therapeutic strategies for different NDDs [110, 246]. It is accepted that progression of NDDs is largely mediated at the protein level, thus investigating NDD-related proteins and their contexts seems to be a promising approach to decipher disease mechanisms [246].

1.2 Huntington's disease

HD is a rare, autosomal dominant, neurodegenerative disease which was first described in 1842, by Charles Oscar Waters, in a letter to Robley Dunglison's Practice of Medicine. There, Waters reported the hereditary nature of a movement disorder that showed involuntary twitches. Other early descriptions were also made, such as the one made by Charles Gorman in 1846, who mentioned the localized incidence of HD in specific geographical regions; or Johan Christian Lund in 1860, who depicted also the hereditary nature of dementia linked to certain arrhythmic movements. However, the most accurate description of HD was made in 1872 by George Huntington, an American doctor, who reported patients with hereditary dance-like movements and cognitive deficits in the adulthood, which ultimately lead to insanity and suicide [114]. These dyskinetic muscle twitchings were referred to as *chorea*, which derives from Ancient Greek and means *dance*, therefore the disease was called Huntington's chorea.

HD's global incidence is reported to be 3 per 100,000 [203]. The disease prevalence, however, varies more than tenfold between different geographical regions [209], with lower incidence in Asian populations and a higher one in places such as Australia, North America and western Europe, where prevalence can reach 1 per 10,000 [44, 203]. HD's onset tipically occurs in the third and fourth life decades [65]; nevertheless, there are patient cases ranging from infancy to 80 years of age.

The different symptoms characterizing HD can be categorized in three groups. Motor symptoms include the named chorea and ataxia in initial stages of the disease; tics, gait balance impairments, dysarthria and dysphagia. As the disease progresses in later stages, dystonia and bradykinesia take place [186]. Cognitive symptoms include impaired working memory, executive dysfunction, problems with attention or memory and progressive dementia; all together appearing before motor manifestations [199]. Lastly, psychiatric symptoms comprise depression, anxiety, irritability, apathy and obsessive-compulsive dis-

orders [200, 124]. Progressively, patients are not able to talk, walk or maintain personal needs. In the very late stages of HD, this leads to the risk of infections, falls or choking [218]; psychosis and suicidal thoughts are prominent as well [267, 230].

Taking all this into account, life expectancy after a clinical diagnosis usually lies between 15 to 20 years due to the progressive action of the disease [260, 25]. Despite the lack of a current cure for HD, different efforts have been taken to develop sypmtomatic treatments [1, 271].

1.2.1 Genetics of HD

Despite the observations of the hereditary nature of the disease from the original descriptions, the first clue on the genetic origin of the disease did not arrive until 1983 [93], when the defect was mapped to chromosome 4 (4p16.3). Specifically, HD is caused by the expansion of a polyglutamine-coding trinucleotide repeat (CAG; cytosine, adenine and guanine) at the N-terminus of the first exon in the mutated huntingtin (*HTT*) gene [151]. The severity of the disease depends on the length of these polyQ stretches. Subjects with CAG lengths less than 36 will not develop the disease and subjects bearing an intermediate range of 36-39 CAG repeats, could display incomplete penetrance. Patients, however, with a range above 40 repeats will display full-penetrance HD [180, 9].

The number of CAG repeats also inversely correlates with age of onset [9]. There is a genetic anticipation phenomenon, which names the tendency for the age of onset to be younger in the offspring than in the affected parent. Thus, pathological CAG repeat segments can expand in successive generations leading to an increased disease severity and/or decreased age of onset [206]. Molecularly, this has been attributed to the presence of a meiotically unstable intermediate allele [82], which can cause both sporadic and inherited cases of HD. This anticipation is more common in paternal alleles as the CAG segment is more unstable during spermatogenesis [215]. Instability of CAG-repeat lengths, however, is also present in somatic cells, such as cortical neurons of HD patients, but not in blood cells [245].

Nevertheless, CAG repeat length might be responsible only for 40% of the onset variation in patients [268]. There are other factors associated with onset and progression of the disease. For instance, genetic modifiers involved in the pathology, such as SNPs, present in the *HTT* gene, but also in genes implicated in transcriptional regulation (PGC-

1α), neurotransmission (GluR6, A2A, NR receptors), intracellular transport and endocytosis (HTT-associated protein-1, HAP1), autophagy (autophagy-related related gene, Atg7), peroxisomal function (peroxisome proliferator-activated receptor C coactivator 1a, PPARGC1A) and proteolysis (ubiquitin C-terminal hydrolase, UCHL1) [234].

1.2.2 Huntingtin protein

HTT is a soluble protein encompassing 3,144 aminoacids, which is ubiquitously expressed, with remarkable high levels through the nervous system [236]. In neurons, it localizes in both soma and dendrites [60]. The role of HTT is fundamental in early embryonic development [36] and it was illustrated with the lethality of knock-out (KO) mouse models and targeted gene disruption, where mice died before embryonic day 9 [183, 66].

Cellular functions of HTT have been shown to be multiple and variable. It serves different organelles and compartments and therefore it comprises several essential cellular tasks, such as vesicle transport, interacting with vesicle membranes [79, 60]; cell division, interacting with microtubules, the ER and the Golgi apparatus [68]; and cellular transcription, interacting with nuclear proteins and chromatine [104, 227]. It also plays a role in neuronal survival. Its inactivation in postmitotic neurons drives the neuron to degeneration, causing motor deficits and finally, lethality [63]. On the contrary, its overexpression protects striatal neurons in culture from apoptotic death after starvation and heat stress [216].

Over the years, there have been several efforts to identify the structure of HTT protein by modelling and crystallography [128, 129]. Due to the large size of the protein, along with the high number of protein interactors [144], these goal remained unresolved. Recently, however, the structure of full length HTT was resolved by cryo-EM [92], supporting the concept that HTT serves as a multivalent interaction hub [227].

HTT protein contains different functional domains apart from its polyQ stretch (Figure 1.1). At the amino terminus, just up-stream to the polyQ sequence, there is the N17 domain, a highly-conserved stretch of 17 residues necessary for HTT nuclear/cytosol localization, acting as a nuclear export signal (NES) [284]. N17 also incorporates a binding site for the nuclear exporter Trp (translocated promoter region) [45], which might cause mHTT accumulation in nuclei when affected. Furthermore, it has been shown that these first 17 aminoacids modify nuclear pathogenesis and disease severity in HD mouse

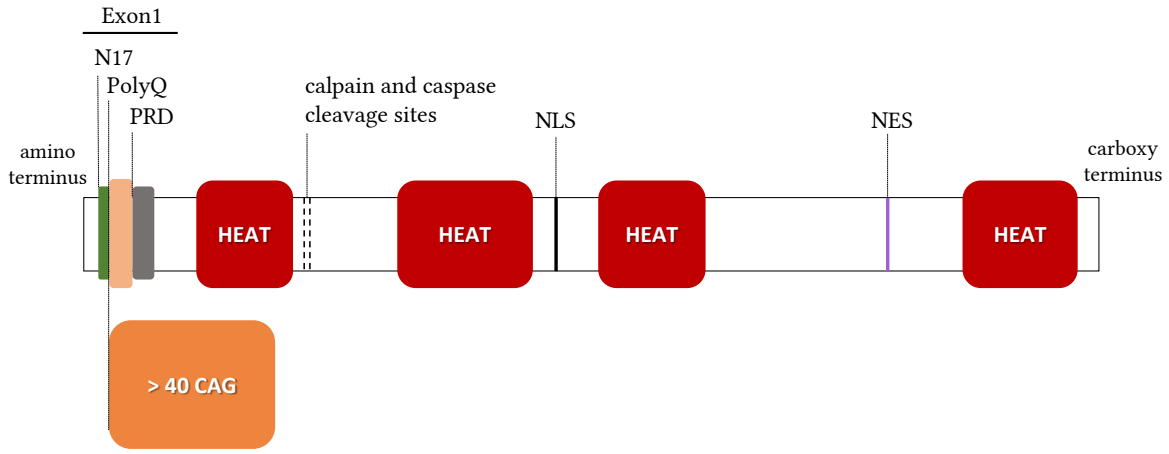

Figure 1.1 – Schematic representation of HTT protein functional domains. HTT protein depicts different functional domains. At the N-terminal end there is N17, a highly-conserved 17-residue stretch essential for HTT nuclear/cytosol localization. Downstream there is the polyQ sequence, expanded in HD, followed by PRD. Exon 1 displays these three domains. Several clusters of HEAT repeat sequences are also schematically represented, along with NLS and NES sequences.

models by regulating subcellular localization of known nuclear pathogenic mHTT species [90]. Downstream the polyQ stretch there is a proline rich domain (PRD), exclusive of mammals [250], which has a role in HTT aggregation [57], HTT turnover [241] and protein-protein recognition [77]. In addition, HTT also displays a nuclear export signal (NLS) [21], and a NES sequence at the C-terminus [273]. HTT possesses several HEAT repeat sequences (Htt, Elongation factor 3, the PR65/A subunit of protein phosphatase 2A, and the lipid kinase TOR), which usually mediate protein-protein interactions involved in cytoplasmic and nuclear transport, microtubule dynamics, and chromosome segregation [248, 92].

Nonetheless, the specific role of HTT in neurodegeneration, remains yet undefined. PolyQ repeats are not exclusive of mHTT and are present in other proteins [80]; it has been suggested that they form a polar zipper structure neccessary for some transcription factors [201]. In mHTT, however, the CAG expansion alters the three-dimensional conformation of the protein, which modifies its molecular interactions, both with other interactors and with itself [185]. The specific cascade of events that drives mHTT to cause HD, remains insufficiently explored.

1.2.3 Protein aggregation and toxicity

As the CAG expansion leads mHTT to aggregate, the first option for its HD related toxicity would be a loss-of-function situation. However, it has been shown that a conditional loss of endogenous HTT after embryonic development or heterozygosity does not lead to HD phenotypes in mice or humans [63]. To the contrary, a gain-of-function situation might explain HD toxicity derived from the expanded polyQ stretch.

Upon processing, mHTT undergoes caspase or calpain proteolysis through its overlapping cleavage sites (Figure 1.1) [266, 76]. This process generates soluble monomeric N-terminal fragments, which are considered to be more harmful to the cell compared to the full mHTT [138]. These mHTT monomers accumulate in the cytoplasm until their concentration exceeds a certain threshold value; then, monomers dimerize to form soluble intermediate oligomers which are in equilibrium with the monomer population [193]. These two species react subsequently together forming glutamine-amine bonds between different mHTT molecules, driving the formation of inclusion bodies (IBs) in the nucleus, as well as in the cytoplasm [138, 156]. These fragments are considered to be responsible for the formation of nuclear and perinuclear IBs, both in patients and mouse models [61, 54]. IBs are a notable hallmark of the disease, but mHTT can form multiple intermediates, as mentioned. Solving which species exist *in situ* and their pathogenic significance is critical for uncovering HD molecular pathogenesis and therapeutic targets.

The role of these mHTTs IBs in neurodegeneration remains unclear. Some studies have correlated directly IB formation and toxicty [54]. In HD, IBs contain different proteins in different proportions. IBs are strongly ubiquitinated and they contain proteasome-associated proteins, which supports the consequence of a subsequent failure of the degradation system and, eventually, cell death [100, 43]. The pool of chaperones is also affected since many of them are sequestered into the IBs, leading to abnormal protein folding [101]. Overexpression of different chaperones, such as Hsp70, ChiP or TRiC, has been shown to shield against this misfolded-protein toxicity *in vitro* and *in vivo* [171, 249]. In addition, toxicity from the IBs could also come from the seclusion of differen transcription factors [64, 280]. IBs were suggested also to interfere with nuclear transport [89], as well as with cellular membranes [17]. This sequestration leads ultimately to inactivation of essential proteins from the celullar pool [130, 108, 107].

Other studies, in contrast, have proposed a protective role for IBs. For example, IB formation over time correlates with neuronal survival and decreases toxic intracellular

levels of diffused soluble mHTT [10]. The R6/2 mouse model displays prominent intranuclear mHTT IBs, but shows minor cell death [54, 62]. It has also been observed that many of the IBs in striatum are present in neurons that are neurodegeneration resistant [137]. After treatment with antiapoptotic compounds or neurotrophic factors striatal neurons in culture showed a reduction in cell death but an increase in the number of IBs [226]. Last but not least, some neuropathological studies with HD-affected patients showed a poor correlation in *post mortem* brains between mHTT IBs and intensity of clinical features [94].

Thus, it is possible that IBs are a mechanism of protection used by the cell to minimize mHTT toxicity. One of the hallmarks of human HD, which is not so prominent in mouse models, is the outstanding loss of the striatum (up to 30% of total brain mass), prior to death [261], and yet, it is possible to spot IBs in the remaining neurons of *post mortem* sections [61]. As the IBs could be the cause of cell death, one possibility could be that those visualized neurons are on their way to death. However, another hypothesis is that these neurons have been surviving longer not despite, but due to the IB presence. Aggregation would then be a protective phenomenon by which monomers and oligomers of mHTT would be the toxicity-causing agents [191]. However, the question whether IBs are neuroprotective or neurotoxic needs further investigation.

1.3 Neuropathology in HD

1.3.1 Impaired striatal circuitry

The pathology of HD mainly strikes the basal ganglia and, specifically, the caudate nucleus and putamen within the striatum [102]. The focus on the striatum, however, should not dim the evidence that HD impacts the whole brain. Other brain regions are also affected, such as cortex, thalamus and also the white matter [55, 102]. The vulnerability to HD, however, is not the same across all of these structures. As mentioned, the most vulnerable is striatum, followed by cortex, while the hippocampus is involved at a later stage, and the cerebellum remains exempt even longer [155, 260].

The aberrant function of the basal ganglia causes most of the neuropathological conditions in HD [212], as they control voluntary actions. As previously mentioned, the neuropathology arises in the main structure of the basal ganglia, the striatum and the cortex, which provides different input categories to modulate accurate behavioral responses in

the subject [172]. Because HD affects directly this corticostriatal circuitry mechanism, these behavioral actions are disrupted. To comprehend the action and progression of HD it is essential to understand the basics of this connection.

About 95% of striatal neurons are GABAergic medium-size spiny neurons (MSNs). The current model of basal ganglia function displays two circuits with opposite effects on movement, the direct and indirect pathways [6]. The two pathways originate from two different populations of MSNs and form separate projections to different output structures. MSNs expressing enkephalin and dopamine D2 receptors form the indirect pathway, which comprises the most vulnerable neurons in HD and the ones which are lost from early stages of the disease. MSNs expressing substance P and D1 receptors, correspond to the direct pathway and appear to resist the progression of HD until later stages [261, 214].

In a non-pathological context, the indirect pathway acts to inhibit movement [6, 134]. Striatopallidal MSNs inhibit GABAergic neurons in the GPe. This results in less inhibition of the glutamatergic projection in the STN. In turn, the glutamatergic projections from the STN excite the GABAergic neurons in the GPi which results in greater inhibition to the thalamus and decreased signaling to the motor cortex (Figure 1.2 A). Thus, dysregulation of MSNs in the indirect pathway results in uncontrolled involuntary movements, such as chorea and tremor [16]. A schematic view of this alteration is shown in Figure 1.2 B.

On the contrary, the direct pathway is implicated in movement facilitation [6, 134]. Striatonigral MSNs in the striatum receive excitatory, glutamatergic projections from the cortex and thalamus. This results in excitation of the striatal GABAergic MSNs, which in turn inhibits the GABAergic projection in the GPi. The inhibition of the inhibitory GABAergic neurons in the GPi results in less inhibition on the thalamus glutamatergic neurons. This results in excitation of the motor cortex and initiation of voluntary movement (Figure 1.2 A). Taking this into account, dysregulation of this subset of MSN projection neurons would result in rigidity and bradykinesias [16], as showed in Figure 1.2 C. This dichotomy might explain the characteristic biphasic symptomology of HD, as it depicts early involuntary movements but a characteristic slowness of movement in later disease progression. Interestingly, most interneurons are largely spared. This morphological and functional difference has been speculated to play a role in the differential vulnerability of neurons observed in HD [42].

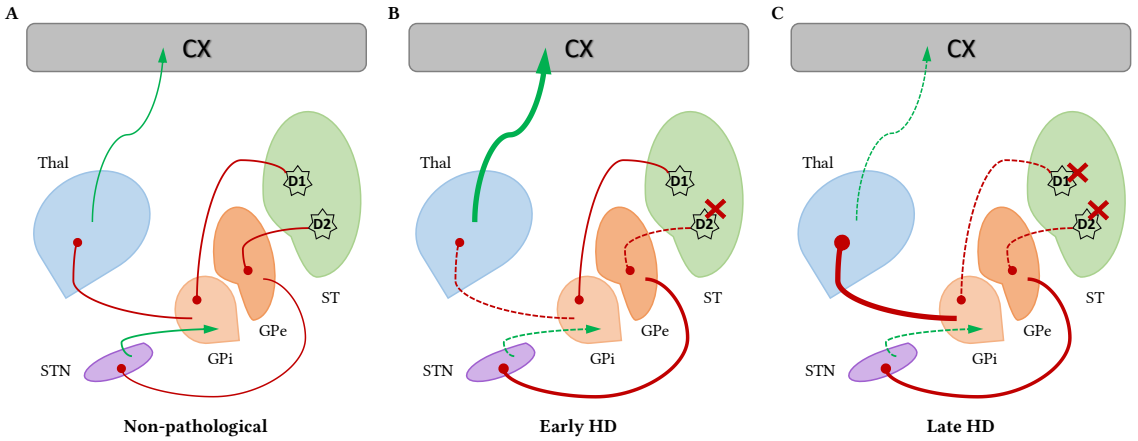

Figure 1.2 – Schematic overview of the HD pathology. (A) Non-pathological context. (B) Early HD, excessive movement. MSNs in the indirect pathway of the basal ganglia project to the GPe and are affected early in the course of the disease (D2). This results in a reduced inhibition of the thalamus and therefore an increased excitability of the motor cortex. (C) Late HD, inhibited movement. As HD progresses, MSNs projecting to the internal segment of the GPi via the direct pathway (D1) are also impaired, leading to a strong increase in the thalamus inhibition and a consequent abnormal reduction in the input to the motor cortex. ST, striatum; GPe, external globus pallidus; GPi, internal globus pallidus; STN, subthalamic nucleus; Thal, thalamus; CX, cortex. Red lines, inhibitory projections; green lines, excitatory projections; dashed lines, impaired projections.

1.3.2 Cellular traits in the pathology

As described above, the specific loss of striatal GABAergic MSNs affects the proper functioning of the corticostriatal circuitry. This reduction of MSNs can be traced by the decreased expression of several receptor subtypes such as D1 and D2 receptors [48], CB1 receptors [164], NMDA receptors [150] or TrkB receptors [81]. A variation of this nature can alter the neural transmission balance between the two pathways, direct and indirect. Moreover, there is a loss of GABA neurotransmitter in HD patients [125] and some studies have shown loss of D1 and D2 receptors in asymptomatic subjects [13], suggesting a dysfunction prior to the onset of the disease.

There are other features at the cellular level that characterize the dysfunction of the corticostriatal tract in HD. Previous studies have described the downregulation of synaptic vesicle fusion proteins (SNARE proteins) [177], as well as a hypometabolism of glucose in asymptomatic patients [163], backing up the statements of different impairments prior to a disease onset.

1.3.3 Molecular traits in the pathology

IBs that arise from mHTT protein develop in neurons of HD affected subjects [261] and they might appear in asymptomatic patients, as described in the previous section

[84]. For years, it was thought that glial cells did not display these inclusions [94]. However, recent evidence postulates certain aggregate load in oligodendrocytes and astrocytes of HD subjects and several HD mouse models [120].

Neurons hold only one IB in the nucleus [19, 61] with ubiquitin immunoreactivity [238]. Although reports of HD brains described IBs mainly in the nucleus, other work found ubiquitinated accumulations of mHTT in some neuronal processes undergoing dysthrophia and in the cytoplasm [94, 61]. These characteristic nuclear IBs are located all accross the brain in the caudate nucleus, putamen, globus pallidus, substantia nigra, hippocampus, thalamus, subthalamic nucleus, cortex and amygdala [186, 238].

mHTT also promotes mitochondrial dysfunction by decreasing ATP biogenesis [233], affecting calcium buffering [196] and lowering mitochondrial trafficking [145]. This might be one of the factors that explain increased MSN vulnerability to mitochondrial function since they consume large amounts of ATP in order to keep a hyperpolarized state [31, 99]. Another disease risk could be axonal transport impairments caused by mHTT [176, 99], which affect growth and maintenance of neuronal projections in MSNs bearing IBs.

1.4 Models for studying HD

1.4.1 *In vitro* models of HD

One of the very first *in vitro* models to study HD was generated in yeast, *Saccharomyces cerevisiae*. Yeast represents a useful tool to expose genes implicated in IB formation, to study the potential toxicity of different polyQ lengths or to screen potential pharmacological compounds [161]. Yeast models have been of major relevance for HD, for example, for unraveling the relevance of chaperone-mediated folding of polyQ expansions. Chaperone Hsp104 was published to be a modulator of aggregation of polyQ-containing proteins [135] and overexpression of Hsp70 and Hsp40 inhibited the formation of amyloid-like deposits by promoting detergent-soluble inclusions [179]. More recently, it has been reported that the ribosome quality control machinery has a protective role in yeast, as nuclear accumulation of Httex1-103Q enhances its cytotoxicity [283]. However, it is unclear whether this situation resembles what takes place in mammalian neurons.

Cellular models are useful tools to investigate HD pathology and to understand possible mechanisms of the disease. Different mammalian cell types in mitotic phase are

available to study HD. This pool of different profiles allows to examine the pathology in a variety of tissues in which the expression and impact of HD pathology is significant and less discerned [225]. Some cell lines have been used to model HD features through transfection of different constructs and evaluation of toxicity, aggregate kinetics, aggregate localization or antibody suitability, such as human embryonic cell lines (HEK293T) [97], monkey kidney fibroblast lines (COS-7) [194], mouse neuroblastoma (Neuro2a) [190, 277], human neuroblastoma (SH-SY5Y) [263], or rat pheochromocytoma (PC12) [240], among others.

Interestingly, various inducible cell models have also been generated to study mHTT dynamics and generation of aggregates in a controlled manner by modulating the expression. The advantage of these systems lies in the time- and inducer-dependent regulation of the gene of interest. With this approach, mostly cell lines with neuronal phenotypes have been used in order to reproduce more accurately HD characteristics. For example, Neuro2a (N2a), a cell line expressing HttEx1 under muristerone A-inducible promoter [262] showed sensitivity to aggregates in a dose- and time-dependent manner; the NG108-15 cell line expresses either full-length or truncated *Htt* gene under the Tet promoter and shows formation of cytoplasmic and nuclear inclusions in a time- and polyQ length-dependent manner [149]; the PC12 cell line has been a useful tool, expressing different versions of HttEx1-eGFP under the Tet promoter, both ON and OFF, displaying inhibition of neurite outgrowth, as well as cell death coupled with transcriptional dysregulation [272, 116]. Although many cell lines have been used, there can be differences when compared to primary cells. Therefore, primary neurons transiently transfected with mHTT or prepared from HD transgenic mice are frequently used as *in vitro* model [254].

In vitro models are also a precious instrument to integrate and validate *in vivo* observations. Despite the variety of available cell lines, a major drawback is the lack of human neuronal cell lines that can be representative of early neuronal differentiation. Currently, induced pluripotent stem cells (iPCs) derived from either HD murine models or patients are drawing more and more attention. These cells can be collected and subsequently reprogrammed for a different somatic fate [32]. mHTT does not impair the reprogramming into neuronal progenitors or mature neurons [197]. HD iPSCs and the neural cell types derived from them recapitulate some disease phenotypes found in both human patients and animal models. These new tools are fundamental to better understand how mHTT affects neuronal cells in a more physiological manner and to identify potential factors responsible for the higher susceptibility of MSNs to degenerate [253, 117]. Nevertheless, the use of iPSCs has been limited due to some of the inherent problems with cell line

reproducibility and technological differences between laboratories.

1.4.2 *In vivo* models of HD

The development of transgenic models marked a breakthrough in HD research as they represented valuable tools not only for characterizing HD associated molecular changes, but also for identifying cytotoxic pathways related to mHTT and potentially testing possible therapies. The nematode *Caenorhabditis elegans* is the simplest established animal model in HD [198]. Its simplicity of 302 neurons along with its transparency allows a whole set of biochemical and behavioral studies that can be combined with longitudinal live imaging experiments [28].

Another invertebrate model is the fruit fly, *Drosophila melanogaster*. It bears a fully functional nervous system with a separation among specialized functions such as vision, olfaction, learning and memory. Comparative genome analysis reported a similarity of 50% between fly and human genes [219]. As an important advantage, foreign genes in *Drosophila* can be engineered to be expressed in a tissue- and time-specific manner, in addition to the fantastic resource of available genetic tools [157]. Typically, polyQ-expressing flies form nuclear inclusions and display protein aggregation, neurodegeneration, behavioral deficits and a reduced lifespan [141].

One of the most important advances in HD research has been the generation of various mouse models. Before it was possible to model the genetics of HD researchers used lesion-based models where excitotoxic injuries were introduced in the striatum of the animals to research the functional role of this brain structure in HD [47, 224, 26]. These lesions typically induced cell death by excitotoxic mechanisms or by disruption of the mitochondrial machinery, generated with the application of different aminoacids such as quinolinic acid or 3-nitropropionic acid, which caused massive apoptotic cell death [59]. Some of these models reproduce motor abnormalities present in late stage HD patients [18]. These classical lesion models produce behavioral responses and have contributed substantially to the understanding of the corticostriatal pathway and the striatum in HD. However, their nature does not consistently match the genetic basis and progressive worsening of the human disease; there is no clear association between their mechanism of action and the genetic cause of HD. Additionally, cell death in HD is progressive and the age of onset inversely proportional to the number of CAG repeats in the mHTT protein [9], whereas cell death in the toxin models is immediate and not progressive due to the acute type of the lesions.

The description of the genetic cause, the mutated *HTT* gene [151], was the starting point for different attempts in the generation of genetic models suitable for not only mimicking of the human symptoms, but also research in an appropriate proteomic and genomic context. In fact, the first models showed the relevance of HTT protein in early embryonic development, as they were KO models and demonstrated embryonic lethality [213, 66]. These discoveries, however, did not lead to a broader knowledge of how mHTT causes HD and it was still necessary to generate genetically modified animals more similar to the human pathology. From there on, different mouse models for HD have been widely generated, from transgenic ones expressing mHTT-Exon1, through full-length transgenic models, to full-length knock-in (KI) ones.

Mouse models are widely used in research, as they show relatively rapid and progressive neurological phenotypes. However, there is still discussion regarding the point that the adult-onset disease takes years to manifest in humans. Rodents are limited by two main issues; their small brain size and neuroanatomical organization compared to humans, as well as their shorter lifespans. To face these constraints, large animal models expressing mHTT are also being used, such as sheep [118], minipigs [274] and non-human primates [275]. The use of these animal models can be specially relevant in some aspects that are particularly challenging in rodents. For example, mapping the progression of HD in the presymptomatic stages or testing new therapeutic vectors in larger brains, which could address long term safety and set a maximal therapeutic effect. Nevertheless, the use of these animals in preclinical studies is expensive, their accessibility by all researchers is limited and they need a very long term study plan, as compared to rodents.

The R6/2 mouse model

The first genetically modified mouse models of HD expressed a fragment of exon 1 of human HTT randomly integrated into the murine genome [168], specifically, the R6 lines, which included R6/0, R6/T, R6/1, R6/2, and R6/5 [154]. From those five R6 lines originally generated, the two most widely used are R6/1 and R6/2. As the mHTT-Exon1 fragment that these lines carry is integrated randomly into the genome, transgenic mHTT is expressed along with both endogenous *Htt* alleles. Regarding this point, these lines are criticized for the fact that they only express a shortened HTT form, questioning its physiological validity. However, N-terminal fragments are believed to be the most toxic species in the mHTT cleveage process [83]. Both, R6/1 and R6/2 lines have been extensively

studied and they resemble HD symptomology in a similar manner, being comparable to some KI models [270].

In particular, the R6/2 line carried 144 CAG repeats at the time of publication. However, due to the intrinsic instability of the repeats, they have expanded over time. The R6/2 model presents motor deficits as early as 5 weeks of age [154, 34], such as decline on the rotarod test. Onset of motor symptoms takes place around the age of 8 weeks, where motor and balance coordination are impaired, showing resting tremor, chorea-like movements, stereotypies, clasping behavior, epileptic seizures, narcolepsy, weight loss and spontaneous shuddering movements [207]. At this age, it was also shown by a MRI-based study that there is a lack of striatal growth, instead of striatal atrophy, correlating the motor symptoms with the brain volume loss [208]. Cognitive impairment was also characterized by different behavioral tests [147], as well as other defects such as weight loss, diabetes, resting tremor or seizures [154, 115]. All this eventually results in premature death at around 12 weeks of age (Figure 1.3). In fact, at autopsy, brain weight is significantly reduced, whereas neuronal death is minimal compared with behavioral symptoms [62]. In contrast, one of the main characteristics of human HD is the massive loss of striatal neurons [56]. It is possible that cell death follows a long phase of neuronal dysfunction in both mice and humans, but it remains unsolved why this transgenic model does not show marked cell death until the last stages of the disease. An explanation might be the short lifespan of the model, which might be caused by general metabolic disease and seizures. Alternatively, because R6/2 mice are relatively resistant to kainic acid *in vivo*, they might have protective mechanisms that are not present in humans [256, 264].

At the celullar level, the R6/2 model presents mHTT-associated inclusions in striatum

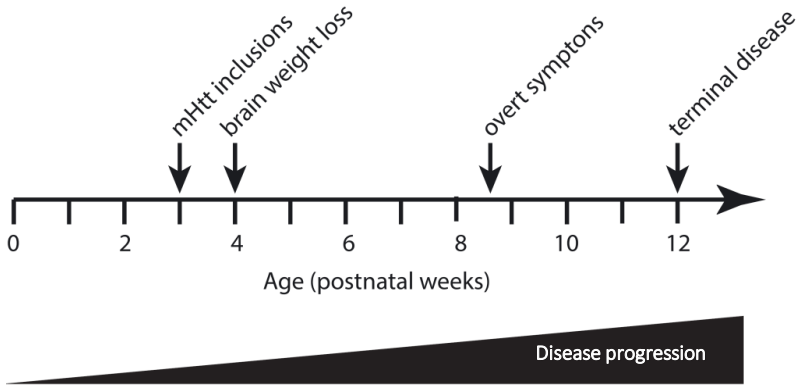

Figure 1.3 – Timeline overview of the R6/2 mouse model. Schematic representation of the life timeline of the R6/2 mouse model, depicting the main prototypical and molecular events.

and cortex as early as 3 weeks of age [167], similar to HD inclusions, which exhibit an amyloid-like structure [166]. Although different brain regions have different proportion of inclusions along the lifetime of the model, at the terminal disease stage there are inclusions in almost all neurons. For example, in the most vulnerable region in HD, the striatum, it has been published that 98% of MSNs are inclusion positive by that time point, in contrast to interneurons, which exhibit fewer inclusions [167, 133].

1.5 Proteomics in neurodegenerative diseases

The term *proteome* describes the whole protein load of a cell line, tissue, or organism. Proteomic analysis takes an integrative view of biological processes by considering all the proteins of a cell [37]. It includes different techniques, such as protein microarrays, two-hybrid assays in yeast, crystallization or mass-spectometry (MS). Specifically, this last approach is considered a key instrument for the field and both, its development and improvement have been essential in studies of protein semi-quantitative measurements, protein-protein interactions, protein localization and protein function [136]. Currently, MS is the most popular method for detection and characterization of proteins since it provides not only details regarding the expression levels or post-translational modifications, but also it is relevant for the identification of potential biomarkers in different disease backgrounds.

In a context of neurodegeneration, finding biomarkers is a robust instrument for NDD diagnostics and treatment evaluation [184]. For example, the analysis of CSF has been shown to be a perfect biological source for different conditions that affect the CNS [37, 53]. Different studies have recognized CSF proteins that might act as possible biomarkers for AD, PD or ALS [132, 95]. As another example, proteomics have also been used for analyzing oxidative stress in patients affected by NDDs such as AD [210].

The great power of proteomic approaches in the neurodegeneration field certainly complements traditional procedures and allows the identification of multiple proteins that were not previously linked to a specific disease. The identification of markers and an the understanding of their interactions will help new potential therapeutic drugs to be developed for early treatments of different NDDs.

In other diseases, such as HD, proteomics has become a progressively useful tool. Different interesting insights in HD have been reported thanks to the proteomic approach.

Some studies have attempted to elucidate potential biomarkers through the CSF [52], as well as more recently through the metabolome [87]. Analysis of the human HD brain proteome suggested a link to different NDDs and to type-2 diabetes [229], which highlighted the interlinked processes of the disease.

1.6 Therapeutic approaches in HD

To date, there is unfortunately no cure for HD and no therapies that reverse or prevent symptoms. There is a large and ongoing search for pharmacological interventions for HD, but there is no treatment to terminate motor, cognitive, or psychological dysfunctions [165]. Because of the vast neurodegeneration and resulting symptoms, the probability that only one therapy will treat the mentioned symptoms is unlikely. Medical management in HD consists of treating each symptom area separately, although this is ineffective. For example, choreatic movements may be treated with tetrabenazine, psychological symptoms with neuroleptics, and cognitive symptoms with minocycline [25]. Another issue arises when looking at the side effects of the medications because treatment of one symptom increases the prominence of another [30, 25].

Different approaches have been proposed to interfere directly with mHTT toxicty. They could be categorized in blockade of HTT proteolysis with caspases or calpain inhibitors, decrease of aggregates or mHTT toxicity with chaperones and chemical compounds, up-regulation of transcription with histone deacetylase inhibitors, re-supply of the lost WT HTT protein functions, application of metabolic enhancers, blockade of excitotoxicity with NMDA antagonists and suppresion of mHTT with siRNA and anti-sense oligonucleotide (ASOs) [110, 221]. Other approaches, instead of interfering with some of the effects in the pathology, focuses on restorative strategies, typically on the striatal neuronal loss [211]. For example, reconstruction of neuronal circuits in the brain by intrastriatal transplantation of striatal neuroblasts from human fetuses was reported as a possible option [202]; or, neuroprotective strategies such as the delivery of neurotrophic factors, as such proteins have shown a strong protection of neurons in various animal models of striatal injuries [5].

1.6.1 Neurotrophic factors in HD

Neurotrophic factors (NF) are proteins which promote the survival of specific neuronal populations. The course of action of these proteins includes the induction of

different physiological effects such as morphological differentiation, nerve regeneration, neurotransmitter expression and gene expression. Endogenous levels of NF usually elicit an increase in the response to neuronal damage, suggesting a physiological regenerative reaction [111]. Neurotrophins, glial cell line-derived neurotrophic factor family members and ciliary neurotrophic factor (CNTF) have neuroprotective effects on different striatal neuronal populations. Additionally, they maintain the integrity of the corticostriatal pathway. Many neurotrophic and growth factors are localized to the nigrostriatal system, suggesting a physiological role in the development, maintenance and/or recovery of these neurons. In fact, many of the factors localized to the nigrostriatal system have neuroprotective actions in HD animal models with exogenous administration [7]. Due to these characteristics, NF may be suitable for the development of a neuroprotective therapy for NDDs, including HD [5].

Among the studied NFs in HD, there are two interesting examples that may result in viable candidates for treatment of the disease and have been under the scrutiny of scientists for some time. The first one is CNTF, a member of an α-helical cytokine superfamily that includes IL-6, LIF and leptin. CNTF is found in glia cells, both within the CNS and the peripheral nervous system (PNS). CNTF is considered an *injury factor* and it has been already reported its neuroprotective role in different models of NDDs [5]. CNTF was delivered by different ways into striatal neurons in experimental animals and it has shown to preserve the neurons in both, chemically-induced model of HD and a transgenic one [8, 69, 279]. These and some other evidence led to the initiation of a clinical trial in order to determine the effects of CNTF in HD patients [14]. CNTF was delivered *ex vivo* by encapsulated baby hamster kidney cells implanted into the lateral ventricle of HD patients. The trial reported the successful possibility of a long-term delivery of CNTF in human brain with the encapsulation method. However, the diffusion of the factor from the ventricle to the parenchyma was limited, as revealed in primates [174], therefore providing only little benefit to the patients [24].

The second NF of interest is brain-derived neurotrophic factor (BDNF), a member of the neurotrophins family, which acts through the interaction with two distinct receptors, the p75 neurotrophin receptor (p75NTR) and a member of the tropomyosine kinase (Trk) receptor family, TrkB. BDNF is produced by cortical neurons in layers V and VI, anterogradely transported, released and finally taken up by GABAergic striatal neurons [159]. Wildtype HTT protein is assumed to regulate the activity of the BDNF promoter II, affecting BDNF transcription [286]. Furthermore, downregulation of BDNF transcripts in cortical neurons is induced by mHTT through an effect on DNA methylation [195].

Accumulation of mHTT can lead therefore to a lower BDNF concentration in the striatum, and reduced BDNF transcription; in addition, mHTT will also reduce BDNF vesicle transport along microtubules [259]. Degeneration of cortical afferents also contributes to the diminished BDNF support of striatal neurons [223]. Different studies have attempted to enhance BDNF signaling in order to improve the HD phenotype. For example, the peptide P42 was reported to act on the aggregation process at early stages of the disease [11] and more recently, to ameliorate R6/2 behavior through BDNF signaling in pre- and post-symptomatic phases [12, 46].

The substantial overlap between neurothrophins signaling pathways and those dysregulated by mHTT provides some support for targeting NF receptors as a therapeutic strategy for HD. Support for this approach is provided by preclinical studies showing that small molecule ligands for both types of NF receptors, Trks and p75NTR, reduce degenerative signaling or increase trophic signaling to prevent HD-related pathology in mouse models of the disease [239]. Regarding Trk ligands, future studies will determine if novel small molecules with optimized bioavailability can be identified and improve cognition and/or motor ability in HD. Since the p75NTR ligand, LM11A-31, is already in Phase II clinical trials for AD in the USA (Reference at ClinicalTrials.gov: NCT03069014), current work is focused on preparing for HD clinical trials, including development of non-invasive biomarkers capable of detecting the therapeutic efficacy of LM11A-31.

There are other NF which also promote survival of neurons and regulate normal function in the CNS, such as glial cell-line derived neurotrophic factor (GDNF) or fibroblast growth factor (FGF) [112, 122, 5]. However, whether these NFs are a promising alternative for human therapy, remains unknown. The main challenge with NFs is their direct delivery, since a systemic one is often associated with side effects as their receptors are widely distributed over the organism and the proteins do not cross the blood-brain barrier. The chosen delivery method depends on the application, the delivery area, the treatment duration and the balance of risks versus benefits. All of this points need to be addressed in the future.

1.6.2 HDGF: a trophic factor harbored in the nucleus

HDGF, also known as high mobility group protein 1-like 2 (HMG-1L2), is a 27 kDa protein implicated in multiple cellular functions, initially purified from the supernatant of human hepatoma cell lines [182, 181]. HDGF-related proteins (HRPs) comprise a family

with six members which subclassify in different groups depending on their charge, size and sequence [58]. Specifically, HDGF is categorized as a small acidic protein within the family [58]. HDGF is widely expressed with high levels in the brain, testis, lung and spleen [70, 2], as well as in developing heart and tumoral cells [72]. Zhou *et al.* shed some light onto its distribution, examining the localization of HDGF in the mouse nervous system, where they found it to be abundantly expressed [285]. Expression of HDGF within the brain takes place in different cell types, neurons, astrocytes, microglia and oligodendrocytes [67].

HDGF is mainly localized to the nucleus and this localization is mandatory for its mitogenic activity [131, 72]. Early studies also found the protein in the cytosol [189]. However, it was demonstrated that the full-length protein is exclusively expressed in the nucleus [73]. The differential localization could be explained taking into account that HDGF resides both in the cytoplasm and the nucleus depending on cell type, phase of cell cycle and its specific function [73].

HDGF contains a well-conserved N-terminal amino acid sequence, the HATH domain (homologous to the amino terminus of HDGF) [58]. The HATH domain comprises the aminoacids 1-98 of HDGF and it is also referred to as the PWWP domain [58, 244]. Proteins including the PWWP domain are involved in transcriptional regulation, DNA methylation, histone modification and DNA repair by interacting with histones, DNA and proteins such as heparin [38, 113, 217]. The type of PWWP domain modulates its binding and protein-protein interactions [113] and it often involves chromatin-associated biological processes [205]. Zhao *et al.* identified the interactome of HDGF trough the PWWP domain and found that HDGF it is a multifunctional protein which participates in several cellular activities, such as ribosome biogenesis, RNA processing, splicing and DNA damage repair [282].

HDGF can be secreted into the extracellular space [252], suggesting a role in auto/paracrine communication. More recently, it was reported that HDGF is secreted via exosomes as a mechanism to release HDGF [187]. Extracellular HDGF appears to signal through transduction pathways from the cell surface [3]. The function of the protein is, nevertheless, not clear. It seems that HDGF plays a role in renal [189], liver [71] and heart [72] development. On the other hand, it seems to be involved in cancer development as well [188, 109, 20], as proliferation-inducing factor. In postmitotic neurons, HDGF may have merely a neurotrophic function. Related to this, HDGF has been found to have a neuroprotective role against motor neuron degeneration [160] and for injured adult retinal

ganglion cells [106]. However, HDGF still misses a detailed characterization in this field, especially in a neuronal disease context and only little information is available. Moreover, HDGF has not been studied in the context of HD.

1.7 Aim of the thesis

The main focus of the present thesis can be divided into the following aims:

1. Investigation of molecular neurodegenerative signatures in the R6/2 HD mouse model.
2. Functional characterization of protein candidates influencing mHTT toxicity.
3. Assessment of the therapeutic potential of HDGF overexpression in cell and animal HD models.

CHAPTER 2

RESULTS

2.1 R6/2 mouse model characterization

R6/2 transgenic mice express mHTT-Exon1 under the control of the human *HTT* promoter [154], as described in previous section. It has been shown that mouse colonies raised in different laboratories display some differences in phenotype [105], which can be due to genetic drift, dietary factors or housing conditions. Therefore, to establish a basal line for our R6/2 colony, we characterized several parameters, both molecular and behavioral.

For study time points we selected an early one at 5 weeks, before disease onset; an intermediate time point at 8 weeks, on the border of visible motor deficits; and a late time point at 12 week old, at the end of the lifespan of R6/2 mice [34, 54]. In agreement with previous studies [54, 167], brains of R6/2 mice already displayed widespread IBs at 5 weeks, with striatal IBs being more abundant over time compared with the cortical region, but significantly smaller than cortical IBs (Figure 2.1).

R6/2 mice were also tested for locomotor activity on an accelerating rotarod and in an open field (Figure 2.2), since the exact time point for the onset of motor impairments varies between colonies and it depends also on the CAG length. It has been previously published that very high repeat numbers lead to a delayed onset of disease, as well as an attenuation of the HD-related phenotype [178, 51]. This variation occurs due to the genetic instability of the CAG repeats, whose transcription elongation is regulated in a tissue-dependent manner and therefore, contributes to the tissue-specific instability [85].

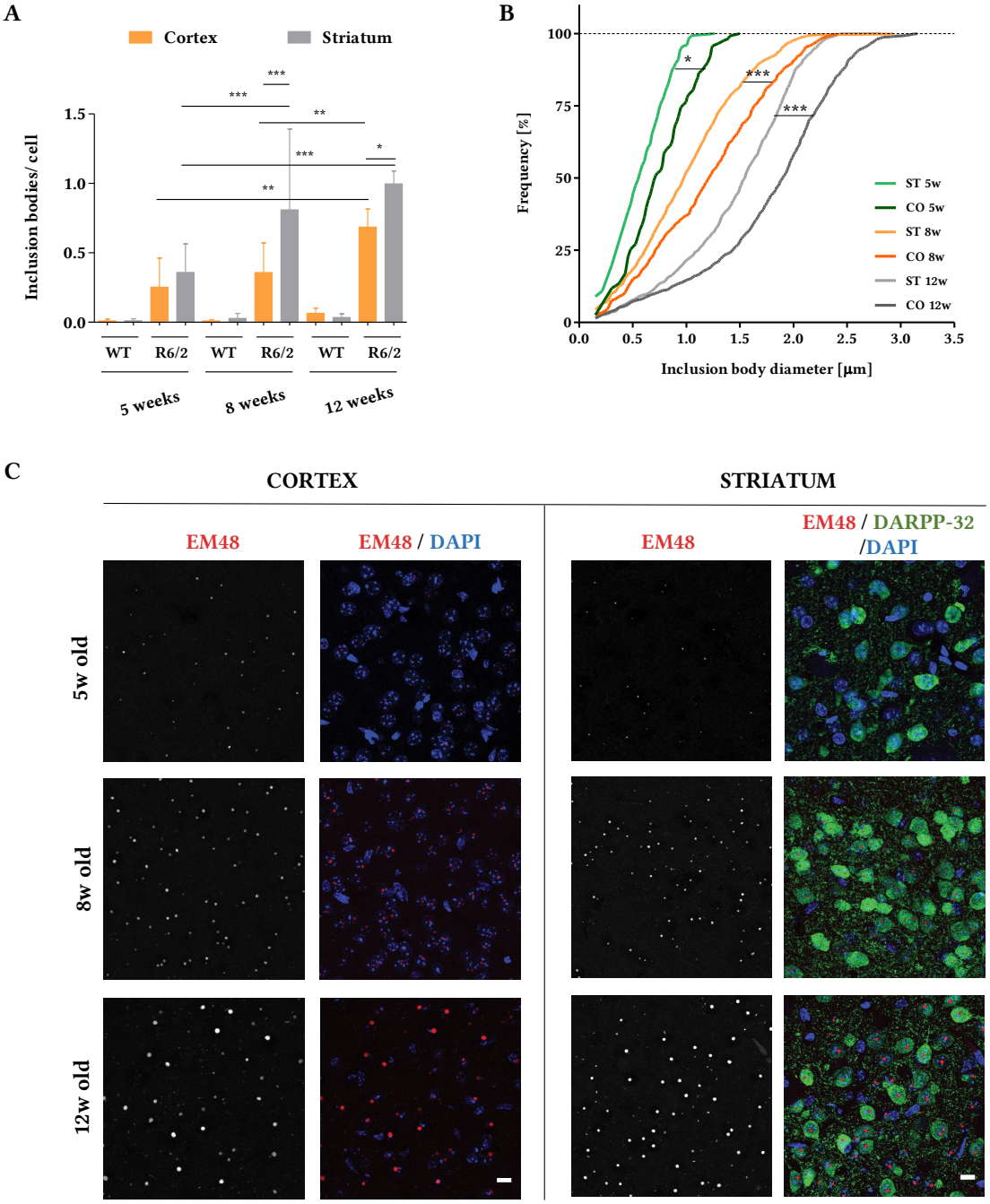

Figure 2.1 – Histological characterization of IBs in R6/2 mice. (A) Immunohistochemistry-based counting of IB, as frequency of IBs per cell from 5, 8 or 12 week old R6/2 and WT mice; one-way ANOVA with Bonferroni's multiple comparison test, * $p<0.05$, ** $p<0.01$, *** $p<0.001$; n=3. Values are mean± SD (B) IB diameter; one-way ANOVA with Bonferroni's multiple comparison test, * $p<0.05$, ** $p<0.01$, *** $p<0.001$; n=3. (C) Immunohistochemistry staining of cortical and striatal tissue of R6/2 mice; DAPI, blue; DARPP-32 for MSNs, green; EM48 for HTT inclusion staining, red; scale bar is 10 µm.

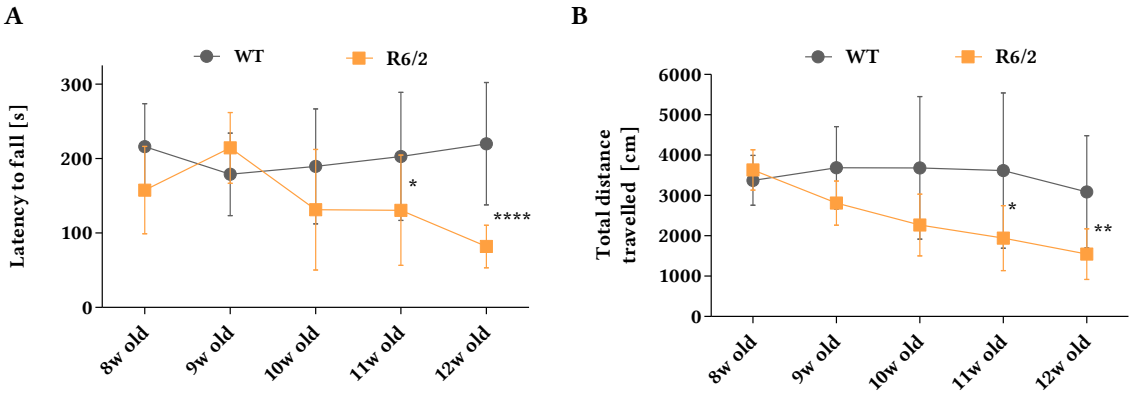

Figure 2.2 – Behavioral characterization of the R6/2 mice. (A) Latency to fall on the accelerating rotarod, n=6-14. (B) Distance traveled in the open field. WT, 6-12 mice, R6/2, 8-18 mice. Two-way ANOVA with Bonferroni's multiple comparison test, * $p<0.05$, ** $p<0.01$, *** $p<0.001$, **** $p<0.0001$. Values are mean± SD.

Our R6/2 colony had a CAG repeat length ranging from 160 to 190 repeats, which translated into a minor delay in the disease progression compared to the original R6/2 line [154]. This slight increment delayed the onset of motor defects in our colony to 10 weeks onwards, compared to published data [34]. R6/2 mice at 8 to 9 weeks of age displayed no significant deficits on the accelerated rotarod and normal locomotion in the open field, whereas at 11-12 weeks of age, the mutants were severely impaired in both tests (Figure 2.2). Taken together, these data show that the R6/2 mice in our colony develop the characteristic phenotypes described for this model, however, the onset of the behavioral defects is slightly delayed compared to the original line.

2.2 Proteomic screening

2.2.1 The proteomic study: a spatiotemporal approach

For the analysis of proteome changes linked to neurodegeneration at the same time points selected, we processed extracts from four brain regions related to the differential vulnerability to HD: striatum (ST), being the most affected region; cortex (CO), hippocampus (HC) and cerebellum (CE), as the region that remains relatively spared until an advanced HD stage [260] (Figure 2.3). From each tissue sample, soluble and insoluble proteomes were measured by single-run LC-MS/MS. All proteomic analyses were performed by Fabian Hosp at the Department of Proteomics and Signal Transduction, in the Max Planck of Biochemistry, as stated in Appendix C.

2.2.2 Proteome remodeling in R6/2 mice after disease onset

Through the experimental design described in Figure 2.3, we identified ∼ 12,500 proteins in the soluble proteome. The soluble brain region data of WT mice provided a communal resource with a spatiotemporal resolution for ∼8,500 proteins after filtering for valid values [107].

As shown in Figure 2.4 A, the principal-component analysis (PCA) indicated a strong separation on the soluble proteomes of R6/2 and WT mice. Firstly, there is an extensive proteome remodeling during the disease progression shown by the clear separation of R6/2 mice from other samples right before the onset and at the final stage of the disease (8 and 12 week old). Secondly, proteomes from CE samples were strongly separated from other brain regions, highlighting the fact that all the other three regions belong to the forebrain. Thirdly, samples from R6/2 at 5 week old grouped indistinguishable with WT samples, suggesting that at this early stage of the disease no major changes took place yet.

The analysis of the expression profiles of the animals, highlighted the remarkable similarity between 5 week-old R6/2 and WT mice. There are, however, some protein clusters which are already differentiated in their expression (green square, Figure 2.4 B). The expression of mHTT causes a drastic proteome remodeling only three weeks later, at 8 weeks of age, with several clusters strongly up- or down-regulated (colored clusters, Figure 2.4 B). Clusters 2 and 3 include enriched up-regulated proteins related to chaperonin complex and proteasome accessory complex, respectively. On the contrary, clusters

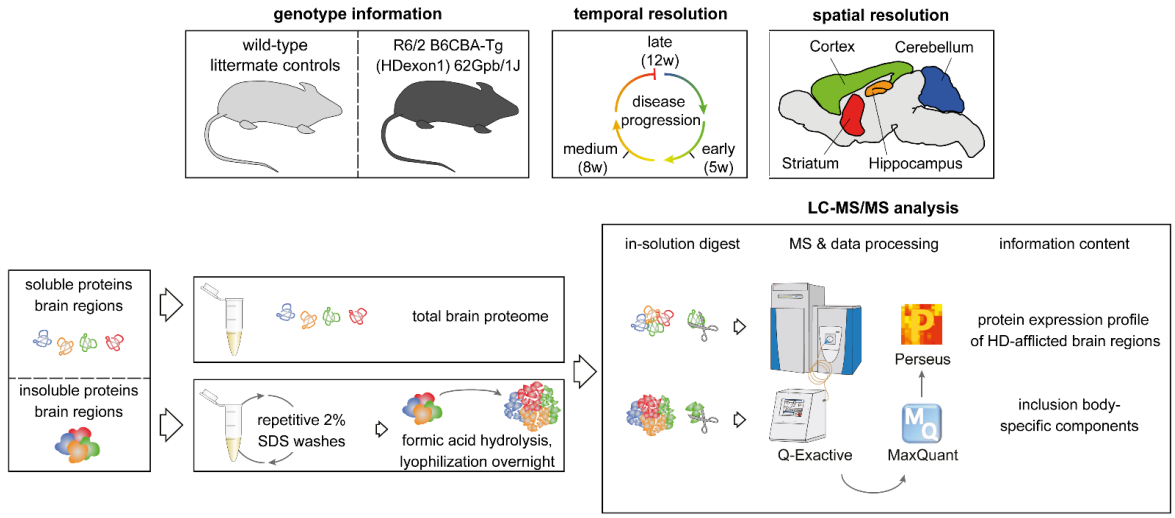

Figure 2.3 – Experimental workflow scheme. Brain regions from R6/2 and WT mice were assessed by quantitative LC-MS/MS. 5 week old,4 R6/2 and 4 WT; 8 week old, 3 R6/2 and 3 WT; 12 week old, 4 R6/2 and 4 WT.

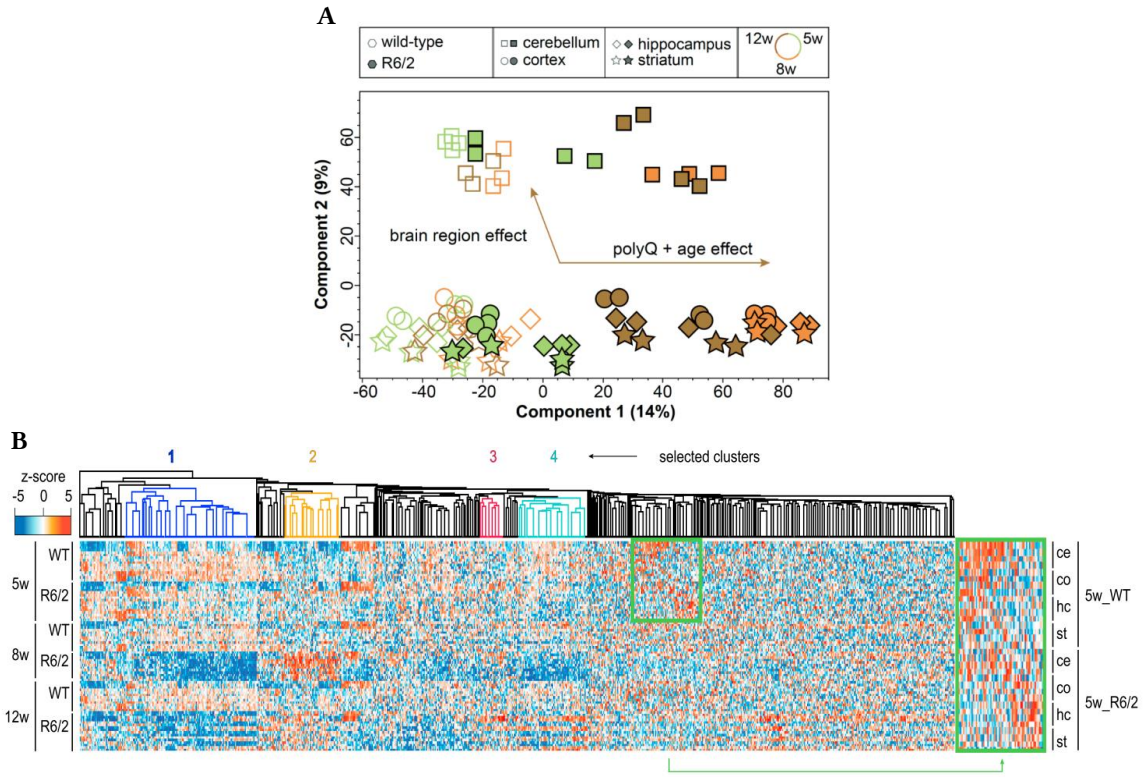

Figure 2.4 – Analysis of the soluble proteome: PCA analysis and proteome remodeling of R6/2 samples. (A) PCA projections of all soluble samples reveal specific effects on the proteome driven by the genotype, age, and differential spatial expression. (B) Hierarchical clustering of protein expression over time shows substantial proteome shifts from early stages of HD onward. The two most up-regulated (red and orange) or down-regulated (blue and cyan) clusters are indicated.

1 and 4 comprise enriched down-regulated proteins associated to the ribosome and energy transport across the mitochondrial electron transfer chain, respectively. These observations are in line with the deficient energy metabolism and impairment of the ubiquitin-proteasome system caused by HD [4, 192]. Overall, this proteomic analysis supplies a detailed overview of protein changes in the R6/2 model on a proteome-wide scale.

2.2.3 Characterization of polyQ aggregates

A distinctive feature of HD is the presence of IBs, consisting of mHTT and sequestered proteins. The identity of those proteins, however, remains unknown. To analyze the insoluble proteome of R6/2, which is largely composed of IBs, we had to pre-treat the samples for MS analysis. The extreme insolubility of the IBs makes them resistant to proteolytic digestion. Therefore, we purified polyQ aggregates in formic acid [130] previous to tissue-based quantitative proteomics (Figure 2.3), which allowed to identify several hundred proteins and shown extensive protein sequestration to the insoluble fraction in

the R6/2 brain.

We estimated protein abundances for a quantitative analysis of the aggregate composition through the iBAQ algorithm, which can roughly estimate the relative abundance of proteins within each sample [231]. Only 10 proteins constituted more than 50% and the top 50 proteins constituted more than 75% of the aggregate mass in 12 week old R6/2 striatum (Figure 2.5 A). These included not only histones and RNA-binding proteins, but also proteins involved in neuronal plasticity, as well as myelin components [107]. This last observation resulted a surprise, considering that the majority of inclusions are found

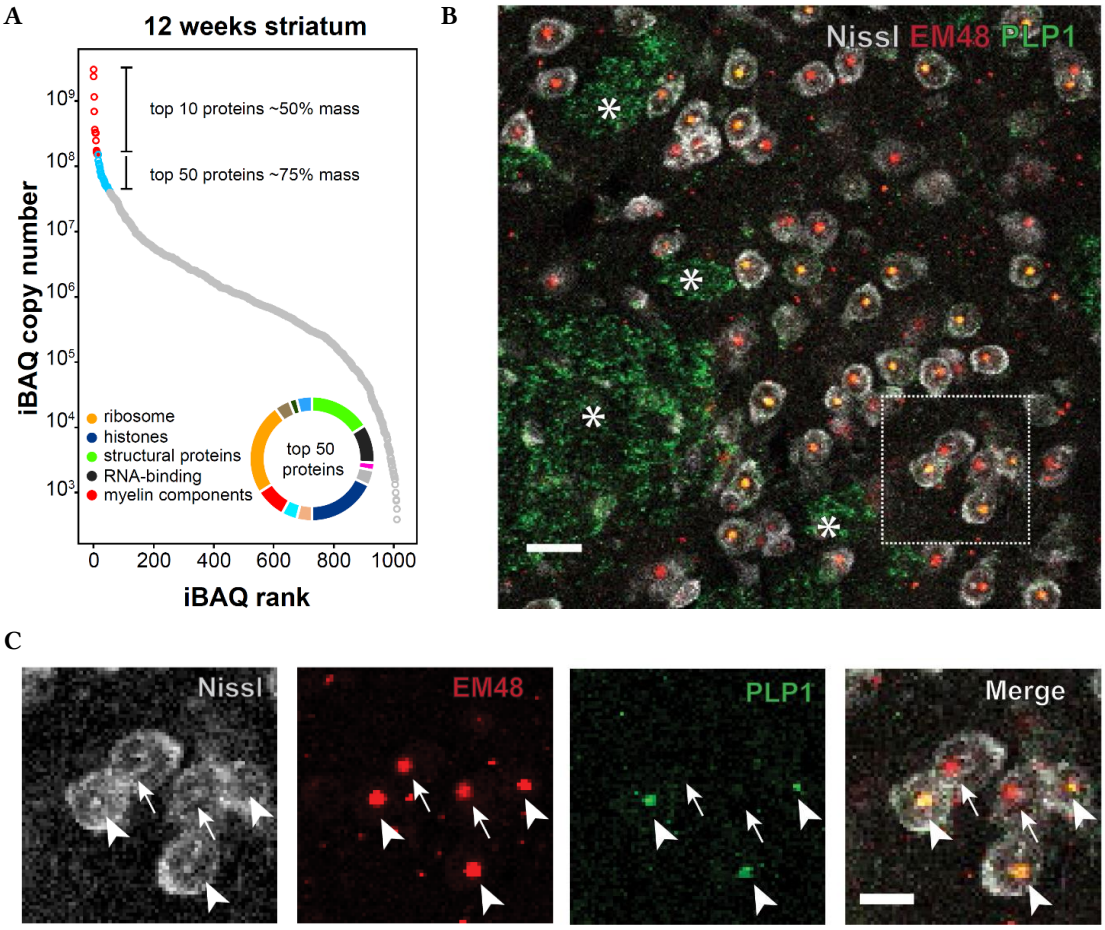

Figure 2.5 – Characterization of polyQ Aggregates. (A) Distribution of iBAQ values for 12 week old R6/2 striata. Pie chart distribution of annotations for the top 50 proteins. (B) Representative single-plane immunofluorescence in a 12 week old R6/2 striatum showing colocalization of PLP1 protein with IBs; Nissl staining for neurons, grey; EM48 staining for HTT IBs, red; PLP1 staining, green; asterisks mark white matter bundles of the striatum; scale bar is 20 µm. (C) Close-up of the colocalization; arrowheads point to PLP1 sequestered in IBs; arrows point to IBs without colocalization; scale bar is 10 µm.)

in neurons. Co-immunostainings for the myelin protein Plp1, HttEx1 IBs, and a neuronal marker revealed co-localization of Plp1 with aggregated HttEx1 in many neuronal IBs, confirming that myelin proteins are true components of neuronal inclusions and excluding the possibility of contamination (Figure 2.5 B and C).

We mapped the soluble proteome data to the insoluble fraction, based on the hypothesis that such extensive proteome remodeling (Figure 2.4 B) should be mirrored in the insoluble counterpart. This revealed that a high number of proteins down-regulated in the soluble proteome, were enriched in the IBs (blue and cyan in Figure 2.6 A), implying sequestration of those proteins and therefore, an extensive loss of function. This depletion of sequestered proteins from the cellular pool likely impairs normal cellular function. Interestingly, a large number of proteins up-regulated in the soluble proteome were also enriched in the insoluble fraction (orange and red in Figure 2.6 A), such as proteins related to the proteasome complex. This finding points to the up-regulation and participation of chaperones and related proteins, which interact with the IBs and become trapped.

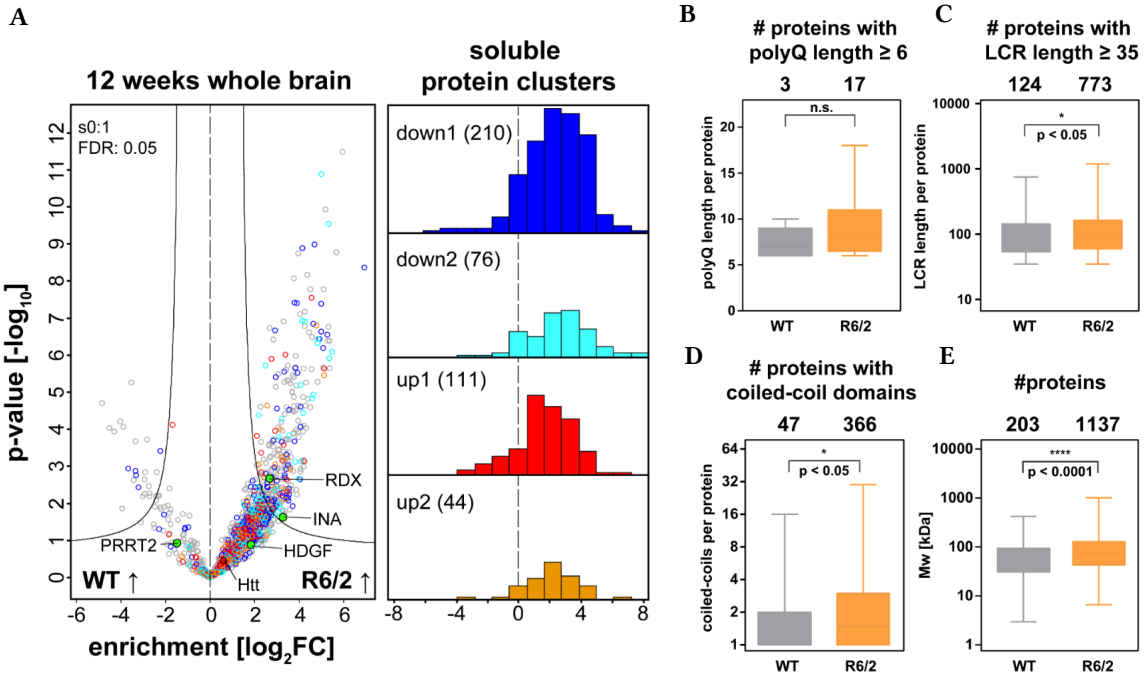

Figure 2.6 – Analysis of the insoluble proteome. (A) Volcano plot of the whole brain insoluble fraction, superimposing enrichment of the proteins that are dysregulated in the soluble fraction. The main protein candidates followed up later on and endogenous Htt are indicated. Color code as in Figure 2.4. (B, C, D, F) Significant enrichment of proteins with longer polyQ. (B) and LCRs (C), more CCDs (D), and higher molecular weight (MW) (E) in 12 week old R6/2 over WT striata. Values are mean± SD. Mann-Whitney U test.

We also analyzed common biophysical features of the IB component proteins that could correlate to the protein sequestration. As shown in Figure 2.6 B-E, we evaluated different motifs known to modulate aggregation: polyQ length, low complexity regions (LCRs) length and number of coiled-coiled domains (CCDs) [228, 126, 74]. Insoluble fractions from R6/2 striata contained significantly more aggregation-prone proteins than WT controls, with a significant difference in CCDs and LCRs and a small trend for polyQ length (Figure 2.6 B-D). Moreover, R6/2 samples were significantly enriched for proteins with higher molecular weight (MW) (Figure 2.6 E). Due to their larger size, these proteins are less stable, thermodynamically speaking, which might explain why their folding is affected under conformational stress conditions [235].

Lastly, we estimated absolute protein abundance in IBs to quantify the degree of sequestration at the different time points and compared the amount of each protein in both proteomes, soluble and insoluble (Figure 2.7). The efficient enrichment of insoluble proteins in our approach is confirmed by the observation of the insoluble ECM proteins with the smallest soluble proportion (Figure 2.7, red dots). Endogenous Htt was also recruited into the aggregates (Figure 2.7, pink dots). Lastly, in agreement with the increase in aggregate size, we observed higher sequestration of protein mass over time, suggesting progressive depletion of the pool of functional proteins. In 8-week-old animals, 80% of

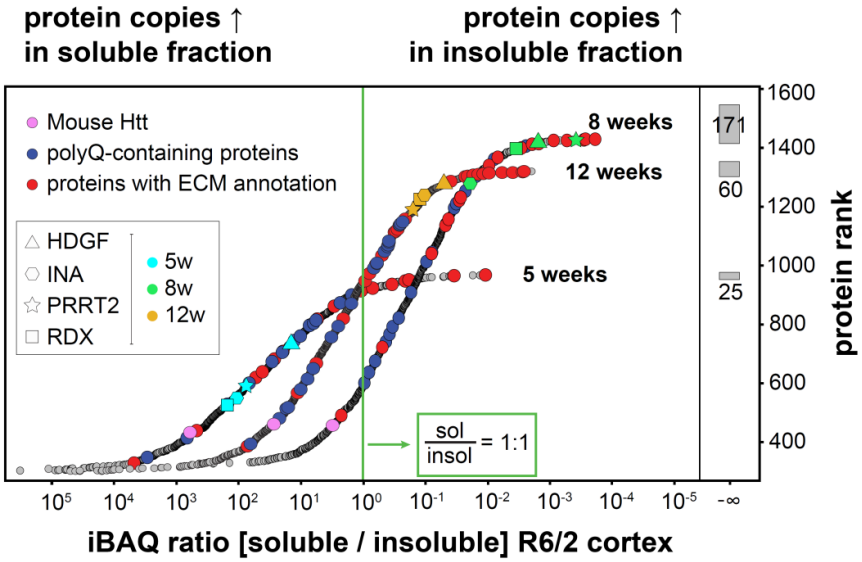

Figure 2.7 – **Protein sequestration degree in IBs.** Ranking of proteins by iBAQ ratios representing protein sequestration from the soluble to the insoluble proteome in R6/2 cortices. Gray boxes show the number of proteins that were only identified in the insoluble proteome per age group, indicated by infinite iBAQ ratios. Proteins investigated in more depth in further experiments are indicated on the curves.

proteins were at least in a 1:1 ratio in the cortical IBs compared to the soluble pool.

2.3 Validation of protein candidates

2.3.1 Protein candidates selection and validation

From all the proteomic analysis, we were able to identify ∼300 proteins depleted from the soluble proteome pool and at the same time enriched in the insoluble IBs. For our initial selection of follow-up candidates outlined in Figure 2.8 A we applied the following main selection factors: we focused on the protein candidates which were depleted from the soluble fraction, enriched in the striatal R6/2 insoluble fraction compared to the control, and at the same time their levels were significantly changed according to the three-way ANOVA statistical analysis of age, genotype and brain region differences [107]. Filtering through several other criteria (regulation statistically affected, literature evaluation and available molecular tools), we selected a group of 19 candidates (Figure 2.8, Table 2.1) for functional follow-up.

To validate the changes revealed by the proteomic analyses, we performed Western blots (WB) for several candidates (HSP90, KIF3B and hnRNPA2/B1), and confirmed their reduction in the soluble fraction at 8 and 12 weeks, which was in all cases significant for the ST brain region (Figure 2.9 A-C).

One of the validated proteins was the amytrophic lateral sclerosis (ALS)-associated protein hnRNPA2B1. ALS-linked hnRNPA2B1 mutations lead to an accumulation of insoluble protein in the nucleus [158]. Through immunostaining, we demostrated that

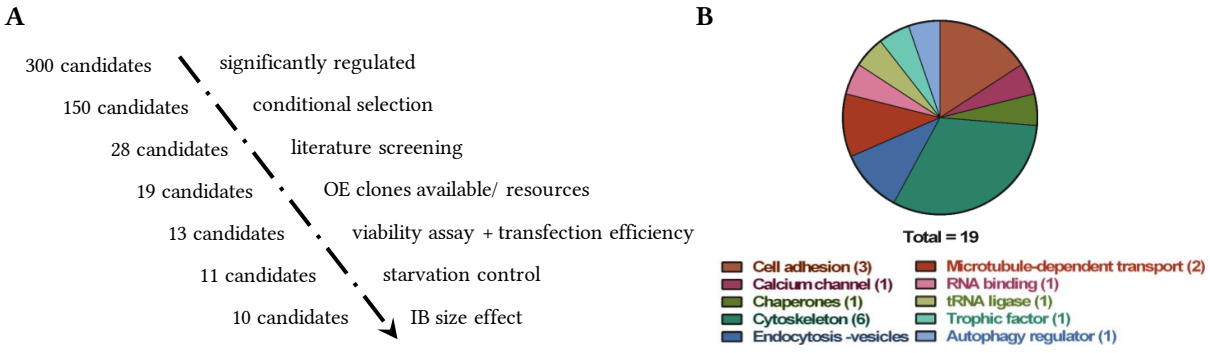

Figure 2.8 – Candidates selection. (A) Schematic summary of the validation steps in the protein candidates follow-up. (B) Distribution of the protein candidates into functional groups, comprising a wide variety of functions.

Table 2.1 – Information of protein candidates.

Gene Names	Protein Name	Function	Localization	Known link to Huntington's disease	Other
AARS	Alanine-tRNA ligase, cytoplasmic	Catalyzes the attachment of alanine to tRNA (alanine)	Cytoplasm	None	Mutations in Aars invovled in Charcot-Marie-Tooth disease
AP2A2	AP-2 complex subunit alpha-2	Component of the adaptor protein complex 2 (AP-2) involved in protein transport via transport vesicles in different membrane traffic pathways.	Membrane	Found as Htt interaction partner	-
CACNB3	Voltage-dependent L-type calcium channel subunit beta-3	Mediates calcium entry to excitable cells	Membrane	None	Deranged calcium signaling in SCA1, SCA2, HD
CHMP3	Charged multivesicular body protein 3	Core component of endosomal sorting machinery, invovled in vesicular trafficking	cytoplasm, endosome	None	-
CNP	2,3-cyclic-nucleotide 3-phosphodiesterase	May participate in RNA metabolism in the myelinating cell	Membrane	None	-
DCTN1	Dynactin subunit 1	Plays a key role in dynein-mediated retrograde transport of vesicles and organelles along microtubules by recruiting and tethering dynein to microtubules	Cytoplasm, nuclear envelope	None	
DNM1	Dynamin-1	Microtubele-associated, involved in vesicular trafficking & endocytosis, GTP-hydrolyzing potential	Cytoplasm, cytoskeleton	None	mHtt binds Drp1 (Dnm1-related protein) and increases it's enzymatic activity
DPYSL2	Dihydropyrimidinase-related protein 2	Plays a role in neuronal development and polarity, as well as in axon growth and guidance, neuronal growth cone collapse and cell migration	Cytoplasm, membrane	Reduced Dpysl2 phosphorylation in HD cortex	Crmp1 acts as chaperone on HTT, reduced expression in HD patients
HDGF	Hepatoma derived growth factor	Trophic factor harbored in the nucleus	Nucleus	None	Involved in some malignant diseases
HNRNPA2B1	Heterogeneous nuclear ribonucleoproteins A2/B1	Associates with nascent pre-mRNAs, packaging them into hnRNP particles	Nucleus, cytoplasmic granules	None	Mutations cause multisystem proteinopathy and ALS
HSP90AA1	Heat shock protein HSP 90-alpha	Molecular chaperone that promotes the maturation, structural maintenance and proper regulation of specific target proteins involved for instance in cell cycle control and signal transduction	Cytoplasm, cell membrane	Reduced expression in HD patients	-
INA	Alpha-internexin	Class-IV neuronal intermediate filament that is able to self-assemble	Extracellular space, cytoskeleton, nucleoplasm, cytoplasmic granules	None	Implicated in ALS, PD and other neuropathies
KIF3B	Kinesin-like protein KIF3B	Involved in tethering the chromosomes to the spindle pole and in chromosome movement	Nucleus, Golgi apparatus	None	-
MAPT	Microtubule-associated protein tau	Promotes microtubule assembly and stability, and might be involved in the establishment and maintenance of neuronal polarity	Cytoplasm	Tau pathologies observed in HD patients	Tau hyperphosphorylation involved in AD nad PD pathologies
NCAM1	Neural cell adhesion molecule 1	Cell adhesion molecule involved in neuron-neuron adhesion, neurite fasciculation, outgrowth of neurites,	Cell membrane	Polysialyted Ncam1 strongly reduced in hippocampus and cortex of HD mice	-
NFASC	Neurofascin	Cell adhesion, ankyrin-binding protein which may be involved in neurite extension, axonal guidance, synaptogenesis, myelination and neuron-glial cell interactions	Cell membrane	Upregulated expression in R6/2 mice	-
PRRT2	Proline rich transmembrane protein 2	Multi-pass membrance protein; component of the outer core of AMPAR complex	Cell membrane	None	
RAC1	Ras-related C3 botulinum toxin substrate 1	Plasma membrane-associated small GTPase which cycles between active GTP-bound and inactive GDP-bound states	Cytoplasm, cell membrane	HTT toxicity modifier	-
RDX	Radixin	Binds the ends of actin filaments to the plasma membrane, concentrated at adherens junctions	Cell membrane	None	Might be involved in axonal regeneration
SBF1	Myotubularin-related protein 5 (Mtrm5)	Probable pseudophosphatase, GEF activity, can bind phosphorylated substrates	Nucleus	None	Mtmr8 and Mtrm9 involved in autophagy
SRGAP3	SLIT-ROBO Rho GTPase-activating protein 3	GTPase-activating protein for RAC1 and perhaps CDC42, but not for RhoA small GTPase	Cytoplasm	None	-

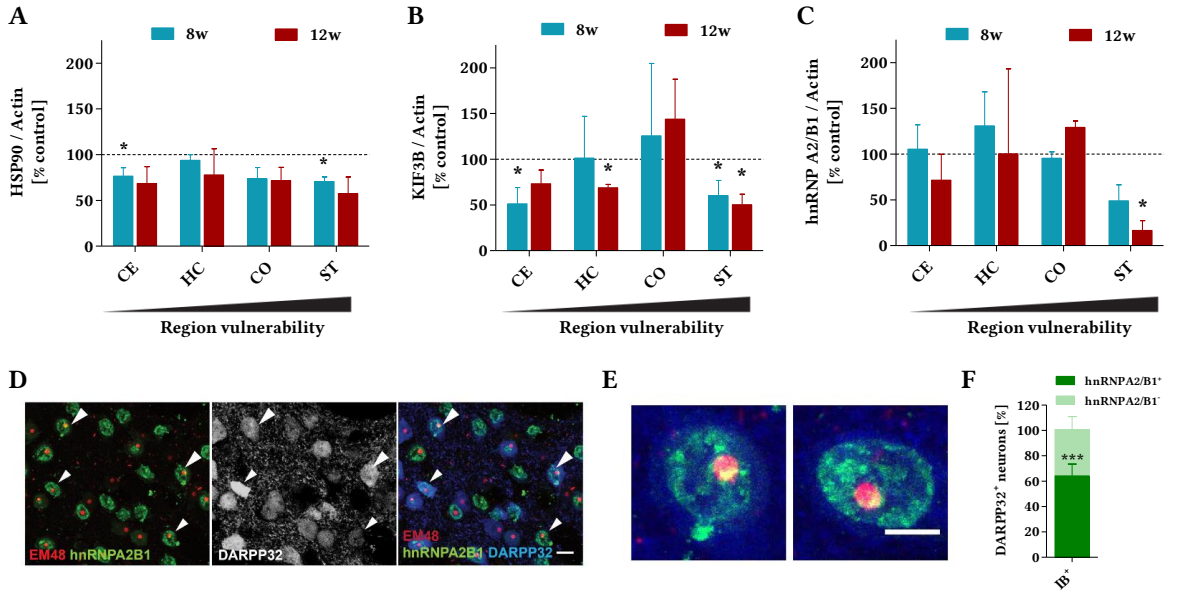

Figure 2.9 – Validation of candidates from the proteomic screen: HSP90, KIF3B and hnRNPA2B1. (A-C) Quantification of candidates in immunoblots of brain regions from 8 and 12 week old R6/2 mice, normalized to WT controls (dotted line); Student's t-test, *p<0.05; n=3-4. Values are mean± SD. (D) Representative single-plane images of 12-week-old R6/2 striatum with nuclear hnRNPA2B1 accumulations; EM48 staining for HTT IBs, red; hnRNPA2B1, green; DARPP-32 staining for MSNs, blue; arrowheads, DARPP32$^+$ neurons containing IBs and showing a nuclear accumulation of hnRNPA2/B1; scale bar is 10 µm. (E) Examples of two DARPP32$^+$ neurons showing colocalization (yellow) of hnRNPA2B1 with the IB; scale bar is 5 µm. (F) Quantification of nuclear accumulation of hnRNPA2/B1 in DARPP32$^+$ neurons with IBs, in the striatum of 12-week-old R6/2 mice; Student's t-test, *** p<0.001; Values are mean± SD; n=3 mice; 7 image fields each.

in R6/2 ST there is a nuclear accumulation of hnRNPA2B1 in most MSNs, as well as its co-localization with HttEx1 IBs (Figure 2.9 D-F). In all neurons with hnRNPA2B1 accumulation, which represent 62% of all DARPP32 $^+$ cells (Figure 2.9 F), some degree of colocalization was always observed between the IB and hnRNPA2B1, as shown in Figure 2.9 E, confirming its sequestration and therefore the enrichment in the insoluble proteome fraction.

2.3.2 Overexpression of loss-of-function candidates in a HD cell model

For the follow-up of the selected protein we initially tested the Neuro2a (N2a) *in vitro* cell model. N2a stable cell lines express C-terminally eGFP-tagged HttEx1 upon induction with ponasterone in three different polyQ lengths, Q18, Q64, and Q180 [262], Figure 2.10 A. Unfortunately, these cell lines repeatedly showed cell death resistance upon expression of the pathogenic polyQ lengths with no significant reduction either after 3 days (Figure 2.10 B) or 4 days (Figure 2.10 C) expressing time.

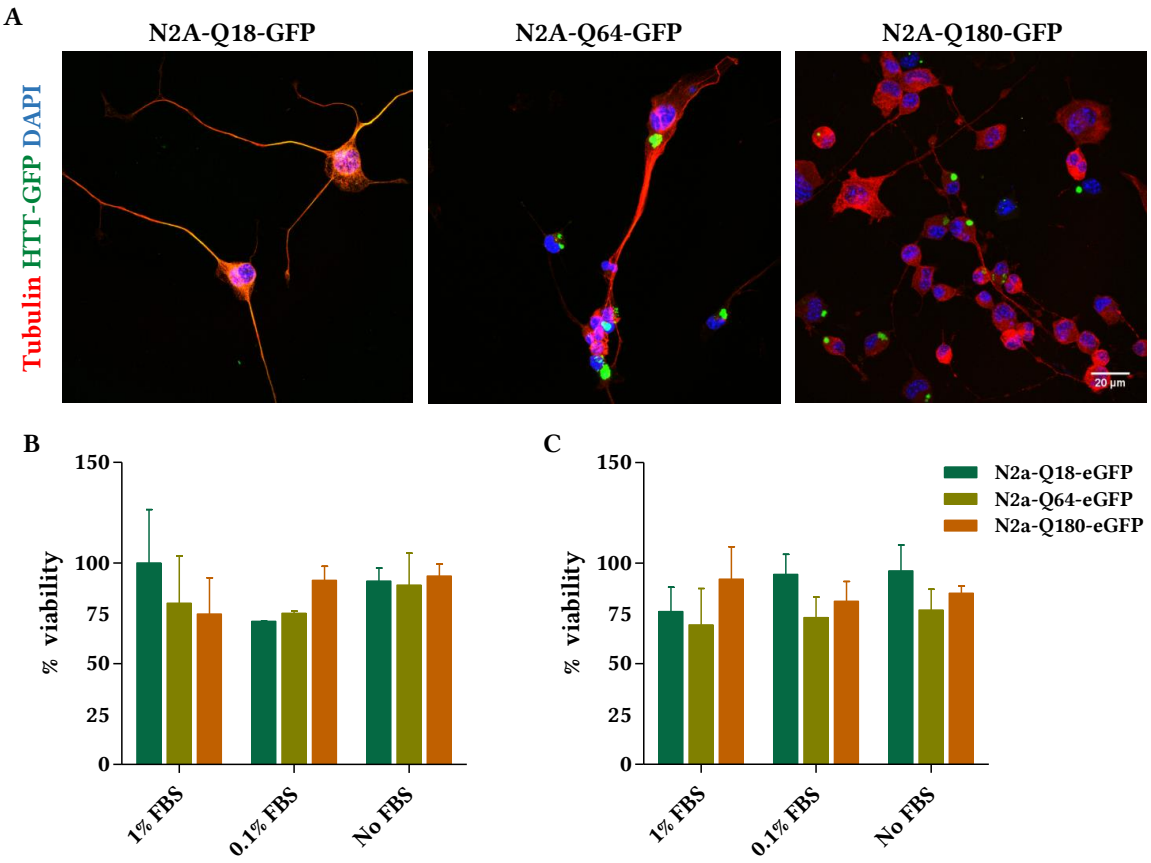

Figure 2.10 – **N2a *in vitro* cell line is not suitable.** (A) Representative images of N2a-Q18, Q64 and Q180-GFP. Blue, DAPI; green, HttEx1-GFP; red, tubulin; scale bar, 20 µm. (B) Induction of HttEx1 does not cause cell death, as measure by MTT assay after 3 days expressing the different polyQ lenghts. (C) Same assessment as in (A) but after 4 days expressing the polyQ lengths.

We then decided to move on to a different *in vitro* model and used inducible neuron-like PC12 cells with stably integrated GFP-tagged HttEx1 with either 23 or 74 glutamines (HD-Q23 and HD-Q74 cells) [272]. Upon induction with doxycycline to express HttEx1, significant reduction in cell viability is observed for HD-Q74, but not HD-Q23 cells (Figure 2.11 A-C). We first checked through quantitative proteomics that all candidates were expressed in this cell line. Indeed, all of them were endogenously expressed with medium to high abundance (Figure 2.11 D). The soluble proportion of most cellular proteins increased significantly after overexpression of the candidates in HD-Q74 cells, as well as, in most cases, the soluble proportion of the candidate itself [107], meaning that the overexpressed protein is either blocking the IB sequestration of other proteins or the candidate is indeed acting specifically. Moreover, transfection of a candidate increased its protein levels compared to non-transfected controls [107].

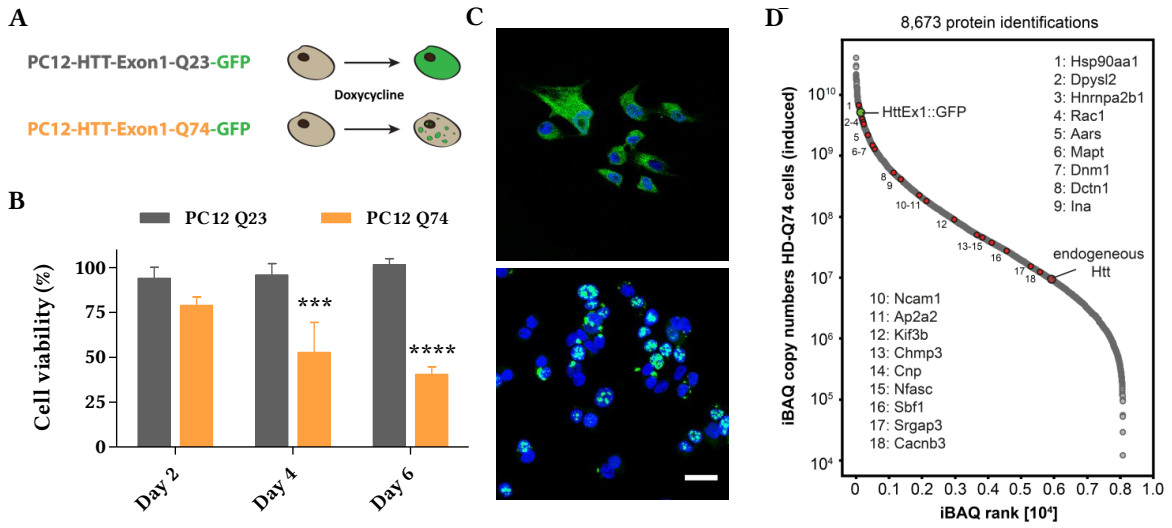

Figure 2.11 – Assessment of the *in vitro* model PC12-HTT-Exon1. (A) Scheme of the PC12-HTT-Exon1 induction in the HD-Q23 and HD-Q74 cell lines. (B) Induction of HttEx1 expression in PC12 cells leads to polyQ length-dependent cell death, as measure by MTT assay; multiple t-test (two-tailed) with Benjamini-Hochberg correction; *FDR<0.05, ***FDR<0.001; n=3. (C) Representative images of HD-Q23 (top) and HD-Q74 (bottom) cell lines 60 hours after induction. Blue, DAPI; green, HttEx1-GFP; scale bar, 20 µm. (D) Ranking of HD-Q74 proteins by iBAQ copy numbers, selected candidates are indicated in red.

Under the hypothesis that the selected protein candidates are in a context of loss of function in the R6/2 brains, we overexpressed them in the *in vitro* system to evaluate their effect on mHTT-induced toxicity. As shown in Figure 2.12 A (orange, lower panel), overexpression of individual candidates significantly improved the viability of HD-Q74 cells in 12 of 18 cases, with a mean survival increase of 40%. For further analysis, we excluded proteins that increased viability in the control HD-Q23 as well (Figure 2.12 A (grey, upper panel), AP2A2, NFASC and MAPT, as well as two other proteins that repeatedly showed low transfection rates (DCTN1 and SBF1).

The influence of the overexpression on the viability, however, could be independent of mHtt-Ex1 and due to a general effect on cell survival. Therefore, to rule out this possibility, we tested whether the candidates rescued the viability of non-induced HD-Q74 cells under starvation conditions. We observed a significant rescue with CNP (Figure 2.12 B), which was subsequently removed from the follow-up, along with DNM1 (FDR = 0.07). Thus, we proved that for all the remaining candidates, there is a specific involvement in mutant HttEx1 toxicity.

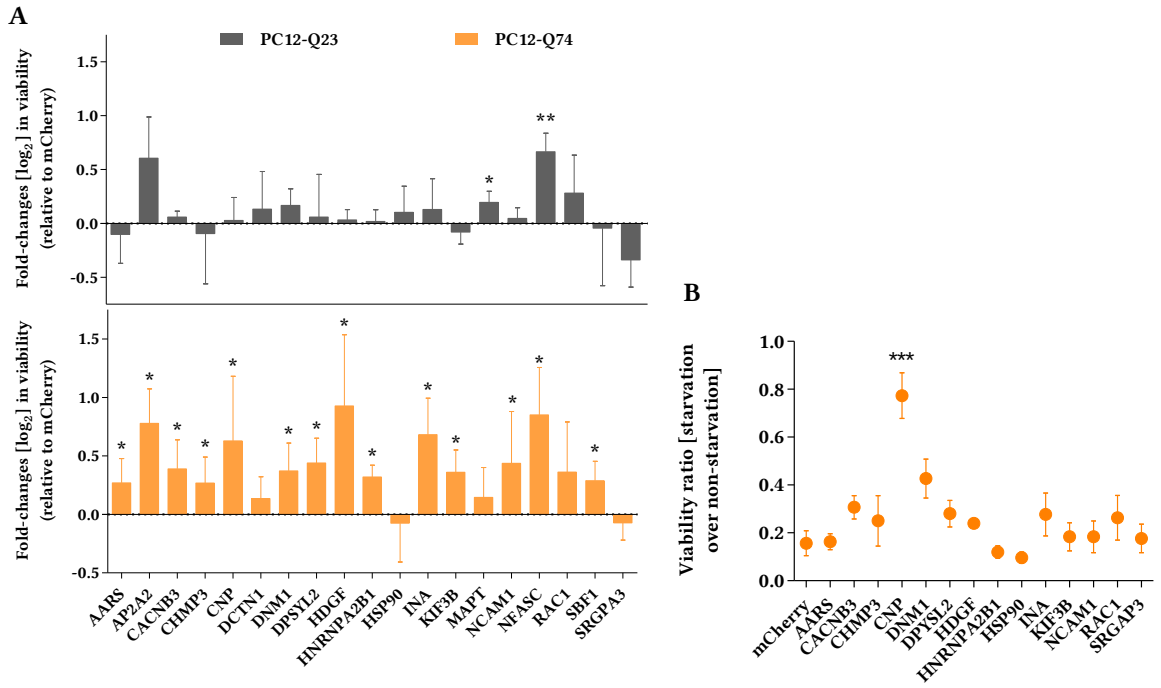

Figure 2.12 – Overexpression of loss-of-function candidates reduces HttEx1 toxicity. (A) Log_2 fold changes (log_2FCs) in viability of HD-Q23 (upper panel) or HD-Q74 (lower panel) cells transfected with the candidates as measured by LDH assay; multiple one-tailed t-test with Benjamini-Hochberg correction; *FDR<0.05, **FDR<0.01; normalized to mCherry controls; n = 4. (B) Candidates' effects on the viability of starved, non-induced HD-Q74 cells; multiple two-tailed t test with Benjamini-Hochberg correction; *FDR<0.05; n = 3.

2.3.3 Characterization of the candidates' rescue effect

To deeper characterize the effect of the candidates' overexpression, we asked whether there was an influence on aggregation as well. Overexpression of the candidates did not have a significant effect on the number of GFP^+ foci per cell (Figure 2.13 A), but their size was significantly reduced in 10 of 11 cases (Figure 2.13 B).

In a more detailed analysis of this size reduction, we could show that the percentage of small foci (<1 µm in diameter) increased significantly in 8 of the 11 cases, whereas the percentage of large foci (>2.5 µm) was significantly reduced in all cases (Figure 2.13 C and D). These findings indicate that overexpression of the proteins sequestered to HttEx1 IBs ameliorates mutant HttEx1 toxicity and decreases aggregate size, but not load.

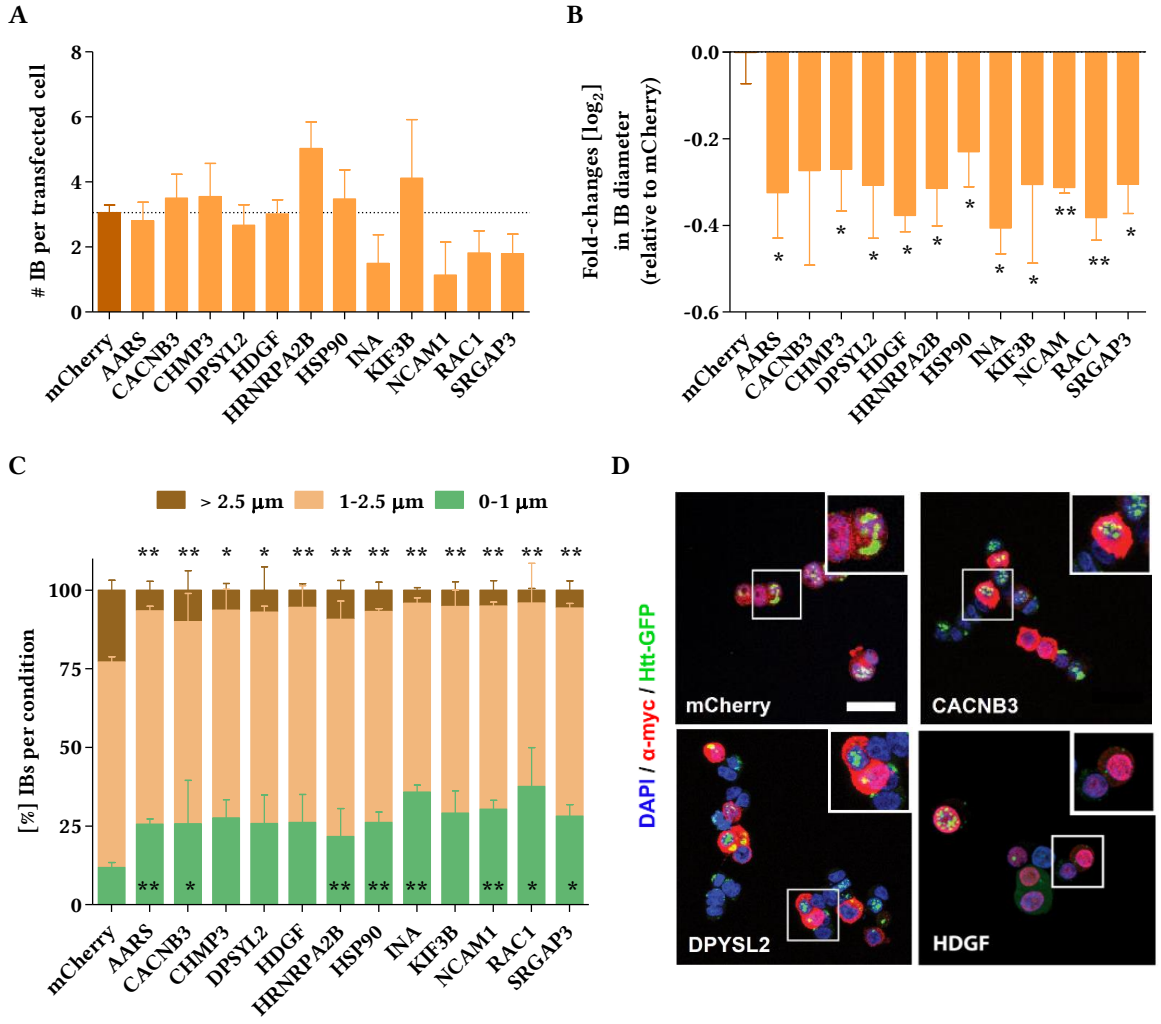

Figure 2.13 – **Characterization of candidates overexpression effect in IBs.** (A) Number of IBs per cell in HD-Q74 cells transfected with the candidates; multiple two-tailed t-test with Benjamini-Hochberg correction; *FDR < 0.05; n=3. (B) Log_2FCs in IB diameter in HD-Q74 cells transfected with the candidates. Multiple two-tailed t test with Benjamini-Hochberg correction; *FDR < 0.05, **FDR < 0.01; normalized to mCherry; n = 3. (C) Distribution of IB diameter bins in HD-Q74 cells transfected with the candidates. Green, <1 µm; orange, 1 - 2.5 µm; brown, >2.5 µm. Multiple two-tailed t test with Benjamini-Hochberg correction; *FDR < 0.05, **FDR < 0.01; n = 3. (D) Representative images of HD-Q74 cells transfected with the indicated candidates or mCherry as control. Blue, DAPI; red, myc candidate; green, HttEx1-GFP; scale bar, 20 µm.

2.4 Follow-up of mHTT-toxicity modifying candidates in primary neurons and *in vivo*

2.4.1 Evaluation of HDGF effect in primary neurons through transfection

One of the protein candidates, HDGF, had a remarkable effect on the PC12-Q74 survival when overexpressed (Table 2.1, Figure 2.12). We then decided to further analyze its toxicity-modifying potential by overexpressing it in primary cortical neurons. Trans-

fection of polyQ-expanded HTT-Q97-mCherry, but not control HTT-Q25-mCherry or mCherry, causes a significant reduction in neuronal survival (Figure 2.14). Remarkably, co-transfection of HDGF significantly rescues neuronal viability, compared to the control condition with GFP.

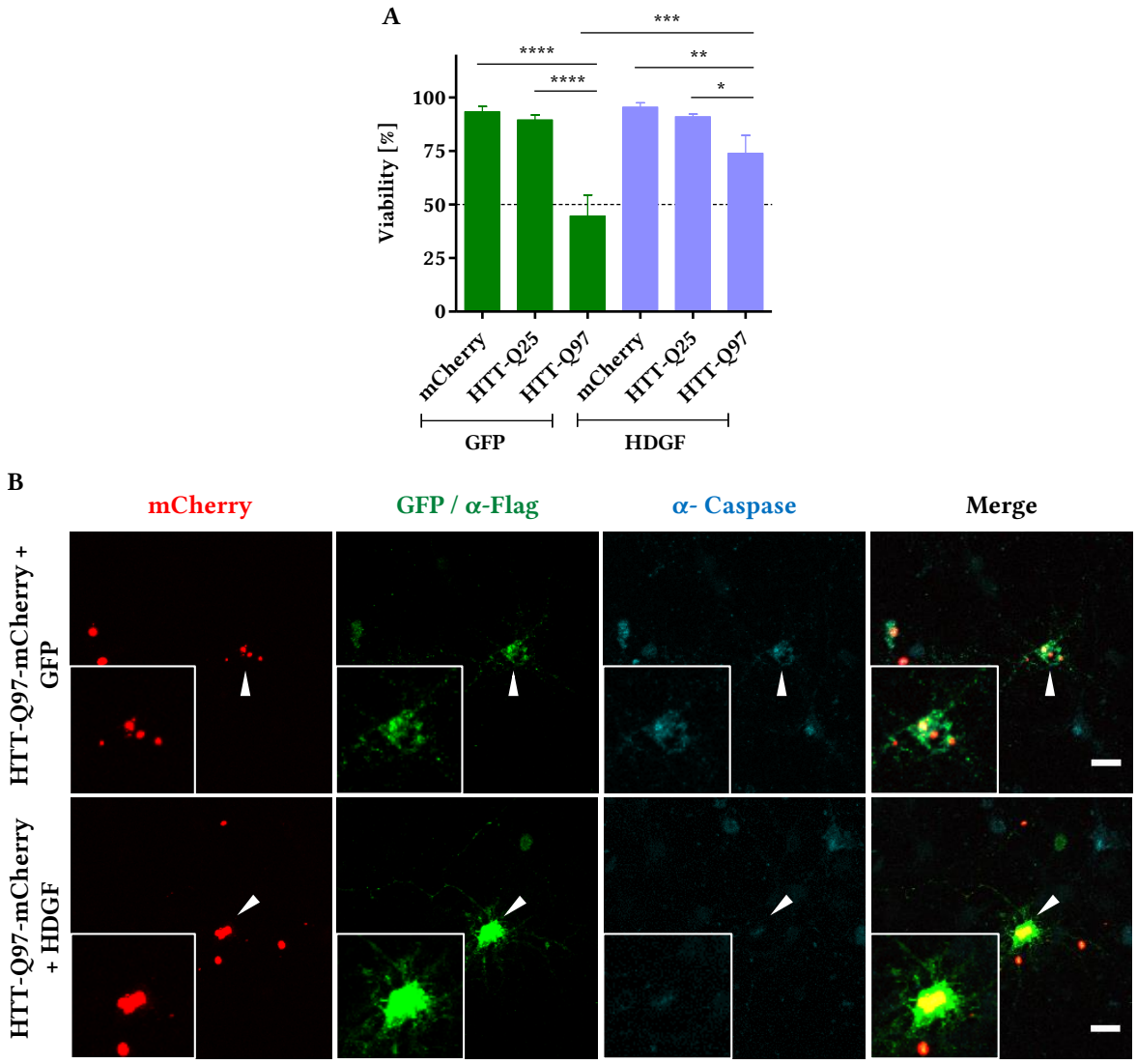

Figure 2.14 – Viability assessment upon HDGF overexpression in cortical neurons. (A) Quantification of caspase-3 positive neurons to assess viability at DIV 7+2.; two-way ANOVA, *<0.05, **< 0.01, ***< 0.001, ****<0.0001; values are mean± SD; n=4 experiments; 30-70 neurons counted per condition/ experiment. (B) Representative maximum projections of neurons overexpressing HTT-Q97 and GFP (upper panels) or HDGF (lower panels). Arrow heads point to cells shown at a higher magnification in the insets. Red, HTT-Q97-mCherry; green, GFP or Flag tag; cyan, caspase-3; scale bar, 20 µm.

2.4.2 Evaluation of candidates' effect in primary neurons through transduction

In addition to HDGF, we selected several other protein candidates for a more detailed follow-up based on their effect in the PC12 survival experiments (INA, Table 2.1, Figure 2.12) or their significant down-regulation in the proteomic analysis (RDX, PRRT2, Table 2.1) [107]. The degree of enrichment of these four candidates in the insoluble fraction for the 12-week-old whole brain is displayed in Figure 2.6, as well as their degree of sequestration over disease progression in Figure 2.7.

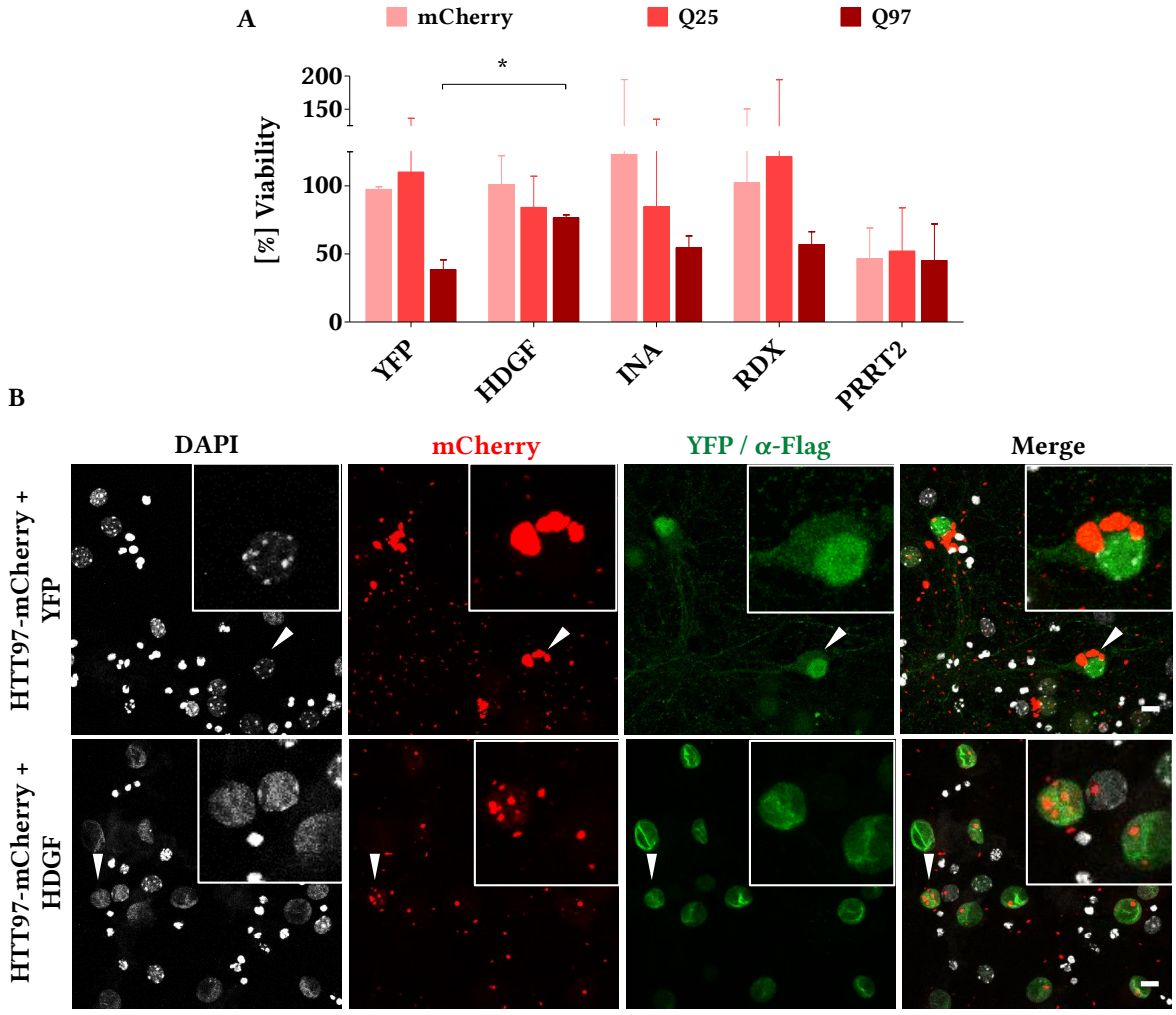

Figure 2.15 – Viability assay upon viral transduction of protein candidates. (A) Quantification of neuronal survival upon the lentiviral co-transduction of the selected candidates along with mCherry, HTT-Q25 or HTT-Q97 at DIV 7+20. Results are normalized to the control condition transduced with mCherry + YFP and measured by MTT; two-tailed multiple t-test with Holm-Sidak correction; *<0.05; values are mean± SD; n=4, DIV 7+20. (B) Representative maximum projections of DIV 7+12 neurons transduced with HTT-Q97 and YFP (upper pannels) or HDGF (lower pannels). Arrowheads point to cells shown in the insets. White, DAPI; red, HTT-Q97-mCherry; green, YFP or Flag tag; scale bar, 20 µm;

In total, four candidates and YFP as control were co-overexpressed in cortical neurons through lentiviral constructs, along with mCherry, HTT-Q25-mCherry or HTT-Q97-mCherry. We confirmed HDGF rescue in this experimental approach as well, compared to the control condition YFP + HTT-Q97-mCherry (Figure 2.15 A). There was no significant effect for the rest of protein candidates and one of them, PRRT2, itself caused neuronal toxicity (Figure 2.15 A). This lentiviral transduction allows a more detailed characterization compared to a transient transfection. This is represented in the observation of a possible effect on the IB size, amount and localization (Figure 2.15 B), as it seems that the overexpression of HDGF in presence of HTT-Q97-mCherry leads to a general nuclear localization of the IBs, compared to their predominantly cytoplasmic localization in the YFP control. Moreover, it might affect the IB size compared to the YFP condition. Another intriguing observation is reflected in the decompression of heterocromatin shown by the DAPI staining in the neurons overexpressing HDGF. These exciting preliminary findings require further quantification and more detailed analysis.

2.4.3 Characterization of HDGF effects *in vivo*

After suggesting that HDGF has a strong effect on the survival of both PC12-Q74 cell line (Figure 2.12) and primary neurons (both trough transient transfection, Figure 2.14, and lentiviral transduction, Figure 2.15), we speculated that it might have an effect *in vivo* as well. To test our hypothesis, we performed intrastriatal injections of AAV8 constructs, bearing either HDGF or YFP, in R6/2 mice and their WT littermates at 4 weeks of age (Figure 2.16 A. Figure 2.16 B demonstrates the successful overexpression of both vectors in the striatum after 3 weeks of expression.

We evaluated the experimental groups at 12 weeks of age in different behavior assays to check whether the overexpression of HDGF in the striatum has an effect at an advanced stage of HD. Behavioral evaluation consisted of an assessment of the motor performance by rotarod, angled horizontal ladder, open field and additionally, clasping phenotype (Figure 2.16). There was no improvement in the rotarod performance; R6/2 mice injected with AAV8-HDGF had a similar latency to fall as R6/2 mice injected with YFP (Figure 2.16 C). Due to the limited suitability of the rotarod to detect minor defects or improvements in coordination, we also evaluated the performance in an angled horizontal ladder, measuring both hindlimbs and forelimbs and quantifying the mistakes in three different categories (hesitation, slip and miss, see Material and Methods). We found no significant difference in any of the experimental groups for the ladder assessment

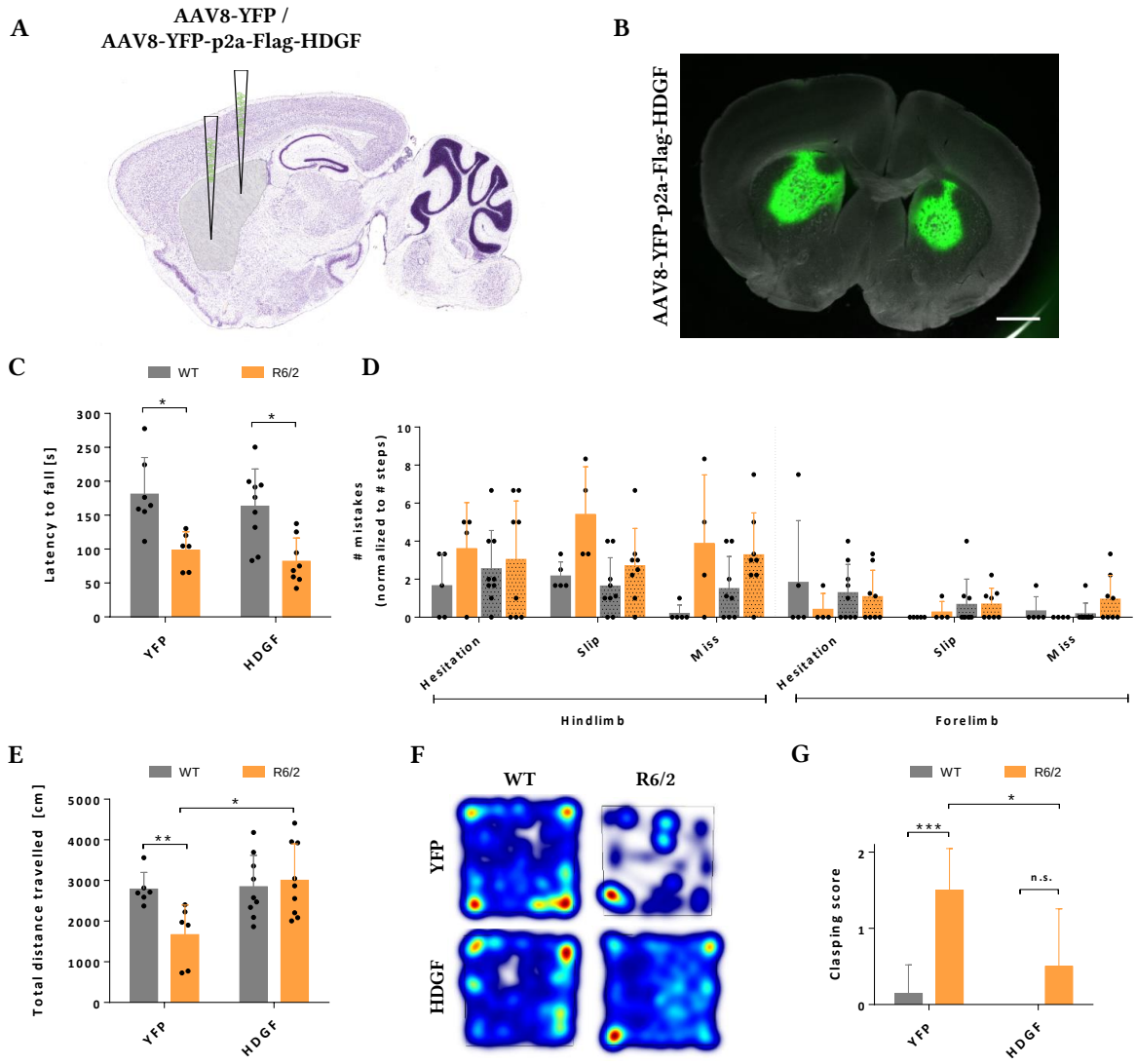

Figure 2.16 – Behavioral assessment of AAV-injected mice. (A) Sagittal mouse brain section stained with Nissl to schematically represent the injection sites of either AAV8-YFP or AAV8-YFP-p2a-Flag-HDGF. Grey area represents the striatum. An identical pair of injections were performed in the contralateral hemisphere. (B) Representative picture of the AAV8-YFP-p2a-Flag-HDGF expression after 3 weeks from the injection date, to check the proper functioning of the viral constructs; scale bar, 1 mm. (C) Rotarod. (D) Angled horizontal ladder. (E) Open field. (F) Representative heatmaps of open field. (G) Clasping score ; two-tailed multiple t-test with Holm-Sidak correction (in A, C and E) or two-way ANOVA (in B); *<0.05, **< 0.01, ***< 0.001; values are mean± SD; n= 6-9 mice per group.

(Figure 2.16 D). Interestingly, the total distance traveled in the open field was rescued in HDGF-injected R6/2 mice up to WT levels (Figure 2.16 E and F). Moreover, we observed a rescue of the clasping phenotype (Figure 2.16 G).

After being behaviorally tested, all animals were sacrificed and their brains were processed to histologically assess HDGF overexpression. Upon a close look, one can notice a

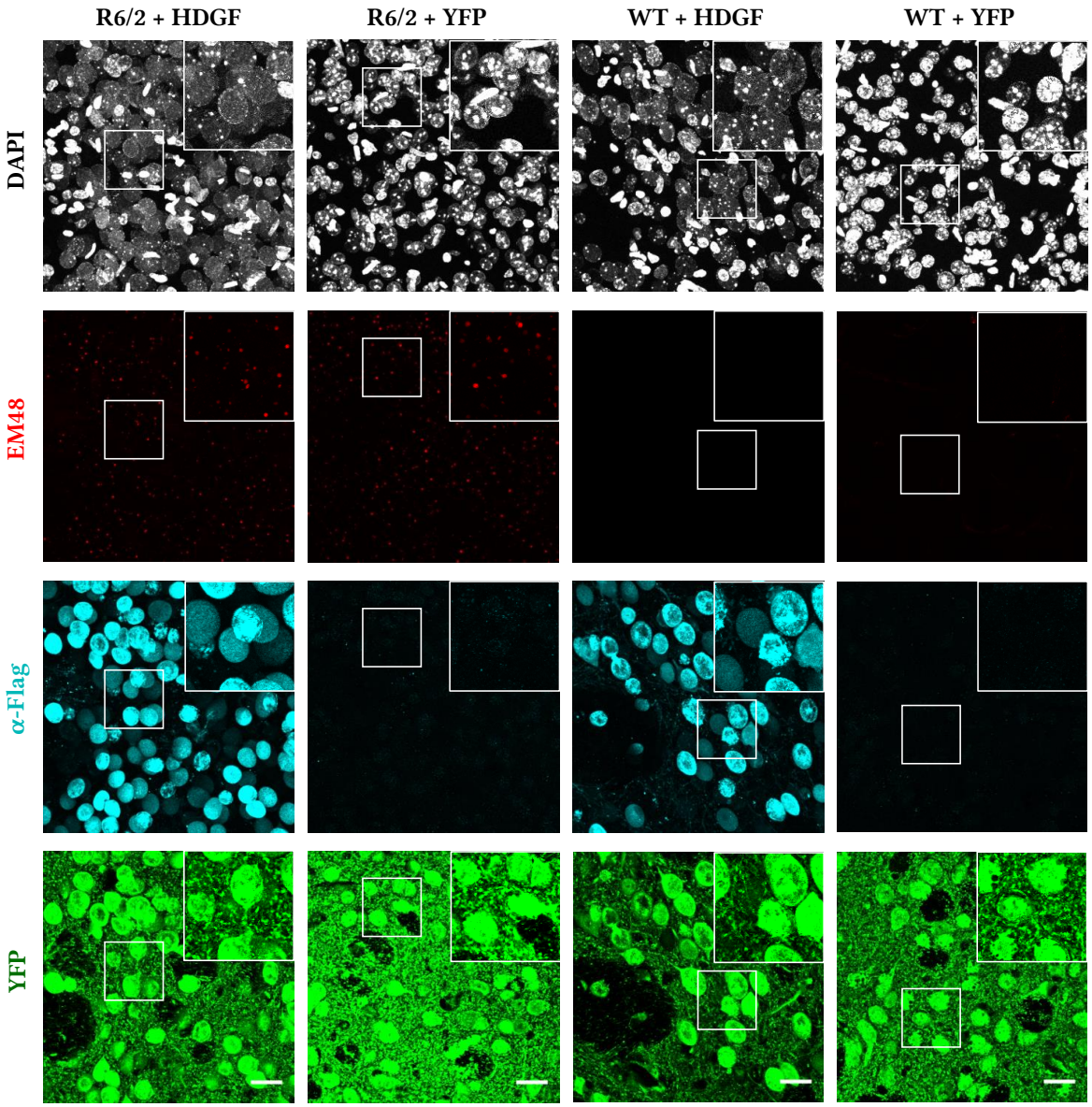

Figure 2.17 – Intrastriatal injections in R6/2 and WT mice. Representative maximum projections of AAV8 overexpression of YFP or HDGF in 12 week old R6/2 and WT littermates. White, DAPI; red, mHTT ; cyan, flag tag; green, YFP; scale bar, 15 µm.

difference in the DAPI staining (Figure 2.17). While neurons overexpressing YFP display a normal DAPI staining, the neurons overexpressing HDGF exhibit an intriguing decompression of constitutive heterocromatin foci, which could be related to a transcriptional event. These results suggest that the overexpression of HDGF in the striatum has a beneficial effect on some HD features in the R6/2 model.

CHAPTER 3

DISCUSSION

3.1 A spatiotemporal proteomic profiling in HD

We characterized the brain proteome of R6/2 and WT mice applying quantitative proteomics. This spatiotemporal approach granted the investigation of molecular neurodegenerative signatures in the HD model with a novel depth of more than 12,000 proteins. Other studies have addressed HD through a proteomic approach [148, 278, 40], where they also focused in the striatum and cortex, two primary regions of HD dysfunction, with different success in the numbers of identified proteins, as well as the achieved depth in the results. The more recent work of Langfelder *et al.* expanded the approach strategy to more brain regions and different tissues, as well as different time points in a KI HD mouse model [139]. To date, however, proteomic approximations exploring HD pathogenesis centered either on expression level changes or on soluble HTT interactions. Our approach, similarly to Langfelder *et al.*, included other relevant regions for the evaluation of HD pathogenesis, apart from cortex and striatum. However, we focused into broadening the knowledge of the interplay between soluble and insoluble aspects of the proteome, a limited aspect of study [15], specifically when following disease progression over time and in differentially affected brain regions.

The characterization of the soluble proteome during disease progression exposed extensive alterations in brain regions that are vulnerable to HD. At an early stage of the disease, 5 weeks old, the expression profile of R6/2 mice appears almost identical to WT. Nevertheless, it is worth noticing how some protein clusters already show differential expression. The remodeling appears to be most extensive at 8 weeks of age in the mice expressing mHTT, the time point when this HD model enters in the onset of the disease,

with crucial down-regulation and up-regulation of protein clusters compared to an early stage of the disease. One hypothesis is that there is a massive stress condition on the cells due to the aberrant mHTT expression and this leads to an up-regulation of chaperones and proteasome components implicated in dealing with this misfolded protein, as shown by the up-regulation of clusters 2 and 3. In parallel, down-regulation of clusters 1 and 4, related to ribosome and energy metabolism, highly affects the proteome remodeling. One of the causes could be related to protein sequestration induced by mHTT and the dysfunction of linked biochemical processes. In fact, defects in energy metabolism have been observed in pre-symptomatic and symptomatic HD subjects, leading to evident oxidative damage by, for example, impairing the SOD activity and decreasing the ascorbic acid flux, a known antioxidant in the brain [4].

The fact that our PCA analysis groups the samples in such clear distribution not only highlights the previous point regarding the early-stage versus advanced-stage, but also the difference between cerebellar samples and all remaining brain regions. This divergence might be due to the different embryonic origin of the cerebellum, which may play a role in the vulnerability of the different cells when dealing with mHTT.

It is interesting to mention the apparent discrepancy in both, the gradual alteration of the soluble proteome over time and the degree of protein sequestration. In both cases, the 8 week-old time point shows a stronger differentiation compared to the 12 week-old time point. One might expect that the further in the disease development, the stronger the alteration and the sequestration. There are two possible answers for this result, that are not mutually exclusive. First, it can be that the general aging context at 12 week old alters the already affected cellular environment. Second, from the 12 week-old animals, two of them came directly from the Jackson Laboratory, as described in the subsection 5.1.7, whereas the rest of animals were obtained from the established in-house colony. As mentioned previously, the gradual expansion of CAG repeats that inevitably occurs during breeding of these mice might have led to an amelioration of the HD phenotypes, including differences at a molecular level.

Our MS-based approach allowed us characterize in detail HttEx1 aggregates from the different disease stages and the different brain regions. The data show that, at late stage of the disease, mature aggregates are composed of several hundred of proteins, in line with the increased size of IBs in the progression of HD in both, animal models and patients. Interestingly, only a few proteins which are specifically expressed in the brain form the bulk of the IB. This implies that the IB composition in HD is highly tissue specific, which

would be important when considering mechanisms of toxicity. As the presence of myelin components in such proportion in the insoluble fraction was surprising, one possibility could be that some myelin from oligodendrocytes was being isolated through our protocol. We could confirm its direct sequestration in the neurons by immunostaining, demonstrating that Plp1 (and probably other myelin proteins detected in the insoluble fraction) is a true component of neuronal IBs and not a contaminant from oligodendrocytes. This is in agreement with previous studies that also described the presence of myelin in neurons [235, 258].

Regarding the molecular composition of the IBs, we identified a significant fraction of constituent proteins bearing some common characteristics in their aminoacid sequence. Specifically, these proteins were rich in aggregation-prone sequence motifs, such as CCDs or LCRs, which are known to facilitate co-aggregation with other proteins. CCDs are implicated in protein interactions and appear to interact with polyQ proteins, promoting their pathogenic features [74]. On the other hand, LCRs act as molecular determinants of RNA granule assembly [126] and therefore, are highly enriched in RNA-binding proteins. It is no surprise then, that these proteins have a prominent presence in the IB composition since these domains exacerbate aggregation in an unbalanced protein interaction situation, potentially giving place to some pathologies [50]. In a HD context, it was recently published that LCR domains co-aggregate with mHTT and other LCR-containing proteins in a HD *in vitro* model, increasing the formation of aggregates [130].

An interesting question that could be analyzed in further studies would be whether these protein domains are also detected in insoluble aggregates found in other NDDs. However, the only available studies to compare have taken place in *post mortem* human tissue [98, 140]; taking into account that the frequency enrichment analysis of mouse versus human motifs is problematic, it leads to a limited statistical power. Additionally, it is hard to compare human data obtained from patients with a progression of years into the disease to our study in the R6/2 model, which develops aggregates in a time window of several weeks.

One critical advantage of the present study is the integration of the soluble and insoluble proteome analysis with a defined spatiotemporal resolution. This allowed to draw molecular neurodegeneration signatures that have not yet been linked to HD pathogenesis. The R6/2 model is one of the best characterized and most widely used within HD research, as reviewed in 1.4.2. Comparative studies have shown its similarity to full-length models at different levels. However, it would be important to compare our spatiotemporal analysis with other full-lenght HD models. As of today, there are only proteomic studies

of full-length HD mice that either focus on protein interactors of the HTT protein [237] or studies with limited sensitivity and resolution, usually reporting only a few tens of significantly regulated proteins [265, 139].

In our study, one striking observation was the prevalent sequestration of proteins exhibiting dysregulated expression levels in the soluble proteome. While up-regulation of proteins in HD mice was more common for lower abundant proteins, down-regulation was significantly more common for highly abundant proteins; for example, members of the Crmp family, where one of its members has been shown to be a HTT-toxicity suppresor [242]. Given that the majority of these proteins were depleted from the soluble protein pool and sequestered into the aggregates, it suggests widespread loss-of-protein function during HD progression. While it has been reported that IBs can be protective by sequestering the more toxic soluble oligomers [10, 96], the persistent recruitment of soluble proteins observed here argues that IBs have a deleterious impact on the cell, causing a major impairment of protein homeostasis by a widespread loss-of-function situation.

3.1.1 Considerations and outlook

The amount of data generated by the present spatiotemporal study can be overwhelming. In this regard, different criteria than the used here could have been applied for following analysis. For example, we selected candidates which were mainly depleted from the soluble fraction as well as highly represented in the striatal insoluble fraction. However, if the proteomic data would be analyzed based on other criteria, it is logical to assume that other protein candidates would have been revealed. These assumption opens numerous possibilities for studying not only the data, but the biological information that we could extract from it.

For future considerations, the proteomic approach could be further improved by additional cellular and subcellular fractionation steps. Brain regions posses great complexity and present certain cellular heterogeneity where mixed populations with different vulnerability could lead to more specific answers, if analyzed individually. One way of approaching this challenge could be the application of laser-capture microdissection along with automated methods to collect cells. This would facilitate the specific isolation and offer the possibility to investigate small defined areas or individual neurons, aiding data interpretation. Another possibility would be to use FACS sorting of genetically labeled cell types.

3.2 mHTT-toxicity modifiers revealed

Our rescue experiments suggested that re-supplying potential loss-of-function candidates improved the viability of an *in vitro* cell model in the context of HttEx1 toxicity. This effect was probably underestimated given that the overexpression assays were done in population-based conditions, with transfection rates from 20 to 40%, which means that the further selected candidates had a clear strong effect on the rescue. A possibility for future studies could be to follow up the two specific candidates that were excluded due to their viability improvement in the starvation condition (CNP and DNM1). All the protein candidates that were further analyzed did not have any beneficial effect under the stress of starvation, which points to the fact that none of those candidates affected the activation of the general survival pathways, thus being specific actors in the toxicity related to mHTT. Nevertheless, it would be interesting to investigate whether the two excluded candidates can further affect not only the aggregate load and the size of the IBs, but also whether they would improve a HD pathological context more significantly than the other selected candidates.

Surprisingly, a large number of our candidates reduced aggregate size but not overall aggregation load. It is possible that each of the selected candidates is essential for cell survival and their overexpression simply re-supplies the cell with a necessary factor. Besides, it is important to consider that a protein with a high affinity for the IBs may occupy much of the interaction surface and thereby, decrease sequestration of endogenous proteins, as implicated by the increase of the soluble proportion of most proteins upon transfection of the candidates into HD-Q74 cells. This scenario may also explain why many of the candidates reduced IB size. It must be noted, interestingly, that SRGAP3 did not improve the viability of the *in vitro* model but it did, on the other hand, reduce the IBs size. This would argue that blocking the sequestration capacity of the IBs by SRGAP3 overexpression is not sufficient for subsequently improving cell survival. The rescue effect of the other candidates is therefore likely not entirely due to shielding the IB surface and preventing other proteins from interacting with the IBs. Our data suggest that overexpression of candidate proteins could increase cell viability by interfering with multistage aggregate formation, but this is one possibility which does not exclude other simultaneous processes. The analyzed candidates are somehow able to promote overall recovery but the molecular mechanism underlying the observed increase in cell viability requires further analysis for each individual case.

An arguable limitation to the *in vitro* validation could be the failure to differentiate the PC12-HD lines to neuron-like cells. In response to NGF, PC12 cells differentiate into sympathetic-like neurons and extend long neurites, providing a useful model for the investigation of neuronal differentiation, signaling and other neurobiological events [88], such as the context of our study. The lack of differentiation in our case could be due, as one explanation out of many, to a loss or mutation in the NGF receptor, which would impair subsequent signaling cascades leading to neurite formation. To prevent proliferation, we maintained the cell lines in minimal serum conditions in the experimental setup so they remained in a quiescent-like state. Other studies have used PC12 cell lines as well without differentiating for addressing questions related to HD [242]. Nevertheless, to overcome this limitation, we addressed the capacity of some of the candidates in a more physiological system, primary cortical neurons, where we could confirm the effect on the viability in the context of mHTT toxicity.

Transient transfection allows to evaluate the effect of a protein of interest in a relatively fast and convenient way. However, it depends on the expression and transfection efficiency of such protein. From the four proteins selected from the proteomic study to follow up in primary neurons (HDGF, INA, RDX and PRRT2), only HDGF was suitable for an evaluation through transient transfection. To overcome this drawback and also to perform a deeper characterization of the candidates' effect, we developed in-house lentivirus for each of the candidate constructs. This approach conceded a longer time of expression and therefore a more detailed analysis. For example, PRRT2 expression resulted in toxicity, independently of the protein co-overexpressed. A study from 2017 [22], showed that overexpression of PRRT2 strongly impaired the cell viability and promoted cell apoptosis in glioma cells, where it is also down-regulated compared to normal brain tissue. There is a possibility that this anti-apoptotic effects take place, in a similar manner, in the cortical neuron milieu. Whether a finer tritation of the lentivirus would make a difference in the toxicity, remains unclear. In any case, because of methodological difficulties we did not pursue this candidate further.

RDX and INA did not cause a significant improvement in the neuronal viability in the presence of HTT-Q97-mCherry, whereas the beneficial effect of HDGF was confirmed again. Interestingly, a couple of observations stand out from the evaluation. Firstly, the IB load derived from the aggregation of HTT-Q97-mCherry in the HDGF transduced condition seems not only strikingly smaller, but the IBs mostly localize within the nucleus, in contrast to the YFP transduced control, where they lie in the cytoplasm. The

location of protein aggregates firmly influences the survival of cells. While aggregates within the nucleus barely influence cellular function, deposits of identical proteins within the cytoplasm interfere with important transport pathways between the nucleus and the cytoplasm [269]. This results in a blockage of protein and RNA transport in and out of the nucleus. In a long-term context, this leads to the death of the affected cells and progression of the pathology. Nevertheless, how all this process develops, mechanistically speaking, should be further addressed.

Secondly, there is the differential decompression of constitutive heterocromatin foci. In a murine nucleus in interphase, pericentric constitutive heterochromatin (PCH) can be visualized as dense DAPI regions, termed chromocenters, with each chromocenter consisting of multiple pericentric regions from different chromosomes [91]. PCH is the main constituent of mouse heterochromatin and is formed by major satellite repeats that comprise 10% of the genome. They are critical for genetic stability and centromere formation. Some controlled dynamical changes of pericentric heterochromatin structure may occur, which associate with brief bursts of major satellite transcription, such as cell differentiation [251, 86] or embryonic development [35, 220]. Nevertheless, in most somatic cells, PCH is transcriptionally repressed with high levels of H3K9me3 and condensed chromatin fibers [222]. Regarding HDGF, there is published evidence of its PWWP domain acting as a histone methyl-lysine reader [217], recognizing both DNA and histone methylated lysines. This involvement in chromatin-associated processes could be the starting point for elucidating the consequences of its overexpression in the future.

3.2.1 Considerations and outlook

The multiplicity of gene copies that are carried by transgenic mice (two murine copies plus the mutated human one) have risen awareness about how representative are these models in the genetics of the human disease. Although transgenic mice show many features, both behavioral and neuropathological when compared to humans patients, they do not match perfectly. For instance, IB formation in the R6/2 line is more extensive and neuronal loss is less striking than in human HD [62]. In addition, supplementary pathology not associated with the disease could be taking place due to the random insertion of the human *HTT* gene in the mouse genome [119]. This could eventually interfere with the proper function of other genes unrelated to HD. The pathogenic mechanism of the truncated HTT in the R6/2 model could be questionable since that fragment may not be produced in the human HD brain. HTT is a big protein with many potential functional

domains and its conformation and function may show variable changes. Therefore, it is likely that we are creating artificial properties when HTT is cut into different fragment sizes.

All these concerns motivated the generation of KI models. These models replace a portion of the mouse *Htt* gene with a mutant human copy that contains an expanded CAG region. The zQ175 KI line was developed in an attempt to have the *HTT* gene in a proper genetic context and displays a more similar phenotype to adult-onset HD [169]. The recent availability of this model in the lab will allow not only to validate the proteomic study, but also to confirm the potential therapeutic effect shown *in vivo* by one of the follow-up candidates, HDGF. On the other hand, it is important to mention that the exon1 of *HTT* is enough to recapitulate many HD features and additionally, R6/2 mice have extensive similarities with KI models on pathological, transcriptional, and electrophysiological levels [51, 139, 270].

3.3 HDGF as possible therapeutic candidate in HD

Our data revealed that HDGF rescues neuronal viability *in vitro* in the context of HttEx1 toxicity. Given our hypothesis of loss-of-function protein candidates, we approached it experimentally with their overexpression. In the case of HDGF, this could be a concern due to the published evidence on the protein in relation with its dysregulation in different cancer types. It is reported that HDGF is an important regulator of many cancer cell activities during transformation, apoptosis, angiogenesis and metastasis, [127] and it appears to function as an unfavorable prognostic marker for human glioma [276], carcinoma [142] and cervical adenocarcinoma [255], among others. As a summary of previous studies, a reduction of HDGF in tumor cells gives as outcome smaller tumors, less angiogenesis and reduced metastatic capacity. However, Sedlmaier *et al.* investigated the direct influence of an initial overexpression of HDGF, showing that there is no evidence of the HDGF transforming capacity in tumor development [232]. They proposed, instead, that HDGF has a possible role in cell differentiation and that it promotes tumor progression after secondary up-regulation [232].

Despite its known role in the development and pathogenesis of some malignancies, there is not much known about HDGF in a neurological context. The distribution of the protein in the murine brain has been characterized in two publications [2, 67]. The signaling pathway for growth factors implies induction of a typical kinase pathway at the

plasma membrane, which leads to an intracellular phosphorylation cascade. Recently, it has been reported that growth factors act as transcriptional cofactors in the nucleus. Although HDGF has been identified as a growth factor, its receptor on the cell membrane remains unclear. One candidate is nucleolin, which has been identified and validated as a HDGF-interacting membrane protein in hepatoma cells. Upon binding to nucleolin, HDGF activates the downstream PI3K/AKT signaling pathway [39]. Similar to other cell types, HDGF is targeted to the nucleus in neurons. Nuclear localization of HDGF is critical for the mitogenic activity of HDGF in different cells [131] and it promotes *de novo* lipogenesis through activating SREBP-1-mediated lipogenic gene transcription [173], which is neccessary for proliferation. However, the clear presence of HDGF mRNA in post-mitotic neurons and the extranuclear expression of the growth factor in cultured differentiated neurons [2], points to a function that is not limited to proliferative activity. Interestingly, LEDGF, which is also a member of the HRP family, enhances the survival of skin fibroblasts, keratinocytes, photoreceptor and retinal pigment epithelial cells [162, 152]. Thus, HDGF might also function as survival factor in adult brain. Indeed, its role in neuronal survival has been demonstrated for hippocampal and spinal motor neurons *in vitro* [160, 285], as well as for retinal ganglion cells *in vivo* [106].

Little is also known about the potential role HDGF may play in a neurodegenerative context. There is, however, a relevant hint from published work some years ago that could point in the appropriate direction. HDGF bears a 32% aminoacid homology to HMG1, which has been reported to have intranuclear and extracellular functions [175] and it is an abundant constituent of mammalian nuclei [23]. The work of Qi *et al.* suggested that a compensatory expression of HMGs ameliorates polyQ-induced pathology in primary neurons and in *Drosophila* polyQ models [204]. In addition, HMGs repress toxic stress signals induced by mHTT or transcriptional repression [204]. The possibility that HMGs may be regulators of polyQ disease pathology opens the door to a robust evidence for HDGF as well. Among the different roles in which HMGs have been implicated, they can act as a factor related to tumor metastasis [247], sustaining the thought that they function in the extracellular space. In HDGF, the absence of the HMG box, which is essential for binding DNA, also suggests that HDGF has extracellular roles, which is supported by the evidence of HDGF secretion [187].

Our results show a remarkable rescue in the open field traveled distance in the HDGF-injected animals, comparable to WT levels. The open field test is classically used to assess animal basal locomotor activity and exploration. The test is based on conflicting innate tendencies of avoiding bright light and open spaces, which ethologically mimic a situation

of predator risk, and of exploring novel environment. It can also be used for general assessment of anxiety in murine models. It had been shown that anxiolytics administration increases exploration time in the center of the open field, while stressful stimuli decrease the number of center visits [41]. However, there is an intrinsic challenge to dissociate impaired locomotor activity from anxiety-induced suppression of exploration. Therefore, it remains unclear whether this rescue in our tested animals is due to an improvement in some specific motor functions or a reduction in the anxiety levels. A possible complementary analysis to help the distinction could be to quantify the rearing frequency, in which rodents stand on their hindlimbs to explore [243]. Pairing the open field analysis with other anxiety measures, such as elevated plus maze, could help the clarification.

Interestingly, HDGF-injected mice were also rescued in the clasping phenotype. Normal mice spread their four limbs when suspended by their tails, whereas R6/2 mice tightly clasp their hind- and forelimbs against their thorax and abdomen. The pathophysiology of this abnormal response is not fully understood. Nevertheless, the paw clasping test is a very widely used way of characterizing HD mouse models, and is often used in studies examining novel treatments, partly due to it being easy and fast to perform [143]. It is tempting to speculate that HDGF overexpression has a wider effect than its cellular context, influencing not only the striatum but also the connectivity associated and responsible for this phenotype.

For all the animals that have undergone behavior experiments it would be essential to check the accuracy of the injection sites. It will be interesting to assess different histological parameters that could shed some light onto the mechanism of rescue *in vivo*, such as evaluation of any change in the IB size and/or amount, quantification of a possible reduction in the inflammation markers and the evaluation of HDGF levels in different brain regions. It also remains an open question, up to further analysis, whether some of the neurons containing HDGF could have taken it up from the neighboring secretion, in a paracrine manner, and whether HDGF might perform a specific function in the cytoplasm related to mHTT.

In order to approach a more exhaustive evaluation of the effect of HDGF overexpression in HD, different lines of action can be taken. Firstly, there are several motor tests that could help narrowing the characterization of the phenotype in the injected R6/2, such as measuring the grip strength, climbing or the running wheel test, which could detect improvement with different group sizes. This test can be automated, requiring a low amount of manual input, making it suitable for preclinical drug testing [103]. Sec-

ondly, it would be very interesting to analyze whether the lifespan of the HDGF-injected R6/2 is affected. Since the R6/2 is such a dramatic model, even a mild extension could mean a significant improvement, mechanistically speaking. Thirdly, an important insight could come into play by applying transcriptomic, as well as proteomic analysis. Such approaches could answer different questions at a molecular level regarding, for example, how are the mHTT levels affected under the overexpression of HDGF, which other protein sets are responding in the same context, how are the protein interactions changing among each other, etc.

Last, but not least, a catalog of different possibilities also opens when discussing injection sites. The observed effect upon overexpression of HDGF arises from two pair of striatal injections in each hemisphere. However, it remains an open question whether the same improvement, or a different one, in the phenotype could be achieved with cortical localized injections or a combination of both, striatal and cortical, given the relevance of the cortiostriatal pathway.

3.3.1 Considerations and outlook

In this project, I have shown HDGF to be a promising mHTT-toxicity modifier. However, many open questions still remain. First, it is not clear through which receptor HDGF might exert its action in neurons. The work from Chen *et al.* demonstrated the function of nucleolin as a cell surface receptor for HDGF in hepatocellular carcinoma cells [39]. However, additional molecules may participate in the formation of surface HDGF-nucleolin signaling complex. The published work postulates that nucleolin protein may serve as high-affinity receptor for HDGF, whereas the other co-receptor proteins may confer the specificity for HDGF recognition in the signaling cascade. The identity and functions of these HDGF-binding membrane proteins remain unclear and require further characterization. Moreover, it is still an open question whether this signaling axis acts similarly in neurons.

The localization of the protein should also be interrogated in future studies. In a mHTT-toxicity context, which effect would it have to fully re-locate the protein to the cytoplasm? HDGF is harbored in the nucleus, but it might be able to exert its neuroprotective role from a different biological compartment. This information would be useful to mechanistically characterize the effect of the protein towards mHTT toxicity.

Another open line for studying is the extracellular application of HDGF. The fact

that the protein can act in a para- and autocrine manner through a cell surface receptor is a clear advantage for future therapeutic approaches. HDGF could be then exogenously applied to the targeted cells with an adequate concentration, which would remove the drawback of an endogenous cell delivery method.

Finally, as it would be interesting to confirm HDGF effect in a different HD mouse model, such as the zQ175 KI line, the targeted time points relevant for the disease should be adapted since it develops HD in a more delayed manner compared to the R6/2 model. It would represent another step into a possible pre-clinical HD treatment.

CHAPTER 4

CONCLUSION

4.1 Concluding remarks

In the present work, I provided an array of data which displays a quantitative picture of the dynamics of the aggregate proteome in relation to the brain proteome, by studying HD progression in the R6/2 mouse model in a spatiotemporal manner.

In summary, the thesis contributed to a more detailed description of the HD pathogenesis on (1) proteome changes upon disease progression and (2) the characterization of polyQ aggregates. The overexpression of different loss-of-function protein candidates, which arose from the proteomic data set, (3) showed an improvement in the viability of a HD cell model. (4) The follow-up of one of those proteins, HDGF, revealed an enhancement in the phenotype of the R6/2 mice when overexpressed in the striatum by AAV.

These findings provide new insights into the molecular pathways underlying HD pathogenesis, and pave the way for development of more refined therapies.

4.2 Thesis graphical overview

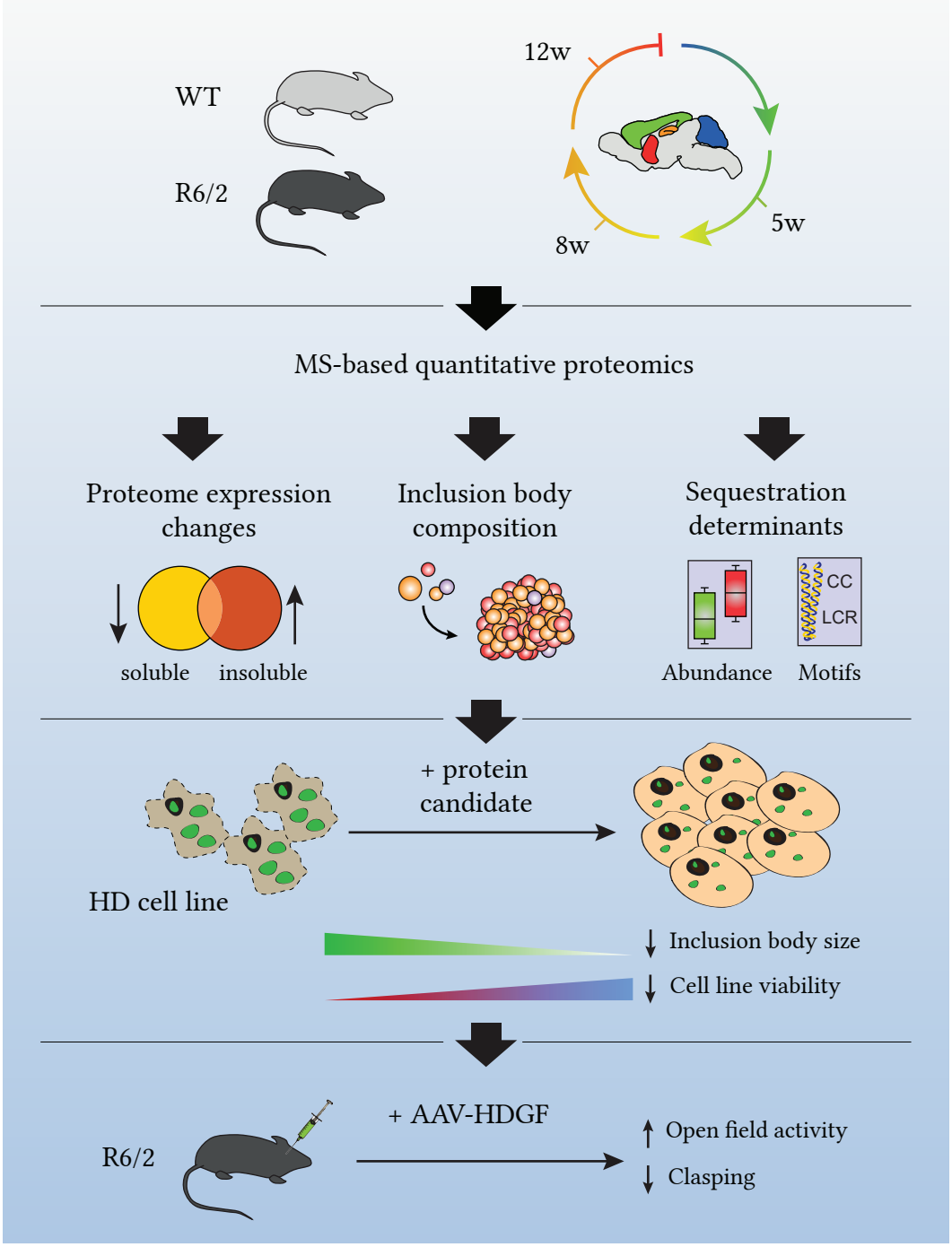

Figure 4.1 – Graphical schematic summary of the thesis. Summary of the developed thesis showing the different phases of the study.

CHAPTER 5

MATERIALS AND METHODS

5.1 Materials

5.1.1 Reagents

Table 5.1 – List of critical reagents used.

Name	Source	Identifier
TransIT-Lenti	Mirus	# MIR6603
16% PFA	Electron Microscopy Sciences	# 15710
Doxycycline	Sigma-Aldrich	# D9891
G418	Thermo Fisher Scientific	# 10131035
Hygromycin B	Thermo Fisher Scientific	# 10687010
Laminin	Thermo Fisher Scientific	# 23017015
Lipofectamine 2000	LifeTechnologies	# 11668027
Lipofectamine LTX with Plus Reagent	LifeTechnologies	# P36930
MTT reagent	Sigma-Aldrich	# M5655
Poly D-Lysin	Sigma-Aldrich	# P7886

5.1.2 Genotyping primers

Table 5.2 – Primers used for genotyping

Name	Sequence
R6/2 Forward	CCG CTC AGG TTC TGC TTT TA
R6/2 Reverse	TGG AAG GAC TTG AGG GAC TC

5.1.3 Buffers

Table 5.3 – List of buffers

Buffer name	Composition
PBS, pH 7.3	137 mM NaCl 2.7 mM KCl 4.3 mM $Na_2HPO_4 \cdot 7H_2O$ 1.4 mM KH_2PO_4
TBS-T	20 mM Tris, pH 7.5 120 mM NaCl 0.1% Tween 20
TAE	2 M Tris acetate 50 mM EDTA
Borate, pH 8.5	50 mM Boric acid 12.5 mM Sodium tetraborate (Borax)
TBS-5	50 mM Tris-HCl, pH 7.8 130 mM NaCl 10 mM KCl 5 mM $MgCl_2$
Citrate	10 mM sodium citrate, pH 6 0.05% Tween 20
Electrophoresis 5x (10 l)	154.5 g Tris base 721 g Glycine 50 g SDS
Protein transfer (1 l)	3.03 g Tris base 14.4 g SDS 200 ml Methanol
Protein running 5x (10 l)	154.5 g Tris base 721 g Glycine 50 g SDS

Table 5.4 – List of solutions

Solution name	Composition
Lysis	50 mM Tris, pH 7.5 150 mM NaCl 2 mM EDTA 1% TritonX-100 Protease inhibitor (Roche)
Blocking	0.2% BSA 5% DS 0.2% lysine 0.2% glycin 0.02% SA
Primary antibody blocking	PBS 0.3 % Triton X-100 2 % BSA 0.02 % SA
Secondary antibody blocking	PBS 0.3 % Triton X-100 3 % DS
Albumin-gelatin	45% albumin 1.5% gelatin 1 M SA, pH 6.5

5.1.4 Commercial kits

Table 5.5 – List of critical commercial kits used.

Kit name	Source	Identifier
NucleoBond Xtra Maxi	Macherey-Nagel	# 740414.5
QIAprep Spin Miniprep	Quiagen	# 27106
Nucleo Spin Gel and PCR Clean-up	Quiagen	# 740609.25
Pierce LDH Cytotoxicity Assay Kit	Thermo Fisher Scientific	# 88953
CalPhos mammalian transfection kit	ClonTech	# K2051-1

5.1.5 Media

Table 5.6 – List of media

Media name	Composition
PC12 culture	DMEM (+ 4.5 g/l D-Glucose, - Pyruvate) 1 % Penicilin/ Streptomicin 1 % G418 Hygromicin B, 70 µg/ml 5% FBS 10% FHS 1 % Glutamax
HEK293T maintenance	DMEM (+ 4.5 g/l D-Glucose, - Pyruvate) 1 % Penicilin/ Streptomicin 1 % G418 1 % Glutamax 10% FBS 1% G418
HEK293T lentivirus production	DMEM (+ 4.5 g/l D-Glucose, - Pyruvate) 1 % Glutamax 10% FBS 1 % NEAA 1 % HEPES
Neuronal dissection	HBSS (+ CaCl2, + MgCl2) 1 % Penicilin/ Streptomicin 1% HEPES 1% Mg_2SO_4
Primary neuronal culture	Neurobasal medium (- L-Glutamine) 1 % Penicilin/ Streptomicin 1 % L-Glutamine 1x B27 supplement

5.1.6 Molecular constructs

Plasmid constructs

Table 5.7 – List of plasmids.

Plasmid Insert	Backbone	Tag	Resistance	Source	Identifier
AARS	pCMV6-Entry	Myc-Flag	Kan	BioCat	RC202136-OR
AP2A2	pCMV6-Entry	Myc-Flag	Kan	BioCat	RC203018-OR
CACNB3	pCMV6-Entry	Myc-Flag	Kan	BioCat	RC207229-OR
CHMP3	pCMV6-Entry	Myc-Flag	Kan	BioCat	RC220006-OR
CNP	pCMV6-Entry	Myc-Flag	Kan	BioCat	RC207038-OR
DCTN1	pCMV6-Entry	Myc-Flag	Kan	BioCat	RC211975-OR
DNM1	pCMV6-Entry	Myc-Flag	Kan	BioCat	RC206284-OR
DPSYL2	pCMV6-Entry	Myc-Flag	Kan	BioCat	RC231368-OR
HDGF	pCMV6-Entry	Myc-Flag	Kan	BioCat	RC204148-OR
HNRNPA2B1	pCMV6-Entry	Myc-Flag	Kan	BioCat	RC219318-OR
HSP90AA1	pcDNA3	HA	Amp	Sessa lab (YSM)	AddGene #22487 [78]
HTT-Q25	pcDNA	Myc-mCherry	Amp	Hartl lab (MPIB)	n/a
HTT-Q97	pcDNA	Myc-mCherry	Amp	Hartl lab (MPIB)	n/a
INA	pCMV6-Entry	Myc-Flag	Kan	BioCat	RC202877-OR
KIF3B	pCMV6-Entry	Myc-Flag	Kan	BioCat	RC213911-OR
MAPT	mApple-C1	mApple	Kan	Davidson lab (NHMFL)	AddGene #54924
NCAM1	pCMV6-Entry	Myc-Flag	Kan	BioCat	RC207890-OR
NFASC	Modified pEGFP-N1	HA	Kan	Bennett lab (DUSOM)	AddGene #31061 [281]
PRRT2	pCMV6-Entry	Myc-Flag	Kan	BioCat	RC202304-OR
RAC1	pRK5-myc	Myc	Amp	Kirschner lab (OSU)	AddGene #37030 [153]
RDX	pCMV6-Entry	Myc-Flag	Kan	BioCat	RC207953-OR
SBF1	pCMV6-Entry	Myc-Flag	Kan	BioCat	RC222090-OR
SRGAP3	pCMV6-Entry	Myc-Flag	Kan	BioCat	RC214288-OR
mCherry	pcDNA	n/a	Kan	Hartl lab (MPIB)	n/a
GFP	PCI-Neo	HA	Amp	Klein lab (MPIN)	n/a
pSPAX2	pSPAX2	n/a	Amp	Edbauer lab (GCND)	n/a
pVSVg	pVSVg	n/a	Amp	Edbauer lab (GCND)	n/a

For the remaining plasmids used in this study but not presented in Table 5.7, they were acquired using the gene synthesis services of GenScript.

Viral constructs

Table 5.8 – List of viral constructs.

Type	Plasmid Insert	Backbone	Promoter	Tag	Titer	Resistance	Source
Lentivirus	YFP	pFhSynW2	Synapsin	N/A	4.46E+05	Amp	This study
	YFP-HDGF	pFhSynW2	Synapsin	Flag	6.58E+04	Amp	This study
	YFP-INA	pFhSynW2	Synapsin	Flag	5.88E+04	Amp	This study
	YFP-PRRT2	pFhSynW2	Synapsin	Flag	2.57E+04	Amp	This study
	YFP-RDX	pFhSynW2	Synapsin	Flag	3.01E+04	Amp	This study
	mCherry	pFhSynW2	Synapsin	Myc	3.81E+05	Amp	Klein lab
	HttQ25-mCherry	pFhSynW2	Synapsin	Myc	6.40E+04	Amp	Klein lab
	HttQ97-mCherry	pFhSynW2	Synapsin	Myc	6.57E+03	Amp	Klein lab
AAV	YFP	AAV2/8	CAG	n/a	2.40E+12	n/a	UAB (Spain)
	YFP-HDGF	AAV2/8	CAG	Flag	5.59E+12	n/a	UAB (Spain)

5.1.7 Experimental models

Bacterial Strains

Table 5.9 – List of bacterial strains

Bacterial strain	Source	Identifier
DH5α	In-house production	n/a
Stellar	ClonTech	# 636763

Cell lines

Table 5.10 – List of cell lines

Cell line	Origin	Source	Identifier
N2a HDExon1-Q18	Mouse neuroblastoma	Nukina lab (JUIC)	n/a
N2a HDExon1-Q64	Mouse neuroblastoma	Nukina lab (JUIC)	n/a
N2a HDExon1-Q180	Mouse neuroblastoma	Nukina lab (JUIC)	n/a
PC12 HDExon1-Q23	Rat pheochromocytoma	Rubensztein lab (CU)	n/a
PC12 HDExon1-Q74	Rat pheochromocytoma	Rubensztein lab (CU)	n/a
HEK293T	Human embrionic kidney	ClonTech	# 632180

Mouse lines

Table 5.11 – List of mouse lines

Mouse line	Source	Identifier
CBA	In-house colony	n/a
C57BL/6	In-house colony	n/a
CD1	In-house colony	n/a
R6/2 (B6CBA-Tg (HDexon1) 62gpb/1J)	The Jackson Laboratory	# 002810

R6/2 mice were generated in the lab of Gillian Bates [154]. For the proteomic study, female R6/2 mice (B6CBA-Tg(HDexon1)62gpb/1J) carrying a 150 ± 5 CAG repeat expansion and female non-transgenic littermate controls at five weeks of age were obtained from the Jackson Laboratory (Bar Harbor, Maine, USA).

For further studies, an R6/2 colony was established at the animal facility of the Max Planck Institute of Biochemistry (Martinsried, Germany) from male R6/2 mice (B6CBA-Tg(HDexon1)62gpb/1J) obtained from Jackson Laboratory. The colony was maintained by crossing carrier males to CBA x C57BL/6 F1 females. Only female R6/2 mice were used for experiments. All mice were housed under SPF conditions with *ad libitum* access

to standard food and water. They were maintained consistent with local animal welfare guidelines (Regierung von Oberbayern).

5.1.8 Antibodies

Primary antibodies

Table 5.12 – List of primary antibodies.

Antigen	Species	Dilution	Source	Application	Identifier
anti-Caspase-3	Rabbit	1:500	Cell Signaling	IF	# 9661S
anti-DARPP-32	Rabbit	1:500	Abcam	IF	# ab40801
anti-DARPP-32	Goat	1:250	Lifespan Biosciences	IF	# LS-C150127
anti-flag	Mouse	1:1000	Origene	IF	# TA50011
anti-flag	Rabbit	1:500	Sigma-Aldrich	IF or MS	# F7425
anti-GAPDH	Rabbit	1:5000	Cell Signaling	WB	# 2118
anti-GFP	Chicken	1:1000	Invitrogen	IF	# 110262
anti-GFP	Rat	1:1000	Chromotek	MS	# 3h9
anti-HA	Rat	1:500	Sigma-Aldrich	IF	# 11867423001
anti-HA	Rabbit	1:500	Sigma-Aldrich	IF	# H6908
anti-HDGF	Rabbit	1:200	Abcam	IF	# ab128921
anti-hnRNPA2B1	Mouse	1:100 or 1:500	Santa Cruz Biotechnology	IF or WB	# sc-514165
anti-HSP90	Rabbit	1:1000	New England Biolabs	WB	# 4877
anti-Huntingtin (EM48)	Mouse	1:500	Milipore	IF	# MAB5374
anti-Huntingtin(MW8)	Mouse	1:500	DSHB	IF	MW8
anti-KIF3B	Mouse	1:500	Santa Cruz Biotechnology	WB	# sc-514165
anti-myc	Rabbit	1:250	Cell Signaling	IF	# 2278
anti-myc	Rabbit		Sigma-Aldrich	IF	# C3956
anti-NeuN	Mouse	1:1000	Milipore	IF	# MAB377
anti-PLP1	Rabbit	1:100	Abcam	IF	# ab28486
anti-β-Actin	Mouse	1:2500	Sigma-Aldrich	WB	# A5316
NeuroTrace 640/660 Nissl Stain	n/a	1:1000	Thermo Fisher Scientific	IF	# N21483

Secondary antibodies

Table 5.13 – List of secondary antibodies.

Antigen	Species	Dilution	Source	Application
anti-rabbit, mouse, goat, chicken IgG, Cy2/Cy3/Cy5-conjugate	Donkey	1:200	Jackson ImmunoResearch	IF
anti-rabbit, mouse, goat, chicken IgG, HRP-linked	Donkey	1:1000 - 1:5000	Cell Signaling or Jackson ImmunoResearch	WB

5.1.9 Instruments and equipment

Table 5.14 – List of critical equipment and instruments used.

Instruments and equipment	Resource
Confocal TCS SP8 microscope	Leica
C1000 Touch thermocycler	Biorad
Vibratome 1000S	Leica
Rotarod NG	Ugo Basile
Stereotaxic frame	Kopf Instruments
TriStar 942 plate reader	Berthold Technologies
Avanti JXN-30 ultracentrifuge	Beckman Coulter

5.1.10 Software

Table 5.15 – List of used software.

Name	Resource
Perseus v1.5.2.11	[257]
ImageJ v1.49i	NIH
EthoVision XT	Noldus
Cell Profiler v2.1.1	[123]
GraphPad v5.00	GraphPad Software

5.2 Methods

5.2.1 Mouse husbandry

Genotyping

For the genetic analysis, 1 mm of tail from each mouse was lysed in 100 µl of 50 mM NaOH for 45 min at 95 °C, vortexing every 15 min and subsequently neutralized by adding 100 µl of 1.5 M Tris-HCl pH 8.8. Tail lysates were stored at 4 °C until further use. This DNA solution was used for the genotyping by PCR. A PCR master mix was prepared and mixed with 1 µl of the respective DNA sample to a total volume of 50 µl:

Table 5.16 – PCR master mix

Master mix for genotyping	
Volume (µl)	**Reagent**
42	H_2O
0.5	Forward primer
0.5	Reverse primer
5	Thermo Pol Reaction buffer (New England Biolabs)
0.5	dNTPs-mix (25 mM each) (Fermentas)
0.5	Taq Polymerase (New England Biolabs)

The resulting mix was run with the following programm:

Table 5.17 – PCR programm for R6/2 genotyping

Step #	Temp °C	Time	Note
1	94	2 min	
2	94	20 sec	
3	65	15 sec	-0.5 °C per cycle decrease
4	68	10 sec	
5			Repeat steps 2-4 for 10 cycles (Touchdown)
6	94	15 sec	
7	60	15 sec	
8	72	10 sec	
9			Repeat steps 6-8 for 28 cycles
10	72	2 min	
11	10		Hold infinite

Determination of CAG repeats

During the study, CAG repeat length was determined from ear punches by the service of Laragen. Only males with CAG repeats under 180 were used for breedings.

Preparation of Mouse Brain Regions

Mice were euthanized by carbondioxide inhalation. Whole brains were then dissected from each mouse, washed once in ice-cold PBS and divided in halves by sagittal dissection on ice. One cerebral hemisphere was further dissected at 4 °C in order to obtain CE, HC, ST and CO. Dissected brain regions were immediately flash-frozen in liquid nitrogen and stored at -80 °C until further use.

Transcardial perfusions

Mice were injected with a mixture of 1.6 % ketamine (Medistar) and 0.08 % xylazine (Bernburg) in saline. After checking for the absence of reflex, mice were transcardially perfused for 4 min at a speed of 1.5 ml/min with cold PBS and for additional 4 min with cold 4 % PFA . Brains were subsequently removed and post-fixed in 4 % PFA overnight. Brains were stored at 4 °C in PBS with 0.02 % sodium azide until further use.

5.2.2 Molecular biology and biochemistry

DNA constructs cloning and amplification

DNA of interest was digested overnight with the corresponding enzyme (New England Biolabs) following manufacturer's instructions. Proper digestion of the construct of interest was checked on a 2% agarose gel following electrophoresis.

DNA fragments were amplified using PFU polymerase (Promega) according to manufacturer's instructions. Both vectors and inserts of interest were purified from agarose gels following electrophoresis with QIAquick Gel Extraction Kit (Quiagen) following manufacturer's instructions. Ligation between vector and insert was performed using T4 DNA ligase (New England Biolabs) overnight at 16°C, in a total volume of 30 µl. Amount of vector was 50 ng and amount of insert used varied based on different stoichiometric ratios (1:1, 1:3, 1:5 and a negative control without insert). Then, 1-5 µl of the ligation reaction were used for transforming 50 µl of either DH5α or Stellar (ClonTech) electro-competent cells in a pre-chilled cuvette (Bio-Rad, Gene Pulser Cuvettes, 0.2 cm electrodes). Cuvettes were exposed to a pulse in the electroporation chamber (Bio-Rad, Puls Controller), and cells were subsequently transferred to a 14 ml Falcon tube in 200 µl LB medium. The

transformed cells were incubated for 1 h at 37°C and 230 rpm shaking. Subsequently, they were plated on LB agar plates containing ampicillin or kanamycin, depending on the insert resistance and left to grow overnight at 37 °C. Cultures of single colonies were grown overnight at 37 °C and 230 rpm in LB medium supplemented with 100 µg/ml ampicillin or kanamycin as required. For purification of the plasmid DNA, maxi-prep or mini-prep kit were used. Plasmid DNA concentration was measured using a NanoDrop 1000 Spectrophotometer (Thermo Scientific). Sequences of all constructs were verified by sequencing at Eurofins.

DNA electrophoresis

Depending on the size of the DNA fragments needed to be separated, 1 or 2 % agarose gels were prepared in TAE buffer. The agarose was dissolved in the buffer by boiling. Subsequently, SYBR Safe (Thermo Fisher) was added to a concentration of 0.6 %. The solution was then poured into a plastic tray and left to cool until polymerized. Gel electrophoresis was performed at 150-200 V, and DNA fragments were visualized by UV light using a Gel Doc XR+ (Biorad).

Western Blotting

Dissected brain regions were homogenized in lysis solution. For SDS-PAGE, 100 µg of proteins were separated in a 10% gradient gel and transferred to a PVDF membrane. The membrane was blotted with the following primary antibodies: hnRNPA2B1, HSP90, KIF3B and Beta-Actin. After incubation with HRP-conjugated secondary antibodies, bound antibodies were visualized by chemiluminescence. The intensity of the bands was quantified by Image J software.

5.2.3 Cell lines and primary neurons

Immortalized cell lines

Mouse N2a neuroblastoma cell lines were a kind gift from Professor Nobuyuki Nukina (Juntendo University Graduate School of Medicine). The three lines were cultured and induced as instructed. Briefly, cells were maintained in media comparable to the HEK293T one, line at 37°C, 10% CO_2 and treated with 2.5 mM dbcAMP (Sigma) for differentiation and 1 μM ponasterone A (Thermo Fisher) for induction of HttEx1-Q18/Q64/Q180. When cells were reaching a confluency around 70-80%, they were washed with pre-warmed PBS and incubated with Trypsin-EDTA (Sigma) for 3 min. Subsequently, cells were taken

up and newly seeded as needed

Rat PC12 pheochromocytoma cell lines stably transfected with either GFP-fused Huntingtin Exon1-Q23 or Q74 were a kind gift from Professor David Rubinsztein (Cambridge Institute for Medical Research). Both lines were cultured and induced as described in Wyttenbach *et. al.*[272]. Briefly, cells were maintained with medium for PC12 cell line at 37°C, 10% CO_2. When cells were reaching a confluency around 70-80%, they were washed with pre-warmed PBS and subsequently, cells were taken up and newly seeded as needed. Induction of the Htt-Exon1-Q23 or Q74 was carried out by adding doxycycline (Sigma-Aldrich) at 1 µg/ml. After induction with doxycycline, cells were kept at 1% HS to maintain them in a quiescent-like state.

Human HEK293T cell line was maintained in medium for HEK293T cells at 37°C, 10% CO_2. At a confluency of 80%, cells were re-seeded as described above.

Lentiviral production

Viral productions were performed in HEK293T cells as previously described [75]. Briefly, HEK293T were seeded with culture media for viral production at a confluency of 75-80%. Subsequently, they were cotransfected using TransIT-Lenti (Mirus) with the cDNA of interest and the lentiviral expression constructs psPAX2 and pVSVg with a ratio of 2,9: 1,7: 1, respectively. After 6 h of transfection, media was renewed. After another 48 h, supernatant was harvested and spun down at 600 g for 5 min to remove cell debris. Subsequently, virus particles were filtered through 0.45 µm filters and concentrated by ultracentrifugation at 100000 g during 2 h in an Avanti JXN-30 ultracentrifuge (Beckman Coulter). Pellets were then left in TBS-5 buffer at 4 °C overnight. On the next day they were aliquoted and stored at - 80°C until further use. Lentiviral titers ranged from $4,55 \cdot 10^5$ as the highest (YFP lentivirus), to $6,9 \cdot 10^4$ as the lowest (Q97-mCherry lentivirus).

Primary neuronal cell culture

For all primary neuronal cultures, plates or coverslips were coated with 0.5 µg/ml poly-D-lysine (Sigma) for 2 - 12 h. After washing with PBS, they were coated with 5 µg/ml laminin (Gibco) for a minimum of 2 - 4 h. All cultures were made using E15-E15.5 CD1 embryos in medium for neuronal dissection. Briefly, brain was dissected out of the skull and hemispheres were cut off the rest of the brain. Meninges were removed

and then the cortex was dissected. Tissue was then trypsinized in 2 ml Trypsin at 37 °C for 20 min. Trypsin activity was neutralized by adding 5 % FBS in medium for primary neuronal culture. FBS was subsequently removed by two washes with medium for primary neuronal culture. Cells were then mechanically dissociated in 1 ml of medium by pipetting around 20 times and diluted in extra medium. Cell counting was conducted in 10 µl volume in a Neubauer counting chamber (Blaubrand, Brand). Neurons were seeded at different densities depending on the culture plate used in primary neuronal culture media and maintained at 37°C, 5% CO_2. Half of the medium was changed after 6-7 days in culture.

Neuronal transfection and transduction

Transfection of primary neurons was performed by the calcium phosphate method as described by Jiang *et al.* [121]. Briefly, a transfection mix was prepared by adding DNA and calcium chloride into H_2O. After mixing by flicking the tube, HBS 2x solution was layered on top of the solution in a drop-wise manner. The solution was then briefly mixed by flicking the tube. The transfection mix was left incubating for 30 min at RT. Coverslips with neurons were transferred into fresh plating medium and 30 µl of the transfection mix was added per 24 well plate well in a dropwise manner. Cells were incubated at 37 °C for 2 - 3 h and then transferred into another plating medium, which had been acidified for at least 30 min at 10 % CO_2. After 30 min neurons were transferred back into their original medium.

Transduction of primary neurons was carried out by adding adjusted amounts, according to their titer, of the different lentivirus. The lentiviral microvolume was mixed with some media from the cultured wells and then added back to the plates.

Cell toxicity assays

N2a and PC12 cells were seeded on coverslips in 24-well cell culture plates for both immunofluorescence microscopy studies and viability assays. After 12 h PC12 cells were transfected with either mCherry plasmid as control, or the different candidates' plasmids and induced 5 h after transfection. All plasmid transfections were performed with Lipofectamine LTX with Plus Reagent (Thermo Fisher Scientific) according to manufacturer's instructions. For viability studies, 50 µl of the medium from each well and each condition were taken at 60 h post-transfection. The LDH assay was performed according to manufacturer's instructions (Pierce LDH cytotoxicity Assay Kit, Thermo Fisher Scientific) and absorbance was measured at 490 nm in a TriStar 942 plate reader (Berthold

Technologies). For the starvation assay in PC12 cells, all serum was removed from the beginning of the experiment.

Alternatively, MTT at 5 mg/ml in PBS was used as another colorimetric assay for assessing viability of cell lines and primary neurons. For this, 20% of the original well volume was added in form of MTT and incubated at 37°C, 10% CO_2 for 2 h. Then, 100 % of the original volume was added in form of solubilizer solution and incubated at 37°C, 10% CO_2 overnight. On the next day absorbance was measured at 570 nm in the plate reader.

5.2.4 Histology

Tissue preparation and immunohistochemistry

Brains of female R6/2 mice and control littermates of different ages were collected after transcardial perfusion with 4% PFA in PBS, followed by overnight fixation in 4% PFA in PBS. Whole brains were then embedded in albumin-gelatin medium and sectioned on a vibratome 1000S (Leica). For some stainings, antigen retrieval was performed in 10 mM sodium citrate buffer at 90 °C for 20 min. Floating sections of 50 µm were permeabilized with 0.5% TritonX-100 for 20 min and then blocked for 2 h with blocking solution. Sections were incubated with the primary antibody overnight at 4 °C . The following primary antibodies were used in primary antibody solution for brain sections: anti-mHtt (EM48 and/or MW8), anti-DARPP-32, anti-PLP1, anti-hnRNPA2B1, anti-HDGF. After washing three times with PBS, sections were incubated with the secondary antibodies in the secondary antibody solution: Cy2-, Cy3- or Cy5-conjugated against the respective species of the primary antibody. NeuroTrace 640/660 Nissl Stain was added with the secondary antibodies in some cases. Nuclei were counterstained with DAPI (Sigma-Aldrich). Sections were washed three times with PBS and mounted with Mowiol (in-house preparation).

Immunocytochemistry

PC12 cells coverslips were fixed 60 h post-transfection in 4% PFA in PBS for 15 min, then permeabilized in 0.1% TritonX-100 for 5 min and washed three times in PBS. Primary neurons coverslips were fixed either at 48 h post-transfection or 7 to 10 days post-transduction. Blocking was performed for 30 min as described above. Coverslips were incubated for 1 h at RT with primary antibodies: anti-myc, anti-flag and anti-HA, followed by Cy3-conjugated anti-rabbit secondary antibody. Nuclei were counterstained with DAPI and coverslips were mounted with ProLong Gold antifade reagent (Life Tech-

nologies). Sections and coverslips were examined at a Confocal TCS SP8 microscope (Leica). Images were taken using a 20x and a 40x objective.

Aggregate quantification in cells and tissue

Aggregates were quantified using an in-house macro on the freeware ImageJ version 1.49i (NIH). For R6/2 brain sections, aggregates were counted in 20 different confocal stacks in each brain region, in a total of three independent experiments. For PC12 cells, aggregates were analyzed in 20 different fields of view for each candidate, in a total of three independent experiments. For the quantification of cells with hnRNPA2B1 nuclear accumulation, images were analyzed with an in-house developed pipeline for CellProfiler [33], in 20 different fields of view for each mouse brain, in a total of three R6/2 mouse brains. The fluorescence intensity analysis was conducted with ImageJ. All quantification were performed in a blinded setting.

5.2.5 *In vivo* experiments

Surgical procedures

R6/2 mice and their littermates underwent surgical procedures at 4 weeks of age. Mice were injected intraperitoneally with 20% mannitol to improve spreading of the virus in the brain tissue [29], administered a painkiller (metamizol, 10 µl/ 10 mg body weight), anesthetized for surgery with isoflurane (1.5 to 2 %, Cp-pharma) and placed in a stereotaxic frame (Kopf Instruments). Body temperature was maintained with a heating pad, and a systemic anesthetic (carprofen, 100 µl/10 mg body weight) was administered subcutaneously. After opening the head skin and aligning to bregma for the accuracy of the injections, the skull was drilled. Mice were bilaterally injected with 0.2 µl of the AAV virus (with a final concentration of 7% mannitol [29]) in the striatum by using the following coordinates, adjusted for 4 week-old mice, calculated with respect to the bregma:

Table 5.18 – Set of coordinates used for the stereotaxic injections

	Stereotaxic injection			
Axis	**Left hemisphere**		**Right hemisphere**	
A/P	-1.7	-2.1	1.7	2.1
M/L	1	0.3	1	0.3
D/V	-3	-3	-3	-3

Viral titers of AAV8-CAG-eYFP and AAV8-CAG-eYFP-p2a-Flag-HDGF were $2,4 \cdot 10^{12}$ gc/ml and $5,59 \cdot 10^{12}$ gc/ml, respectively. For each of the four injections the glass capillary was left in position for 3 min. For all mice, skull holes were covered with bone wax and the incision was closed with sutures. Body weight was measured before surgery and the following week to control the recovery. In total, 31 mice where injected, distributed in the following experimental groups:

Table 5.19 – Experimental groups for the injected mice

WT		**R6/2**	
AAV8-CAG-eYFP	**AAV8-CAG-eYFP-p2a-Flag-HDGF**	**AAV8-CAG-eYFP**	**AAV8-CAG-eYFP-p2a-Flag-HDGF**
8	9	6	8

All the experimental procedures and postoperative care was carried out in accordance with regulations from the government of Upper Bavaria.

Behavior

For the characterization of the basal colony, motor performance was measured weekly from 8 to 12 weeks of age. Mice injected with the virus were assessed at 12 weeks of age. Rotarod analysis was performed on a Rota-Rod NG (Ugo Basile), set to accelerate from 5 to 40 rpm over a 300 s period, after a training period of two consecutive days at 5 rpm during 300 s. Latency to fall was recorded on three trials, with each trial separated by a 15 min rest period. The average of the three trials was considered the resulting data point for each mouse.

Locomotive activity was assessed as well using the open field test. To best measure the activity of the mice, trials were conducted one hour after the beginning of their dark cycle. Mice were placed into a custom-made 40x40 cm open field box arena and total distance traveled was recorded for 10 min. Between trials, the floor of each chamber was washed to minimize any odors left by mice on previous trials that could potentially affect exploratory behavior.

Finally, mice were placed upon a custom-made horizontal ladder with a descending slope of 30°C. The apparatus was made of clear Pexiglas walls and metal rungs inserted

to create a floor. The number of times the animal mistakes through the ladder (total error score) was evaluated by using a variation of a published scoring system [170] through video recording after a training period of two consecutive days. Briefly, the three categories used for quantifying the number of mistakes consisted in hesitation, when the limb aimed for one rung but was placed on another one; slip, when the limp was placed on a rung, then slipped off when bearing weight; miss, when the limb missed the rung and a fall occurred. Distance between ladder rungs in the training was set at 1 cm and increased to 2 cm for the experiment. All tests were carried out blindly to the treatment.

5.2.6 Data analysis

The type of statistical analysis is indicated in the figure legend. The same case applies for statistical information such as the value of n, mean, SD and significance level. If asterisks are used to point the significance level, then the key is reported in the figure legend as well. Statistical analysis were performed using Perseus or GraphPad Prism v5.00 (GraphPad Software, USA).

REFERENCES

[1] G. O. Abdulrahman. Therapeutic advances in the management of Huntington's disease. *Yale J Biol Med*, 84(3):311–319, Sep 2011.

[2] M. M. Abouzied, S. L. Baader, F. Dietz, J. Kappler, V. Gieselmann, and S. Franken. Expression patterns and different subcellular localization of the growth factors hdgf (hepatoma-derived growth factor) and hrp-3 (hdgf-related protein-3) suggest functions in addition to their mitogenic activity. *The Biochemical journal*, 378:169–176, Feb. 2004.

[3] M. M. Abouzied, H. M. El-Tahir, L. Prenner, H. HÃďberlein, V. Gieselmann, and S. Franken. Hepatoma-derived growth factor. significance of amino acid residues 81-100 in cell surface interaction and proliferative activity. *The Journal of biological chemistry*, 280:10945–10954, Mar. 2005.

[4] A. I. Acuña, M. Esparza, C. Kramm, F. A. Beltran, A. V. Parra, C. Cepeda, C. A. Toro, R. L. Vidal, C. Hetz, I. I. Concha, S. Brauchi, M. S. Levine, and M. A. Castro. A failure in energy metabolism and antioxidant uptake precede symptoms of Huntington's disease in mice. *Nat Commun*, 4:2917, 2013.

[5] J. Alberch, E. Perez-Navarro, and J. M. Canals. Neurotrophic factors in huntington's disease. *Progress in brain research*, 146:195–229, 2004.

[6] R. L. Albin, A. B. Young, and J. B. Penney. The functional anatomy of basal ganglia disorders. *Trends Neurosci.*, 12(10):366–375, Oct 1989.

[7] T. Alexi, C. V. Borlongan, R. L. Faull, C. E. Williams, R. G. Clark, P. D. Gluckman, and P. E. Hughes. Neuroprotective strategies for basal ganglia degeneration: Parkinson's and huntington's diseases. *Progress in neurobiology*, 60:409–470, Apr. 2000.

[8] K. D. Anderson, N. Panayotatos, T. L. Corcoran, R. M. Lindsay, and S. J. Wiegand. Ciliary neurotrophic factor protects striatal output neurons in an animal model of huntington disease. *Proceedings of the National Academy of Sciences of the United States of America*, 93:7346–7351, July 1996.

[9] S. E. Andrew, Y. P. Goldberg, B. Kremer, H. Telenius, J. Theilmann, S. Adam, E. Starr, F. Squitieri, B. Lin, and M. A. Kalchman. The relationship between trinucleotide (CAG) repeat length and clinical features of Huntington's disease. *Nat. Genet.*, 4(4):398–403, Aug 1993.

[10] M. Arrasate, S. Mitra, E. S. Schweitzer, M. R. Segal, and S. Finkbeiner. Inclusion body formation reduces levels of mutant huntingtin and the risk of neuronal death. *Nature*, 431(7010):805–810, Oct 2004.

[11] Y. Arribat, N. Bonneaud, Y. Talmat-Amar, S. Layalle, M.-L. Parmentier, and F. Maschat. A huntingtin peptide inhibits polyq-huntingtin associated defects. *PloS one*, 8:e68775, 2013.

[12] Y. Arribat, Y. Talmat-Amar, A. Paucard, P. Lesport, N. Bonneaud, C. Bauer, N. Bec, M.-L. Parmentier, L. Benigno, C. Larroque, P. Maurel, and F. Maschat. Systemic delivery of p42 peptide: a new weapon to fight huntington's disease. *Acta neuropathologica communications*, 2:86, Aug. 2014.

[13] S. J. Augood, R. L. Faull, and P. C. Emson. Dopamine D1 and D2 receptor gene expression in the striatum in Huntington's disease. *Ann. Neurol.*, 42(2):215–221, Aug 1997.

[14] A. C. Bachoud-Levi, N. Deglon, J. P. Nguyen, J. Bloch, C. Bourdet, L. Winkel, P. Remy, M. Goddard, J. P. Lefaucheur, P. Brugieres, S. Baudic, P. Cesaro, M. Peschanski, and P. Aebischer. Neuroprotective gene therapy for huntington's disease using a polymer encapsulated bhk cell line engineered to secrete human cntf. *Human gene therapy*, 11:1723–1729, Aug. 2000.

[15] B. Baldo, P. Paganetti, S. Grueninger, D. Marcellin, L. S. Kaltenbach, D. C. Lo, M. Semmelroth, A. Zivanovic, D. Abramowski, D. Smith, G. P. Lotz, G. P. Bates, and A. Weiss. Tr-fret-based duplex immunoassay reveals an inverse correlation of soluble and aggregated mutant huntingtin in huntington's disease. *Chemistry & biology*, 19:264–275, Feb. 2012.

[16] H. S. Bateup, E. Santini, W. Shen, S. Birnbaum, E. Valjent, D. J. Surmeier, G. Fisone, E. J. Nestler, and P. Greengard. Distinct subclasses of medium spiny neu-

rons differentially regulate striatal motor behaviors. *Proc. Natl. Acad. Sci. U.S.A.*, 107(33):14845–14850, Aug 2010.

[17] F. J. B. Bauerlein, I. Saha, A. Mishra, M. Kalemanov, A. Martinez-Sanchez, R. Klein, I. Dudanova, M. S. Hipp, F. U. Hartl, W. Baumeister, and R. Fernandez-Busnadiego. In Situ Architecture and Cellular Interactions of PolyQ Inclusions. *Cell*, 171(1):179–187, Sep 2017.

[18] M. F. Beal, N. W. Kowall, K. J. Swartz, R. J. Ferrante, and J. B. Martin. Systemic approaches to modifying quinolinic acid striatal lesions in rats. *J. Neurosci.*, 8(10):3901–3908, Oct 1988.

[19] M. W. Becher, J. A. Kotzuk, A. H. Sharp, S. W. Davies, G. P. Bates, D. L. Price, and C. A. Ross. Intranuclear neuronal inclusions in Huntington's disease and dentatorubral and pallidoluysian atrophy: correlation between the density of inclusions and IT15 CAG triplet repeat length. *Neurobiol. Dis.*, 4(6):387–397, Apr 1998.

[20] K. Bernard, E. Litman, J. L. Fitzpatrick, Y. G. Shellman, G. Argast, K. Polvinen, A. D. Everett, K. Fukasawa, D. A. Norris, N. G. Ahn, and K. A. Resing. Functional proteomic analysis of melanoma progression. *Cancer research*, 63:6716–6725, Oct. 2003.

[21] D. A. Bessert, K. L. Gutridge, J. C. Dunbar, and L. R. Carlock. The identification of a functional nuclear localization signal in the huntington disease protein. *Brain research. Molecular brain research*, 33:165–173, Oct. 1995.

[22] G. Bi, J. Yan, S. Sun, and X. Qu. Prrt2 inhibits the proliferation of glioma cells by modulating unfolded protein response pathway. *Biochemical and biophysical research communications*, 485:454–460, Apr. 2017.

[23] M. E. Bianchi and M. Beltrame. Upwardly mobile proteins. workshop: the role of hmg proteins in chromatin structure, gene expression and neoplasia. *EMBO reports*, 1:109–114, Aug. 2000.

[24] J. Bloch, A. C. Bachoud-Levi, N. DÃĪglon, J. P. Lefaucheur, L. Winkel, S. Palfi, J. P. Nguyen, C. Bourdet, V. Gaura, P. Remy, P. BrugiÃĺres, M.-F. Boisse, S. Baudic, P. Cesaro, P. Hantraye, P. Aebischer, and M. Peschanski. Neuroprotective gene therapy for huntington's disease, using polymer-encapsulated cells engineered to secrete human ciliary neurotrophic factor: results of a phase i study. *Human gene therapy*, 15:968–975, Oct. 2004.

[25] R. M. Bonelli and M. F. Beal. Huntington's disease. *Handb Clin Neurol*, 106:507–526, 2012.

[26] C. V. Borlongan, T. K. Koutouzis, T. B. Freeman, D. W. Cahill, and P. R. Sanberg. Behavioral pathology induced by repeated systemic injections of 3-nitropropionic acid mimics the motoric symptoms of Huntington's disease. *Brain Res.*, 697(1-2):254–257, Oct 1995.

[27] D. E. Bredesen, R. V. Rao, and P. Mehlen. Cell death in the nervous system. *Nature*, 443:796–802, Oct. 2006.

[28] H. R. Brignull, J. F. Morley, S. M. Garcia, and R. I. Morimoto. Modeling polyglutamine pathogenesis in c. elegans. *Methods in enzymology*, 412:256–282, 2006.

[29] C. Burger, F. N. Nguyen, J. Deng, and R. J. Mandel. Systemic mannitol-induced hyperosmolality amplifies rAAV2-mediated striatal transduction to a greater extent than local co-infusion. *Mol. Ther.*, 11(2):327–331, 2005.

[30] J.-M. Burgunder, M. Guttman, S. Perlman, N. Goodman, D. P. van Kammen, and L. Goodman. An international survey-based algorithm for the pharmacologic treatment of chorea in huntington's disease. *PLoS currents*, 3:RRN1260, Aug. 2011.

[31] P. Calabresi, M. De Murtas, A. Pisani, A. Stefani, G. Sancesario, N. B. Mercuri, and G. Bernardi. Vulnerability of medium spiny striatal neurons to glutamate: role of Na+/K+ ATPase. *Eur. J. Neurosci.*, 7(8):1674–1683, Aug 1995.

[32] S. Camnasio, A. Delli Carri, A. Lombardo, I. Grad, C. Mariotti, A. Castucci, B. Rozell, P. Lo Riso, V. Castiglioni, C. Zuccato, C. Rochon, Y. Takashima, G. Diaferia, I. Biunno, C. Gellera, M. Jaconi, A. Smith, O. Hovatta, L. Naldini, S. Di Donato, A. Feki, and E. Cattaneo. The first reported generation of several induced pluripotent stem cell lines from homozygous and heterozygous huntington's disease patients demonstrates mutation related enhanced lysosomal activity. *Neurobiology of disease*, 46:41–51, Apr. 2012.

[33] A. E. Carpenter, T. R. Jones, M. R. Lamprecht, C. Clarke, I. H. Kang, O. Friman, D. A. Guertin, J. H. Chang, R. A. Lindquist, J. Moffat, P. Golland, and D. M. Sabatini. CellProfiler: image analysis software for identifying and quantifying cell phenotypes. *Genome Biol.*, 7(10):R100, 2006.

[34] R. J. Carter, L. A. Lione, T. Humby, L. Mangiarini, A. Mahal, G. P. Bates, S. B. Dunnett, and A. J. Morton. Characterization of progressive motor deficits in mice

transgenic for the human Huntington's disease mutation. *J. Neurosci.*, 19(8):3248–3257, 1999.

[35] M. Casanova, M. Pasternak, F. El Marjou, P. Le Baccon, A. V. Probst, and G. Almouzni. Heterochromatin reorganization during early mouse development requires a single-stranded noncoding transcript. *Cell reports*, 4:1156–1167, Sept. 2013.

[36] E. Cattaneo, D. Rigamonti, D. Goffredo, C. Zuccato, F. Squitieri, and S. Sipione. Loss of normal huntingtin function: new developments in Huntington's disease research. *Trends Neurosci.*, 24(3):182–188, Mar 2001.

[37] P. Chaurand, M. E. Sanders, R. A. Jensen, and R. M. Caprioli. Proteomics in diagnostic pathology: profiling and imaging proteins directly in tissue sections. *Am. J. Pathol.*, 165(4):1057–1068, Oct 2004.

[38] L.-Y. Chen, Y.-C. Huang, S.-T. Huang, Y.-C. Hsieh, H.-H. Guan, N.-C. Chen, P. Chuankhayan, M. Yoshimura, M.-H. Tai, and C.-J. Chen. Domain swapping and smyd1 interactions with the pwwp domain of human hepatoma-derived growth factor. *Scientific reports*, 8:287, Jan. 2018.

[39] S.-C. Chen, T.-H. Hu, C.-C. Huang, M.-L. Kung, T.-H. Chu, L.-N. Yi, S.-T. Huang, H.-H. Chan, J.-H. Chuang, L.-F. Liu, H.-C. Wu, D.-C. Wu, M.-C. Chang, and M.-H. Tai. Hepatoma-derived growth factor/nucleolin axis as a novel oncogenic pathway in liver carcinogenesis. *Oncotarget*, 6:16253–16270, June 2015.

[40] M.-C. Chiang, C.-G. Juo, H.-H. Chang, H.-M. Chen, E. C. Yi, and Y. Chern. Systematic uncovering of multiple pathways underlying the pathology of huntington disease by an acid-cleavable isotope-coded affinity tag approach. *Molecular & cellular proteomics : MCP*, 6:781–797, May 2007.

[41] E. Choleris, A. W. Thomas, M. Kavaliers, and F. S. Prato. A detailed ethological analysis of the mouse open field test: effects of diazepam, chlordiazepoxide and an extremely low frequency pulsed magnetic field. *Neuroscience and biobehavioral reviews*, 25:235–260, May 2001.

[42] F. Cicchetti, L. Prensa, Y. Wu, and A. Parent. Chemical anatomy of striatal interneurons in normal individuals and in patients with huntington's disease. *Brain research. Brain research reviews*, 34:80–101, Nov. 2000.

[43] A. Ciechanover and P. Brundin. The ubiquitin proteasome system in neurodegenerative diseases: sometimes the chicken, sometimes the egg. *Neuron*, 40(2):427–446, Oct 2003.

[44] P. M. Conneally. Huntington disease: genetics and epidemiology. *Am. J. Hum. Genet.*, 36(3):506–526, May 1984.

[45] J. Cornett, F. Cao, C. E. Wang, C. A. Ross, G. P. Bates, S. H. Li, and X. J. Li. Polyglutamine expansion of huntingtin impairs its nuclear export. *Nat. Genet.*, 37(2):198–204, Feb 2005.

[46] S. Couly, A. Paucard, N. Bonneaud, T. Maurice, L. Benigno, C. Jourdan, C. Cohen-Solal, M. Vignes, and F. Maschat. Improvement of bdnf signalling by p42 peptide in huntington's disease. *Human molecular genetics*, June 2018.

[47] J. T. Coyle and R. Schwarcz. Lesion of striatal neurones with kainic acid provides a model for Huntington's chorea. *Nature*, 263(5574):244–246, Sep 1976.

[48] Z. R. Crook and D. E. Housman. Dysregulation of dopamine receptor D2 as a sensitive measure for Huntington disease pathology in model mice. *Proc. Natl. Acad. Sci. U.S.A.*, 109(19):7487–7492, May 2012.

[49] A. M. Cuervo, E. S. P. Wong, and M. Martinez-Vicente. Protein degradation, aggregation, and misfolding. *Movement disorders : official journal of the Movement Disorder Society*, 25 Suppl 1:S49–S54, 2010.

[50] A. Cumberworth, G. Lamour, M. M. Babu, and J. Gsponer. Promiscuity as a functional trait: intrinsically disordered regions as central players of interactomes. *The Biochemical journal*, 454:361–369, Sept. 2013.

[51] D. M. Cummings, Y. Alaghband, M. A. Hickey, P. R. Joshi, S. C. Hong, C. Zhu, T. K. Ando, V. M. Andre, C. Cepeda, J. B. Watson, and M. S. Levine. A critical window of CAG repeat-length correlates with phenotype severity in the R6/2 mouse model of Huntington's disease. *J. Neurophysiol.*, 107(2):677–691, 2012.

[52] A. Dalrymple, E. J. Wild, R. Joubert, K. Sathasivam, M. Bjoerkqvist, A. Petersen, G. S. Jackson, J. D. Isaacs, M. Kristiansen, G. P. Bates, B. R. Leavitt, G. Keir, M. Ward, and S. J. Tabrizi. Proteomic profiling of plasma in huntington's disease reveals neuroinflammatory activation and biomarker candidates. *Journal of proteome research*, 6:2833–2840, July 2007.

[53] P. Davidsson and M. SjÃűgren. The use of proteomics in biomarker discovery in neurodegenerative diseases. *Disease markers*, 21:81–92, 2005.

[54] S. W. Davies, M. Turmaine, B. A. Cozens, M. DiFiglia, A. H. Sharp, C. A. Ross, E. Scherzinger, E. E. Wanker, L. Mangiarini, and G. P. Bates. Formation of neuronal

intranuclear inclusions underlies the neurological dysfunction in mice transgenic for the HD mutation. *Cell*, 90(3):537–548, 1997.

[55] S. M. de la Monte, J. P. Vonsattel, and E. P. Richardson. Morphometric demonstration of atrophic changes in the cerebral cortex, white matter, and neostriatum in Huntington's disease. *J. Neuropathol. Exp. Neurol.*, 47(5):516–525, Sep 1988.

[56] S. M. de la Monte, J. P. Vonsattel, and E. P. Richardson. Morphometric demonstration of atrophic changes in the cerebral cortex, white matter, and neostriatum in huntington's disease. *Journal of neuropathology and experimental neurology*, 47:516–525, Sept. 1988.

[57] B. Dehay and A. Bertolotti. Critical role of the proline-rich region in huntingtin for aggregation and cytotoxicity in yeast. *The Journal of biological chemistry*, 281:35608–35615, Nov. 2006.

[58] F. Dietz, S. Franken, K. Yoshida, H. Nakamura, J. Kappler, and V. Gieselmann. The family of hepatoma-derived growth factor proteins: characterization of a new member hrp-4 and classification of its subfamilies. *The Biochemical journal*, 366:491–500, Sept. 2002.

[59] M. DiFiglia. Excitotoxic injury of the neostriatum: a model for Huntington's disease. *Trends Neurosci.*, 13(7):286–289, Jul 1990.

[60] M. DiFiglia, E. Sapp, K. Chase, C. Schwarz, A. Meloni, C. Young, E. Martin, J. P. Vonsattel, R. Carraway, and S. A. Reeves. Huntingtin is a cytoplasmic protein associated with vesicles in human and rat brain neurons. *Neuron*, 14(5):1075–1081, May 1995.

[61] M. DiFiglia, E. Sapp, K. O. Chase, S. W. Davies, G. P. Bates, J. P. Vonsattel, and N. Aronin. Aggregation of huntingtin in neuronal intranuclear inclusions and dystrophic neurites in brain. *Science*, 277(5334):1990–1993, Sep 1997.

[62] L. Dodds, J. Chen, K. Berggren, and J. Fox. Characterization of striatal neuronal loss and atrophy in the r6/2 mouse model of huntington's disease. *PLoS currents*, 6, Jan. 2014.

[63] I. Dragatsis, M. S. Levine, and S. Zeitlin. Inactivation of Hdh in the brain and testis results in progressive neurodegeneration and sterility in mice. *Nat. Genet.*, 26(3):300–306, Nov 2000.

[64] A. W. Dunah, H. Jeong, A. Griffin, Y. M. Kim, D. G. Standaert, S. M. Hersch, M. M. Mouradian, A. B. Young, N. Tanese, and D. Krainc. Sp1 and TAFII130 transcriptional activity disrupted in early Huntington's disease. *Science*, 296(5576):2238–2243, Jun 2002.

[65] M. Duyao, C. Ambrose, R. Myers, A. Novelletto, F. Persichetti, M. Frontali, S. Folstein, C. Ross, M. Franz, and M. Abbott. Trinucleotide repeat length instability and age of onset in Huntington's disease. *Nat. Genet.*, 4(4):387–392, Aug 1993.

[66] M. P. Duyao, A. B. Auerbach, A. Ryan, F. Persichetti, G. T. Barnes, S. M. McNeil, P. Ge, J. P. Vonsattel, J. F. Gusella, and A. L. Joyner. Inactivation of the mouse Huntington's disease gene homolog Hdh. *Science*, 269(5222):407–410, Jul 1995.

[67] H. M. El-Tahir, F. Dietz, R. Dringen, K. Schwabe, K. Strenge, S. Kelm, M. M. Abouzied, V. Gieselmann, and S. Franken. Expression of hepatoma-derived growth factor family members in the adult central nervous system. *BMC neuroscience*, 7:6, Jan. 2006.

[68] S. Elias, M. S. Thion, H. Yu, C. M. Sousa, C. Lasgi, X. Morin, and S. Humbert. Huntingtin regulates mammary stem cell division and differentiation. *Stem Cell Reports*, 2(4):491–506, Apr 2014.

[69] D. F. Emerich, S. R. Winn, P. M. Hantraye, M. Peschanski, E. Y. Chen, Y. Chu, P. McDermott, E. E. Baetge, and J. H. Kordower. Protective effect of encapsulated cells producing neurotrophic factor cntf in a monkey model of huntington's disease. *Nature*, 386:395–399, Mar. 1997.

[70] H. Enomoto, H. Nakamura, W. Liu, and S. Nishiguchi. Hepatoma-derived growth factor: Its possible involvement in the progression of hepatocellular carcinoma. *International journal of molecular sciences*, 16:14086–14097, June 2015.

[71] H. Enomoto, K. Yoshida, Y. Kishima, Y. Okuda, and H. Nakamura. Participation of hepatoma-derived growth factor in the regulation of fetal hepatocyte proliferation. *Journal of gastroenterology*, 37 Suppl 14:158–161, Nov. 2002.

[72] A. D. Everett. Identification, cloning, and developmental expression of hepatoma-derived growth factor in the developing rat heart. *Developmental dynamics : an official publication of the American Association of Anatomists*, 222:450–458, Nov. 2001.

[73] A. D. Everett, D. R. Lobe, M. E. Matsumura, H. Nakamura, and C. A. McNamara. Hepatoma-derived growth factor stimulates smooth muscle cell growth and is ex-

pressed in vascular development. *The Journal of clinical investigation*, 105:567–575, Mar. 2000.

[74] F. Fiumara, L. Fioriti, E. R. Kandel, and W. A. Hendrickson. Essential role of coiled coils for aggregation and activity of Q/N-rich prions and PolyQ proteins. *Cell*, 143(7):1121–1135, Dec 2010.

[75] D. Fleck, F. van Bebber, A. Colombo, C. Galante, B. M. Schwenk, L. Rabe, H. Hampel, B. Novak, E. Kremmer, S. Tahirovic, D. Edbauer, S. F. Lichtenthaler, B. Schmid, M. Willem, and C. Haass. Dual cleavage of neuregulin 1 type III by BACE1 and ADAM17 liberates its EGF-like domain and allows paracrine signaling. *J. Neurosci.*, 33(18):7856–7869, 2013.

[76] J. Gafni, E. Hermel, J. E. Young, C. L. Wellington, M. R. Hayden, and L. M. Ellerby. Inhibition of calpain cleavage of huntingtin reduces toxicity: accumulation of calpain/caspase fragments in the nucleus. *J. Biol. Chem.*, 279(19):20211–20220, May 2004.

[77] Y.-G. Gao, X.-Z. Yan, A.-X. Song, Y.-G. Chang, X.-C. Gao, N. Jiang, Q. Zhang, and H.-Y. Hu. Structural insights into the specific binding of huntingtin proline-rich region with the sh3 and ww domains. *Structure (London, England : 1993)*, 14:1755–1765, Dec. 2006.

[78] G. Garcia-Cardena, R. Fan, V. Shah, R. Sorrentino, G. Cirino, A. Papapetropoulos, and W. C. Sessa. Dynamic activation of endothelial nitric oxide synthase by Hsp90. *Nature*, 392(6678):821–824, 1998.

[79] L. R. Gauthier, B. C. Charrin, M. Borrell-Pages, J. P. Dompierre, H. Rangone, F. P. Cordelieres, J. De Mey, M. E. MacDonald, V. Lessmann, S. Humbert, and F. Saudou. Huntingtin controls neurotrophic support and survival of neurons by enhancing BDNF vesicular transport along microtubules. *Cell*, 118(1):127–138, Jul 2004.

[80] H. P. Gerber, K. Seipel, O. Georgiev, M. Hofferer, M. Hug, S. Rusconi, and W. Schaffner. Transcriptional activation modulated by homopolymeric glutamine and proline stretches. *Science*, 263(5148):808–811, Feb 1994.

[81] S. Gines, M. Bosch, S. Marco, N. Gavalda, M. Diaz-Hernandez, J. J. Lucas, J. M. Canals, and J. Alberch. Reduced expression of the TrkB receptor in Huntington's disease mouse models and in human brain. *Eur. J. Neurosci.*, 23(3):649–658, Feb 2006.

[82] Y. P. Goldberg, B. Kremer, S. E. Andrew, J. Theilmann, R. K. Graham, F. Squitieri, H. Telenius, S. Adam, A. Sajoo, and E. Starr. Molecular analysis of new mutations for huntington's disease: intermediate alleles and sex of origin effects. *Nature genetics*, 5:174–179, Oct. 1993.

[83] Y. P. Goldberg, D. W. Nicholson, D. M. Rasper, M. A. Kalchman, H. B. Koide, R. K. Graham, M. Bromm, P. Kazemi-Esfarjani, N. A. Thornberry, J. P. Vaillancourt, and M. R. Hayden. Cleavage of huntingtin by apopain, a proapoptotic cysteine protease, is modulated by the polyglutamine tract. *Nat. Genet.*, 13(4):442–449, Aug 1996.

[84] E. Gomez-Tortosa, M. E. MacDonald, J. C. Friend, S. A. Taylor, L. J. Weiler, L. A. Cupples, J. Srinidhi, J. F. Gusella, E. D. Bird, J. P. Vonsattel, and R. H. Myers. Quantitative neuropathological changes in presymptomatic Huntington's disease. *Ann. Neurol.*, 49(1):29–34, Jan 2001.

[85] A. V. Goula, A. Stys, J. P. Chan, Y. Trottier, R. Festenstein, and K. Merienne. Transcription elongation and tissue-specific somatic CAG instability. *PLoS Genet.*, 8(11):e1003051, 2012.

[86] J. Govin, E. Escoffier, S. Rousseaux, L. Kuhn, M. Ferro, J. ThÃĬvenon, R. Catena, I. Davidson, J. Garin, S. Khochbin, and C. Caron. Pericentric heterochromatin reprogramming by new histone variants during mouse spermiogenesis. *The Journal of cell biology*, 176:283–294, Jan. 2007.

[87] S. F. Graham, P. Kumar, R. O. Bahado-Singh, A. Robinson, D. Mann, and B. D. Green. Novel metabolite biomarkers of huntington's disease as detected by high-resolution mass spectrometry. *Journal of proteome research*, 15:1592–1601, May 2016.

[88] L. A. Greene and A. S. Tischler. Establishment of a noradrenergic clonal line of rat adrenal pheochromocytoma cells which respond to nerve growth factor. *Proceedings of the National Academy of Sciences of the United States of America*, 73:2424–2428, July 1976.

[89] J. C. Grima, J. G. Daigle, N. Arbez, K. C. Cunningham, K. Zhang, J. Ochaba, C. Geater, E. Morozko, J. Stocksdale, J. C. Glatzer, J. T. Pham, I. Ahmed, Q. Peng, H. Wadhwa, O. Pletnikova, J. C. Troncoso, W. Duan, S. H. Snyder, L. P. W. Ranum, L. M. Thompson, T. E. Lloyd, C. A. Ross, and J. D. Rothstein. Mutant Huntingtin Disrupts the Nuclear Pore Complex. *Neuron*, 94(1):93–107, Apr 2017.

[90] X. Gu, J. P. Cantle, E. R. Greiner, C. Y. Lee, A. M. Barth, F. Gao, C. S. Park, Z. Zhang, S. Sandoval-Miller, R. L. Zhang, M. Diamond, I. Mody, G. Coppola, and X. W. Yang. N17 Modifies mutant Huntingtin nuclear pathogenesis and severity of disease in HD BAC transgenic mice. *Neuron*, 85(4):726–741, Feb 2015.

[91] M. Guenatri, D. Bailly, C. Maison, and G. Almouzni. Mouse centric and pericentric satellite repeats form distinct functional heterochromatin. *The Journal of cell biology*, 166:493–505, Aug. 2004.

[92] Q. Guo, B. Huang, C. J., and et al. The cryo-electron microscopy structure of huntingtin. *Nature*, 555:117–120, 2018.

[93] J. F. Gusella, N. S. Wexler, P. M. Conneally, S. L. Naylor, M. A. Anderson, R. E. Tanzi, P. C. Watkins, K. Ottina, M. R. Wallace, and A. Y. Sakaguchi. A polymorphic DNA marker genetically linked to Huntington's disease. *Nature*, 306(5940):234–238, 1983.

[94] C. A. Gutekunst, S. H. Li, H. Yi, J. S. Mulroy, S. Kuemmerle, R. Jones, D. Rye, R. J. Ferrante, S. M. Hersch, and X. J. Li. Nuclear and neuropil aggregates in Huntington's disease: relationship to neuropathology. *J. Neurosci.*, 19(7):2522–2534, Apr 1999.

[95] Z. H., R. U., P. E., B. G., A. U., B. K., and B. A. Clinical proteomics in neurodegenerative disorders. *Acta Neurologica Scandinavica*, 118(1):1–11, 2008.

[96] C. Haass and D. J. Selkoe. Soluble protein oligomers in neurodegeneration: lessons from the alzheimer's amyloid beta-peptide. *Nature reviews. Molecular cell biology*, 8:101–112, Feb. 2007.

[97] A. S. Hackam, R. Singaraja, T. Zhang, L. Gan, and M. R. Hayden. In vitro evidence for both the nucleus and cytoplasm as subcellular sites of pathogenesis in huntington's disease. *Human molecular genetics*, 8:25–33, Jan. 1999.

[98] C. M. Hales, E. B. Dammer, Q. Deng, D. M. Duong, M. Gearing, J. C. Troncoso, M. Thambisetty, J. J. Lah, J. M. Shulman, A. I. Levey, and N. T. Seyfried. Changes in the detergent-insoluble brain proteome linked to amyloid and tau in alzheimer's disease progression. *Proteomics*, 16:3042–3053, Dec. 2016.

[99] I. Han, Y. You, J. H. Kordower, S. T. Brady, and G. A. Morfini. Differential vulnerability of neurons in Huntington's disease: the role of cell type-specific features. *J. Neurochem.*, 113(5):1073–1091, Jun 2010.

[100] D. G. Hay, K. Sathasivam, S. Tobaben, B. Stahl, M. Marber, R. Mestril, A. Mahal, D. L. Smith, B. Woodman, and G. P. Bates. Altered proteasomal function due to the expression of polyglutamine-expanded truncated N-terminal huntingtin induces apoptosis by caspase activation through mitochondrial cytochrome c release. *Hum. Mol. Genet.*, 10(10):1049–1059, 2001.

[101] D. G. Hay, K. Sathasivam, S. Tobaben, B. Stahl, M. Marber, R. Mestril, A. Mahal, D. L. Smith, B. Woodman, and G. P. Bates. Progressive decrease in chaperone protein levels in a mouse model of Huntington's disease and induction of stress proteins as a therapeutic approach. *Hum. Mol. Genet.*, 13(13):1389–1405, Jul 2004.

[102] H. Heinsen, M. Strik, M. Bauer, K. Luther, G. Ulmar, D. Gangnus, G. Jungkunz, W. Eisenmenger, and M. Gotz. Cortical and striatal neurone number in Huntington's disease. *Acta Neuropathol.*, 88(4):320–333, 1994.

[103] M. A. Hickey, K. Gallant, G. G. Gross, M. S. Levine, and M.-F. Chesselet. Early behavioral deficits in r6/2 mice suitable for use in preclinical drug testing. *Neurobiology of disease*, 20:1–11, Oct. 2005.

[104] P. Hilditch-Maguire, F. Trettel, L. A. Passani, A. Auerbach, F. Persichetti, and M. E. MacDonald. Huntingtin: an iron-regulated protein essential for normal nuclear and perinuclear organelles. *Hum. Mol. Genet.*, 9(19):2789–2797, Nov 2000.

[105] E. Hockly, B. Woodman, A. Mahal, C. M. Lewis, and G. Bates. Standardization and statistical approaches to therapeutic trials in the R6/2 mouse. *Brain Res. Bull.*, 61(5):469–479, 2003.

[106] A. Hollander, P. M. D'Onofrio, M. M. Magharious, M. D. Lysko, and P. D. Koeberle. Quantitative retinal protein analysis after optic nerve transection reveals a neuroprotective role for hepatoma-derived growth factor on injured retinal ganglion cells. *Investigative ophthalmology & visual science*, 53:3973–3989, June 2012.

[107] F. Hosp, S. Gutierrez-Angel, M. H. Schaefer, J. Cox, F. Meissner, M. S. Hipp, F. U. Hartl, R. Klein, I. Dudanova, and M. Mann. Spatiotemporal Proteomic Profiling of Huntington's Disease Inclusions Reveals Widespread Loss of Protein Function. *Cell Rep*, 21(8):2291–2303, Nov 2017.

[108] F. Hosp, H. Vossfeldt, M. Heinig, D. Vasiljevic, A. Arumughan, E. Wyler, and et al. Quantitative interaction proteomics of neurodegenerative disease proteins. *Cell Rep*, 11(7):1134–1146, May 2015.

[109] T.-H. Hu, C.-C. Huang, L.-F. Liu, P.-R. Lin, S.-Y. Liu, H.-W. Chang, C.-S. Changchien, C.-M. Lee, J.-H. Chuang, and M. H. Tai. Expression of hepatoma-derived growth factor in hepatocellular carcinoma. *Cancer*, 98:1444–1456, Oct. 2003.

[110] W.-J. Huang, W.-W. Chen, and X. Zhang. Huntington's disease: Molecular basis of pathology and status of current therapeutic approaches. *Experimental and therapeutic medicine*, 12:1951–1956, Oct. 2016.

[111] P. E. Hughes, T. Alexi, M. Walton, C. E. Williams, M. Dragunow, R. G. Clark, and P. D. Gluckman. Activity and injury-dependent expression of inducible transcription factors, growth factors and apoptosis-related genes within the central nervous system. *Progress in neurobiology*, 57:421–450, Feb. 1999.

[112] S. Humbert, E. A. Bryson, F. P. CordeliÃÍres, N. C. Connors, S. R. Datta, S. Finkbeiner, M. E. Greenberg, and F. Saudou. The igf-1/akt pathway is neuroprotective in huntington's disease and involves huntingtin phosphorylation by akt. *Developmental cell*, 2:831–837, June 2002.

[113] Y.-L. Hung, H.-J. Lee, I. Jiang, S.-C. Lin, W.-C. Lo, Y.-J. Lin, and S.-C. Sue. The first residue of the pwwp motif modulates hath domain binding, stability, and protein-protein interaction. *Biochemistry*, 54:4063–4074, July 2015.

[114] G. Huntington and G. Huntington. On chorea. George Huntington, M.D. *J Neuropsychiatry Clin Neurosci*, 15(1):109–112, 2003.

[115] M. S. Hurlbert, W. Zhou, C. Wasmeier, F. G. Kaddis, J. C. Hutton, and C. R. Freed. Mice transgenic for an expanded CAG repeat in the Huntington's disease gene develop diabetes. *Diabetes*, 48(3):649–651, Mar 1999.

[116] S. Igarashi, H. Morita, K. M. Bennett, Y. Tanaka, S. Engelender, M. F. Peters, J. K. Cooper, J. D. Wood, A. Sawa, and C. A. Ross. Inducible pc12 cell model of huntington's disease shows toxicity and decreased histone acetylation. *Neuroreport*, 14:565–568, Mar. 2003.

[117] H. iPSC Consortium. Developmental alterations in huntington's disease neural cells and pharmacological rescue in cells and mice. *Nature neuroscience*, 20:648–660, May 2017.

[118] J. C. Jacobsen, C. S. Bawden, S. R. Rudiger, C. J. McLaughlan, S. J. Reid, H. J. Waldvogel, M. E. MacDonald, J. F. Gusella, S. K. Walker, J. M. Kelly, G. C. Webb,

R. L. M. Faull, M. I. Rees, and R. G. Snell. An ovine transgenic huntington's disease model. *Human molecular genetics*, 19:1873–1882, May 2010.

[119] J. C. Jacobsen, S. Erdin, C. Chiang, C. Hanscom, R. R. Handley, D. D. Barker, A. Stortchevoi, I. Blumenthal, S. J. Reid, R. G. Snell, M. E. MacDonald, A. J. Morton, C. Ernst, J. F. Gusella, and M. E. Talkowski. Potential molecular consequences of transgene integration: The r6/2 mouse example. *Scientific reports*, 7:41120, Jan. 2017.

[120] A. H. Jansen, M. van Hal, I. C. Op den Kelder, R. T. Meier, A. A. de Ruiter, M. H. Schut, D. L. Smith, C. Grit, N. Brouwer, W. Kamphuis, H. W. Boddeke, W. F. den Dunnen, W. M. van Roon, G. P. Bates, E. M. Hol, and E. A. Reits. Frequency of nuclear mutant huntingtin inclusion formation in neurons and glia is cell-type-specific. *Glia*, 65(1):50–61, 01 2017.

[121] M. Jiang and G. Chen. High Ca2+-phosphate transfection efficiency in low-density neuronal cultures. *Nat Protoc*, 1(2):695–700, 2006.

[122] K. Jin, M. LaFevre-Bernt, Y. Sun, S. Chen, J. Gafni, D. Crippen, A. Logvinova, C. A. Ross, D. A. Greenberg, and L. M. Ellerby. Fgf-2 promotes neurogenesis and neuroprotection and prolongs survival in a transgenic mouse model of huntington's disease. *Proceedings of the National Academy of Sciences of the United States of America*, 102:18189–18194, Dec. 2005.

[123] T. R. Jones, I. H. Kang, D. B. Wheeler, R. A. Lindquist, A. Papallo, D. M. Sabatini, P. Golland, and A. E. Carpenter. Cellprofiler analyst: data exploration and analysis software for complex image-based screens. *BMC bioinformatics*, 9:482, Nov. 2008.

[124] C. L. Julien, J. C. Thompson, S. Wild, P. Yardumian, J. S. Snowden, G. Turner, and D. Craufurd. Psychiatric disorders in preclinical Huntington's disease. *J. Neurol. Neurosurg. Psychiatry*, 78(9):939–943, Sep 2007.

[125] I. Kanazawa, H. Sasaki, O. Muramoto, M. Matsushita, T. Mizutani, K. Iwabuchi, T. Ikeda, and N. Takahata. Studies on neurotransmitter markers and striatal neuronal cell density in Huntington's disease and dentatorubropallidoluysian atrophy. *J. Neurol. Sci.*, 70(2):151–165, Sep 1985.

[126] M. Kato, T. W. Han, S. Xie, K. Shi, X. Du, L. C. Wu, H. Mirzaei, E. J. Goldsmith, J. Longgood, J. Pei, N. V. Grishin, D. E. Frantz, J. W. Schneider, S. Chen, L. Li, M. R. Sawaya, D. Eisenberg, R. Tycko, and S. L. McKnight. Cell-free formation of RNA granules: low complexity sequence domains form dynamic fibers within hydrogels. *Cell*, 149(4):753–767, May 2012.

[127] B. Kazeminezhad, B. Baradaran, and M. R. Hafezi Ahmadi. The evaluation of hepatoma-derived growth factor in determining of prognosis and estimating of invasive probability of tumoral cells, recurrent, and metastasis of lymphatic glands in breast carcinoma. *Journal of family medicine and primary care*, 6:770–774, 2017.

[128] N. W. Kelley, X. Huang, S. Tam, C. Spiess, J. Frydman, and V. S. Pande. The predicted structure of the headpiece of the Huntingtin protein and its implications on Huntingtin aggregation. *J. Mol. Biol.*, 388(5):919–927, May 2009.

[129] M. W. Kim, Y. Chelliah, S. W. Kim, Z. Otwinowski, and I. Bezprozvanny. Secondary structure of Huntingtin amino-terminal region. *Structure*, 17(9):1205–1212, Sep 2009.

[130] Y. E. Kim, F. Hosp, F. Frottin, H. Ge, M. Mann, M. Hayer-Hartl, and F. U. Hartl. Soluble Oligomers of PolyQ-Expanded Huntingtin Target a Multiplicity of Key Cellular Factors. *Mol. Cell*, 63(6):951–964, Sep 2016.

[131] Y. Kishima, H. Yamamoto, Y. Izumoto, K. Yoshida, H. Enomoto, M. Yamamoto, T. Kuroda, H. Ito, K. Yoshizaki, and H. Nakamura. Hepatoma-derived growth factor stimulates cell growth after translocation to the nucleus by nuclear localization signals. *The Journal of biological chemistry*, 277:10315–10322, Mar. 2002.

[132] M. A. Korolainen, T. A. Nyman, T. Aittokallio, and T. PirttilÃd. An update on clinical proteomics in alzheimer's research. *Journal of Neurochemistry*, 112(6):1386–1414, mar 2010.

[133] C. M. Kosinski, J. H. Cha, A. B. Young, L. Mangiarini, G. Bates, J. Schiefer, and M. Schwarz. Intranuclear inclusions in subtypes of striatal neurons in Huntington's disease transgenic mice. *Neuroreport*, 10(18):3891–3896, Dec 1999.

[134] A. V. Kravitz, L. D. Tye, and A. C. Kreitzer. Distinct roles for direct and indirect pathway striatal neurons in reinforcement. *Nat. Neurosci.*, 15(6):816–818, Jun 2012.

[135] S. Krobitsch and S. Lindquist. Aggregation of huntingtin in yeast varies with the length of the polyglutamine expansion and the expression of chaperone proteins. *Proceedings of the National Academy of Sciences of the United States of America*, 97:1589–1594, Feb. 2000.

[136] A. C. Kroksveen, J. A. Opsahl, T. T. Aye, R. J. Ulvik, and F. S. Berven. Proteomics of human cerebrospinal fluid: discovery and verification of biomarker candidates in neurodegenerative diseases using quantitative proteomics. *J Proteomics*, 74(4):371–388, Apr 2011.

[137] S. Kuemmerle, C. A. Gutekunst, A. M. Klein, X. J. Li, S. H. Li, M. F. Beal, S. M. Hersch, and R. J. Ferrante. Huntington aggregates may not predict neuronal death in Huntington's disease. *Ann. Neurol.*, 46(6):842–849, Dec 1999.

[138] C. Landles, K. Sathasivam, A. Weiss, B. Woodman, H. Moffitt, S. Finkbeiner, B. Sun, J. Gafni, L. M. Ellerby, Y. Trottier, W. G. Richards, A. Osmand, P. Paganetti, and G. P. Bates. Proteolysis of mutant huntingtin produces an exon 1 fragment that accumulates as an aggregated protein in neuronal nuclei in Huntington disease. *J. Biol. Chem.*, 285(12):8808–8823, Mar 2010.

[139] P. Langfelder, J. P. Cantle, D. Chatzopoulou, N. Wang, F. Gao, I. Al-Ramahi, X.-H. Lu, E. M. Ramos, K. El-Zein, Y. Zhao, S. Deverasetty, A. Tebbe, C. Schaab, D. J. Lavery, D. Howland, S. Kwak, J. Botas, J. S. Aaronson, J. Rosinski, G. Coppola, S. Horvath, and X. W. Yang. Integrated genomics and proteomics define huntingtin cag length-dependent networks in mice. *Nature neuroscience*, 19:623–633, Apr. 2016.

[140] J. B. Leverenz, I. Umar, Q. Wang, T. J. Montine, P. J. McMillan, D. W. Tsuang, J. Jin, C. Pan, J. Shin, D. Zhu, and J. Zhang. Proteomic identification of novel proteins in cortical lewy bodies. *Brain pathology (Zurich, Switzerland)*, 17:139–145, Apr. 2007.

[141] E. A. Lewis and G. A. Smith. Using drosophila models of huntington's disease as a translatable tool. *Journal of neuroscience methods*, 265:89–98, May 2016.

[142] D. Li, Z. Han, J. Liu, X. Zhang, J. Ren, L. Yan, H. Liu, and Z. Xu. Upregulation of nucleus hdgf predicts poor prognostic outcome in patients with penile squamous cell carcinoma bypass vegf-a and ki-67. *Medical oncology (Northwood, London, England)*, 30:702, Dec. 2013.

[143] J. Y. Li, N. Popovic, and P. Brundin. The use of the r6 transgenic mouse models of huntington's disease in attempts to develop novel therapeutic strategies. *NeuroRx : the journal of the American Society for Experimental NeuroTherapeutics*, 2:447–464, July 2005.

[144] S. H. Li and X. J. Li. Huntingtin-protein interactions and the pathogenesis of Huntington's disease. *Trends Genet.*, 20(3):146–154, Mar 2004.

[145] X. J. Li, A. L. Orr, and S. Li. Impaired mitochondrial trafficking in Huntington's disease. *Biochim. Biophys. Acta*, 1802(1):62–65, Jan 2010.

[146] V. Limviphuvadh, S. Tanaka, S. Goto, K. Ueda, and M. Kanehisa. The commonality of protein interaction networks determined in neurodegenerative disorders (ndds). *Bioinformatics (Oxford, England)*, 23:2129–2138, Aug. 2007.

[147] L. A. Lione, R. J. Carter, M. J. Hunt, G. P. Bates, A. J. Morton, and S. B. Dunnett. Selective discrimination learning impairments in mice expressing the human Huntington's disease mutation. *J. Neurosci.*, 19(23):10428–10437, Dec 1999.

[148] X. Liu, B. R. Miller, G. V. Rebec, and D. E. Clemmer. Protein expression in the striatum and cortex regions of the brain for a mouse model of huntington's disease. *Journal of proteome research*, 6:3134–3142, Aug. 2007.

[149] A. Lunkes and J. L. Mandel. A cellular model that recapitulates major pathogenic steps of huntington's disease. *Human molecular genetics*, 7:1355–1361, Sept. 1998.

[150] R. Luthi-Carter, B. L. Apostol, A. W. Dunah, M. M. DeJohn, L. A. Farrell, G. P. Bates, A. B. Young, D. G. Standaert, L. M. Thompson, and J. H. Cha. Complex alteration of NMDA receptors in transgenic Huntington's disease mouse brain: analysis of mRNA and protein expression, plasma membrane association, interacting proteins, and phosphorylation. *Neurobiol. Dis.*, 14(3):624–636, Dec 2003.

[151] M. E. MacDonald, C. M. Ambrose, M. P. Duyao, R. H. Myers, C. Lin, L. Srinidhi, G. Barnes, and et al. A novel gene containing a trinucleotide repeat that is expanded and unstable on Huntington's disease chromosomes. The Huntington's Disease Collaborative Research Group. *Cell*, 72(6):971–983, Mar 1993.

[152] S. Machida, P. Chaudhry, T. Shinohara, D. P. Singh, V. N. Reddy, L. T. Chylack, P. A. Sieving, and R. A. Bush. Lens epithelium-derived growth factor promotes photoreceptor survival in light-damaged and rcs rats. *Investigative ophthalmology & visual science*, 42:1087–1095, Apr. 2001.

[153] P. K. Manchanda, G. N. Jones, A. A. Lee, D. R. Pringle, M. Zhang, L. Yu, K. M. La Perle, and L. S. Kirschner. Rac1 is required for Prkar1a-mediated Nf2 suppression in Schwann cell tumors. *Oncogene*, 32(30):3491–3499, 2013.

[154] L. Mangiarini, K. Sathasivam, M. Seller, B. Cozens, A. Harper, C. Hetherington, M. Lawton, Y. Trottier, H. Lehrach, S. W. Davies, and G. P. Bates. Exon 1 of the HD gene with an expanded CAG repeat is sufficient to cause a progressive neurological phenotype in transgenic mice. *Cell*, 87(3):493–506, 1996.

[155] D. M. Mann, R. Oliver, and J. S. Snowden. The topographic distribution of brain atrophy in Huntington's disease and progressive supranuclear palsy. *Acta Neuropathol.*, 85(5):553–559, 1993.

[156] D. Marcellin, D. Abramowski, D. Young, J. Richter, A. Weiss, A. Marcel, J. Maassen, M. Kauffmann, M. Bibel, D. R. Shimshek, R. L. Faull, G. P. Bates, R. R. Kuhn, P. H. Van der Putten, P. Schmid, and G. P. Lotz. Fragments of HdhQ150 mutant huntingtin form a soluble oligomer pool that declines with aggregate deposition upon aging. *PLoS ONE*, 7(9):e44457, 2012.

[157] J. L. Marsh, J. Pallos, and L. M. Thompson. Fly models of huntington's disease. *Human molecular genetics*, 12 Spec No 2:R187–R193, Oct. 2003.

[158] F. J. Martinez, G. A. Pratt, E. L. Van Nostrand, R. Batra, S. C. Huelga, K. Kapeli, P. Freese, S. J. Chun, K. Ling, C. Gelboin-Burkhart, L. Fijany, H. C. Wang, J. K. Nussbacher, S. M. Broski, H. J. Kim, R. Lardelli, B. Sundararaman, J. P. Donohue, A. Javaherian, J. Lykke-Andersen, S. Finkbeiner, C. F. Bennett, M. Ares, C. B. Burge, J. P. Taylor, F. Rigo, and G. W. Yeo. Protein-RNA Networks Regulated by Normal and ALS-Associated Mutant HNRNPA2B1 in the Nervous System. *Neuron*, 92(4):780–795, Nov 2016.

[159] S. Marty, B. MdaP, and B. Berninger. Neurotrophins and activity-dependent plasticity of cortical interneurons. *Trends in neurosciences*, 20:198–202, May 1997.

[160] S. Marubuchi, T. Okuda, K. Tagawa, Y. Enokido, D. Horiuchi, R. Shimokawa, T. Tamura, M.-L. Qi, Y. Eishi, K. Watabe, M. Shibata, M. Nakagawa, and H. Okazawa. Hepatoma-derived growth factor, a new trophic factor for motor neurons, is up-regulated in the spinal cord of pqbp-1 transgenic mice before onset of degeneration. *Journal of neurochemistry*, 99:70–83, Oct. 2006.

[161] R. P. Mason and F. Giorgini. Modeling huntington disease in yeast: perspectives and future directions. *Prion*, 5:269–276, 2011.

[162] H. Matsui, L. R. Lin, D. P. Singh, T. Shinohara, and V. N. Reddy. Lens epithelium-derived growth factor: increased survival and decreased dna breakage of human rpe cells induced by oxidative stress. *Investigative ophthalmology & visual science*, 42:2935–2941, Nov. 2001.

[163] J. C. Mazziotta, M. E. Phelps, J. J. Pahl, S. C. Huang, L. R. Baxter, W. H. Riege, J. M. Hoffman, D. E. Kuhl, A. B. Lanto, and J. A. Wapenski. Reduced cerebral glucose metabolism in asymptomatic subjects at risk for Huntington's disease. *N. Engl. J. Med.*, 316(7):357–362, Feb 1987.

[164] E. A. McCaw, H. Hu, G. T. Gomez, A. L. Hebb, M. E. Kelly, and E. M. Denovan-Wright. Structure, expression and regulation of the cannabinoid receptor gene (CB1) in Huntington's disease transgenic mice. *Eur. J. Biochem.*, 271(23-24):4909–4920, Dec 2004.

[165] P. McColgan and S. J. Tabrizi. Huntington's disease: a clinical review. *European journal of neurology*, 25:24–34, Jan. 2018.

[166] D. P. McGowan, W. van Roon-Mom, H. Holloway, G. P. Bates, L. Mangiarini, G. J. Cooper, R. L. Faull, and R. G. Snell. Amyloid-like inclusions in Huntington's disease. *Neuroscience*, 100(4):677–680, 2000.

[167] C. A. Meade, Y. P. Deng, F. R. Fusco, N. Del Mar, S. Hersch, D. Goldowitz, and A. Reiner. Cellular localization and development of neuronal intranuclear inclusions in striatal and cortical neurons in R6/2 transgenic mice. *J. Comp. Neurol.*, 449(3):241–269, 2002.

[168] L. B. Menalled and M. F. Chesselet. Mouse models of Huntington's disease. *Trends Pharmacol. Sci.*, 23(1):32–39, Jan 2002.

[169] L. B. Menalled, A. E. Kudwa, S. Miller, J. Fitzpatrick, J. Watson-Johnson, N. Keating, M. Ruiz, R. Mushlin, W. Alosio, K. McConnell, D. Connor, C. Murphy, S. Oakeshott, M. Kwan, J. Beltran, A. Ghavami, D. Brunner, L. C. Park, S. Ramboz, and D. Howland. Comprehensive behavioral and molecular characterization of a new knock-in mouse model of huntington's disease: zq175. *PloS one*, 7:e49838, 2012.

[170] G. A. Metz and I. Q. Whishaw. Cortical and subcortical lesions impair skilled walking in the ladder rung walking test: a new task to evaluate fore- and hindlimb stepping, placing, and co-ordination. *Journal of neuroscience methods*, 115:169–179, Apr. 2002.

[171] V. M. Miller, R. F. Nelson, C. M. Gouvion, A. Williams, E. Rodriguez-Lebron, S. Q. Harper, B. L. Davidson, M. R. Rebagliati, and H. L. Paulson. CHIP suppresses polyglutamine aggregation and toxicity in vitro and in vivo. *J. Neurosci.*, 25(40):9152–9161, Oct 2005.

[172] A. J. Milnerwood and L. A. Raymond. Early synaptic pathophysiology in neurodegeneration: insights from Huntington's disease. *Trends Neurosci.*, 33(11):513–523, Nov 2010.

[173] X. Min, J. Wen, L. Zhao, K. Wang, Q. Li, G. Huang, J. Liu, and X. Zhao. Role of hepatoma-derived growth factor in promoting de novo lipogenesis and tumorigenesis in hepatocellular carcinoma. *Molecular oncology*, July 2018.

[174] V. Mittoux, J. M. Joseph, F. Conde, S. Palfi, C. Dautry, T. Poyot, J. Bloch, N. Deglon, S. Ouary, E. A. Nimchinsky, E. Brouillet, P. R. Hof, M. Peschanski, P. Aebischer, and P. Hantraye. Restoration of cognitive and motor functions by ciliary neurotrophic factor in a primate model of huntington's disease. *Human gene therapy*, 11:1177–1187, May 2000.

[175] S. MÃijller, P. Scaffidi, B. Degryse, T. Bonaldi, L. Ronfani, A. Agresti, M. Beltrame, and M. E. Bianchi. New embo members' review: the double life of hmgb1 chromatin protein: architectural factor and extracellular signal. *The EMBO journal*, 20:4337–4340, Aug. 2001.

[176] G. A. Morfini, Y. M. You, S. L. Pollema, A. Kaminska, K. Liu, K. Yoshioka, B. Bjorkblom, E. T. Coffey, C. Bagnato, D. Han, C. F. Huang, G. Banker, G. Pigino, and S. T. Brady. Pathogenic huntingtin inhibits fast axonal transport by activating JNK3 and phosphorylating kinesin. *Nat. Neurosci.*, 12(7):864–871, Jul 2009.

[177] A. J. Morton, R. L. Faull, and J. M. Edwardson. Abnormalities in the synaptic vesicle fusion machinery in Huntington's disease. *Brain Res. Bull.*, 56(2):111–117, Sep 2001.

[178] A. J. Morton, D. Glynn, W. Leavens, Z. Zheng, R. L. Faull, J. N. Skepper, and J. M. Wight. Paradoxical delay in the onset of disease caused by super-long CAG repeat expansions in R6/2 mice. *Neurobiol. Dis.*, 33(3):331–341, 2009.

[179] P. J. Muchowski, G. Schaffar, A. Sittler, E. E. Wanker, M. K. Hayer-Hartl, and F. U. Hartl. Hsp70 and hsp40 chaperones can inhibit self-assembly of polyglutamine proteins into amyloid-like fibrils. *Proceedings of the National Academy of Sciences of the United States of America*, 97:7841–7846, July 2000.

[180] R. H. Myers. Huntington's disease genetics. *NeuroRx*, 1(2):255–262, Apr 2004.

[181] H. Nakamura, Y. Izumoto, H. Kambe, T. Kuroda, T. Mori, K. Kawamura, H. Yamamoto, and T. Kishimoto. Molecular cloning of complementary dna for a novel human hepatoma-derived growth factor. its homology with high mobility group-1 protein. *The Journal of biological chemistry*, 269:25143–25149, Oct. 1994.

[182] H. Nakamura, H. Kambe, T. Egawa, Y. Kimura, H. Ito, E. Hayashi, H. Yamamoto, J. Sato, and S. Kishimoto. Partial purification and characterization of human

hepatoma-derived growth factor. *Clinica chimica acta; international journal of clinical chemistry*, 183:273–284, Aug. 1989.

[183] J. Nasir, S. B. Floresco, J. R. O'Kusky, V. M. Diewert, J. M. Richman, J. Zeisler, A. Borowski, J. D. Marth, A. G. Phillips, and M. R. Hayden. Targeted disruption of the Huntington's disease gene results in embryonic lethality and behavioral and morphological changes in heterozygotes. *Cell*, 81(5):811–823, Jun 1995.

[184] A. Nayak, G. Salt, S. K. Verma, and U. Kishore. Proteomics Approach to Identify Biomarkers in Neurodegenerative Diseases. *Int. Rev. Neurobiol.*, 121:59–86, 2015.

[185] Y. Nekooki-Machida, M. Kurosawa, N. Nukina, K. Ito, T. Oda, and M. Tanaka. Distinct conformations of in vitro and in vivo amyloids of huntingtin-exon1 show different cytotoxicity. *Proc. Natl. Acad. Sci. U.S.A.*, 106(24):9679–9684, Jun 2009.

[186] M. J. Novak and S. J. Tabrizi. Huntington's disease. *BMJ*, 340:c3109, Jun 2010.

[187] J. Nuesse, E.-M. Blumrich, U. Mirastschijski, L. Kappelmann, S. Kelm, and F. Dietz. Intra- or extra-exosomal secretion of hdgf isoforms: the extraordinary function of the hdgf-a n-terminal peptide. *Biological chemistry*, 398:793–811, June 2017.

[188] Y. Okuda, H. Nakamura, K. Yoshida, H. Enomoto, H. Uyama, T. Hirotani, M. Funamoto, H. Ito, A. D. Everett, T. Hada, and I. Kawase. Hepatoma-derived growth factor induces tumorigenesis in vivo through both direct angiogenic activity and induction of vascular endothelial growth factor. *Cancer science*, 94:1034–1041, Dec. 2003.

[189] J. A. Oliver and Q. Al-Awqati. An endothelial growth factor involved in rat renal development. *The Journal of clinical investigation*, 102:1208–1219, Sept. 1998.

[190] M. A. Olshina, L. M. Angley, Y. M. Ramdzan, J. Tang, M. F. Bailey, A. F. Hill, and D. M. Hatters. Tracking mutant huntingtin aggregation kinetics in cells reveals three major populations that include an invariant oligomer pool. *The Journal of biological chemistry*, 285:21807–21816, July 2010.

[191] Z. Ortega, M. Diaz-Hernandez, C. J. Maynard, F. Hernandez, N. P. Dantuma, and J. J. Lucas. Acute polyglutamine expression in inducible mouse model unravels ubiquitin/proteasome system impairment and permanent recovery attributable to aggregate formation. *J. Neurosci.*, 30(10):3675–3688, Mar 2010.

[192] Z. Ortega and J. J. Lucas. Ubiquitin-proteasome system involvement in Huntington's disease. *Front Mol Neurosci*, 7:77, 2014.

[193] G. Ossato, M. A. Digman, C. Aiken, T. Lukacsovich, J. L. Marsh, and E. Gratton. A two-step path to inclusion formation of huntingtin peptides revealed by number and brightness analysis. *Biophys. J.*, 98(12):3078–3085, Jun 2010.

[194] G. Ossato, M. A. Digman, C. Aiken, T. Lukacsovich, J. L. Marsh, and E. Gratton. A two-step path to inclusion formation of huntingtin peptides revealed by number and brightness analysis. *Biophysical journal*, 98:3078–3085, June 2010.

[195] Y. Pan, T. Daito, Y. Sasaki, Y. H. Chung, X. Xing, S. Pondugula, S. J. Swamidass, T. Wang, A. H. Kim, and H. Yano. Inhibition of dna methyltransferases blocks mutant huntingtin-induced neurotoxicity. *Scientific reports*, 6:31022, Aug. 2016.

[196] A. V. Panov, C. A. Gutekunst, B. R. Leavitt, M. R. Hayden, J. R. Burke, W. J. Strittmatter, and J. T. Greenamyre. Early mitochondrial calcium defects in Huntington's disease are a direct effect of polyglutamines. *Nat. Neurosci.*, 5(8):731–736, Aug 2002.

[197] I.-H. Park, N. Arora, H. Huo, N. Maherali, T. Ahfeldt, A. Shimamura, M. W. Lensch, C. Cowan, K. Hochedlinger, and G. Q. Daley. Disease-specific induced pluripotent stem cells. *Cell*, 134:877–886, Sept. 2008.

[198] J. A. Parker, J. B. Connolly, C. Wellington, M. Hayden, J. Dausset, and C. Neri. Expanded polyglutamines in caenorhabditis elegans cause axonal abnormalities and severe dysfunction of plm mechanosensory neurons without cell death. *Proceedings of the National Academy of Sciences of the United States of America*, 98:13318–13323, Nov. 2001.

[199] J. S. Paulsen and J. D. Long. Onset of Huntington's disease: can it be purely cognitive? *Mov. Disord.*, 29(11):1342–1350, Sep 2014.

[200] J. S. Paulsen, R. E. Ready, J. M. Hamilton, M. S. Mega, and J. L. Cummings. Neuropsychiatric aspects of Huntington's disease. *J. Neurol. Neurosurg. Psychiatry*, 71(3):310–314, Sep 2001.

[201] M. F. Perutz, T. Johnson, M. Suzuki, and J. T. Finch. Glutamine repeats as polar zippers: their possible role in inherited neurodegenerative diseases. *Proc. Natl. Acad. Sci. U.S.A.*, 91(12):5355–5358, Jun 1994.

[202] M. Peschanski, A.-C. Bachoud-LÃľvi, and P. Hantraye. Integrating fetal neural transplants into a therapeutic strategy: the example of huntington's disease. *Brain : a journal of neurology*, 127:1219–1228, June 2004.

[203] T. Pringsheim, K. Wiltshire, L. Day, J. Dykeman, T. Steeves, and N. Jette. The incidence and prevalence of Huntington's disease: a systematic reviewand meta-analysis. *Mov. Disord.*, 27(9):1083–1091, Aug 2012.

[204] M.-L. Qi, K. Tagawa, Y. Enokido, N. Yoshimura, Y.-i. Wada, K. Watase, S.-i. Ishiura, I. Kanazawa, J. Botas, M. Saitoe, E. E. Wanker, and H. Okazawa. Proteome analysis of soluble nuclear proteins reveals that hmgb1/2 suppress genotoxic stress in polyglutamine diseases. *Nature cell biology*, 9:402–414, Apr. 2007.

[205] S. Qin and J. Min. Structure and function of the nucleosome-binding pwwp domain. *Trends in biochemical sciences*, 39:536–547, Nov. 2014.

[206] J. Quigley. Juvenile Huntington's Disease: Diagnostic and Treatment Considerations for the Psychiatrist. *Curr Psychiatry Rep*, 19(2):9, Feb 2017.

[207] S. Ramaswamy, J. L. McBride, and J. H. Kordower. Animal models of huntington's disease. *ILAR journal*, 48:356–373, 2007.

[208] I. Rattray, E. Smith, R. Gale, K. Matsumoto, G. P. Bates, and M. Modo. Correlations of behavioral deficits with brain pathology assessed through longitudinal MRI and histopathology in the R6/2 mouse model of HD. *PLoS ONE*, 8(4):e60012, 2013.

[209] M. D. Rawlins, N. S. Wexler, A. R. Wexler, S. J. Tabrizi, I. Douglas, S. J. Evans, and L. Smeeth. The Prevalence of Huntington's Disease. *Neuroepidemiology*, 46(2):144–153, 2016.

[210] T. T. Reed, W. M. Pierce, W. R. Markesbery, and D. A. Butterfield. Proteomic identification of hne-bound proteins in early alzheimer disease: Insights into the role of lipid peroxidation in the progression of ad. *Brain Research*, 1274:66 – 76, 2009.

[211] A. Reiner, R. L. Albin, K. D. Anderson, C. J. D'Amato, J. B. Penney, and A. B. Young. Differential loss of striatal projection neurons in huntington disease. *Proceedings of the National Academy of Sciences of the United States of America*, 85:5733–5737, Aug. 1988.

[212] A. Reiner and Y. P. Deng. Disrupted striatal neuron inputs and outputs in Huntington's disease. *CNS Neurosci Ther*, 24(4):250–280, Apr 2018.

[213] A. Reiner, I. Dragatsis, S. Zeitlin, and D. Goldowitz. Wild-type huntingtin plays a role in brain development and neuronal survival. *Mol. Neurobiol.*, 28(3):259–276, Dec 2003.

[214] E. K. Richfield, K. A. Maguire-Zeiss, H. E. Vonkeman, and P. Voorn. Preferential loss of preproenkephalin versus preprotachykinin neurons from the striatum of Huntington's disease patients. *Ann. Neurol.*, 38(6):852–861, Dec 1995.

[215] R. M. Ridley, C. D. Frith, T. J. Crow, and P. M. Conneally. Anticipation in Huntington's disease is inherited through the male line but may originate in the female. *J. Med. Genet.*, 25(9):589–595, Sep 1988.

[216] D. Rigamonti, J. H. Bauer, C. De-Fraja, L. Conti, S. Sipione, C. Sciorati, E. Clementi, A. Hackam, M. R. Hayden, Y. Li, J. K. Cooper, C. A. Ross, S. Govoni, C. Vincenz, and E. Cattaneo. Wild-type huntingtin protects from apoptosis upstream of caspase-3. *J. Neurosci.*, 20(10):3705–3713, May 2000.

[217] G. B. Rona, E. C. A. Eleutherio, and A. S. Pinheiro. Pwwp domains and their modes of sensing dna and histone methylated lysines. *Biophysical reviews*, 8:63–74, Mar. 2016.

[218] R. A. Roos. Huntington's disease: a clinical review. *Orphanet J Rare Dis*, 5:40, Dec 2010.

[219] G. M. Rubin, M. D. Yandell, J. R. Wortman, G. L. Gabor Miklos, C. R. Nelson, I. K. Hariharan, M. E. Fortini, P. W. Li, R. Apweiler, W. Fleischmann, J. M. Cherry, S. Henikoff, M. P. Skupski, S. Misra, M. Ashburner, E. Birney, M. S. Boguski, T. Brody, P. Brokstein, S. E. Celniker, S. A. Chervitz, D. Coates, A. Cravchik, A. Gabrielian, R. F. Galle, W. M. Gelbart, R. A. George, L. S. Goldstein, F. Gong, P. Guan, N. L. Harris, B. A. Hay, R. A. Hoskins, J. Li, Z. Li, R. O. Hynes, S. J. Jones, P. M. Kuehl, B. Lemaitre, J. T. Littleton, D. K. Morrison, C. Mungall, P. H. O'Farrell, O. K. Pickeral, C. Shue, L. B. Vosshall, J. Zhang, Q. Zhao, X. H. Zheng, and S. Lewis. Comparative genomics of the eukaryotes. *Science (New York, N.Y.)*, 287:2204–2215, Mar. 2000.

[220] F. Rudert, S. Bronner, J. M. Garnier, and P. DollÃĺ. Transcripts from opposite strands of gamma satellite dna are differentially expressed during mouse development. *Mammalian genome : official journal of the International Mammalian Genome Society*, 6:76–83, Feb. 1995.

[221] D. W. Y. Sah and N. Aronin. Oligonucleotide therapeutic approaches for huntington disease. *The Journal of clinical investigation*, 121:500–507, Feb. 2011.

[222] N. Saksouk, E. Simboeck, and J. DÃĺjardin. Constitutive heterochromatin formation and transcription in mammals. *Epigenetics & chromatin*, 8:3, 2015.

[223] P. Samadi, A. Boutet, V. V. Rymar, K. Rawal, J. Maheux, J.-C. Kvann, M. Tomaszewski, F. Beaubien, J. F. Cloutier, D. Levesque, and A. F. Sadikot. Relationship between bdnf expression in major striatal afferents, striatum morphology and motor behavior in the r6/2 mouse model of huntington's disease. *Genes, brain, and behavior*, 12:108–124, Feb. 2013.

[224] P. R. Sanberg, S. F. Calderon, M. Giordano, J. M. Tew, and A. B. Norman. The quinolinic acid model of Huntington's disease: locomotor abnormalities. *Exp. Neurol.*, 105(1):45–53, Jul 1989.

[225] J. Sassone, C. Colciago, G. Cislaghi, V. Silani, and A. Ciammola. Huntington's disease: the current state of research with peripheral tissues. *Experimental neurology*, 219:385–397, Oct. 2009.

[226] F. Saudou, S. Finkbeiner, D. Devys, and M. E. Greenberg. Huntingtin acts in the nucleus to induce apoptosis but death does not correlate with the formation of intranuclear inclusions. *Cell*, 95(1):55–66, Oct 1998.

[227] F. Saudou and S. Humbert. The Biology of Huntingtin. *Neuron*, 89(5):910–926, Mar 2016.

[228] M. H. Schaefer, E. E. Wanker, and M. A. Andrade-Navarro. Evolution and function of CAG/polyglutamine repeats in protein-protein interaction networks. *Nucleic Acids Res.*, 40(10):4273–4287, May 2012.

[229] S. J. Schoenberger, D. Jezdic, R. L. M. Faull, and G. J. S. Cooper. Proteomic analysis of the human brain in huntington's disease indicates pathogenesis by molecular processes linked to other neurodegenerative diseases and to type-2 diabetes. *Journal of Huntington's disease*, 2:89–99, 2013.

[230] M. Schoenfeld, R. H. Myers, L. A. Cupples, B. Berkman, D. S. Sax, and E. Clark. Increased rate of suicide among patients with Huntington's disease. *J. Neurol. Neurosurg. Psychiatry*, 47(12):1283–1287, Dec 1984.

[231] B. Schwanhausser, D. Busse, N. Li, G. Dittmar, J. Schuchhardt, J. Wolf, W. Chen, and M. Selbach. Global quantification of mammalian gene expression control. *Nature*, 473(7347):337–342, May 2011.

[232] A. Sedlmaier, N. Wernert, R. GallitzendÃűrfer, M. M. Abouzied, V. Gieselmann, and S. Franken. Overexpression of hepatoma-derived growth factor in melanocytes does not lead to oncogenic transformation. *BMC cancer*, 11:457, Oct. 2011.

[233] I. S. Seong, E. Ivanova, J. M. Lee, Y. S. Choo, E. Fossale, M. Anderson, J. F. Gusella, J. M. Laramie, R. H. Myers, M. Lesort, and M. E. MacDonald. HD CAG repeat implicates a dominant property of huntingtin in mitochondrial energy metabolism. *Hum. Mol. Genet.*, 14(19):2871–2880, Oct 2005.

[234] H. Shang, A. Danek, B. Landwehrmeyer, and J. M. Burgunder. Huntington's disease: new aspects on phenotype and genotype. *Parkinsonism Relat. Disord.*, 18 Suppl 1:S107–109, Jan 2012.

[235] K. Sharma, S. Schmitt, C. G. Bergner, S. Tyanova, N. Kannaiyan, N. Manrique-Hoyos, K. Kongi, L. Cantuti, U. K. Hanisch, M. A. Philips, M. J. Rossner, M. Mann, and M. Simons. Cell type- and brain region-resolved mouse brain proteome. *Nat. Neurosci.*, 18(12):1819–1831, Dec 2015.

[236] A. H. Sharp, S. J. Loev, G. Schilling, S. H. Li, X. J. Li, J. Bao, M. V. Wagster, J. A. Kotzuk, J. P. Steiner, and A. Lo. Widespread expression of Huntington's disease gene (IT15) protein product. *Neuron*, 14(5):1065–1074, May 1995.

[237] D. I. Shirasaki, E. R. Greiner, I. Al-Ramahi, M. Gray, P. Boontheung, D. H. Geschwind, J. Botas, G. Coppola, S. Horvath, J. A. Loo, and X. W. Yang. Network organization of the huntingtin proteomic interactome in mammalian brain. *Neuron*, 75:41–57, July 2012.

[238] K. A. Sieradzan, A. O. Mechan, L. Jones, E. E. Wanker, N. Nukina, and D. M. Mann. Huntington's disease intranuclear inclusions contain truncated, ubiquitinated huntingtin protein. *Exp. Neurol.*, 156(1):92–99, Mar 1999.

[239] D. A. Simmons. Modulating neurotrophin receptor signaling as a therapeutic strategy for huntington's disease. *Journal of Huntington's disease*, 6:303–325, 2017.

[240] C. Song, G. Perides, and Y. F. Liu. Expression of full-length polyglutamine-expanded huntingtin disrupts growth factor receptor signaling in rat pheochromocytoma (pc12) cells. *The Journal of biological chemistry*, 277:6703–6707, Feb. 2002.

[241] A. L. Southwell, A. Khoshnan, D. E. Dunn, C. W. Bugg, D. C. Lo, and P. H. Patterson. Intrabodies binding the proline-rich domains of mutant huntingtin increase its turnover and reduce neurotoxicity. *The Journal of neuroscience : the official journal of the Society for Neuroscience*, 28:9013–9020, Sept. 2008.

[242] M. Stroedicke, Y. Bounab, N. Strempel, K. Klockmeier, S. Yigit, R. P. Friedrich, G. Chaurasia, S. Li, F. Hesse, S.-P. Riechers, J. Russ, C. Nicoletti, A. Boeddrich,

T. Wiglenda, C. Haenig, S. Schnoegl, D. Fournier, R. K. Graham, M. R. Hayden, S. Sigrist, G. P. Bates, J. Priller, M. A. Andrade-Navarro, M. E. Futschik, and E. E. Wanker. Systematic interaction network filtering identifies crmp1 as a novel suppressor of huntingtin misfolding and neurotoxicity. *Genome research*, 25:701–713, May 2015.

[243] O. Sturman, P.-L. Germain, and J. Bohacek. Exploratory rearing: a context- and stress-sensitive behavior recorded in the open-field test. *Stress (Amsterdam, Netherlands)*, pages 1–10, Feb. 2018.

[244] S.-C. Sue, W.-T. Lee, S.-C. Tien, S.-C. Lee, J.-G. Yu, W.-J. Wu, W.-g. Wu, and T.-h. Huang. Pwwp module of human hepatoma-derived growth factor forms a domain-swapped dimer with much higher affinity for heparin. *Journal of molecular biology*, 367:456–472, Mar. 2007.

[245] M. Swami, A. E. Hendricks, T. Gillis, T. Massood, J. Mysore, R. H. Myers, and V. C. Wheeler. Somatic expansion of the Huntington's disease CAG repeat in the brain is associated with an earlier age of disease onset. *Hum. Mol. Genet.*, 18(16):3039–3047, Aug 2009.

[246] P. Sweeney, H. Park, M. Baumann, J. Dunlop, J. Frydman, R. Kopito, A. McCampbell, G. Leblanc, A. Venkateswaran, A. Nurmi, and R. Hodgson. Protein misfolding in neurodegenerative diseases: implications and strategies. *Translational neurodegeneration*, 6:6, 2017.

[247] A. Taguchi, D. C. Blood, G. del Toro, A. Canet, D. C. Lee, W. Qu, N. Tanji, Y. Lu, E. Lalla, C. Fu, M. A. Hofmann, T. Kislinger, M. Ingram, A. Lu, H. Tanaka, O. Hori, S. Ogawa, D. M. Stern, and A. M. Schmidt. Blockade of rage-amphoterin signalling suppresses tumour growth and metastases. *Nature*, 405:354–360, May 2000.

[248] H. Takano and J. F. Gusella. The predominantly HEAT-like motif structure of huntingtin and its association and coincident nuclear entry with dorsal, an NF-kB/Rel/dorsal family transcription factor. *BMC Neurosci*, 3:15, Oct 2002.

[249] S. Tam, R. Geller, C. Spiess, and J. Frydman. The chaperonin TRiC controls polyglutamine aggregation and toxicity through subunit-specific interactions. *Nat. Cell Biol.*, 8(10):1155–1162, Oct 2006.

[250] M. Tartari, C. Gissi, V. Lo Sardo, C. Zuccato, E. Picardi, G. Pesole, and E. Cattaneo. Phylogenetic comparison of huntingtin homologues reveals the appearance of

a primitive polyq in sea urchin. *Molecular biology and evolution*, 25:330–338, Feb. 2008.

[251] R. Terranova, S. Sauer, M. Merkenschlager, and A. G. Fisher. The reorganisation of constitutive heterochromatin in differentiating muscle requires hdac activity. *Experimental cell research*, 310:344–356, Nov. 2005.

[252] K. Thakar, T. KrÃűcher, S. Savant, D. Gollnast, S. Kelm, and F. Dietz. Secretion of hepatoma-derived growth factor is regulated by n-terminal processing. *Biological chemistry*, 391:1401–1410, Dec. 2010.

[253] A. Tousley and K. B. Kegel-Gleason. Induced Pluripotent Stem Cells in Huntington's Disease Research: Progress and Opportunity. *Journal of Huntington's disease*, 5:99–131, June 2016.

[254] F. Trettel, D. Rigamonti, P. Hilditch-Maguire, V. C. Wheeler, A. H. Sharp, F. Persichetti, E. Cattaneo, and M. E. MacDonald. Dominant phenotypes produced by the hd mutation in sthdh(q111) striatal cells. *Human molecular genetics*, 9:2799–2809, Nov. 2000.

[255] C.-C. Tsai, S.-C. Huang, M. H. Tai, C.-C. C. Chien, C.-C. Huang, and Y.-C. Hsu. Hepatoma-derived growth factor upregulation is correlated with prognostic factors of early-stage cervical adenocarcinoma. *International journal of molecular sciences*, 15:21492–21504, Nov. 2014.

[256] M. Turmaine, A. Raza, A. Mahal, L. Mangiarini, G. P. Bates, and S. W. Davies. Nonapoptotic neurodegeneration in a transgenic mouse model of huntington's disease. *Proceedings of the National Academy of Sciences of the United States of America*, 97:8093–8097, July 2000.

[257] S. Tyanova, T. Temu, P. Sinitcyn, A. Carlson, M. Y. Hein, T. Geiger, M. Mann, and J. Cox. The perseus computational platform for comprehensive analysis of (prote)omics data. *Nature methods*, 13:731–740, Sept. 2016.

[258] M. Uhlen, L. Fagerberg, B. M. HallstrÃűm, C. Lindskog, P. Oksvold, A. Mardinoglu, s. Sivertsson, C. Kampf, E. SjÃűstedt, A. Asplund, I. Olsson, K. Edlund, E. Lundberg, S. Navani, C. A.-K. Szigyarto, J. Odeberg, D. Djureinovic, J. O. Takanen, S. Hober, T. Alm, P.-H. Edqvist, H. Berling, H. Tegel, J. Mulder, J. Rockberg, P. Nilsson, J. M. Schwenk, M. Hamsten, K. von Feilitzen, M. Forsberg, L. Persson, F. Johansson, M. Zwahlen, G. von Heijne, J. Nielsen, and F. PontÃĺn. Proteomics. tissue-based map of the human proteome. *Science (New York, N.Y.)*, 347:1260419, Jan. 2015.

[259] A. Volterra, D. Trotti, S. Floridi, and G. Racagni. Reactive oxygen species inhibit high-affinity glutamate uptake: molecular mechanism and neuropathological implications. *Annals of the New York Academy of Sciences*, 738:153–162, Nov. 1994.

[260] J. P. Vonsattel and M. DiFiglia. Huntington disease. *J. Neuropathol. Exp. Neurol.*, 57(5):369–384, May 1998.

[261] J. P. Vonsattel, R. H. Myers, T. J. Stevens, R. J. Ferrante, E. D. Bird, and E. P. Richardson. Neuropathological classification of Huntington's disease. *J. Neuropathol. Exp. Neurol.*, 44(6):559–577, Nov 1985.

[262] G. H. Wang, K. Mitsui, S. Kotliarova, A. Yamashita, Y. Nagao, S. Tokuhiro, T. Iwatsubo, I. Kanazawa, and N. Nukina. Caspase activation during apoptotic cell death induced by expanded polyglutamine in n2a cells. *Neuroreport*, 10:2435–2438, Aug. 1999.

[263] H.-Q. Wang, Y.-X. Xu, X.-Y. Zhao, H. Zhao, J. Yan, X.-B. Sun, J.-C. Guo, and C.-Q. Zhu. Overexpression of f(0)f(1)-atp synthase alpha suppresses mutant huntingtin aggregation and toxicity in vitro. *Biochemical and biophysical research communications*, 390:1294–1298, Dec. 2009.

[264] L.-h. Wang and Z.-h. Qin. Animal models of huntington's disease: implications in uncovering pathogenic mechanisms and developing therapies. *Acta pharmacologica Sinica*, 27:1287–1302, Oct. 2006.

[265] M. Wegrzynowicz, H. K. Holt, D. B. Friedman, and A. B. Bowman. Changes in the striatal proteome of yac128q mice exhibit gene-environment interactions between mutant huntingtin and manganese. *Journal of proteome research*, 11:1118–1132, Feb. 2012.

[266] C. L. Wellington, L. M. Ellerby, C. A. Gutekunst, D. Rogers, S. Warby, R. K. Graham, O. Loubser, J. van Raamsdonk, R. Singaraja, Y. Z. Yang, J. Gafni, D. Bredesen, S. M. Hersch, B. R. Leavitt, S. Roy, D. W. Nicholson, and M. R. Hayden. Caspase cleavage of mutant huntingtin precedes neurodegeneration in Huntington's disease. *J. Neurosci.*, 22(18):7862–7872, Sep 2002.

[267] H. H. Wetzel, C. R. Gehl, L. Dellefave-Castillo, J. F. Schiffman, K. M. Shannon, J. S. Paulsen, P. Hedges, E. McCusker, S. Pearce, R. Trent, D. Abwender, P. Como, I. Gardiner, C. Hickey, E. Kayson, K. Kieburtz, F. Marshall, N. Pearson, I. Shoulson, C. Zimmerman, E. Louis, K. Marder, C. Moskowitz, C. Polanco, S. Taylor, N. Zubin, C. Brown, M. Guttman, S. Russell, D. Stewart, J. Thomson, D. S.

Sax, M. Saint-Hilaire, J. Gray, C. Hunter, E. Siemers, J. Wojcieszek, T. Dawson, E. Leritz, A. Rosenblatt, M. Sherr, C. Young, T. Ashizawa, J. Beach, J. Jankovic, J. Jaglin, K. Shannon, A. Auchus, J. T. Greennamyre, S. Hersch, R. Jones, D. Olson, J. H. Cha, M. Cudkowicz, W. Koroshetz, G. Rudolf, P. Sexton, A. B. Young, R. Albin, K. Wernette, D. S. Higgins, C. Reider, V. Hunt, F. Walker, B. Gray, R. Hauser, J. Sanchez-Ramos, A. Walker, M. Nance, J. Corey-Bloom, M. Swenson, N. Swerdlow, H. Paulson, R. Rodnizky, L. Vining, J. Paulsen, W. Martin, M. Wieler, A. Faxca, G. Rey, W. Weiner, C. Adler, J. Caviness, C. Lied, S. Newman, B. Shannon, J. Ayan, K. Caplan, J. Celler, K. Marek, M. Hayden, L. Raymond, G. Rohs, L. S. Dure, J. Lane, D. Brown, S. Factor, E. Molho, M. Harrison, C. Manning, E. Rost-Ruffner, J. Adams, R. Cummings, V. Wheelock, R. Dubinsky, C. Gray, A. C. Bachoud-Levi, H. Meierkord, J. Friedman, M. Lannon, J. Lawrence, A. Rubin, R. Schwarz, and D. Oakes. Suicidal ideation in Huntington disease: the role of comorbidity. *Psychiatry Res*, 188(3):372–376, Aug 2011.

[268] N. S. Wexler, J. Lorimer, J. Porter, F. Gomez, C. Moskowitz, E. Shackell, K. Marder, G. Penchaszadeh, S. A. Roberts, J. Gayan, D. Brocklebank, S. S. Cherny, L. R. Cardon, J. Gray, S. R. Dlouhy, S. Wiktorski, M. E. Hodes, P. M. Conneally, J. B. Penney, J. Gusella, J. H. Cha, M. Irizarry, D. Rosas, S. Hersch, Z. Hollingsworth, M. MacDonald, A. B. Young, J. M. Andresen, D. E. Housman, M. M. De Young, E. Bonilla, T. Stillings, A. Negrette, S. R. Snodgrass, M. D. Martinez-Jaurrieta, M. A. Ramos-Arroyo, J. Bickham, J. S. Ramos, F. Marshall, I. Shoulson, G. J. Rey, A. Feigin, N. Arnheim, A. Acevedo-Cruz, L. Acosta, J. Alvir, K. Fischbeck, L. M. Thompson, A. Young, L. Dure, C. J. O'Brien, J. Paulsen, A. Brickman, D. Krch, S. Peery, P. Hogarth, D. S. Higgins, and B. Landwehrmeyer. Venezuelan kindreds reveal that genetic and environmental factors modulate Huntington's disease age of onset. *Proc. Natl. Acad. Sci. U.S.A.*, 101(10):3498–3503, Mar 2004.

[269] A. C. Woerner, F. Frottin, D. Hornburg, L. R. Feng, F. Meissner, M. Patra, J. Tatzelt, M. Mann, K. F. Winklhofer, F. U. Hartl, and M. S. Hipp. Cytoplasmic protein aggregates interfere with nucleocytoplasmic transport of protein and rna. *Science (New York, N.Y.)*, 351:173–176, Jan. 2016.

[270] B. Woodman, R. Butler, C. Landles, M. K. Lupton, J. Tse, E. Hockly, H. Moffitt, K. Sathasivam, and G. P. Bates. The Hdh(Q150/Q150) knock-in mouse model of HD and the R6/2 exon 1 model develop comparable and widespread molecular phenotypes. *Brain Res. Bull.*, 72(2-3):83–97, Apr 2007.

[271] K. J. Wyant, A. J. Ridder, and P. Dayalu. Huntington's Disease-Update on Treatments. *Curr Neurol Neurosci Rep*, 17(4):33, Apr 2017.

[272] A. Wyttenbach, J. Swartz, H. Kita, T. Thykjaer, J. Carmichael, J. Bradley, R. Brown, M. Maxwell, A. Schapira, T. F. Orntoft, K. Kato, and D. C. Rubinsztein. Polyglutamine expansions cause decreased CRE-mediated transcription and early gene expression changes prior to cell death in an inducible cell model of Huntington's disease. *Hum. Mol. Genet.*, 10(17):1829–1845, 2001.

[273] J. Xia, D. H. Lee, J. Taylor, M. Vandelft, and R. Truant. Huntingtin contains a highly conserved nuclear export signal. *Hum. Mol. Genet.*, 12(12):1393–1403, Jun 2003.

[274] D. Yang, C.-E. Wang, B. Zhao, W. Li, Z. Ouyang, Z. Liu, H. Yang, P. Fan, A. O'Neill, W. Gu, H. Yi, S. Li, L. Lai, and X.-J. Li. Expression of huntington's disease protein results in apoptotic neurons in the brains of cloned transgenic pigs. *Human molecular genetics*, 19:3983–3994, Oct. 2010.

[275] S.-H. Yang, P.-H. Cheng, H. Banta, K. Piotrowska-Nitsche, J.-J. Yang, E. C. H. Cheng, B. Snyder, K. Larkin, J. Liu, J. Orkin, Z.-H. Fang, Y. Smith, J. Bachevalier, S. M. Zola, S.-H. Li, X.-J. Li, and A. W. S. Chan. Towards a transgenic model of huntington's disease in a non-human primate. *Nature*, 453:921–924, June 2008.

[276] Y. Yang, S. Liang, Y. Li, F. Gao, L. Zheng, S. Tian, P. Yang, and L. Li. Hepatoma-derived growth factor functions as an unfavorable prognostic marker of human gliomas. *Oncology letters*, 14:7179–7184, Dec. 2017.

[277] C. Ye, Y. Zhang, W. Wang, J. Wang, and H. Li. Inhibition of neurite outgrowth and promotion of cell death by cytoplasmic soluble mutant huntingtin stably transfected in mouse neuroblastoma cells. *Neuroscience letters*, 442:63–68, Sept. 2008.

[278] C. Zabel, L. Mao, B. Woodman, M. Rohe, M. A. Wacker, Y. KlÃđre, A. Koppelstaetter, G. Nebrich, O. Klein, S. Grams, A. Strand, R. Luthi-Carter, D. Hartl, J. Klose, and G. P. Bates. A large number of protein expression changes occur early in life and precede phenotype onset in a mouse model for huntington disease. *Molecular & cellular proteomics : MCP*, 8:720–734, Apr. 2009.

[279] D. Zala, J.-C. Bensadoun, L. Pereira de Almeida, B. R. Leavitt, C.-A. Gutekunst, P. Aebischer, M. R. Hayden, and N. DÃľglon. Long-term lentiviral-mediated expression of ciliary neurotrophic factor in the striatum of huntington's disease transgenic mice. *Experimental neurology*, 185:26–35, Jan. 2004.

[280] W. Zhai, H. Jeong, L. Cui, D. Krainc, and R. Tjian. In vitro analysis of huntingtin-mediated transcriptional repression reveals multiple transcription factor targets. *Cell*, 123(7):1241–1253, Dec 2005.

[281] X. Zhang, J. Q. Davis, S. Carpenter, and V. Bennett. Structural requirements for association of neurofascin with ankyrin. *The Journal of biological chemistry*, 273:30785–30794, Nov. 1998.

[282] J. Zhao, H. Yu, L. Lin, J. Tu, L. Cai, Y. Chen, F. Zhong, C. Lin, F. He, and P. Yang. Interactome study suggests multiple cellular functions of hepatoma-derived growth factor (hdgf). *Journal of proteomics*, 75:588–602, Dec. 2011.

[283] J. Zheng, J. Yang, Y.-J. Choe, X. Hao, X. Cao, Q. Zhao, Y. Zhang, V. Franssens, F. U. Hartl, T. NystrÃűm, J. Winderickx, and B. Liu. Role of the ribosomal quality control machinery in nucleocytoplasmic translocation of polyq-expanded huntingtin exon-1. *Biochemical and biophysical research communications*, 493:708–717, Nov. 2017.

[284] Z. Zheng, A. Li, B. B. Holmes, J. C. Marasa, and M. I. Diamond. An n-terminal nuclear export signal regulates trafficking and aggregation of huntingtin (htt) protein exon 1. *The Journal of biological chemistry*, 288:6063–6071, Mar. 2013.

[285] Z. Zhou, Y. Yamamoto, F. Sugai, K. Yoshida, Y. Kishima, H. Sumi, H. Nakamura, and S. Sakoda. Hepatoma-derived growth factor is a neurotrophic factor harbored in the nucleus. *The Journal of biological chemistry*, 279:27320–27326, June 2004.

[286] C. Zuccato, A. Ciammola, D. Rigamonti, B. R. Leavitt, D. Goffredo, L. Conti, M. E. MacDonald, R. M. Friedlander, V. Silani, M. R. Hayden, T. Timmusk, S. Sipione, and E. Cattaneo. Loss of huntingtin-mediated bdnf gene transcription in huntington's disease. *Science (New York, N.Y.)*, 293:493–498, July 2001.

APPENDIX A

CURRICULUM VITAE

Personal information

Name	Sara Gutiérrez Ángel
Birth date	03.02.1988, Spain
Nationality	Spanish

University education

2014 – 2018 International PhD at the Max Planck Institute of Neurobiology (Germany)
Thesis with Prof. Dr. Ruediger Klein
Mutant Huntingtin toxicity modifiers revealed by a spatiotemporal proteomic profiling

2012 – 2014 International Master in Biomedical Biotechnology
Thesis at Cold Spring Harbor Laboratory (USA) with Prof. Dr. Gregory Hannon
A molecular framework for understanding DCIS

2006 – 2012 National Degree in Molecular Biology (equivalent to MSc) at Autonomous University of Madrid (Spain)
Thesis at the Spanish National Cardiovascular Research Centre (Spain) with Dr. Pilar Martin
Role of the CD69 receptor in the modulation of cardiac inflammation through microRNAs

APPENDIX B

LIST OF PUBLICATIONS

B.1 Spatiotemporal Proteomic Profiling of Huntington's Disease Inclusions Reveals Widespread Loss of Protein Function

Resource

Cell Reports

Spatiotemporal Proteomic Profiling of Huntington's Disease Inclusions Reveals Widespread Loss of Protein Function

Graphical Abstract

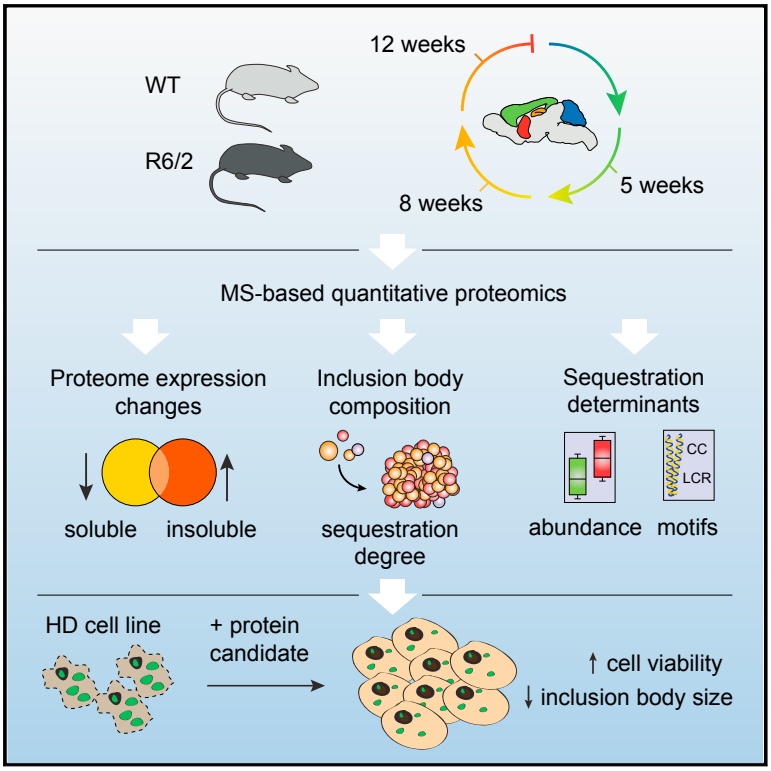

Highlights

- Spatiotemporally resolved brain proteome of wild-type and HD mice
- Quantitative characterization of huntingtin inclusion bodies *in vivo*
- Sequestration correlates with protein expression levels and specific sequence features
- Resupplying sequestered proteins ameliorates HTT-induced toxicity and inclusion size

Authors

Fabian Hosp, Sara Gutiérrez-Ángel, Martin H. Schaefer, ..., Rüdiger Klein, Irina Dudanova, Matthias Mann

Correspondence

idudanova@neuro.mpg.de (I.D.), mmann@biochem.mpg.de (M.M.)

In Brief

Hosp et al. use quantitative proteomics to describe the soluble and insoluble proteome of several brain regions in a mouse model of Huntington's disease at various stages of disease progression. Their findings suggest that widespread sequestration of proteins into mutant huntingtin inclusion bodies contributes to HD pathogenesis.

Data and Software Availability

PXD004973

Hosp et al., 2017, Cell Reports *21*, 2291–2303
November 21, 2017
https://doi.org/10.1016/j.celrep.2017.10.097

CellPress

Cell Reports
Resource

Spatiotemporal Proteomic Profiling of Huntington's Disease Inclusions Reveals Widespread Loss of Protein Function

Fabian Hosp,[1,9] Sara Gutiérrez-Ángel,[2,9] Martin H. Schaefer,[3,4] Jürgen Cox,[5] Felix Meissner,[6] Mark S. Hipp,[7,8] F.-Ulrich Hartl,[7,8] Rüdiger Klein,[2,8] Irina Dudanova,[2,*] and Matthias Mann[1,10,*]
[1]Department of Proteomics and Signal Transduction, Max Planck Institute of Biochemistry, Am Klopferspitz 18, 82152 Martinsried, Germany
[2]Department Molecules-Signaling-Development, Max Planck Institute of Neurobiology, Am Klopferspitz 18, 82152 Martinsried, Germany
[3]EMBL/CRG Systems Biology Research Unit, Centre for Genomic Regulation (CRG), Barcelona Institute of Science and Technology, Dr. Aiguader 88, 08003 Barcelona, Spain
[4]Universitat Pompeu Fabra (UPF), 08003 Barcelona, Spain
[5]Computational Systems Biochemistry Laboratory, Max Planck Institute of Biochemistry, Am Klopferspitz 18, 82152 Martinsried, Germany
[6]Experimental Systems Immunology Laboratory, Max Planck Institute of Biochemistry, Am Klopferspitz 18, 82152 Martinsried, Germany
[7]Department of Cellular Biochemistry, Max Planck Institute of Biochemistry, Am Klopferspitz 18, 82152 Martinsried, Germany
[8]Munich Cluster for Systems Neurology (SyNergy), 80336 Munich, Germany
[9]These authors contributed equally
[10]Lead Contact
*Correspondence: idudanova@neuro.mpg.de (I.D.), mmann@biochem.mpg.de (M.M.)
https://doi.org/10.1016/j.celrep.2017.10.097

SUMMARY

Aggregation of polyglutamine-expanded huntingtin exon 1 (HttEx1) in Huntington's disease (HD) proceeds from soluble oligomers to late-stage inclusions. The nature of the aggregates and how they lead to neuronal dysfunction is not well understood. We employed mass spectrometry (MS)-based quantitative proteomics to dissect spatiotemporal mechanisms of neurodegeneration using the R6/2 mouse model of HD. Extensive remodeling of the soluble brain proteome correlated with insoluble aggregate formation during disease progression. In-depth and quantitative characterization of the aggregates uncovered an unprecedented complexity of several hundred proteins. Sequestration to aggregates depended on protein expression levels and sequence features such as low-complexity regions or coiled-coil domains. In a cell-based HD model, overexpression of a subset of the sequestered proteins in most cases rescued viability and reduced aggregate size. Our spatiotemporally resolved proteome resource of HD progression indicates that widespread loss of cellular protein function contributes to aggregate-mediated toxicity.

INTRODUCTION

Cellular environment is characterized by very high protein concentrations, increasing the danger of aggregation. Thus, maintenance of protein solubility is a fundamental aspect of cellular homeostasis. Aggregates play a prominent role in many neurodegenerative diseases (NDDs) (Ross and Poirier, 2004). Misfolding and aggregation can disrupt cellular function in two ways, loss of endogenous protein function or gain of a novel toxic function, and there is evidence that both processes occur in disease (Winklhofer et al., 2008). The aggregation cascade involves multiple intermediate conformations, such as globular and fibrillar structures, up to the late-stage inclusion bodies (IBs) (Knowles et al., 2014).

Huntington's disease (HD) is an autosomal dominant NDD characterized by neuropsychiatric and motor impairments (Saudou and Humbert, 2016). It is caused by a CAG repeat expansion in exon 1 of the huntingtin (*HTT*) gene, which leads to an expanded polyglutamine (polyQ) stretch in the N terminus of the huntingtin protein (The Huntington's Disease Collaborative Research Group, 1993). A hallmark of this disorder is the appearance of cytoplasmic and intranuclear huntingtin aggregates (Davies et al., 1997; DiFiglia et al., 1997), which interfere with several cellular processes, such as proteostasis, transcription, vesicular trafficking, and energy metabolism (Orr and Zoghbi, 2007; Saudou and Humbert, 2016).

Obtaining insights into the composition of huntingtin IBs is of particular importance in understanding HD mechanisms. So far, it has been challenging to characterize the protein composition of IBs, because they remain insoluble even in very high detergent concentrations. Efforts to purify late-stage polyQ aggregates culminated in the identification of only a few tens of proteins, mainly heat shock factors (Mitsui et al., 2002), components of the ubiquitin-proteasome pathway (Doi et al., 2004), and certain transcription factors (Dunah et al., 2002; Shimohata et al., 2000). Given the size of the IBs—up to several micrometers (Gutekunst et al., 1999)—it is likely that they contain far more proteins. Moreover, the quantitative composition of IBs and its variation among brain regions is almost entirely unknown.

Mass spectrometry (MS)-based quantitative proteomics is powerful technology for systems-wide analysis of complex cellular processes (Aebersold and Mann, 2016). To date,

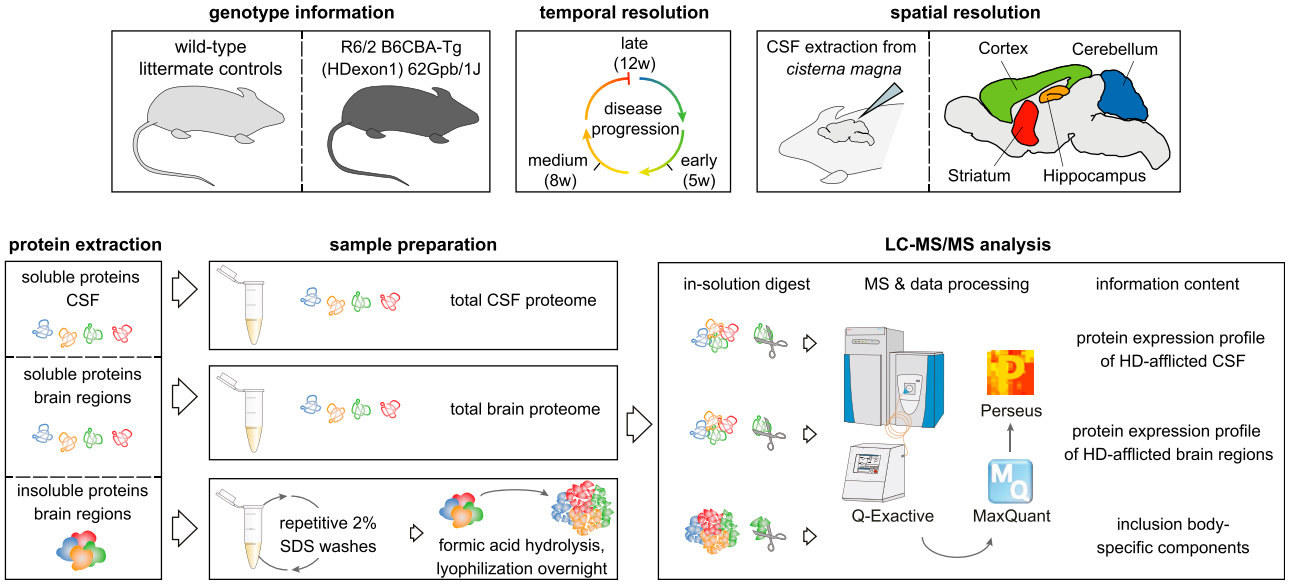

Figure 1. Experimental Design

Brain regions from R6/2 and WT mice were assessed by quantitative LC-MS/MS. From each tissue sample, soluble and insoluble proteomes were measured. IBs were enriched by repetitive SDS washes and hydrolyzed in formic acid. Cerebrospinal fluid from each mouse was also analyzed. Number of animals: 5 weeks, 4 R6/2 and 4 WT; 8 weeks, 3 R6/2 and 3 WT; 12 weeks, 4 R6/2 and 4 WT.

proteomic approaches exploring HD pathogenesis have focused either on expression level changes or on soluble huntingtin interactions (Culver et al., 2012; Langfelder et al., 2016; Shirasaki et al., 2012). In contrast, knowledge of the interplay between soluble and insoluble aspects of the proteome is limited (Baldo et al., 2012), particularly when following disease progression over time and in differentially affected brain regions.

Here, we investigate molecular neurodegeneration signatures in a mouse HD model by MS-based quantitative proteomics with spatiotemporal resolution. We describe the soluble and insoluble proteomes of four brain regions, as well as the cerebrospinal fluid proteome at three time points of disease progression. Acid-based hydrolysis of the aggregates allows us to characterize them in depth by quantitative MS. Our data enable comparison of the degree of protein sequestration from the soluble pool to IBs over time, as well as analysis of sequence features of the sequestered proteins. Functional follow-up in a cellular HD model reveals that increasing expression levels of sequestered proteins in many cases restores cellular function and alters the nature of HttEx1 aggregates, suggesting that widespread loss of protein function due to sequestration contributes to HD pathogenesis.

RESULTS

R6/2 transgenic mice express N-terminal exon 1 of polyQ-expanded huntingtin under control of the human huntingtin promoter (Mangiarini et al., 1996). For our analysis of neurodegeneration-associated proteome changes, we selected an early time point at 5 weeks, before disease onset; an intermediate time point at 8 weeks, on the verge of visible motor deficits; and a late time point at 12 weeks, at the end of the lifespan of R6/2 mice (Carter et al., 1999; Davies et al., 1997). We prepared soluble and insoluble extracts from four brain regions (striatum, cortex, hippocampus, and cerebellum), which show differential vulnerability to HD, with striatum being most severely affected and cerebellum remaining relatively spared until advanced disease stages (Vonsattel and DiFiglia, 1998). To relate the proteome changes in the brain to those in a proximal body fluid, cerebrospinal fluid was also analyzed (Figure 1).

Spatiotemporal Brain Proteome Resource of Wild-Type Mice

Recently, we compiled an in-depth cell-type- and region-specific proteomic catalog of the adult mouse brain with a depth of ~13,000 proteins (Sharma et al., 2015). Building on that analysis by using the peptide identifications as a library (Supplemental Experimental Procedures), we now identified 12,498 proteins in the soluble proteome alone using single-run liquid chromatography-tandem mass spectrometry (LC-MS/MS). Of these, we chose 8,455 proteins by stringent filtering for valid values (Figure 2A; Table S1A; Supplemental Experimental Procedures). Correlation analysis indicated a high degree of reproducibility between replicates (R = 0.84 overall; R = 0.90 for biological replicates) (Figure S1A). First, we investigated the soluble proteome of wild-type (WT) controls. Protein abundances spanned seven orders of magnitude, with only 217 proteins amounting to 50% of the total protein mass (Figure 2A). Gene Ontology (GO) biological processes correlated with overall protein abundances in expected ways (Figure 2A; Tables S1B and S1C). High-abundant proteins tended to have a smaller molecular mass (Figure 2B), as in other tissues (Wiśniewski

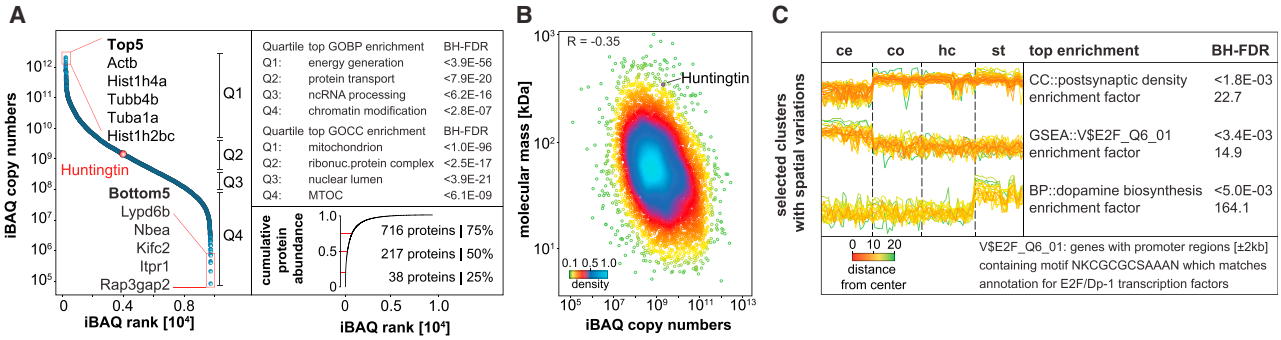

Figure 2. Spatiotemporal Brain Proteome Resource

(A) Ranking of brain proteins by iBAQ (intensity-based absolute quantification) copy numbers from highest to lowest. Strongest enrichment for each quartile is displayed for GO categories "biological process" and "cellular component"; BH-FDR, Benjamini-Hochberg-corrected false discovery rate. Cumulative protein mass from the highest to the lowest abundant protein shows that only a few proteins make up most of the protein mass.

(B) iBAQ copy numbers for ~8,500 proteins inversely correlate with molecular mass. Data points are colored by local point density.

(C) Spatial resolution exposes functional brain region specificity. Three selected clusters display distinct protein expression across the four regions. p value, BH-FDR corrected; EF, enrichment factor of the most enriched GO term; MaxLFQ intensity, normalized label-free protein intensity.

See also Figure S1 and Table S1.

et al., 2014), presumably reflecting evolutionary constraints on biosynthesis costs (Warringer and Blomberg, 2006). Our approach uncovered several brain region-specific protein clusters (Lein et al., 2007; Sharma et al., 2015). For instance, proteins involved in dopaminergic signaling were enriched in the striatum, which receives extensive dopaminergic innervation (Figure 2C; Table S1D) (Gerfen and Surmeier, 2011). As expected for the narrow time window of the analysis compared to the lifespan of WT animals, little changes in protein expression were detected at different time points (Figure S1B) (Walther and Mann, 2011). Collectively, our soluble brain region data of WT mice provide a comprehensive resource for the community, with copy numbers and spatiotemporal resolution for almost 8,500 proteins.

Extensive Brain Proteome Remodeling during Disease Progression in R6/2 Mice

Principal-component analysis (PCA) on the spatiotemporally resolved soluble proteomes of R6/2 and WT mice showed clear separation of samples with two major effects (Figure 3A). First, R6/2 mice after disease onset (8 and 12 weeks) were separated from other samples, reflecting extensive protein remodeling during pathogenesis (Figure 3A). Second, cerebellar proteomes were strongly separated from other brain regions. Only a few proteins were responsible for driving separation in the PCA (Figure 3B). Spatial drivers included brain region-specific proteins, whereas age- and disease-driving proteins were enriched for GO terms such as "regulation of synaptic part" ($p < 6.0E-19$, Benjamini-Hochberg-corrected false discovery rate [BH-FDR]), "neuron projection" ($p < 1.4E-12$), or "associated with oxidative phosphorylation" ($p < 7.5E-9$).

To identify significant differences among the genotypes, brain regions, and time points, we employed three-way ANOVA. This revealed hundreds of significant protein changes for each of the three factorial groups and their combinations (Figure S2A). Concordant with the PCA results, the three individual groups exhibited similar numbers of significant protein changes. The combination of age and genotype contributed almost as much as age and genotype separately, indicating that age and genotype jointly drove the extensive proteome remodeling in our dataset. To investigate spatiotemporal changes of the soluble proteome in more detail, we tested for differences in any functional annotations to the background protein distribution and observed that protein annotations changed spatiotemporally and in accordance with known features of HD progression (Figure S2B; Supplemental Experimental Procedures) (Geiger et al., 2012). One example is the increased expression of proteins involved in neurotransmitter secretion at early disease stages in hippocampus and striatum (8 weeks) followed by a decrease at later stages (12 weeks) (Chen et al., 2013). Another finding is the loss of protein expression associated with the calcineurin complex in the cortex (Gratuze et al., 2015). We have compiled a list of annotation changes across brain regions and time (Table S1E) and find many potentially interesting clues for the selective spatial disease progression, such as reduced cortical expression of annotations associated with amino acid import and ion transmembrane transporter activity or reduced striatal expression of annotations associated with mRNA splicing (Figure S2B). Hence, our dataset provides a rich resource of brain region-specific changes in R6/2 mice to formulate testable hypotheses about HD pathogenesis.

Expression profiles of R6/2 and WT animals at 5 weeks were largely identical, although specific protein clusters already exhibited different expression (Figure 3C). Just three weeks later, expression of mutant HttEx1 caused extensive remodeling of the proteome with marked up- and downregulation of thousands of proteins (Figure 3C, colored clusters). The two upregulated clusters were enriched in proteins of the chaperonin containing TCP1 complex (cluster 2, $p < 2.0E-4$, BH-FDR) and proteasome accessory complex (cluster 3, $p < 4.0E-3$), whereas the two downregulated clusters were enriched in proteins associated with the ribosome (cluster 1, $p < 9.5E-4$) and energy transport

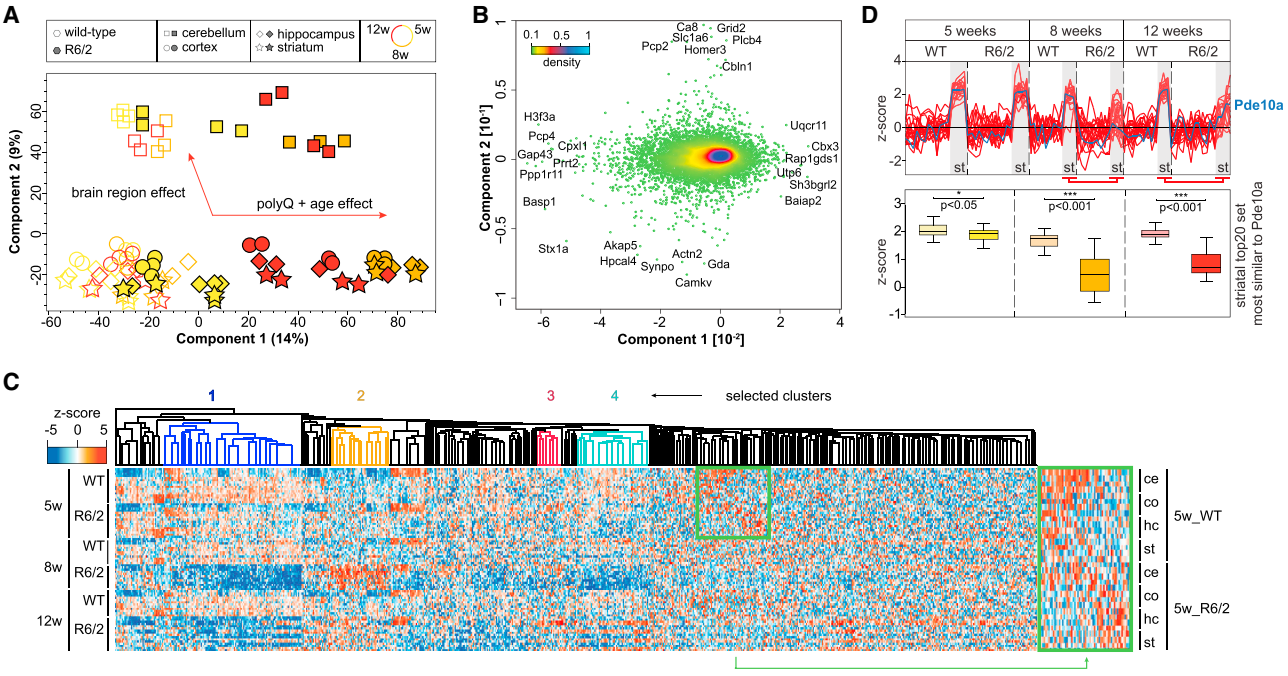

Figure 3. Drastic Proteome Remodeling of R6/2 Mice after Disease Onset

(A and B) PCA projections (A) and PCA loadings (B) of all soluble samples reveal specific effects on the proteome driven by the genotype, age, and differential spatial expression. Data points in (B) are colored by local point density.

(C) Hierarchical clustering of protein expression over time shows substantial proteome shifts from early stages of HD onward. The two most upregulated (red and orange) or downregulated (blue and cyan) clusters are indicated.

(D) Top 20 Euclidean distance tracking of protein expression profiles similar to Pde10a over time and across brain regions; gray boxes indicate striatal expression (upper panel). Boxplots of *Z*-scored MaxLFQ intensities for the striatal top 20 set (lower panel). Reduced expression of all targets in R6/2 samples compared to WT. See also Figure S2.

across the mitochondrial electron transfer chain (cluster 4, $p < 9.0E{-}4$) (Table S1F). This is consistent with the deficient energy metabolism and impairment of the ubiquitin-proteasome system in HD (Acuña et al., 2013; Ortega and Lucas, 2014). Our analysis now provides the underlying protein changes in the R6/2 model on a proteome-wide scale.

A hallmark of HD neuropathology is the selective degeneration of striatal medium spiny neurons (MSNs), which has been linked to transcriptional dysregulation of cyclic AMP (cAMP) and CREB signaling (Vonsattel and DiFiglia, 1998; Wyttenbach et al., 2001). We found Pde10a, a cAMP or cyclic guanosine monophosphate (cGMP)-hydrolyzing enzyme highly enriched in MSNs, to be markedly downregulated in R6/2 striatum (Figure 3D). It is one of the earliest and most significantly downregulated gene products in HD patients and a promising target to restore cyclic nucleotide (cNMP) signaling in affected neurons (Giampà et al., 2010). Furthermore, Pde10a ligands are used in positron emission tomography (PET) to assess the extent of disease and predict conversion to HD (Russell et al., 2014).

We next asked whether other proteins follow the same profile and thus might serve as markers of HD progression. Following the Euclidean distance of the top 20 expression profiles most similar to Pde10a revealed a set of proteins with interrelated functions, such as cNMP metabolism, neurotransmitter, and specifically dopaminergic signaling (Figure 3D; Figure S2C). The first group included Pde10a-related Pde1b, as well as Darpp-32, which is widely used as a marker for both MSNs and the attenuation of dopaminergic signaling in HD (Jiang et al., 2011). Further candidates were also associated with dopamine metabolism, such as Drd1, a dopamine receptor expressed in MSNs whose striatal loss correlates with cognitive decline (Chen et al., 2013). Adenylate cyclase 5 (Adcy5) is predominantly expressed in the striatum and has been linked to rarer forms of chorea and dystonia (Carapito et al., 2015). A transcriptomics and proteomics study identified 17 of our 21 potential markers among the top 50 hub genes of a striatal module negatively associated with CAG repeat length in a different HD mouse model (Langfelder et al., 2016). Thus, our data define a set of MSN-specific proteins that can be used to assess cNMP-linked dopaminergic imbalances.

Inflammatory Profile in the Cerebrospinal Fluid Proteome

The cerebrospinal fluid is an invaluable source in assessing pathological alterations of the CNS (Kroksveen et al., 2011). We next asked whether HD signatures in the soluble brain proteome correlate with changes in the cerebrospinal fluid. A total of 778 cerebrospinal fluid proteins were quantified with our single-shot workflow after filtering out likely contaminants (Table S2A; Supplemental Experimental Procedures). Unsupervised

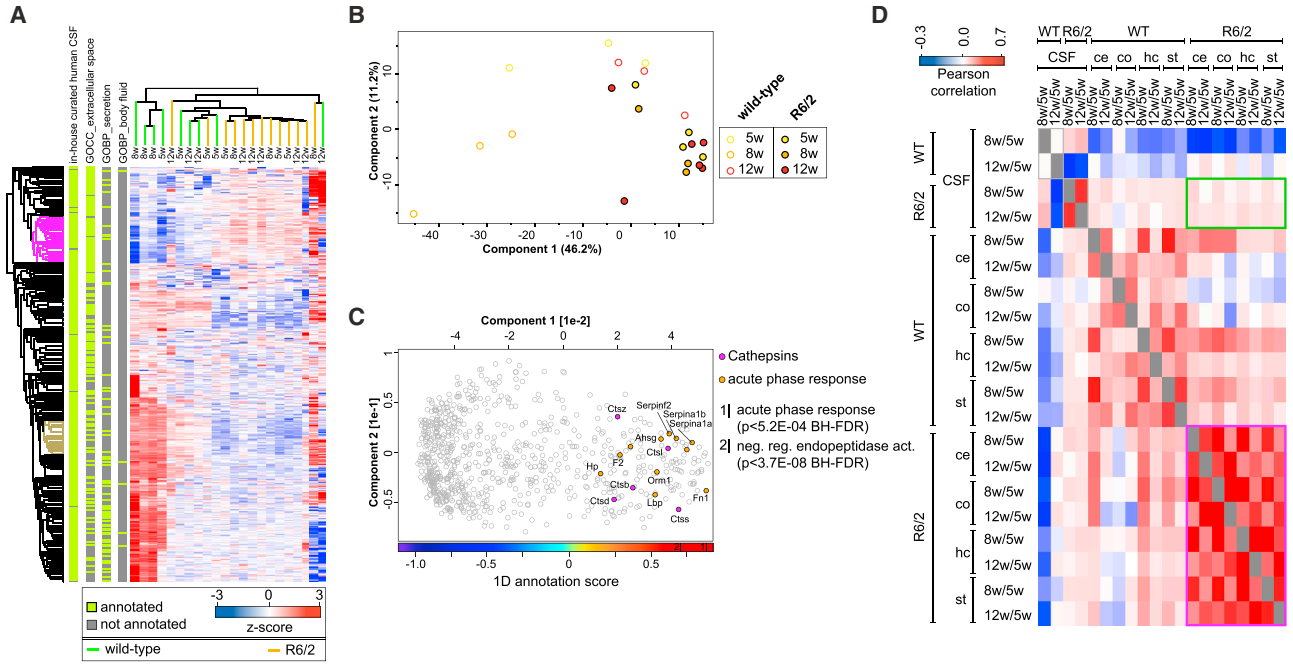

Figure 4. Altered Cerebrospinal Fluid Proteome in R6/2 Mice

(A) Hierarchical clustering of cerebrospinal fluid protein expression reveals good separation of R6/2 and WT mice; row bars indicate filters for known GO annotations related to secretion (see Supplemental Experimental Procedures for details).

(B) PCA projections of all cerebrospinal fluid samples show good separation between WT and R6/2 mice.

(C) Corresponding PCA loadings of (B) reveal strong inflammatory response in R6/2 animals. The color bar displays the 1D annotation score with the two most enriched annotations for R6/2 mice; the annotation score indicates the center of the protein distribution of each significant annotation category relative to the overall distribution of values. p value, BH-FDR corrected.

(D) Correlation of protein expression changes between different disease stages is high within the soluble proteome (purple inlay) but low for the comparison of the soluble proteome with the cerebrospinal fluid (green inlay) of R6/2 mice.

See also Table S2.

hierarchical clustering separated R6/2 and WT samples, indicating changes in protein secretion to the cerebrospinal fluid upon expression of mutant HttEx1 (Figure 4A). Among the most dysregulated proteins we found peptidase regulators increased in the cerebrospinal fluid of R6/2 mice (Figures 4B and 4C; Table S2B). The presence of proteolytic enzymes reflects inflammatory processes, and our data suggest that several members of the cathepsin family dominantly contribute to these processes, because they are major drivers of the PCA separation between R6/2 and WT samples (Ossovskaya and Bunnett, 2004). Finally, we compared correlations of protein expression changes between the brain and the cerebrospinal fluid proteome (Figure 4D). Although expression changes in the brain over time correlated between R6/2 mice ($R > 0.5$), the correlation between soluble brain proteomes and cerebrospinal fluid was low ($R < 0.1$) (Figure 4D). This indicates that global expression changes in the soluble proteome are not necessarily reflected in the cerebrospinal fluid proteome.

In-Depth Characterization of the Insoluble Proteome *In Vivo*

Huntingtin-containing IBs are a hallmark of HD, but the identity and quantity of their constituent proteins are largely unknown. In agreement with previous studies (Davies et al., 1997; Meade et al., 2002), brains of R6/2 mice already displayed widespread IBs at 5 weeks, with striatal IBs being significantly smaller than cortical ones (Figures S3A–S3C).

Although purification of late-stage aggregates is straightforward due to their extreme insolubility, this biophysical property also makes them resistant to proteolytic digestion, a precondition for MS analysis. Concentrated formic acid can dissolve polyQ aggregates (Hazeki et al., 2000; Kim et al., 2016), and here we demonstrate that it is compatible with tissue-based quantitative proteomics (Figure 1; Supplemental Experimental Procedures). This purification approach, when coupled to state-of-the-art MS, identified several hundred proteins and revealed extensive protein sequestration to the insoluble fraction in the R6/2 brain, including endogenous mouse Htt (Figure S4; Table S3). For quantitative analysis of the aggregate composition, we used the iBAQ (intensity-based absolute quantification) algorithm to estimate protein abundances (Schwanhäusser et al., 2011). Only 10 proteins constituted more than 50% and the top 50 proteins constituted more than 75% of the aggregate mass in 12-week-old R6/2 striatum (Figure 5A). Apart from histones and RNA-binding proteins, these included proteins involved in neuronal plasticity, as well as myelin components

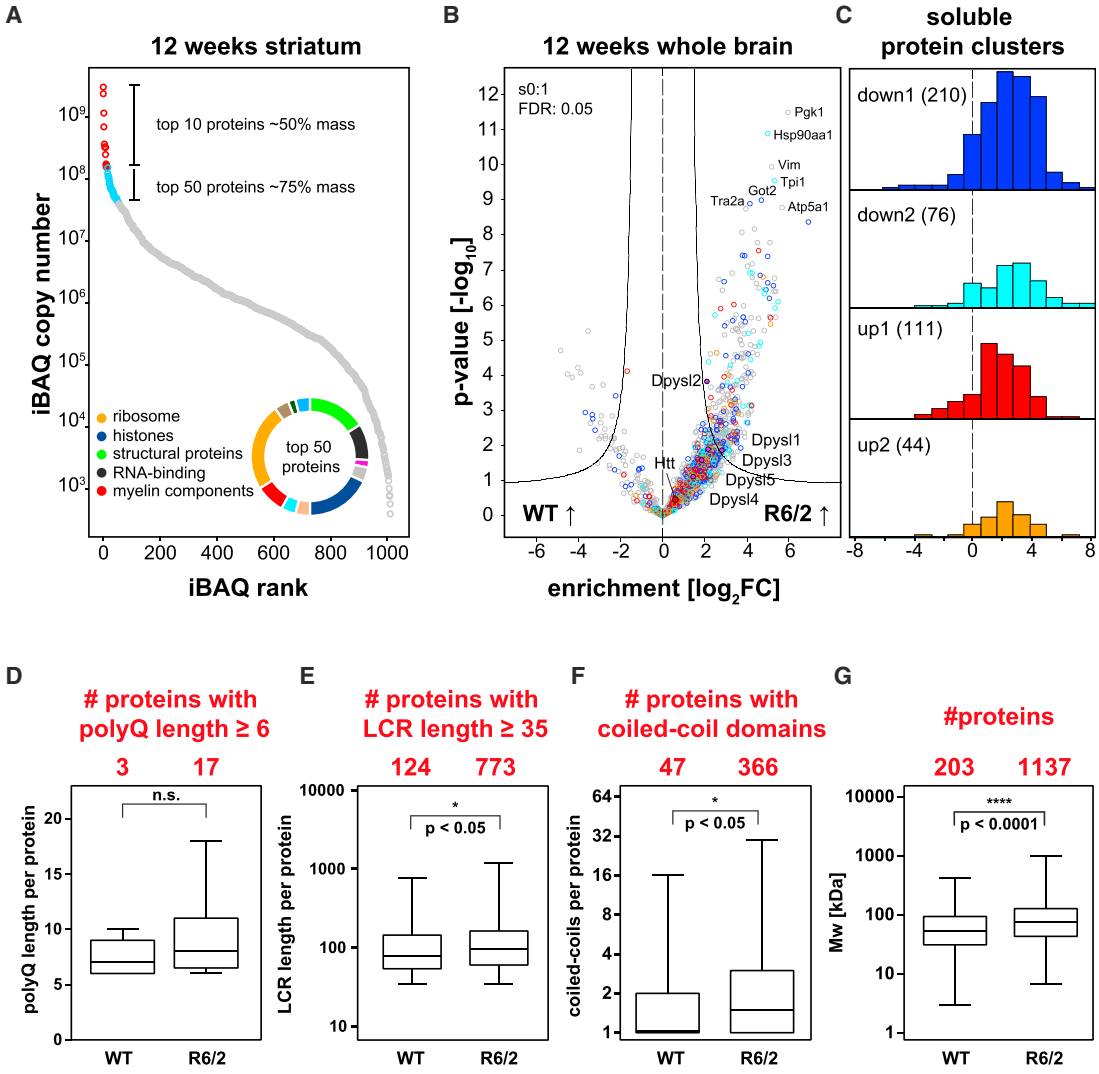

Figure 5. In-Depth Characterization of PolyQ Aggregates

(A) Distribution of iBAQ values for 12 week R6/2 striata. Pie chart distribution of annotations for the top 50 proteins.

(B and C) Proteins with dysregulated soluble expression (color coding from Figure 3C) are enriched in R6/2 insoluble fractions, superimposing enrichment for all 12 week brain regions together. The most enriched insoluble proteins and endogenous Htt is indicated.

(D–G) Significant enrichment of proteins with longer polyQ (D) and LCRs (E), more CCDs (F), and higher molecular weight (MW) (G) in 12 week R6/2 over WT striata. Mann-Whitney U test.

See also Figures S3–S5 and Table S3.

(Table S3). Co-immunostainings for the myelin protein Plp1, aggregated HttEx1, and a neuronal marker revealed co-localization of Plp1 with aggregated HttEx1 in many neuronal IBs, confirming that myelin proteins are true components of neuronal inclusions (Figures S3D and S3E).

Most sequestered proteins contributed little to overall aggregate mass. There was a general tendency for abundant cellular proteins to also be among the more abundant aggregate proteins (median R = 0.40 across all conditions) (Figure S5). GO analysis revealed many proteins associated with native huntingtin function and the proteostasis network to be enriched in the R6/2 insoluble fraction, including known interactors and aggregation modifiers of polyQ-expanded huntingtin. Several members of the TCP-1 ring complex (TRiC) and the Hsp40, Hsp70, and Hsp90 families made up ~1.5% of the insoluble fraction mass. All five members of the collapsin response mediator protein (Crmp) family, also known as dihydropyrimidinase-related proteins (Dpysl), were also enriched (Figure 5B). A study identified Crmp1 as a suppressor of huntingtin toxicity (Stroedicke et al., 2015). Apart from confirming these known aggregate constituents, our data provide a large number of new proteins with potential links to HD (Table S3A).

We hypothesized that the extensive soluble proteome remodeling in HD should be reflected in the insoluble proteome.

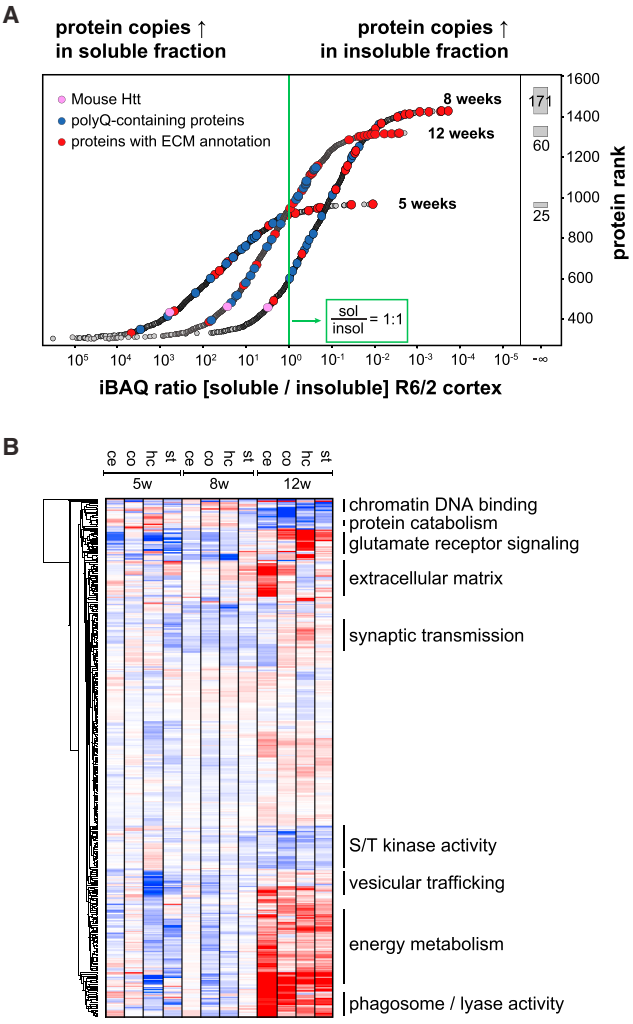

Figure 6. Functional Attributes of PolyQ Aggregates

(A) Ranking of proteins by iBAQ ratios representing protein sequestration from the soluble to the insoluble proteome in R6/2 cortices. Gray boxes show the number of proteins that were only identified in the insoluble proteome per age group, indicated by infinite iBAQ ratios.

(B) Annotation matrix of protein attributes, such as complexes, gene ontologies, and pathways, highlighting changes in the spatiotemporal composition of the insoluble fraction. The color code indicates normalized median abundance of the proteins belonging to each category relative to the distribution of all proteins. Selected annotations are highlighted. Red, most abundant; blue, least abundant. Mann-Whitney U test (BH-FDR < 0.05).

See also Figure S6 and Table S3.

Mapping our soluble proteome data to the insoluble fraction revealed a large number of proteins that were downregulated in the soluble proteome and enriched in the aggregates (blue and cyan in Figures 5B and 5C; Figure S4), suggesting widespread loss of protein function by sequestration. Conversely, we also found many proteins that were upregulated in both the soluble and the aggregate proteomes (orange and red in Figures 5B and 5C; Figure S4; Table S3B). Among the latter, the TRiC chaperonin and the GO term "proteasome accessory complex" were highly overrepresented ($p < 4.0E{-}5$ and $p < 3.2E{-}3$ BH-FDR, respectively) (Table S3E), confirming specific upregulation of chaperones that interact with aggregates but become entangled with them. Potential loss-of-function candidates (reduced in the soluble proteome and increased in the insoluble proteome) often had a significantly higher abundance compared to proteins upregulated in the soluble proteome (Figure S6A), consistent with a sequestration mechanism that depletes the cellular pool of these proteins, thereby impeding cellular function.

Next, we asked whether sequestration into the aggregates correlated with certain biophysical features. We focused on polyQ length, low-complexity regions (LCRs), and coiled-coil domains (CCDs), motifs known to modulate protein aggregation (Fiumara et al., 2010; Kato et al., 2012; Li and Li, 2004; Schaefer et al., 2012). Insoluble fractions from R6/2 striata contained significantly more aggregation-prone proteins than WT controls, with a robust effect size for CCDs and small effect sizes for polyQ and LCRs (Figures 5D–5F; Figures S6B–S6D). In addition, R6/2 samples were significantly enriched for proteins with higher molecular weight (Figure 5G; Figure S6E). Larger proteins tend to be less thermodynamically stable, which may explain why their folding is compromised under conditions of conformational stress (Sharma et al., 2012).

To quantify the degree of sequestration, we estimated absolute protein abundance using the iBAQ algorithm and compared the amount of each protein in the soluble and insoluble proteome (Figure 6A; Figure S6F). Extracellular matrix (ECM) proteins had the least soluble proportion, reflecting their insolubility and demonstrating efficient enrichment of insoluble proteins in our protocol (Figure 6A, marked in red). Endogenous Htt was also recruited into the aggregates (Figure 6A, marked in pink). In concordance with the increase in aggregate size, we observed increased sequestration of protein mass over time, hence progressively depleting the pool of functional proteins. In 8-week-old animals, a full 80% of proteins were at least in a 1:1 ratio in the cortical IBs compared to the soluble pool.

To determine whether the IB composition varies over time and across brain regions, we tested for differences in any functional annotations to the background protein distribution (Figure 6B; Table S3F; Supplemental Experimental Procedures) and found spatiotemporal changes of protein annotations, reflecting many known features of HD pathogenesis. Transcriptional and epigenetic dysregulation is an early event in HD, and we found that IBs at 5 weeks were already significantly enriched in DNA- and chromatin-binding elements (FDR < 0.05). Conversely, late-stage IBs at 8 to 12 weeks were enriched in proteins associated with glutamate receptor signaling and synaptic transmission, correlating with the onset of motor phenotypes (FDR < 0.05, respectively). Similarly, we observed spatial changes such as enrichment of SMAD-binding proteins in cortical IBs (FDR < 0.05), or depletion of proteins involved in Wnt signaling pathways in striatal IBs (FDR < 0.05), linked to synaptic degeneration (Galli et al., 2014). Our proteomic analysis therefore demonstrates that protein sequestration is both brain region and time specific and may link dynamic changes in the IBs to the phenotype.

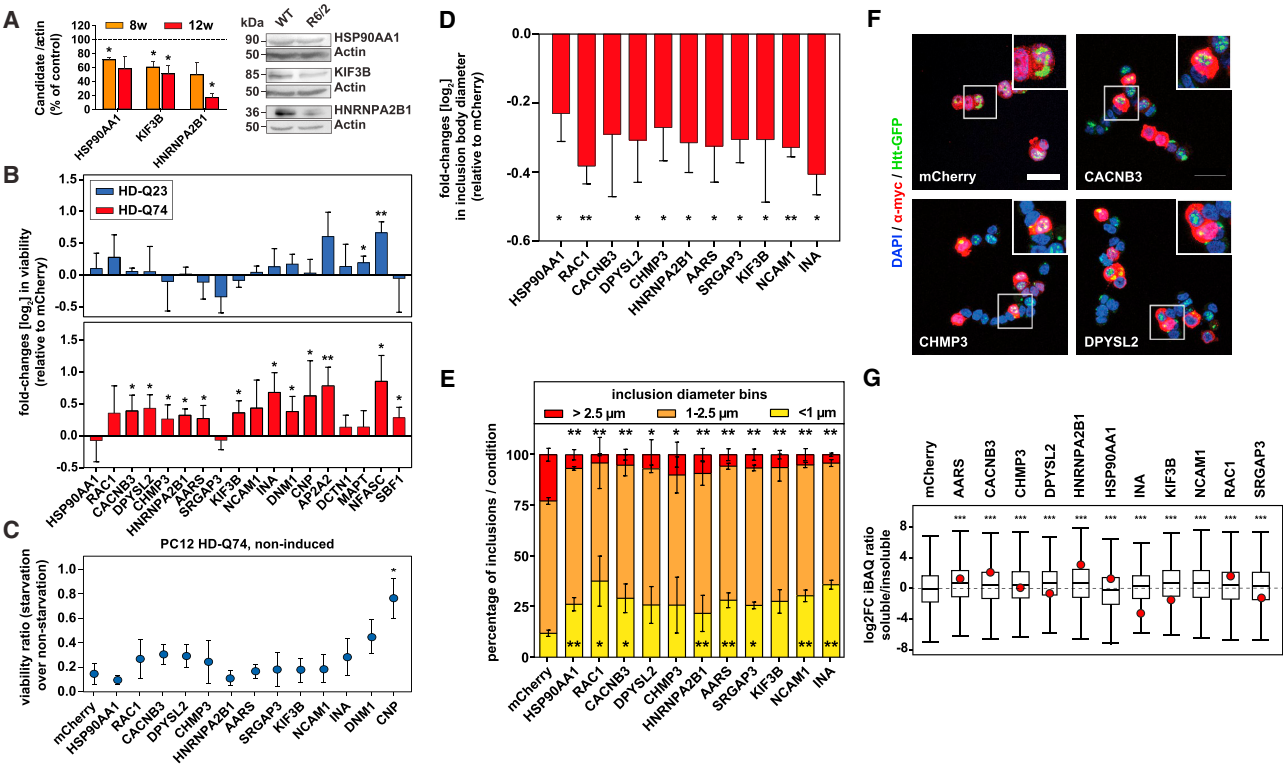

Figure 7. Overexpression of Loss-of-Function Candidates Ameliorates HttEx1 Phenotypes

(A) Left: quantification of candidates in immunoblots of 8- and 12-week-old R6/2 striata, normalized to WT (dotted line). Student's t test, *$p < 0.05$; n = 3–4. Right: representative examples of immunoblots from 12-week-old striata.

(B) Log_2 fold changes (log_2FCs) in viability of HD-Q23 (upper panel) or HD-Q74 (lower panel) cells transfected with the candidates as measured by lactate dehydrogenase (LDH) assay. Multiple one-tailed t test with Benjamini-Hochberg correction; *FDR < 0.05, **FDR < 0.01; normalized to mCherry controls; n = 4.

(C) Candidates' effects on the viability of starved, non-induced HD-Q74 cells. Multiple two-tailed t test with Benjamini-Hochberg correction; *FDR < 0.05; n = 3.

(D) Log_2FCs in IB diameter in HD-Q74 cells transfected with the candidates. Multiple two-tailed t test with Benjamini-Hochberg correction; *FDR < 0.05, **FDR < 0.01; normalized to mCherry; n = 3.

(E) Distribution of IB diameter bins in HD-Q74 cells transfected with the candidates. Yellow, <1 µm; orange, 1–2.5 µm; red, >2.5 µm. Multiple two-tailed t test with Benjamini-Hochberg correction; *FDR < 0.05, **FDR < 0.01; n = 3.

(F) Representative images of HD-Q74 cells transfected with selected candidates. Blue, DAPI; red, myc candidate; green, HttEx1-GFP; scale bar, 20 µm.

(G) Log_2FCs in the soluble fraction of proteins after overexpression of candidates in HD-Q74 cells, determined by changes in iBAQ ratios (soluble to insoluble). The red dot indicates the iBAQ ratio of the candidate. Multiple two-tailed t test with Benjamini-Hochberg correction; ***FDR < 0.001; n = 3. NCAM1 was not identified in the insoluble fraction in this experiment.

See also Figure S7.

Overexpressing Loss-of-Function Candidates Rescues PolyQ Length-Dependent Toxicity and Alters IB Size

We identified several hundred proteins that were depleted from the soluble pool and increased in insoluble aggregates. To test whether this represents widespread loss of protein function, we selected a group of 18 candidates for functional follow-up based on several criteria, including their profiles in the proteomics experiments and association with neuronal functions but no previous link to HD (Figure S7A; Table S4). For several candidates, reduction in protein levels in the soluble fraction was confirmed by western blot (Figure 7A; Figure S7B). Among the selected candidates was the amytrophic lateral sclerosis (ALS)-associated protein hnRNPA2B1. ALS-linked hnRNPA2B1 mutations lead to an accumulation of insoluble protein in the nucleus (Martinez et al., 2016). Immunostaining in R6/2 striatum demonstrated a nuclear accumulation of hnRNPA2B1 in most MSNs, as well as its co-localization with HttEx1 IBs (Figures S7C–S7E).

For the follow-up of the selected proteins, we used inducible neuron-like PC12 cells with stably integrated, GFP-tagged HttEx1 with either 23 or 74 glutamines (HD-Q23 and HD-Q74 cells). Induction of HttEx1 led to polyQ length-dependent cell death (Figure S7F) (Wyttenbach et al., 2001). Quantitative proteomics revealed that all candidates were expressed in this cell line with medium to high abundance (Figure S7G), and induction of HttEx1 did not substantially alter their expression (Figure S7H). Furthermore, in most cases, transfection of a candidate increased its protein levels compared to non-transfected controls (Figure S7I). Overexpression of individual candidates significantly improved the viability of HD-Q74 cells in 12 of 18

cases (BH-FDR < 0.05), with a mean survival increase of 40% (Figure 7B, lower panel). Three proteins (Ap2a2, Mapt, and Nfasc) that increased the viability of control HD-Q23 cells (Figure 7B, upper panel) and two proteins that repeatedly exhibited low transfection rates (Dctn1 and Sbf1) were excluded from further analyses. To distinguish between a general effect on cell survival and a specific involvement in mutant HttEx1 toxicity, we tested whether the candidates rescued the viability of non-induced HD-Q74 cells under starvation and observed a rescue with only one protein, Cnp (Figure 7C). Thus, the effects of the remaining candidates were specific for mutant HttEx1 toxicity.

We next asked whether the HttEx1 toxicity-modifying proteins also had an effect on aggregation. Overexpression of the candidates did not change the number of GFP+ foci per cell (Figure S7J) but did reduce their size in 10 of 11 cases (Figure 7D). Moreover, the percentage of small foci (<1 μm in diameter) increased significantly in 8 of the 11 cases, whereas the percentage of large foci (>2.5 μm) was significantly reduced in all cases (Figures 7E and 7F). As an orthogonal approach, we employed membrane filter trap assay, which also did not reveal a significant change in the aggregation load (Figure S7K). Finally, the soluble proportion of most cellular proteins increased significantly after overexpression of the candidates in HD-Q74 cells, as well as, in most cases, the soluble proportion of the candidate (Figure 7G). Thus, overexpression of the proteins sequestered to HttEx1 IBs ameliorates mutant HttEx1 toxicity and decreases aggregate size, but not load.

DISCUSSION

We applied quantitative proteomics to investigate molecular neurodegeneration signatures in an *in vivo* model of HD. Employing a recently published proteomic resource of the mouse brain (Sharma et al., 2015) and a single-run LC-MS/MS workflow, we characterized the brain proteome of the R6/2 mice and WT controls to a depth of more than 12,000 proteins. Spatiotemporal characterization of the soluble proteome during disease progression uncovered extensive alterations in brain regions vulnerable to HD. The data provide a resource to the community, which is available via a user-friendly database (http://maxqb.biochem.mpg.de/mxdb/). The value of such data is illustrated by the identification of several MSN-specific proteins whose signaling is compromised in HD and that are already used for PET imaging. These clinically relevant proteins emerge from our analysis and thus validate the R6/2 model, which is one of the best characterized and most widely used HD mouse models. Comparative studies demonstrated its extensive similarity with full-length Huntingtin models at pathological, transcriptional, and electrophysiological levels (Cummings et al., 2009; Langfelder et al., 2016; Woodman et al., 2007). Nevertheless, it will be necessary to extend our approach to full-length models in the future.

Furthermore, our dataset contains a number of additional proteins that have closely related expression regulation in the course of HD, making them promising candidates for imaging or other applications. Another example emerged upon matching the soluble brain and cerebrospinal fluid proteomes. Several proteomic analyses have proposed potential biomarkers of HD progression in cerebrospinal fluid , mostly linked to inflammation (Dalrymple et al., 2007; Fang et al., 2009). Here, we also observed a strong inflammatory signature in the cerebrospinal fluid of R6/2 mice. However, proposed biomarkers have failed to be validated for clinical trials (Byrne and Wild, 2016). We found an overall low correlation between changes in the soluble proteome and the cerebrospinal fluid, which needs to be considered when attempting to identify biomarkers in cerebrospinal fluid.

The use of formic acid to chemically cleave aggregated proteins, in combination with quantitative MS, enabled us to perform the first in-depth characterization of HttEx1 aggregates *in vivo* and in a stage- and brain region-dependent manner. This generic approach provides an unbiased tool to study insoluble aggregates in other misfolding diseases. In the case of HD, we find that the insoluble fraction containing late-stage HttEx1 aggregates consists of several hundred proteins, concordant with the very large size of IBs in model systems and patients. Just a few proteins, generally only expressed in the brain, make up the bulk of the aggregate mass. This suggests that the aggregate composition in HD, and perhaps in other NDDs, is highly tissue specific. The presence of several myelin-associated proteins was surprising, because these are expressed mainly in glial cells. However, in our recent brain proteome resource (Sharma et al., 2015), as well as in the Human Protein Atlas (Uhlén et al., 2015), myelin was also detected in neurons, and we could confirm the presence of Plp1 in IBs by immunostaining. Therefore, we believe that these proteins derive mostly from neuronal IBs, not from oligodendrocytes.

Few aggregate constituents were known previously, such as proteostasis network components, native huntingtin interactors, and several transcription factors. However, most identified proteins represent diverse biological functions. We found that these proteins are rich in aggregation-prone motifs, such as CCDs or LCRs. CCDs and LCRs are molecular recognition motifs, regulating oligomerization of higher-order structures among both RNAs and proteins (Cumberworth et al., 2013; Kato et al., 2012). CCDs are prominently involved in protein-protein interactions and can interact with polyQ proteins, promoting their aggregation (Fiumara et al., 2010). RNA-binding proteins, which figure prominently in the aggregates, are particularly rich in LCRs, because they can be molecular determinants of RNA granule assembly (Han et al., 2012; Kato et al., 2012). The formation of such reversible structures allows increase of local concentrations of relevant interactors. However, because LCRs also promote protein binding promiscuity and aggregation propensity, this comes at the cost of undesirable, non-productive interactions, leading to several diseases (Cumberworth et al., 2013). We have shown in a cell model of HD that LCR domains co-aggregate with mutant HTT and other LCR-containing proteins, exacerbating aggregate formation (Kim et al., 2016). Our current results suggest that LCRs are also responsible for promoting co-aggregation *in vivo*. Several elements of the protein folding machinery also contain LCRs (Hageman et al., 2010). It is tempting to speculate that the presence of these sequences in both aggregation-prone and aggregation-counteracting proteins represents a balance that has co-evolved over time.

Our insoluble fraction showed little overlap with recently published protein aggregation sets. Of all insoluble proteins in our dataset, less than 5% overlapped with interactors of artificial

amyloid-like beta sheet proteins (Olzscha et al., 2011), and less than 1% were shared with either RNA-binding proteins containing prion-like domains (Li et al., 2013) or stress granules (Jain et al., 2016). The little overlap between these aggregation-associated proteins indicates that proteins from our insoluble dataset specifically co-aggregate with mutant HttEx1.

The integrative aspect of jointly analyzing the soluble and insoluble proteome, combined with the spatiotemporal resolution, allowed us to elucidate molecular neurodegeneration signatures that have not yet been linked to HD. Hundreds of proteins were downregulated in the soluble proteome and upregulated in the insoluble proteome. This prevalent sequestration of proteins into the aggregates suggests widespread loss of protein function in HD. Although it has been reported that IBs are protective by sequestering toxic soluble oligomers (Arrasate et al., 2004; Haass and Selkoe, 2007), the substantial depletion of soluble proteins observed here suggests a major impairment of protein homeostasis in the cell.

In accordance with this hypothesis, our rescue experiments demonstrated that overexpression of loss-of-function candidates ameliorated HttEx1 toxicity in a cellular HD model. The molecular mechanism underlying the observed increase in cell viability requires further analysis. It is possible that each of the selected candidates is necessary for cell survival and overexpression simply re-supplies the cell with an essential factor. In addition, a protein with a strong affinity for HttEx1 aggregates may occupy much of the aggregates' interaction surface and thereby reduce sequestration of endogenous proteins, as suggested by the increase of the soluble proportion of most proteins upon transfection of the candidates into HD-Q74 cells. The latter scenario may also explain why many of our candidates reduced IB size. Our data therefore suggest that overexpression of candidate proteins could increase cell viability by interfering with multistage aggregate formation. Soluble interactors of both native and mutant NDD proteins have been identified as disease modifiers (Hosp et al., 2015; Kaltenbach et al., 2007). Most proteins in the insoluble aggregates, however, are most likely not associated with the native function of the disease protein. Given the high proportion of toxicity mediators in our validation set, it is likely that the total set of potential loss-of-function proteins contains further candidates that would be interesting to study in the context of HD.

In summary, we provide a rich resource comprising (1) changes in the proteome upon disease progression, (2) protein copy numbers, (3) degree of protein sequestration to the IBs, and (4) correlation of proteomes across different brain regions, time, and aspects of the brain and cerebrospinal fluid proteome. Altogether, these data paint a quantitative picture of the dynamic aggregate proteome in relation to the brain proteome. This highlights the power of integrative approaches to elucidate molecular mechanisms of HD, helping to bridge the gap between identification of disease-associated pathways and their corresponding phenotypes.

EXPERIMENTAL PROCEDURES

Further details and an outline of resources used in this work can be found in Supplemental Experimental Procedures.

Cell Lines

Rat PC12 pheochromocytoma cell lines stably transfected with either GFP-fused Huntingtin Exon1-Q23 or Huntingtin Exon1-Q74 were a gift from David Rubinsztein (Cambridge Institute for Medical Research). Both lines were cultured and induced as described (Wyttenbach et al., 2001). Briefly, cells were maintained at 70 μg/mL hygromycin B (Thermo Fisher Scientific) in standard medium consisting of high-glucose DMEM (Sigma-Aldrich) with 100 U/mL penicillin/streptomycin (Sigma-Aldrich), 2 mM GlutaMAX (Life Technologies), 10% heat-inactivated horse serum (HS) (Life Technologies), 5% Tet-approved fetal bovine serum (Clontech), and 100 μg/mL G418 (Thermo Fisher Scientific) at 37°C, 10% CO2. Induction of HttEx1-Q23 or HttEx1-Q74 was carried out by adding doxycycline (Sigma-Aldrich) at 1 μg/mL. After induction with doxycycline, cells were kept at 1% HS to maintain them in a quiescent-like state.

Mouse Strains

For the proteomic study, female R6/2 mice (B6CBA-Tg(HDexon1)62 gpb/1J) carrying a 150 ± 5 CAG repeat expansion and non-transgenic littermate controls at 5 weeks of age were obtained from the Jackson Laboratory (Bar Harbor, Maine, USA) and sacrificed at the age of 5, 8, and 12 weeks. For further studies, an R6/2 colony was established at the animal facility of the Max Planck Institute of Biochemistry, Martinsried, from male R6/2 mice (B6CBA-Tg(HDexon1)62 gpb/1J) obtained from the Jackson Laboratory. The colony was maintained by crossing carrier males to CBA x C57BL/6 F1 females. Only female R6/2 mice were used for experiments. All animals used in this study had *ad libitum* access to standard mouse food and water and were maintained consistent with an animal protocol approved by the local authorities (Regierung von Oberbayern, animal protocol 55.2-1-54-2532-168-2014).

LC-MS/MS Analysis

MS analysis was performed using Q Exactive mass spectrometers (Thermo Fisher Scientific, Bremen, Germany) coupled online to a nanoflow ultra-high performance liquid chromatography (UHPLC) instrument (Easy1000 nLC, Thermo Fisher Scientific). Peptides were separated on a 50-cm-long (75 μm inner diameter) column packed in house with ReproSil-Pur C18-AQ 1.9 μm resin (Dr. Maisch, Ammerbuch, Germany). Column temperature was kept at 50°C by an in-house-designed oven with a Peltier element, and operational parameters were monitored in real time by the SprayQc software (Scheltema and Mann, 2012). Peptides were loaded with buffer A (0.1% [v/v] formic acid) and eluted with a nonlinear gradient of 5%–60% buffer B (0.1% [v/v] formic acid, 80% [v/v] acetonitrile) at a flow rate of 250 nL/min. Peptide separation was achieved by 245 min gradients (soluble proteome), 120 min gradients (cerebrospinal fluid), or 60 min gradients (insoluble proteome). The survey scans (300–1,700 m/z, target value = 3E6, maximum ion injection times = 20 ms) were acquired at a resolution of 70,000, followed by higher-energy collisional dissociation (HCD)-based fragmentation (normalized collision energy = 25) of up to 10 dynamically chosen, most abundant precursor ions. The MS/MS scans were acquired at a resolution of 17,500 (target value = 1E5, maximum ion injection times = 120 ms). Repeated sequencing of peptides was minimized by excluding the selected peptide candidates for 20 s.

Statistical Analysis

The type of statistical test (e.g., ANOVA or Mann-Whitney U test) is annotated in the figure legend and/or in the Supplemental Experimental Procedures segment specific to the analysis. In addition, statistical parameters such as the value of n, mean or median, SD, and significance level are reported in the figures and/or in the figure legends. When asterisks are used to signify the significance level, the key is reported in the respective figure legend. Statistical analyses were performed using Perseus or R as described in Supplemental Experimental Procedures for individual analysis.

DATA AND SOFTWARE AVAILABILITY

The accession number for the raw and processed data reported in this paper is PRIDE: PXD004973.

SUPPLEMENTAL INFORMATION

Supplemental Information includes Supplemental Experimental Procedures, seven figures, and four tables and can be found with this article online at https://doi.org/10.1016/j.celrep.2017.10.097.

AUTHOR CONTRIBUTIONS

F.H. performed wet lab and MS experiments and analyzed the data. S.G.-A. performed wet lab and imaging experiments and analyzed the data. I.D. performed cerebrospinal fluid extraction and mouse brain dissection. M.H.S. and J.C. developed bioinformatic tools. M.S.H., F.M., and F.-U.H. provided reagents and advised research. F.H., S.G.-A., I.D., R.K., and M.M. interpreted the data. F.H. and M.M. conceived the project and wrote the manuscript. All authors read and approved the manuscript.

ACKNOWLEDGMENTS

We thank our colleagues at the Max Planck Institutes of Biochemistry and Neurobiology, especially G.H.H. Borner and D. Hornburg for help and fruitful discussions; S. Kroiss, K. Mayr, I. Paron, G. Sowa, and B. Splettstösser for excellent technical assistance; and K. Schulz-Trieglaff and the MPIB animal facility for help with the R6/2 breeding and caretaking. We acknowledge the gift of the PC12 HD cell lines from D. Rubinsztein (University of Cambridge, UK). The research leading to these results has received funding from the Munich Cluster for Systems Neurology "SyNergy," the European Research Council Synergy grant "ToPAG—Toxic protein aggregation in neurodegeneration" (ERC-2012-SyG_318987-ToPAG), and the Max Planck Society for the Advancement of Science.

Received: June 23, 2017
Revised: September 13, 2017
Accepted: October 24, 2017
Published: November 21, 2017

REFERENCES

Acuña, A.I., Esparza, M., Kramm, C., Beltrán, F.A., Parra, A.V., Cepeda, C., Toro, C.A., Vidal, R.L., Hetz, C., Concha, I.I., et al. (2013). A failure in energy metabolism and antioxidant uptake precede symptoms of Huntington's disease in mice. Nat. Commun. *4*, 2917.

Aebersold, R., and Mann, M. (2016). Mass-spectrometric exploration of proteome structure and function. Nature *537*, 347–355.

Arrasate, M., Mitra, S., Schweitzer, E.S., Segal, M.R., and Finkbeiner, S. (2004). Inclusion body formation reduces levels of mutant huntingtin and the risk of neuronal death. Nature *431*, 805–810.

Baldo, B., Paganetti, P., Grueninger, S., Marcellin, D., Kaltenbach, L.S., Lo, D.C., Semmelroth, M., Zivanovic, A., Abramowski, D., Smith, D., et al. (2012). TR-FRET-based duplex immunoassay reveals an inverse correlation of soluble and aggregated mutant huntingtin in Huntington's disease. Chem. Biol. *19*, 264–275.

Byrne, L.M., and Wild, E.J. (2016). Cerebrospinal fluid biomarkers for Huntington's disease. J. Huntingtons Dis. *5*, 1–13.

Carapito, R., Paul, N., Untrau, M., Le Gentil, M., Ott, L., Alsaleh, G., Jochem, P., Radosavljevic, M., Le Caignec, C., David, A., et al. (2015). A de novo ADCY5 mutation causes early-onset autosomal dominant chorea and dystonia. Mov. Disord. *30*, 423–427.

Carter, R.J., Lione, L.A., Humby, T., Mangiarini, L., Mahal, A., Bates, G.P., Dunnett, S.B., and Morton, A.J. (1999). Characterization of progressive motor deficits in mice transgenic for the human Huntington's disease mutation. J. Neurosci. *19*, 3248–3257.

Chen, J.Y., Wang, E.A., Cepeda, C., and Levine, M.S. (2013). Dopamine imbalance in Huntington's disease: a mechanism for the lack of behavioral flexibility. Front. Neurosci. *7*, 114.

Culver, B.P., Savas, J.N., Park, S.K., Choi, J.H., Zheng, S., Zeitlin, S.O., Yates, J.R., 3rd, and Tanese, N. (2012). Proteomic analysis of wild-type and mutant huntingtin-associated proteins in mouse brains identifies unique interactions and involvement in protein synthesis. J. Biol. Chem. *287*, 21599–21614.

Cumberworth, A., Lamour, G., Babu, M.M., and Gsponer, J. (2013). Promiscuity as a functional trait: intrinsically disordered regions as central players of interactomes. Biochem. J. *454*, 361–369.

Cummings, D.M., André, V.M., Uzgil, B.O., Gee, S.M., Fisher, Y.E., Cepeda, C., and Levine, M.S. (2009). Alterations in cortical excitation and inhibition in genetic mouse models of Huntington's disease. J. Neurosci. *29*, 10371–10386.

Dalrymple, A., Wild, E.J., Joubert, R., Sathasivam, K., Björkqvist, M., Petersén, A., Jackson, G.S., Isaacs, J.D., Kristiansen, M., Bates, G.P., et al. (2007). Proteomic profiling of plasma in Huntington's disease reveals neuroinflammatory activation and biomarker candidates. J. Proteome Res. *6*, 2833–2840.

Davies, S.W., Turmaine, M., Cozens, B.A., DiFiglia, M., Sharp, A.H., Ross, C.A., Scherzinger, E., Wanker, E.E., Mangiarini, L., and Bates, G.P. (1997). Formation of neuronal intranuclear inclusions underlies the neurological dysfunction in mice transgenic for the HD mutation. Cell *90*, 537–548.

DiFiglia, M., Sapp, E., Chase, K.O., Davies, S.W., Bates, G.P., Vonsattel, J.P., and Aronin, N. (1997). Aggregation of huntingtin in neuronal intranuclear inclusions and dystrophic neurites in brain. Science *277*, 1990–1993.

Doi, H., Mitsui, K., Kurosawa, M., Machida, Y., Kuroiwa, Y., and Nukina, N. (2004). Identification of ubiquitin-interacting proteins in purified polyglutamine aggregates. FEBS Lett. *571*, 171–176.

Dunah, A.W., Jeong, H., Griffin, A., Kim, Y.M., Standaert, D.G., Hersch, S.M., Mouradian, M.M., Young, A.B., Tanese, N., and Krainc, D. (2002). Sp1 and TAFII130 transcriptional activity disrupted in early Huntington's disease. Science *296*, 2238–2243.

Fang, Q., Strand, A., Law, W., Faca, V.M., Fitzgibbon, M.P., Hamel, N., Houle, B., Liu, X., May, D.H., Poschmann, G., et al. (2009). Brain-specific proteins decline in the cerebrospinal fluid of humans with Huntington disease. Mol. Cell. Proteomics *8*, 451–466.

Fiumara, F., Fioriti, L., Kandel, E.R., and Hendrickson, W.A. (2010). Essential role of coiled coils for aggregation and activity of Q/N-rich prions and PolyQ proteins. Cell *143*, 1121–1135.

Galli, S., Lopes, D.M., Ammari, R., Kopra, J., Millar, S.E., Gibb, A., and Salinas, P.C. (2014). Deficient Wnt signalling triggers striatal synaptic degeneration and impaired motor behaviour in adult mice. Nat. Commun. *5*, 4992.

Geiger, T., Wehner, A., Schaab, C., Cox, J., and Mann, M. (2012). Comparative proteomic analysis of eleven common cell lines reveals ubiquitous but varying expression of most proteins. Mol. Cell. Proteomics *11*, M111.014050.

Gerfen, C.R., and Surmeier, D.J. (2011). Modulation of striatal projection systems by dopamine. Annu. Rev. Neurosci. *34*, 441–466.

Giampà, C., Laurenti, D., Anzilotti, S., Bernardi, G., Menniti, F.S., and Fusco, F.R. (2010). Inhibition of the striatal specific phosphodiesterase PDE10A ameliorates striatal and cortical pathology in R6/2 mouse model of Huntington's disease. PLoS ONE *5*, e13417.

Gratuze, M., Noël, A., Julien, C., Cisbani, G., Milot-Rousseau, P., Morin, F., Dickler, M., Goupil, C., Bezeau, F., Poitras, I., et al. (2015). Tau hyperphosphorylation and deregulation of calcineurin in mouse models of Huntington's disease. Hum. Mol. Genet. *24*, 86–99.

Gutekunst, C.A., Li, S.H., Yi, H., Mulroy, J.S., Kuemmerle, S., Jones, R., Rye, D., Ferrante, R.J., Hersch, S.M., and Li, X.J. (1999). Nuclear and neuropil aggregates in Huntington's disease: relationship to neuropathology. J. Neurosci. *19*, 2522–2534.

Haass, C., and Selkoe, D.J. (2007). Soluble protein oligomers in neurodegeneration: lessons from the Alzheimer's amyloid beta-peptide. Nat. Rev. Mol. Cell Biol. *8*, 101–112.

Hageman, J., Rujano, M.A., van Waarde, M.A., Kakkar, V., Dirks, R.P., Govorukhina, N., Oosterveld-Hut, H.M., Lubsen, N.H., and Kampinga, H.H. (2010). A DNAJB chaperone subfamily with HDAC-dependent activities suppresses toxic protein aggregation. Mol. Cell *37*, 355–369.

Han, T.W., Kato, M., Xie, S., Wu, L.C., Mirzaei, H., Pei, J., Chen, M., Xie, Y., Allen, J., Xiao, G., and McKnight, S.L. (2012). Cell-free formation of RNA granules: bound RNAs identify features and components of cellular assemblies. Cell *149*, 768–779.

Hazeki, N., Tukamoto, T., Goto, J., and Kanazawa, I. (2000). Formic acid dissolves aggregates of an N-terminal huntingtin fragment containing an expanded polyglutamine tract: applying to quantification of protein components of the aggregates. Biochem. Biophys. Res. Commun. *277*, 386–393.

Hosp, F., Vossfeldt, H., Heinig, M., Vasiljevic, D., Arumughan, A., Wyler, E., Genetic and Environmental Risk for Alzheimer's Disease GERAD1 Consortium; Landthaler, M., Hubner, N., Wanker, E.E., Lannfelt, L., et al. (2015). Quantitative interaction proteomics of neurodegenerative disease proteins. Cell Rep. *11*, 1134–1146.

Jain, S., Wheeler, J.R., Walters, R.W., Agrawal, A., Barsic, A., and Parker, R. (2016). ATPase-modulated stress granules contain a diverse proteome and substructure. Cell *164*, 487–498.

Jiang, M., Wang, J., Fu, J., Du, L., Jeong, H., West, T., Xiang, L., Peng, Q., Hou, Z., Cai, H., et al. (2011). Neuroprotective role of Sirt1 in mammalian models of Huntington's disease through activation of multiple Sirt1 targets. Nat. Med. *18*, 153–158.

Kaltenbach, L.S., Romero, E., Becklin, R.R., Chettier, R., Bell, R., Phansalkar, A., Strand, A., Torcassi, C., Savage, J., Hurlburt, A., et al. (2007). Huntingtin interacting proteins are genetic modifiers of neurodegeneration. PLoS Genet. *3*, e82.

Kato, M., Han, T.W., Xie, S., Shi, K., Du, X., Wu, L.C., Mirzaei, H., Goldsmith, E.J., Longgood, J., Pei, J., et al. (2012). Cell-free formation of RNA granules: low complexity sequence domains form dynamic fibers within hydrogels. Cell *149*, 753–767.

Kim, Y.E., Hosp, F., Frottin, F., Ge, H., Mann, M., Hayer-Hartl, M., and Hartl, F.U. (2016). Soluble oligomers of polyQ-expanded huntingtin target a multiplicity of key cellular factors. Mol. Cell *63*, 951–964.

Knowles, T.P., Vendruscolo, M., and Dobson, C.M. (2014). The amyloid state and its association with protein misfolding diseases. Nat. Rev. Mol. Cell Biol. *15*, 384–396.

Kroksveen, A.C., Opsahl, J.A., Aye, T.T., Ulvik, R.J., and Berven, F.S. (2011). Proteomics of human cerebrospinal fluid: discovery and verification of biomarker candidates in neurodegenerative diseases using quantitative proteomics. J. Proteomics *74*, 371–388.

Langfelder, P., Cantle, J.P., Chatzopoulou, D., Wang, N., Gao, F., Al-Ramahi, I., Lu, X.H., Ramos, E.M., El-Zein, K., Zhao, Y., et al. (2016). Integrated genomics and proteomics define huntingtin CAG length-dependent networks in mice. Nat. Neurosci. *19*, 623–633.

Lein, E.S., Hawrylycz, M.J., Ao, N., Ayres, M., Bensinger, A., Bernard, A., Boe, A.F., Boguski, M.S., Brockway, K.S., Byrnes, E.J., et al. (2007). Genome-wide atlas of gene expression in the adult mouse brain. Nature *445*, 168–176.

Li, S.H., and Li, X.J. (2004). Huntingtin-protein interactions and the pathogenesis of Huntington's disease. Trends Genet. *20*, 146–154.

Li, Y.R., King, O.D., Shorter, J., and Gitler, A.D. (2013). Stress granules as crucibles of ALS pathogenesis. J. Cell Biol. *201*, 361–372.

Mangiarini, L., Sathasivam, K., Seller, M., Cozens, B., Harper, A., Hetherington, C., Lawton, M., Trottier, Y., Lehrach, H., Davies, S.W., and Bates, G.P. (1996). Exon 1 of the HD gene with an expanded CAG repeat is sufficient to cause a progressive neurological phenotype in transgenic mice. Cell *87*, 493–506.

Martinez, F.J., Pratt, G.A., Van Nostrand, E.L., Batra, R., Huelga, S.C., Kapeli, K., Freese, P., Chun, S.J., Ling, K., Gelboin-Burkhart, C., et al. (2016). Protein-RNA networks regulated by normal and ALS-associated mutant HNRNPA2B1 in the nervous system. Neuron *92*, 780–795.

Meade, C.A., Deng, Y.P., Fusco, F.R., Del Mar, N., Hersch, S., Goldowitz, D., and Reiner, A. (2002). Cellular localization and development of neuronal intranuclear inclusions in striatal and cortical neurons in R6/2 transgenic mice. J. Comp. Neurol. *449*, 241–269.

Mitsui, K., Nakayama, H., Akagi, T., Nekooki, M., Ohtawa, K., Takio, K., Hashikawa, T., and Nukina, N. (2002). Purification of polyglutamine aggregates and identification of elongation factor-1alpha and heat shock protein 84 as aggregate-interacting proteins. J. Neurosci. *22*, 9267–9277.

Olzscha, H., Schermann, S.M., Woerner, A.C., Pinkert, S., Hecht, M.H., Tartaglia, G.G., Vendruscolo, M., Hayer-Hartl, M., Hartl, F.U., and Vabulas, R.M. (2011). Amyloid-like aggregates sequester numerous metastable proteins with essential cellular functions. Cell *144*, 67–78.

Orr, H.T., and Zoghbi, H.Y. (2007). Trinucleotide repeat disorders. Annu. Rev. Neurosci. *30*, 575–621.

Ortega, Z., and Lucas, J.J. (2014). Ubiquitin-proteasome system involvement in Huntington's disease. Front. Mol. Neurosci. *7*, 77.

Ossovskaya, V.S., and Bunnett, N.W. (2004). Protease-activated receptors: contribution to physiology and disease. Physiol. Rev. *84*, 579–621.

Ross, C.A., and Poirier, M.A. (2004). Protein aggregation and neurodegenerative disease. Nat. Med. *10* (*Suppl*), S10–S17.

Russell, D.S., Barret, O., Jennings, D.L., Friedman, J.H., Tamagnan, G.D., Thomae, D., Alagille, D., Morley, T.J., Papin, C., Papapetropoulos, S., et al. (2014). The phosphodiesterase 10 positron emission tomography tracer, [18F]MNI-659, as a novel biomarker for early Huntington disease. JAMA Neurol. *71*, 1520–1528.

Saudou, F., and Humbert, S. (2016). The biology of huntingtin. Neuron *89*, 910–926.

Schaefer, M.H., Wanker, E.E., and Andrade-Navarro, M.A. (2012). Evolution and function of CAG/polyglutamine repeats in protein-protein interaction networks. Nucleic Acids Res. *40*, 4273–4287.

Scheltema, R.A., and Mann, M. (2012). SprayQc: a real-time LC-MS/MS quality monitoring system to maximize uptime using off the shelf components. J. Proteome Res. *11*, 3458–3466.

Schwanhäusser, B., Busse, D., Li, N., Dittmar, G., Schuchhardt, J., Wolf, J., Chen, W., and Selbach, M. (2011). Global quantification of mammalian gene expression control. Nature *473*, 337–342.

Sharma, K., Vabulas, R.M., Macek, B., Pinkert, S., Cox, J., Mann, M., and Hartl, F.U. (2012). Quantitative proteomics reveals that Hsp90 inhibition preferentially targets kinases and the DNA damage response. Mol. Cell. Proteomics *11*, M111.014654.

Sharma, K., Schmitt, S., Bergner, C.G., Tyanova, S., Kannaiyan, N., Manrique-Hoyos, N., Kongi, K., Cantuti, L., Hanisch, U.K., Philips, M.A., et al. (2015). Cell type- and brain region-resolved mouse brain proteome. Nat. Neurosci. *18*, 1819–1831.

Shimohata, T., Nakajima, T., Yamada, M., Uchida, C., Onodera, O., Naruse, S., Kimura, T., Koide, R., Nozaki, K., Sano, Y., et al. (2000). Expanded polyglutamine stretches interact with TAFII130, interfering with CREB-dependent transcription. Nat. Genet. *26*, 29–36.

Shirasaki, D.I., Greiner, E.R., Al-Ramahi, I., Gray, M., Boontheung, P., Geschwind, D.H., Botas, J., Coppola, G., Horvath, S., Loo, J.A., and Yang, X.W. (2012). Network organization of the huntingtin proteomic interactome in mammalian brain. Neuron *75*, 41–57.

Stroedicke, M., Bounab, Y., Strempel, N., Klockmeier, K., Yigit, S., Friedrich, R.P., Chaurasia, G., Li, S., Hesse, F., Riechers, S.P., et al. (2015). Systematic interaction network filtering identifies CRMP1 as a novel suppressor of huntingtin misfolding and neurotoxicity. Genome Res. *25*, 701–713.

The Huntington's Disease Collaborative Research Group (1993). A novel gene containing a trinucleotide repeat that is expanded and unstable on Huntington's disease chromosomes. Cell *72*, 971–983.

Uhlén, M., Fagerberg, L., Hallström, B.M., Lindskog, C., Oksvold, P., Mardinoglu, A., Sivertsson, Å., Kampf, C., Sjöstedt, E., Asplund, A., et al. (2015). Proteomics. Tissue-based map of the human proteome. Science *347*, 1260419.

Vonsattel, J.P., and DiFiglia, M. (1998). Huntington disease. J. Neuropathol. Exp. Neurol. *57*, 369–384.

Walther, D.M., and Mann, M. (2011). Accurate quantification of more than 4000 mouse tissue proteins reveals minimal proteome changes during aging. Mol. Cell. Proteomics *10*, M110.004523.

Warringer, J., and Blomberg, A. (2006). Evolutionary constraints on yeast protein size. BMC Evol. Biol. *6*, 61.

Winklhofer, K.F., Tatzelt, J., and Haass, C. (2008). The two faces of protein misfolding: gain- and loss-of-function in neurodegenerative diseases. EMBO J. *27*, 336–349.

Wiśniewski, J.R., Hein, M.Y., Cox, J., and Mann, M. (2014). A "proteomic ruler" for protein copy number and concentration estimation without spike-in standards. Mol. Cell. Proteomics *13*, 3497–3506.

Woodman, B., Butler, R., Landles, C., Lupton, M.K., Tse, J., Hockly, E., Moffitt, H., Sathasivam, K., and Bates, G.P. (2007). The Hdh(Q150/Q150) knock-in mouse model of HD and the R6/2 exon 1 model develop comparable and widespread molecular phenotypes. Brain Res. Bull. *72*, 83–97.

Wyttenbach, A., Swartz, J., Kita, H., Thykjaer, T., Carmichael, J., Bradley, J., Brown, R., Maxwell, M., Schapira, A., Orntoft, T.F., et al. (2001). Polyglutamine expansions cause decreased CRE-mediated transcription and early gene expression changes prior to cell death in an inducible cell model of Huntington's disease. Hum. Mol. Genet. *10*, 1829–1845.

B.2 Cortical circuit alterations precede disease onset in Huntington's disease mice

Cortical circuit alterations precede disease onset in Huntington's disease mice

Abbreviated title: Cortical circuit changes in HD mice

Johanna Neuner[1,9], Elena Katharina Schulz-Trieglaff[1,9], Sara Gutiérrez-Ángel[1], Fabian Hosp[2], Matthias Mann[2], Thomas Arzberger[3,4,5], Rüdiger Klein[1,6,10], Sabine Liebscher[6,7,8,10,*] and Irina Dudanova[1,10,*]

[1]Department of Molecules – Signaling – Development, Max Planck Institute of Neurobiology, 82152 Martinsried, Germany

[2]Department of Proteomics and Signal Transduction, Max Planck Institute of Biochemistry, 82152 Martinsried, Germany

[3]German Center for Neurodegenerative Diseases (DZNE), 81377 Munich, Germany

[4]Center for Neuropathology and Prion Research, Ludwig-Maximilians University Munich, 81377 Munich, Germany

[5]Department of Psychiatry and Psychotherapy, Ludwig-Maximilians University Munich, 81377 Munich, Germany

[6]Munich Cluster for Systems Neurology (SyNergy), 81377 Munich, Germany

[7]Institute of Clinical Neuroimmunology, Klinikum der Universität München, Ludwig-Maximilians University, 82152 Martinsried, Germany

[8]Biomedical Center, Medical Faculty, Ludwig-Maximilians University Munich, 82152 Martinsried, Germany

[9]These authors contributed equally

[10]These authors contributed equally

* Correspondence: sabine.liebscher@med.uni-muenchen.de (S.L.), idudanova@neuro.mpg.de (I.D.)

Conflicts of Interest

The authors declare no conflicts of interest.

Acknowledgements

We thank Nejc Dolensek for the implementation of the speed sensor; Narasimha Reddy Vaka, Robert Kasper, Diego Sangineto and Henry Haeberle for technical support with microscope hardware; Pieter

Goltstein and Tobias Rose for providing custom-made tools for awake imaging; Hakan Kucukdereli and Pieter Goltstein for insightful discussions; Stefanie Huschenbett, Mario Rivera-Cortes and Eneyda Kowalski for excellent animal care; Julia Boshart for excellent assistance with histology; André Wilke for quantification of immunostainings; André Wilke and Tammo von Knoblauch for mouse genotyping; and Dominique Förster for critically reading the manuscript. This work was funded by the European Research Council Synergy Grant under FP7 GA number ERC-2012-*SyG_318987*-Toxic Protein Aggregation in Neurodegeneration (ToPAG) to R.K. and M.M., and by the Max Planck Society for the Advancement of Science.

Abstract

Huntington's disease (HD) is a devastating hereditary movement disorder, characterized by degeneration of neurons in the striatum and cortex. Studies in human patients and mouse HD models suggest that disturbances of neuronal function in the neocortex play an important role in the disease onset and progression. However, the precise nature and time course of cortical alterations in HD have remained elusive. Here, we use chronic *in vivo* two-photon calcium imaging to monitor the activity of single neurons in layer 2/3 of the primary motor cortex in awake, behaving R6/2 transgenic HD mice and wildtype littermates. R6/2 mice show age-dependent changes in neuronal activity with a clear increase in activity at the age of 8.5 weeks, preceding the onset of motor and neurological symptoms. Furthermore, quantitative proteomics demonstrate a pronounced downregulation of synaptic proteins in the cortex, and histological analyses in R6/2 mice and HD patient samples reveal reduced inputs from parvalbumin-positive interneurons onto layer 2/3 pyramidal cells. Thus, our study provides a time-resolved description as well as mechanistic details of cortical circuit dysfunction in HD.

Significance statement

Funtional alterations in the cortex are believed to play an important role in the pathogenesis of Huntington's disease (HD). However, studies monitoring cortical activity in HD models *in vivo* at a single-cell resultion are still lacking. We have used chronic two-photon imaging to investigate changes in the activity of single neurons in the primary motor cortex of awake presymptomatic HD mice. We show that neuronal activity increases before the mice develop disease symptoms. Our histological analyses in mice and in human HD autopsy cases furthermore demonstrate a loss inhibitory synaptic terminals from parvalbimun-positive interneurons, revealing a potential mechanism of cortical circuit impairment in HD.

Introduction

Huntington's disease (HD) is an incurable hereditary neurodegenerative disorder, characterized by choreatic movements in combination with cognitive decline and psychiatric symptoms. HD is caused by an expansion of the CAG repeat in exon 1 of the Huntingtin gene (Huntington's Disease Collborative Research Group, 1993), resulting in the expression of the aggregation-prone mutant Huntingtin (mHTT) protein with an elongated polyglutamine (polyQ) tract. mHTT interferes with multiple cellular functions, including transcription, energy metabolism, protein homeostasis and intracellular transport (Labbadia and Morimoto, 2013; Saudou and Humbert, 2016). The striatum is the most vulnerable region in HD, however, prominent pathological changes are also observed in the neocortex (Vonsattel and DiFiglia, 1998; Raymond et al., 2011; Waldvogel et al., 2012). Importantly, ample evidence points towards the disturbance of cortical function and impairment of corticostriatal communication as crucial early events in HD (Miller et al., 2011; Unschuld et al., 2012; Estrada-Sanchez and Rebec, 2013; Veldman and Yang, 2017). Imaging studies in HD gene expansion carriers demonstrate that cortical thinning and abnormalities of cortical activity contribute to the onset, progression and clinical variability of HD (Reading et al., 2004; Rosas et al., 2005; Rosas et al., 2008; Schippling et al., 2009; Nopoulos et al., 2010; Orth et al., 2010; Waldvogel et al., 2012). In particular, primary motor cortex (M1) is among the regions showing the earliest changes (Rosas et al., 2008), and the degree of cell loss in this area correlates with the motor impairments (Thu et al., 2010). In addition, analyses of tissue-specific conditional mouse models revealed the requirement of mHTT in both the striatum and the cortex for driving the full extent of HD phenotypes (Gu et al., 2005; Gu et al., 2007). Likewise, mHTT lowering in both regions is necessary for an efficient rescue of HD-related deficits (Wang et al., 2014; Estrada-Sanchez et al., 2015).

Cortical pyramidal neurons (principal cells, PCs) are known to be a vulnerable cell population in HD (Estrada-Sanchez and Rebec, 2013). HD mouse models display multiple morphological and electrophysiological abnormalities in these cells. Reduced dendritic arborizations and a decline in the density and stability of dendritic spines on PCs were observed in the somatosensory cortex (Klapstein et al., 2001; Murmu et al., 2013; Murmu et al., 2015). These defects were paralleled by lower levels of several synaptic proteins and a decrease in excitatory synapse density at an advanced disease stage (Murmu et al., 2015). In addition, electrophysiological recordings revealed changes in both excitatory

and inhibitory inputs onto layer 2/3 (L2/3) PCs (Gu et al., 2005; Spampanato et al., 2008; Cummings et al., 2009).

Although the main focus in cortical HD pathology has been on PCs, there is also increasing evidence for an involvement of cortical interneurons (INs). Reductions in certain populations of INs were detected in human postmortem HD brains (Kim et al., 2014; Mehrabi et al., 2016). Furthermore, studies in conditional mouse models demonstrated the importance of mHTT expression in INs for the development of cortical pathology and behavioral defects (Gu et al., 2005), and attributed certain electrophysiological and behavioral alterations specifically to IN dysfunction (Dougherty et al., 2014). Despite these insights into the impairments occurring in PCs and INs, it has remained unclear how cortical network function is affected *in vivo* before disease onset and at different disease stages, and which molecular and circuit mechanisms underlie these functional alterations.

Here, we use chronic *in vivo* two-photon calcium imaging in awake, behaving HD mice to monitor the activity of large populations of L2/3 neurons in the M1 area at single-cell resolution. Our imaging experiments reveal disturbances of neuronal activity that precede the onset of symptoms. Proteomic analyses show a pronounced downregulation of synaptic proteins in the cortex, whereas histological findings in HD mouse brains and in human postmortem tissue point to a loss of parvalbumin (PV)-positive inhibitory synapses on PCs, providing a possible circuit mechanism for the cortical dysfunction in HD mice.

Materials and Methods

Transgenic mice

R6/2 mice (Mangiarini et al., 1996) transgenic for the 5′ end of the human *huntingtin* gene were maintained in a specific pathogen-free animal facility by crossing R6/2 males to F1 C57Bl6/CBA females. The presence of the transgene was verified by PCR with the following primers: forward, 5′-CCGCTCAGGTTCTGCTTTTA-3′, reverse, 5′- TGGAAGGACTTGAGGGACTC-3′. CAG repeat length was determined by Laragen and averaged 192 repeats. Mice were kept in inverted 14-10 h light-dark cycle from surgery on, had free access to food and water and showed no signs of inflammation or metabolic compromise. All procedures were performed in accordance with mouse protocols approved by the Government of Upper Bavaria (55.2-1-54-2532-168-2014, 55.2-1-54-2532-19-2015).

Behavioral tests

Rotarod. Rotarod test was performed on a Rota-Rod NG (Ugo Basile). Mice were first trained on two consecutive days for 300 s at 5 rpm, and then tested on the accelerating rotarod from 5 to 40 rpm over a 300 s period. Latency to fall was recorded on three trials separated by 15 min resting periods, and the average value was taken for analysis.

Open field. Locomotor activity in the open field was assessed one hour after the beginning of the dark cycle. Mice were placed into a custom-made 40x40 cm arena, and total distance traveled was recorded for 10 min. The floor of the chamber was washed between the trials to minimize any olfactory cues that could affect exploratory behavior.

Virus injection and cranial window surgery

For *in vivo* calcium imaging, an adeno-associated virus (AAV1/2) containing the genetically encoded calcium indicator GCaMP6s (Chen et al., 2013) and the bright structural marker mRuby2 (Lam et al., 2012) under the control of the human synapsin-1 promoter was used to label cortical neurons (Rose et al., 2016). Intracerebral injections of AAV and cranial window implantation were performed within the same surgery in 3.5-week-old mice deeply anesthetized with an intraperitoneal (i.p.) injection of ketamine/xylazine (130 and 10 mg kg^{-1} body weight, respectively). The analgesic carprofen (5 mg kg^{-1} body weight, subcutaneously) and the anti-inflammatory drug dexamethasone (10 mg kg^{-1}, i.p.) were administered shortly before surgery. To increase viral uptake and spread, mannitol (20% solution; 30

ml kg^{-1} body weight, i.p.) was applied 20 min prior to virus injection (Burger et al., 2005). During surgery, the virus (titer: ~10^{12} infecting units per ml) was injected into L2/3 of M1 cortex (3 injection sites with stepwise 300 nl injections at 150, 200 and 250 µm depth). Next, a cranial window over the right cortical hemisphere was implanted as previously described (Holtmaat et al., 2009). Briefly, a circular piece of skull (4 mm in diameter) was removed over the fore- and hindlimb area of M1 (position: 1.3 mm lateral and 1.0 mm anterior to bregma) using a dental drill (Foredom). A round coverslip (VWR; d=4 mm) was glued to the skull using histoacryl glue (B.Braun) and dental acrylic cement (Kerr Vertise Flow). After surgery, mice received a subcutaneous injection of the antibiotic cefotaxime (60 mg kg^{-1}) and were placed in a warm environment for recovery. After 10 days, a small custom-made metal bar (1 cm x 3 cm; 0.06 g) with a round opening was glued onto the coverslip with dental acrylic cement to allow for stable head fixation under the objective and repeated repositioning of mice during subsequent imaging sessions. Imaging began after a 21-day resting period after surgery.

Handling and ball training

At the age of 5 weeks, mice were handled on 5 consecutive days for 10 min until they were familiarized with the trainer and routinely ran from hand to hand. In the subsequent ball training mice got adjusted to the experimental setup and head fixation. Ball training sessions that were repeated on 3 consecutive days were set in the dark (infrared (IR) light source) and lasted for 30 min. Mice were head-fixed by the metal bar to a custom-made holder and placed onto a styrofoam ball (d=20 cm) that floated on pressurized air and was custom-installed under the microscope objective (Dombeck et al., 2007). Mouse behavior (resting or running) was observed with an IR-sensitive camera (USB 2.0, 1/3"CMOS, 744x480 pixel; 8 mm M0814MP2 1.4-16C, 2/3", megapixel c-mount objective; TIS) without exposure to additional stimuli or learning tasks. After the third session, mice had adjusted to the head fixation and showed alternating running and resting behavior.

Two-photon calcium imaging in behaving mice

During the experiment, the same conditions as during ball training were applied. Mouse behavior was tracked at 15 Hz with an IR-sensitive video camera (TIS) and custom software (Input Controller, TIS). In addition, to track ball motion, a computer gaming mouse (G500S, Logitech) was positioned along the ball axis, controlled by a raspberry pi3 and custom written scripts using PuTTY to count ball rotation

events (1000 counts/s). To synchronize *in vivo* two-photon imaging, behavioral video recording and ball speed measurements, a 900s lasting TTL pulse (5V) was sent to relevant hardware using Matlab (Mathworks). *In vivo* calcium imaging was performed with an upright multiphoton microscope (Bergamo II, Thorlabs) equipped with a Ti:Sapphire laser with dual beam (InSight DeepSee, Spectra Physics), a 8 kHz galvo/resonant scanner and a 16x, 0.8 NA water immersion objective (Nikon). The laser intensities were modulated with Pockels cells (Conoptics). The following wavelengths and emission filters were used to simultaneously image the two fluorophores: 920 nm / 525±25 nm (GCaMP6s) and 1040 nm / 607±35 nm (mRuby2). ThorImage 2.4 software (Thorlabs) was used for microscope control and image acquisition. To measure neuronal activity, time series images of selected positions/fields of view (FOVs) with bright expression of the calcium indicator were acquired at 10 Hz for a total duration of 900 s. For each mouse, two FOVs were acquired per imaging time point at the depth of 150-350 μm. Efforts were made to keep the GCaMP6s fluorescence constant throughout the entire experiment ($\leq$50 mW laser power out of objective). For each FOV, an image of the blood vessel map was acquired under epifluorescence light to ensure return to the same position in serial experiments. In addition, the information about XYZ-coordinates provided by the microscope stage was documented for each image position. The structural marker mRuby2 was used to precisely adjust the FOV in the z-plane. After imaging, the animal was returned back to its housing cage for rest. At the last imaging time point, the same FOVs were additionally imaged for 300 s during isoflurane (1.5%) anesthesia.

Time series image processing and data analysis

Image analysis was performed with ImageJ (NIH) and Matlab software using custom written procedures. First, full frame images were registered and motion corrected in ImageJ using the moco plugin (Dubbs et al., 2016). Next, regions of interest (ROIs) were drawn manually around individual somata based on both maximum and mean intensity projections of all frames. For neighboring cells with direct contact, pixels containing signal from both neurons were excluded from the selection. For each imaging time point, the ROIs were visually inspected in the GCaMP and mRuby channel to ensure that the same cells were analyzed throughout the imaging period. The fluorescence intensity of all pixels inside each ROI was averaged and mean values were imported into Matlab for further processing as described previously (Liebscher et al., 2016). To account for neuropil contamination, the following correction method was applied: the initial ROI was fitted with an ellipse and this ellipse was stretched

by 6 pixels. All pixels of the initial ROI, as well as those in neighboring ROIs were excluded from the resulting larger ellipse. Next, the corrected ROI signal was computed as follows: $F_{ROI\_comp} = F_{ROI} - 0.7 \times (F_{neuropil} - \text{median}(F_{neuropil}))$ with F_{ROI_comp} representing the neuropil compensated fluorescence of the ROI, F_{ROI} referring to the fluorescence signal of the initial ROI selection and $F_{neuropil}$ to the signal stemming from the neuropil (Liebscher et al., 2016). To estimate the baseline level (F_0), each fluorescence trace was divided by the median of all values smaller than the 70th percentile of the entire trace and subtracting 1 from those values, which reflects the baseline well as judged by visual inspection. Cells were classified as active in a particular experiment if they crossed a threshold of baseline + 3 x SD of the $\Delta F/F$ trace at least once for a minimum of 10 consecutive frames (1 s).

Video sequences acquired for behavioral tracking were analyzed in EthoVision (Noldus), using the activity analysis tool. Briefly, a ROI was drawn manually around the forepaws. Changes in pixels induced by forepaw movement were registered as activity change and plotted over time by determined algorithms. For direct comparison of video and imaging data at equal frame numbers, the 15 Hz videos were reduced to 10 Hz using the signal.resample function from Scipy and imported into Matlab for further analysis.

MS data analysis and visualization

All data was obtained from the proteomic dataset published by Hosp et al. (2017). Principal component analysis (PCA) was conducted with the Perseus software package (Tyanova et al., 2016). Annotations were based on GOCC, GOBP, GOMF, CORUM, Pfam domains and KEGG pathway annotations with the exception of the main PCA drivers, which were complemented by manual annotations based on literature searches. All other analyses and data visualizations were performed with R software (R Development Core Team, 2008). Significantly changed protein expression was defined as a combination of a p-value lower than 0.05 and an expression change of at least two-fold compared to littermate controls.

Immunofluorescent staining and confocal microscopy

Mice were transcardially perfused with phosphate-buffered saline (PBS) followed by 4% paraformaldehyde (PFA) in PBS. Brains were dissected out, post-fixed in 4% PFA at 4°C for 48 h, and coronal brain sections (70 µm) were cut on a microtome (VT 1000S, Leica). Free-floating sections were

permeabilized in 0.5% TritonX-100 for 30 min and blocked in 5% normal donkey serum, 0.2% bovine serum albumin (BSA), 0.2% glycine, 0.2% lysine, 0.02% sodium azide in PBS for 2 h at room temperature, followed by overnight exposure to primary antibodies in 0.3% TritonX-100, 2% BSA, 0.02% sodium azide in PBS. The following primary antibodies were used: rabbit anti-PV, 1:500 (Abcam); mouse anti-NeuN, 1:500 (Millipore), guinea-pig anti-VGlut1 (Millipore), guinea-pig anti-vGlut2 (Millipore), mouse anti-PSD-95 (Sigma), mouse anti-Gephyrin (Synaptic systems), and rabbit anti-VGAT (Synaptic systems). After several washes with PBS, sections were incubated in corresponding Alexa secondary antibodies (Invitrogen) diluted 1:300 for 2 h followed by 10 min DAPI (Sigma) staining, several PBS washes and mounting with fluorescent mounting medium (DAKO). Fluorescence images were acquired with a Leica TCS SP8 confocal microscope using a 63x, 1.40 NA oil immersion objective (Leica). Image analysis was performed blindly with ImageJ and R. Briefly, images of pre- and postsynaptic stainings were converted into binary masks in ImageJ. Puncta of 2 pixels or less were excluded from further analysis. The coordinates of the remaining puncta were extracted using the "analyze particles" function. The distance of every presynaptic particle to every postsynaptic particle was then calculated using the Pythagorean equation and matrix calculations in R. A distance of 1 μm or less was counted as a synapse. For PV puncta quantification, the PC circumference was traced manually and measured with ImageJ. The area of the cell body and the surrounding PV staining were extracted and the PV-positive pixels counted using a custom written macro. The area of PV terminals around the cell body was normalized to the cell body perimeter.

Patient material

5 μm paraffin sections from the primary motor cortex of 3 HD autopsy cases and 3 age-matched controls were obtained from Neurobiobank Munich, Ludwig-Maximilians University Munich. Demographic information is provided in Table 1. The experiments were approved by the local ethics committee. Sections were deparaffinized in Xylene twice for 5 min, hydrated in a decreasing ethanol concentration series, and transferred to warm tap water for 5 min. Antigen retrieval was conducted in boiling Tris-EDTA buffer (10 mM Tris, 1mM EDTA, 0.05 % Tween 20, pH 9.0) for 15 min. Slides were then transferred to tap water and blocked with BLOXALL Blocking Solution (Vector Laboratories) for 10 min and subsequently with 2.5 % horse serum for 30 min. The following primary antibodies were used: rabbit anti-PV, 1:250 (Abcam) and mouse anti-CamK2α, 1:250 (Abcam). After several washes

with PBS, sections were incubated in corresponding Alexa secondary antibodies (Invitrogen) diluted 1:300, and Neurotrace, 1:500 (Life technologies) for 2 h followed by 10 min DAPI (Sigma) staining, several PBS washes and mounting with fluorescent mounting medium (DAKO). Fluorescence images were acquired with a Leica TCS SP8 confocal microscope using a 63x, 1.40 NA oil immersion objective (Leica). PCs in L2/3 were identified by their triangular shape, the presence of a nucleolus seen with Neurotrace, and/or through Camk2α-positive staining. Image analysis was performed with ImageJ and R. For PV puncta quantification, the circumference of the pyramidal neuron was traced manually, dilated by 1.5 µm and measured with ImageJ. The area of the cell body and the surrounding PV staining was extracted and the PV-positive pixels counted using a custom written macro. The area of PV terminals around the cell body was normalized to the cell body perimeter.

Experimental design and statistical analysis

Female R6/2 mice and female wildtype (WT) littermates were used in all experiments. Behavioral tests were conducted with groups of 7-10 WT and 10 R6/2 mice. For chronic imaging experiments, 6 WT and 5 R6/2 mice were used. Proteomic data was from 4 WT and 4 R6/2 5-week-old mice and 3 WT and 3 R6/2 8-week-old mice. Immunostainings were performed on brain sections of 5 WT and 5 R6/2 mice at 5 weeks of age, and 5 WT and 4 R6/2 mice at 8 weeks of age. Human data was from 3 HD and 3 age-matched control autopsy cases. For behavioral tests, comparisons were made with two-way ANOVA with Bonferroni´s multiple comparison test. Two-way repeated measures ANOVA was used to reveal effects of genotype and time in chronic imaging experiments. Pearson's Chi-square test was applied to evaluate changes in activity categories. Exact binomial two-sided test was used for binomially distributed data. Two-tailed unpaired Student's t-test was applied for comparisons of two groups in histological analyses. Data were analyzed in a blinded manner. Data are expressed as mean ± SEM unless indicated otherwise, with $p<0.05$ defining differences as statistically significant (*$p<0.05$; **$p<0.01$; ***$p<0.001$; n.s. - not significant).

Results

Chronic two-photon calcium imaging in the cortex of R6/2 mice

We investigated neuronal activity in R6/2 transgenic mice, which express mHTT-exon 1 with a pathological polyQ expansion under the human HTT promoter and are characterized by an early onset and rapid progression of disease (Fig. 1A) (Mangiarini et al., 1996; Carter et al., 1999; Meade et al., 2002). In spite of considerable brain atrophy, no obvious cell death is observed in this line until the age of 12 weeks (Mangiarini et al., 1996; Dodds et al., 2014). Overt neurological symptoms such as tremor, dyskinesia and balance impairment start at 9-11 weeks of age (Mangiarini et al., 1996). The exact age of onset of motor impairments varies between different R6/2 colonies and is dependent on the CAG repeat length. Surprisingly, very high repeat numbers, which occur due to the genetic instability of the repeats, lead to a later onset and overall attenuation of the HD-related phenotypes (Morton et al., 2009; Cummings et al., 2012). The CAG repeat length in our colony averaged 192 ± 2 repeats and was higher than in the original line (~150 repeats) (Mangiarini et al., 1996). We therefore characterized the motor phenotype in our colony by testing the mice on an accelerating rotarod and in the open field. 8 to 9-week-old R6/2 mice showed no significant deficits on the rotarod and normal locomotion in the open field, whereas by the age of 12-13 weeks, they were severely impaired in both tests (Two-way ANOVA with Bonferroni´s multiple comparison test; Rotarod, 8-9 weeks, $p>0.05$; 12-13 weeks, $p<0.001$; Open field, 8-9 weeks, $p>0.05$; 12-13 weeks, $p<0.001$; Fig. 1B). We conclude that the onset of motor defects in our colony occurs after 9 weeks of age and is thus slightly delayed compared to other reports (Carter et al., 1999; Murmu et al., 2013), likely due to the expansion of CAG repeats and/or differences in housing conditions.

To study longitudinal changes in neuronal function before and around the onset of disease, we chronically monitored calcium responses in L2/3 neurons in the M1 cortex of R6/2 mice and WT littermates. Mice were injected with AAV1/2-Syn1-mRuby2-P2A-GCaMP6s (Rose et al., 2016), which allows functional imaging along with morphological labeling of the neurons (Fig. 1C-D). Because of the rapid disease progression in this mouse line, we performed virus injections and cranial window implantations at the age of 3.5 weeks (Fig. 1A). Two-photon imaging sessions of 15 min each were started 3 weeks after the surgery and carried out at weekly intervals between 6.5 and 9.5 weeks of age (Fig. 1A). Populations of 100-200 L2/3 neurons were imaged in awake head-restrained animals during

voluntary locomotion in the dark on a spherical treadmill restricted to movement around one axis (Dombeck et al., 2007) (Fig. 1E). The experiments ended before the animals developed overt neurological symptoms. During the imaging sessions, mice exhibited spontaneous running behavior, which was recorded by an IR-sensitive video camera and/or by an optical mouse sensor (Fig. 1E).

Increased neuronal activity in HD mice before disease onset

Calcium responses were observed in many L2/3 neurons, with activity remaining quite stable during the imaging period in WT mice, but increasing on average in R6/2 mutants (Fig. 2A-B). Accordingly, the average frequency of calcium transients stayed unchanged between the imaging sessions in WT mice, while it increased in R6/2 animals starting from 8.5 weeks of age (WT, 1612 neurons from 6 mice; R6/2, 2589 neurons from 5 mice; Repeated measures ANOVA, Genotype: $F(1, 12597) = 2.01$, $p = 0.16$; Age: $F(3, 12597) = 82.91$, $p < 0.001$; Interaction $F(3, 12597) = 101.2$, $p < 0.001$; Fig. 2C). The change in transient frequency was also evident when we only analyzed the periods during which the animal remained stationary (only experiments with a minimum of 1% stationary time were included in the analysis; WT, 1346 neurons from 6 mice; R6/2, 2589 neurons from 5 mice; Repeated measures ANOVA, Genotype: $F(1, 11599) = 0.08$, $p = 0.78$; Age: $F(3, 11599) = 73.43$, $p < 0.001$; Interaction $F(3, 11599) = 102.66$, $p < 0.001$; Fig. 2D), indicating that the elevated activity was independent of locomotion. Next, we quantified the fraction of active cells (exhibiting at least one calcium transient during an imaging session, see Materials and Methods) at different time points. This analysis revealed a higher fraction of active cells in R6/2 mice from 8.5 weeks onwards (WT, 7 FOVs from 6 mice; R6/2, 10 FOVs from 5 mice; Repeated measures ANOVA, Genotype: $F(1, 45) = 1.11$, $p = 0.31$; Age: $F(3, 45) = 3.84$, $p = 0.02$; Interaction $F(3, 45) = 3.73$, $p = 0.02$; Fig. 2E). After the last awake imaging session, mice were also imaged under isoflurane anesthesia. In agreement with previous studies, the fraction of active cells was lower in anesthetized compared to awake animals (Greenberg et al., 2008). However, consistent with our findings in awake animals, we observed more active cells in R6/2 mice than in WT littermates (WT, 1612 neurons from 6 mice; R6/2, 2589 neurons from 5 mice. Wilcoxon rank-sum test, $p=0.038$; Fig. 2F). In summary, these data demonstrate elevated neuronal activity in the cortex of HD mice before the onset of neurological and motor impairments.

Altered dynamics of single-cell activity in HD mice

We next asked whether individual neurons changed their activity levels during the imaging period and whether the presence of mHTT had an impact on this dynamics. For each of the imaging time points, we quantified the reoccurrence rate of active cells, i.e. the fraction of cells that were active at the given imaging time point and remained active in each of the following imaging sessions. In WT mice, the reoccurrence rates of active cells steadily declined throughout the imaging period, consistent with previous studies describing a high variability of neuronal activity patterns in the motor cortex (Rokni et al., 2007; Peters et al., 2014; Clopath et al., 2017). In R6/2 animals this decline also occurred, but slowed down from 8.5 weeks onwards, resulting in a higher reoccurrence rate compared to WT controls (WT, 7 FOVs from 6 mice; R6/2, 10 FOVs from 5 mice; Repeated measures ANOVA, 6.5 to 9.5 weeks: Genotype: $F(1, 45) = 2.61$, $p = 0.12$; Age: $F(3, 45) = 130.0$, $p < 0.001$; Interaction $F(3, 45) = 3.97$, $p = 0.01$. 7.5 to 9.5 weeks: Genotype: $F(1, 30) = 8.59$, $p = 0.01$; Age: $F(2, 30) = 94.42$, $p < 0.001$; Interaction $F(2, 30) = 5.33$, $p = 0.01$. 8.5 to 9.5 weeks: Genotype: $F(1, 15) = 2.01$, $p = 0.18$; Age: $F(1, 15) = 94.42$, $p < 0.001$; Interaction $F(1, 15) = 2.01$, $p = 0.18$; Fig. 3A). These results suggest that the increase in neuronal activity detected in R6/2 mice is at least partially due to more cells staying active between the imaging sessions.

We further examined activity levels of single neurons by subdividing the imaged cells into four activity categories: silent (0 Ca^{2+} transients/min), rarely active (>0-0.5 transients/min), intermediately active (>0.5-4 transients/min), and highly active (>4 transients/min) (Fig. 3B). In the first two imaging sessions, the distribution of cells into these four categories was not significantly different between R6/2 and WT mice (Fig. 3C). However, a clear shift in the distribution was observed in the R6/2 animals between 7.5 and 8.5 weeks of age (WT, 1612 neurons from 6 mice; R6/2, 2589 neurons from 5 mice; Pearson's Chi-square test, R6/2 vs. WT at 6.5 weeks, $p = 0.5347$; at 7.5 weeks, $p = 0.901$; at 8.5 weeks, $p = 0.0495$; at 9.5 weeks, $p=0.0198$), which was due to an increase in the fraction of intermediately active cells, as well as reduction in the fraction of silent cells, while the rarely active and the highly active fractions did not change significantly (Fig. 3C). The increase in the intermediately active category in the R6/2 mice at 8.5 weeks was to a large extent due to cells that were classified as silent at 7.5 weeks (26% of silent cells became intermediately active in WT vs. 54% in R6/2; Exact binomial test, $p = 1.798e-07$). Taken together, these results indicate that activity dynamics are altered in R6/2 mice. The observed increase

in activity can at least in part be attributed to more silent cells changing into the intermediately active category, as well as more cells staying active between the imaging sessions.

Downregulation of synaptic proteins in R6/2 cortex before disease onset

To gain insight into the potential molecular mechanisms underlying the dysregulated activity in the cortex, we took advantage of the spatiotemporally resolved mass spectrometry-based proteomic dataset from R6/2 mice and WT littermates that we obtained previously, including changes in the soluble proteome and composition of insoluble mHTT inclusion bodies (Hosp et al., 2017). For the present study, we focused on cortical samples from 5-week-old (early presymptomatic) and 8-week-old animals (just before the onset of neuronal activity changes). Principal component analysis (PCA) revealed a clear separation of soluble cortical samples of 8-week-old R6/2 mice from the samples of 5-week-old R6/2 and all WT animals (Fig. 4A). We next asked which proteins accounted for this separation. Interestingly, the largest functional group among the main PCA drivers that were downregulated in 8-week-old R6/2 mice were synapse-related proteins (28%, 7 out of 25 proteins; the fraction of synapse-related proteins in the total proteome was 7%, 703 out of 9937 proteins) (Fig. 4B-C, Extended Data Table 4-1). In contrast, no synaptic proteins were found among the main PCA drivers upregulated in R6/2 mice (0 out of 25; Fig. 4B).

While there were no major changes in the soluble cortical proteome of 5-week-old mice, a global downregulation of multiple proteins in the soluble fraction occurred at 8 weeks of age in the R6/2 cortex (Fig. 4D-F), consistent with the data from other brain regions (Hosp et al., 2017). At 8 weeks of age, we also observed a pronounced decrease in synaptic protein levels (Fig. 4F). Importantly, the fraction of downregulated synaptic proteins (19%, 137 out of 703 proteins) was significantly higher than the downregulated fraction of the total proteome (12%, 1153 out of 9938 proteins) (Exact binomial test, $p=0.0434$; Fig. 4D and Extended Data Table 4-2), pointing towards a specific loss of synaptic proteins that is not merely due to the general remodeling of the whole proteome. We next asked if this downregulation of synaptic proteins might be due to their sequestration within mHTT inclusions. Out of 137 synaptic proteins reduced in the soluble fraction at 8 weeks, 60 were detected in the insoluble proteome, which largely consists of mHTT inclusions. Remarkably, only 1 of the detected proteins was significantly increased in R6/2 mice, while 6 were decreased, and 53 not significantly altered (Fig. 4G,

Extended Data Table 4-3). Sequestration within mHTT inclusions is therefore likely not a major mechanism of synaptic protein decrease at an early stage of HD progression. This is distinct from the situation in 12-week-old R6/2 brains, where many proteins downregulated in the soluble pool are enriched in the insoluble material, indicative of their recruitment to mHTT inclusion bodies (Hosp et al., 2017). In summary, our proteomic results reveal a broad downregulation of synaptic components already before disease onset.

Loss of PV-positive inhibitory inputs onto PCs

Lower levels of synaptic proteins in the R6/2 mice might reflect a loss of synapses. A decrease in synapses in the R6/2 cortex at an advanced disease stage has been reported previously (Murmu et al., 2015). However, it has remained unclear whether synapse numbers are already reduced before disease onset. We therefore performed immunostainings for excitatory and inhibitory pre- and postsynaptic markers in L2/3 of the M1 cortex of 8-week-old animals and quantified densities of opposing VGlut1/2; PSD-95 puncta as putative excitatory synapses and opposing VGAT; Gephyrin puncta as putative inhibitory synapses (Fig. 4H-I). These experiments did not reveal significant changes in total excitatory or inhibitory synapse densities at 8 weeks (3 FOVs per mouse from 5 WT and 4 R6/2 mice. Student's t-test; excitatory synapses, p=0.8279; inhibitory synapses, p=0.6773; Fig. 4H-I). However, since cortical thickness is already significantly reduced in R6/2 mice at this age (WT, 5 mice, R6/2, 4 mice; Student's t-test, p=0.0003; Fig. 4K), the overall number of synapses is likely to be decreased. While higher-resolution methods will be required for a more precise quantification, our current results therefore suggest that both excitatory and inhibitory synapse numbers are reduced in R6/2 mice already before disease onset.

We next focused on a more specific subset of synapses, PV-positive IN terminals on PCs. PV cells represent the most numerous IN subtype in the cortex, form synaptic terminals on the perisomatic region of their target cells and constitute the strongest source of inhibition onto PCs (Pfeffer et al., 2013; Tremblay et al., 2016). Interestingly, we found several specific markers of PV INs, including Pvalb, Calb1, and Plcxd3 (Tasic et al., 2016; Tasic et al., 2017; Mayer et al., 2018), to be downregulated in the soluble cortical proteome of R6/2 mice, as well as Synaptotagmin 2, a specific marker of PV synaptic terminals (Sommeijer and Levelt, 2012), to be downregulated in the insoluble fraction (Fig. 4F-G).

Immunostainings revealed a significant reduction in the area of PV+ terminals surrounding NeuN-labeled PC cell bodies in L2/3 of the M1 cortex of R6/2 mice at 8 weeks, but not at 5 weeks of age (WT, 74 PCs from 5 mice and 63 PCs from 5 mice for 5 and 8 weeks of age, respectively; R6/2, 74 PCs from 5 mice and 58 PCs from 4 mice for 5 and 8 weeks of age, respectively; Student's t-test, 5 weeks, p=0.3131; 8 weeks, p=0.0257. Fig. 5A-B).

To validate these histological findings in human disease cases, we performed immunostainings for PV+ terminals in postmortem brain tissue of HD patients and age-matched controls. Consistent with the results from R6/2 mice, we observed a marked reduction in the area of PV+ puncta around L2/3 PCs in the primary motor cortex (Ctrl, 69 PCs from 3 brains; HD, 75 PCs from 3 brains; Student's t-test, p=1.436e-15. Fig. 5C-D). In summary, loss of PV+ inhibitory inputs onto PCs occurs both in R6/2 mice and in human HD cases, suggesting that weakened inhibition from PV+ INs might at least partially explain dysregulated cortical activity in HD.

Discussion

Using chronic *in vivo* imaging in awake animals, we demonstrate an overall increase in cortical activity in HD mice. While our results are in agreement with previous reports describing dysregulation of activity and higher excitability in rodent models of HD (Walker et al., 2008; Cummings et al., 2009; Miller et al., 2011), we were able for the first time to observe these changes at a single-cell resolution, in awake animals already at a presymptomatic stage. Our findings therefore suggest that impaired cortical activity might critically contribute to disease onset. We also show that the excessive activity is not related to voluntary locomotion. This activity might therefore be aberrant, leading to higher noise in the cortical networks and thereby degrading information processing, as observed previously in a mouse model of Alzheimer's disease (Liebscher et al., 2016).

Our chronic imaging approach further revealed altered activity dynamics at single-cell level, with more neurons remaining active between imaging sessions, as well as more cells changing from silent to intermediately active. Highly dynamic activity patterns that are characteristic of the motor cortex and believed to be important for motor learning (Peters et al., 2014) therefore appear to be compromised in these mice. These findings provide a possible mechanism for the motor learning impairments observed in HD mouse models (Trueman et al., 2007; Woodard et al., 2017) as well as HD patients (Heindel et al., 1988).

Dysfunction of cortical circuitry might in turn lead to profound changes of neuronal function in the striatum. Early in HD progression, hyperactivity of striatal neurons was described R6/2 mice (Rebec et al., 2006), and elevated glutamate levels were detected in the striatum of HD patients (Taylor-Robinson et al., 1996). These alterations could in part be due to increased activation of the striatum by cortical inputs. Remarkably, removal of cortical afferents resulted in amelioration of HD phenotypes in R6/2 mice (Stack et al., 2007), and expression of mHTT in cortical neurons was necessary and sufficient to cause functional impairments of the striatal compartment in a corticostriaral network reconstructed *in vitro* (Virlogeux et al., 2018). It remains to be tested whether restoration of normal cortical activity levels, e.g. with the help of chemogenetic tools, would also be sufficient to rescue or delay HD symptoms.

Searching for the underlying circuit mechanisms of impaired cortical activity, we observed a reduction in inhibitory PV+ inputs onto PCs in R6/2 mice, which we confirmed in HD autopsy cases. These findings suggest that abnormalities of cortical function in HD could at least in part be explained by weakened inhibition. Reduced frequency of inhibitory postsynaptic currents has been described in L2/3 PCs in the motor and somatosensory cortex in several HD mouse models at a symptomatic stage (Gu et al., 2005; Spampanato et al., 2008; Cummings et al., 2009). Consistently, human studies with the use of transcranial magnetic stimulation also revealed abnormal cortical excitability due to dysfunctional inhibition in presymptomatic and early-stage HD patients (Schippling et al., 2009; Philpott et al., 2016), emphasizing the translational value of our findings.

Several previous reports suggested that PV cells might play a role in HD pathogenesis. PV INs develop mHTT inclusion bodies and show electrophysiological changes in HD mouse models (Meade et al., 2002; Spampanato et al., 2008). Selective expression of mHTT in this IN population results in specific HD-related phenotypes, including impaired cortical inhibition (Dougherty et al., 2014). It should, however, be noted that our results do not exclude a possible involvement of other IN subtypes in the cortical HD pathology. With the help of the available genetic tools for labeling specific IN subpopulations and manipulating their activity *in vivo* (Taniguchi et al., 2011), in future studies it should be possible to uncover the precise roles of particular IN subtypes in this disease. Interestingly, impairments in the function of inhibitory neurons have also been suggested to underlie neural circuit defects in mouse models of Alzheimer's disease (Verret et al., 2012; Busche and Konnerth, 2016). Excitation/inhibition imbalance and resulting dysregulation of cortical activity may therefore represent common phenomena in various neurodegenerative disorders.

What might be the molecular link between expression of mHTT and defects of neuronal communication in the cortex? Our proteomic analyses demonstrated a major downregulation of synaptic proteins in R6/2 mice. In addition to confirming reductions in synaptic proteins shown at advanced disease stages in HD mice and human brain samples (Morton and Edwardson, 2001; Morton et al., 2001; Smith et al., 2007; Skotte et al., 2018), our dataset reveals a broad downregulation of synaptic components that occurs already before disease onset. Surprisingly, the majority of synaptic proteins that were downregulated in the soluble fraction were not altered in the insoluble material at 8 weeks of age,

arguing against sequestration as a major mechanism of synaptic protein depletion at this disease stage (Murmu et al., 2013; Kim et al., 2016; Hosp et al., 2017). One likely mechanism of synaptic protein reduction might be transcriptional dysregulation, as genes related to synaptic signaling were among the most prominent dysregulated gene clusters in transcriptomic analyses of HD mice and human iPSC-derived neural cultures (Tang et al., 2011; Langfelder et al., 2016; HD iPSC Consortium, 2017). While synapse loss and downregulation of synaptic proteins might be expected to go along with a reduction in neuronal activity, we and others (Cummings et al., 2009) in fact observed the opposite effect in the cortex of HD mice. This underscores the complexity of HD pathogenic mechanisms and the value of *in vivo* imaging studies in deciphering cortical microcircuit alterations in disease models. Taken together, our chronic single-cell resolution imaging approach, in combination with state-of-the-art proteomic analyses and histological experiments, points towards disturbed cortical excitation/inhibition balance preceding disease onset as a key mechanism in HD pathogenesis.

Author Contributions

J.N. and E.K.S.-T. acquired the in vivo imaging data. E.K.S.-T. performed the histological experiments. S.G.-A. conducted the behavioral tests. J.N., E.K.S.-T. and S.L. performed data analysis. F.H. and M.M. provided unpublished proteomic data. T.A. provided the human tissue and gave advice on neuropathological analyses. R.K., S.L. and I.D. supervised the project. J.N., R.K., S.L. and I.D. wrote the paper.

References

Burger C, Nguyen FN, Deng J, Mandel RJ (2005) Systemic mannitol-induced hyperosmolality amplifies rAAV2-mediated striatal transduction to a greater extent than local co-infusion. Mol Ther 11:327-331.

Busche MA, Konnerth A (2016) Impairments of neural circuit function in Alzheimer's disease. Philos Trans R Soc Lond B Biol Sci 371.

Carter RJ, Lione LA, Humby T, Mangiarini L, Mahal A, Bates GP, Dunnett SB, Morton AJ (1999) Characterization of progressive motor deficits in mice transgenic for the human Huntington's disease mutation. J Neurosci 19:3248-3257.

Chen TW, Wardill TJ, Sun Y, Pulver SR, Renninger SL, Baohan A, Schreiter ER, Kerr RA, Orger MB, Jayaraman V, Looger LL, Svoboda K, Kim DS (2013) Ultrasensitive fluorescent proteins for imaging neuronal activity. Nature 499:295-300.

Clopath C, Bonhoeffer T, Hubener M, Rose T (2017) Variance and invariance of neuronal long-term representations. Philos Trans R Soc Lond B Biol Sci 372.

Cummings DM, Andre VM, Uzgil BO, Gee SM, Fisher YE, Cepeda C, Levine MS (2009) Alterations in cortical excitation and inhibition in genetic mouse models of Huntington's disease. J Neurosci 29:10371-10386.

Cummings DM, Alaghband Y, Hickey MA, Joshi PR, Hong SC, Zhu C, Ando TK, Andre VM, Cepeda C, Watson JB, Levine MS (2012) A critical window of CAG repeat-length correlates with phenotype severity in the R6/2 mouse model of Huntington's disease. J Neurophysiol 107:677-691.

Dodds L, Chen J, Berggren K, Fox J (2014) Characterization of Striatal Neuronal Loss and Atrophy in the R6/2 Mouse Model of Huntington's Disease. PLoS currents 6.

Dombeck DA, Khabbaz AN, Collman F, Adelman TL, Tank DW (2007) Imaging large-scale neural activity with cellular resolution in awake, mobile mice. Neuron 56:43-57.

Dougherty SE, Hollimon JJ, McMeekin LJ, Bohannon AS, West AB, Lesort M, Hablitz JJ, Cowell RM (2014) Hyperactivity and cortical disinhibition in mice with restricted expression of mutant huntingtin to parvalbumin-positive cells. Neurobiol Dis 62:160-171.

Dubbs A, Guevara J, Yuste R (2016) moco: Fast Motion Correction for Calcium Imaging. Front Neuroinform 10:6.

Estrada-Sanchez AM, Rebec GV (2013) Role of cerebral cortex in the neuropathology of Huntington's disease. Front Neural Circuits 7:19.

Estrada-Sanchez AM, Burroughs CL, Cavaliere S, Barton SJ, Chen S, Yang XW, Rebec GV (2015) Cortical efferents lacking mutant huntingtin improve striatal neuronal activity and behavior in a conditional mouse model of Huntington's disease. J Neurosci 35:4440-4451.

Greenberg DS, Houweling AR, Kerr JN (2008) Population imaging of ongoing neuronal activity in the visual cortex of awake rats. Nature neuroscience 11:749-751.

Gu X, Andre VM, Cepeda C, Li SH, Li XJ, Levine MS, Yang XW (2007) Pathological cell-cell interactions are necessary for striatal pathogenesis in a conditional mouse model of Huntington's disease. Mol Neurodegener 2:8.

Gu X, Li C, Wei W, Lo V, Gong S, Li SH, Iwasato T, Itohara S, Li XJ, Mody I, Heintz N, Yang XW (2005) Pathological cell-cell interactions elicited by a neuropathogenic form of mutant Huntingtin contribute to cortical pathogenesis in HD mice. Neuron 46:433-444.

HD iPSC Consortium (2017) Developmental alterations in Huntington's disease neural cells and pharmacological rescue in cells and mice. Nature neuroscience 20:648-660.

Heindel WC, Butters N, Salmon DP (1988) Impaired learning of a motor skill in patients with Huntington's disease. Behav Neurosci 102:141-147.

Holtmaat A, Bonhoeffer T, Chow DK, Chuckowree J, De Paola V, Hofer SB, Hubener M, Keck T, Knott G, Lee WC, Mostany R, Mrsic-Flogel TD, Nedivi E, Portera-Cailliau C, Svoboda K, Trachtenberg JT, Wilbrecht L (2009) Long-term, high-resolution imaging in the mouse neocortex through a chronic cranial window. Nat Protoc 4:1128-1144.

Hosp F, Gutierrez-Angel S, Schaefer MH, Cox J, Meissner F, Hipp MS, Hartl FU, Klein R, Dudanova I, Mann M (2017) Spatiotemporal Proteomic Profiling of Huntington's Disease Inclusions Reveals Widespread Loss of Protein Function. Cell Rep 21:2291-2303.

Huntington's Disease Collaborative Research Group (1993) A novel gene containing a trinucleotide repeat that is expanded and unstable on Huntington's disease chromosomes. Cell 72:971-983.

Kim EH, Thu DC, Tippett LJ, Oorschot DE, Hogg VM, Roxburgh R, Synek BJ, Waldvogel HJ, Faull RL (2014) Cortical interneuron loss and symptom heterogeneity in Huntington disease. Ann Neurol 75:717-727.

Kim YE, Hosp F, Frottin F, Ge H, Mann M, Hayer-Hartl M, Hartl FU (2016) Soluble Oligomers of PolyQ-Expanded Huntingtin Target a Multiplicity of Key Cellular Factors. Mol Cell 63:951-964.

Klapstein GJ, Fisher RS, Zanjani H, Cepeda C, Jokel ES, Chesselet MF, Levine MS (2001) Electrophysiological and morphological changes in striatal spiny neurons in R6/2 Huntington's disease transgenic mice. J Neurophysiol 86:2667-2677.

Labbadia J, Morimoto RI (2013) Huntington's disease: underlying molecular mechanisms and emerging concepts. Trends in biochemical sciences 38:378-385.

Lam AJ, St-Pierre F, Gong Y, Marshall JD, Cranfill PJ, Baird MA, McKeown MR, Wiedenmann J, Davidson MW, Schnitzer MJ, Tsien RY, Lin MZ (2012) Improving FRET dynamic range with bright green and red fluorescent proteins. Nat Methods 9:1005-1012.

Langfelder P et al. (2016) Integrated genomics and proteomics define huntingtin CAG length-dependent networks in mice. Nature neuroscience 19:623-633.

Liebscher S, Keller GB, Goltstein PM, Bonhoeffer T, Hubener M (2016) Selective Persistence of Sensorimotor Mismatch Signals in Visual Cortex of Behaving Alzheimer's Disease Mice. Curr Biol 26:956-964.

Mangiarini L, Sathasivam K, Seller M, Cozens B, Harper A, Hetherington C, Lawton M, Trottier Y, Lehrach H, Davies SW, Bates GP (1996) Exon 1 of the HD gene with an expanded CAG repeat is sufficient to cause a progressive neurological phenotype in transgenic mice. Cell 87:493-506.

Mayer C, Hafemeister C, Bandler RC, Machold R, Batista Brito R, Jaglin X, Allaway K, Butler A, Fishell G, Satija R (2018) Developmental diversification of cortical inhibitory interneurons. Nature 555:457-462.

Meade CA, Deng YP, Fusco FR, Del Mar N, Hersch S, Goldowitz D, Reiner A (2002) Cellular localization and development of neuronal intranuclear inclusions in striatal and cortical neurons in R6/2 transgenic mice. The Journal of comparative neurology 449:241-269.

Mehrabi NF, Waldvogel HJ, Tippett LJ, Hogg VM, Synek BJ, Faull RL (2016) Symptom heterogeneity in Huntington's disease correlates with neuronal degeneration in the cerebral cortex. Neurobiol Dis 96:67-74.

Miller BR, Walker AG, Barton SJ, Rebec GV (2011) Dysregulated Neuronal Activity Patterns Implicate Corticostriatal Circuit Dysfunction in Multiple Rodent Models of Huntington's Disease. Front Syst Neurosci 5:26.

Morton AJ, Edwardson JM (2001) Progressive depletion of complexin II in a transgenic mouse model of Huntington's disease. J Neurochem 76:166-172.

Morton AJ, Faull RL, Edwardson JM (2001) Abnormalities in the synaptic vesicle fusion machinery in Huntington's disease. Brain Res Bull 56:111-117.

Morton AJ, Glynn D, Leavens W, Zheng Z, Faull RL, Skepper JN, Wight JM (2009) Paradoxical delay in the onset of disease caused by super-long CAG repeat expansions in R6/2 mice. Neurobiol Dis 33:331-341.

Murmu RP, Li W, Holtmaat A, Li JY (2013) Dendritic spine instability leads to progressive neocortical spine loss in a mouse model of Huntington's disease. J Neurosci 33:12997-13009.

Murmu RP, Li W, Szepesi Z, Li JY (2015) Altered sensory experience exacerbates stable dendritic spine and synapse loss in a mouse model of Huntington's disease. J Neurosci 35:287-298.

Nopoulos PC, Aylward EH, Ross CA, Johnson HJ, Magnotta VA, Juhl AR, Pierson RK, Mills J, Langbehn DR, Paulsen JS, Group P-HICoHS (2010) Cerebral cortex structure in prodromal Huntington disease. Neurobiol Dis 40:544-554.

Orth M, Schippling S, Schneider SA, Bhatia KP, Talelli P, Tabrizi SJ, Rothwell JC (2010) Abnormal motor cortex plasticity in premanifest and very early manifest Huntington disease. J Neurol Neurosurg Psychiatry 81:267-270.

Peters AJ, Chen SX, Komiyama T (2014) Emergence of reproducible spatiotemporal activity during motor learning. Nature 510:263-267.

Pfeffer CK, Xue M, He M, Huang ZJ, Scanziani M (2013) Inhibition of inhibition in visual cortex: the logic of connections between molecularly distinct interneurons. Nature neuroscience 16:1068-1076.

Philpott AL, Cummins TDR, Bailey NW, Churchyard A, Fitzgerald PB, Georgiou-Karistianis N (2016) Cortical inhibitory deficits in premanifest and early Huntington's disease. Behav Brain Res 296:311-317.

R Development Core Team (2008) R: A language and environment for statistical computing. R Foundation for Statistical Computing, Vienna, Austria

Raymond LA, Andre VM, Cepeda C, Gladding CM, Milnerwood AJ, Levine MS (2011) Pathophysiology of Huntington's disease: time-dependent alterations in synaptic and receptor function. Neuroscience 198:252-273.

Reading SA, Dziorny AC, Peroutka LA, Schreiber M, Gourley LM, Yallapragada V, Rosenblatt A, Margolis RL, Pekar JJ, Pearlson GD, Aylward E, Brandt J, Bassett SS, Ross CA (2004) Functional brain changes in presymptomatic Huntington's disease. Ann Neurol 55:879-883.

Rebec GV, Conroy SK, Barton SJ (2006) Hyperactive striatal neurons in symptomatic Huntington R6/2 mice: variations with behavioral state and repeated ascorbate treatment. Neuroscience 137:327-336.

Rokni U, Richardson AG, Bizzi E, Seung HS (2007) Motor learning with unstable neural representations. Neuron 54:653-666.

Rosas HD, Hevelone ND, Zaleta AK, Greve DN, Salat DH, Fischl B (2005) Regional cortical thinning in preclinical Huntington disease and its relationship to cognition. Neurology 65:745-747.

Rosas HD, Salat DH, Lee SY, Zaleta AK, Pappu V, Fischl B, Greve D, Hevelone N, Hersch SM (2008) Cerebral cortex and the clinical expression of Huntington's disease: complexity and heterogeneity. Brain 131:1057-1068.

Rose T, Jaepel J, Hubener M, Bonhoeffer T (2016) Cell-specific restoration of stimulus preference after monocular deprivation in the visual cortex. Science 352:1319-1322.

Saudou F, Humbert S (2016) The Biology of Huntingtin. Neuron 89:910-926.

Schippling S, Schneider SA, Bhatia KP, Munchau A, Rothwell JC, Tabrizi SJ, Orth M (2009) Abnormal motor cortex excitability in preclinical and very early Huntington's disease. Biol Psychiatry 65:959-965.

Skotte NH, Andersen JV, Santos A, Aldana BI, Willert CW, Norremolle A, Waagepetersen HS, Nielsen ML (2018) Integrative Characterization of the R6/2 Mouse Model of Huntington's Disease Reveals Dysfunctional Astrocyte Metabolism. Cell Rep 23:2211-2224.

Smith R, Klein P, Koc-Schmitz Y, Waldvogel HJ, Faull RL, Brundin P, Plomann M, Li JY (2007) Loss of SNAP-25 and rabphilin 3a in sensory-motor cortex in Huntington's disease. J Neurochem 103:115-123.

Sommeijer JP, Levelt CN (2012) Synaptotagmin-2 is a reliable marker for parvalbumin positive inhibitory boutons in the mouse visual cortex. PLoS One 7:e35323.

Spampanato J, Gu X, Yang XW, Mody I (2008) Progressive synaptic pathology of motor cortical neurons in a BAC transgenic mouse model of Huntington's disease. Neuroscience 157:606-620.

Stack EC, Dedeoglu A, Smith KM, Cormier K, Kubilus JK, Bogdanov M, Matson WR, Yang L, Jenkins BG, Luthi-Carter R, Kowall NW, Hersch SM, Beal MF, Ferrante RJ (2007) Neuroprotective effects of synaptic modulation in Huntington's disease R6/2 mice. J Neurosci 27:12908-12915.

Tang B, Seredenina T, Coppola G, Kuhn A, Geschwind DH, Luthi-Carter R, Thomas EA (2011) Gene expression profiling of R6/2 transgenic mice with different CAG repeat lengths reveals genes associated with disease onset and progression in Huntington's disease. Neurobiol Dis 42:459-467.

Taniguchi H, He M, Wu P, Kim S, Paik R, Sugino K, Kvitsiani D, Fu Y, Lu J, Lin Y, Miyoshi G, Shima Y, Fishell G, Nelson SB, Huang ZJ (2011) A resource of Cre driver lines for genetic targeting of GABAergic neurons in cerebral cortex. Neuron 71:995-1013.

Tasic B et al. (2016) Adult mouse cortical cell taxonomy revealed by single cell transcriptomics. Nature neuroscience 19:335-346.

Tasic B et al. (2017) Shared and distinct transcriptomic cell types across neocortical areas. bioRxiv 229542.

Taylor-Robinson SD, Weeks RA, Bryant DJ, Sargentoni J, Marcus CD, Harding AE, Brooks DJ (1996) Proton magnetic resonance spectroscopy in Huntington's disease: evidence in favour of the glutamate excitotoxic theory. Mov Disord 11:167-173.

Thu DC, Oorschot DE, Tippett LJ, Nana AL, Hogg VM, Synek BJ, Luthi-Carter R, Waldvogel HJ, Faull RL (2010) Cell loss in the motor and cingulate cortex correlates with symptomatology in Huntington's disease. Brain 133:1094-1110.

Tremblay R, Lee S, Rudy B (2016) GABAergic Interneurons in the Neocortex: From Cellular Properties to Circuits. Neuron 91:260-292.

Trueman RC, Brooks SP, Jones L, Dunnett SB (2007) The operant serial implicit learning task reveals early onset motor learning deficits in the Hdh knock-in mouse model of Huntington's disease. Eur J Neurosci 25:551-558.

Tyanova S, Temu T, Sinitcyn P, Carlson A, Hein MY, Geiger T, Mann M, Cox J (2016) The Perseus computational platform for comprehensive analysis of (prote)omics data. Nat Methods 13:731-740.

Unschuld PG, Joel SE, Liu X, Shanahan M, Margolis RL, Biglan KM, Bassett SS, Schretlen DJ, Redgrave GW, van Zijl PC, Pekar JJ, Ross CA (2012) Impaired cortico-striatal functional connectivity in prodromal Huntington's Disease. Neurosci Lett 514:204-209.

Veldman MB, Yang XW (2017) Molecular insights into cortico-striatal miscommunications in Huntington's disease. Curr Opin Neurobiol 48:79-89.

Verret L, Mann EO, Hang GB, Barth AM, Cobos I, Ho K, Devidze N, Masliah E, Kreitzer AC, Mody I, Mucke L, Palop JJ (2012) Inhibitory interneuron deficit links altered network activity and cognitive dysfunction in Alzheimer model. Cell 149:708-721.

Virlogeux A, Moutaux E, Christaller W, Genoux A, Bruyere J, Fino E, Charlot B, Cazorla M, Saudou F (2018) Reconstituting Corticostriatal Network on-a-Chip Reveals the Contribution of the Presynaptic Compartment to Huntington's Disease. Cell Rep 22:110-122.

Vonsattel JP, DiFiglia M (1998) Huntington disease. J Neuropathol Exp Neurol 57:369-384.

Waldvogel HJ, Kim EH, Thu DC, Tippett LJ, Faull RL (2012) New Perspectives on the Neuropathology in Huntington's Disease in the Human Brain and its Relation to Symptom Variation. J Huntingtons Dis 1:143-153.

Walker AG, Miller BR, Fritsch JN, Barton SJ, Rebec GV (2008) Altered information processing in the prefrontal cortex of Huntington's disease mouse models. J Neurosci 28:8973-8982.

Wang N, Gray M, Lu XH, Cantle JP, Holley SM, Greiner E, Gu X, Shirasaki D, Cepeda C, Li Y, Dong H, Levine MS, Yang XW (2014) Neuronal targets for reducing mutant huntingtin expression to ameliorate disease in a mouse model of Huntington's disease. Nat Med 20:536-541.

Woodard CL, Bolanos F, Boyd JD, Silasi G, Murphy TH, Raymond LA (2017) An Automated Home-Cage System to Assess Learning and Performance of a Skilled Motor Task in a Mouse Model of Huntington's Disease. eNeuro 4.

Figure legends

Figure 1. Chronic two-photon calcium imaging in R6/2 mice. **A**, Experimental design and timeline of R6/2 phenotypes. **B**, Left: Latency to fall on the accelerating rotarod. Right: Distance travelled in the open field. ***p<0.001. **C**, Scheme of a cranial window over the M1 cortex. **D**, Coronal brain section showing AAV-mediated (AAV1/2-Syn1-mRuby2-P2A-GCaMP6s) expression of mRuby2 (red) and GCaMP6s (green) in L2/3 neurons in M1. **E**, Imaging setup. A mouse head-fixed under a two-photon microscope is placed on a styrofoam ball floating on pressurized air. Neuronal activity is monitored through a cranial window. Running behavior is registered by an IR-sensitive video camera and a speed sensor. Scale bars: D, left image, 50 μm; right image, 20 μm.

Figure 2. Increased neuronal activity before disease onset in R6/2 mice. **A**, Top: Examples of imaged areas in WT and R6/2 cortex superimposed by activity maps. Color coding shows normalized maximal activity. Bottom: Activity traces of neurons labeled on the images above. **B**, Raster plots of neuronal activity in WT and R6/2 mice during the imaging sessions at 6.5 and 8.5 weeks of age. Cells are sorted by activity at 6.5 weeks. Running episodes are depicted in white and stationary periods in black at the bottom of the plots. **C**, Cumulative distributions of calcium transient frequencies at the indicated time points in WT (left) and R6/2 (right) animals. Note a shift in the distribution towards higher frequencies

occurring at 8.5 weeks in R6/2 mice. **D**, Cumulative distributions of calcium transient frequencies during stationary periods at the indicated time points in WT (left) and R6/2 (right) animals. **E**, Fraction of active cells at different imaging time points in WT and R6/2 mice. **F**, Fraction of active cells under isoflurane anesthesia at 9.5 weeks. *p<0.05. Scale bar in a, 50 μm.

Figure 3. Altered dynamics of single-cell activity. **A**, Reoccurrence rate of active cells in WT and R6/2 mice. **B**, Example traces of highly active, intermediately active, rarely active and silent neurons. **C**, Alluvial plots showing changes between the four activity categories at different imaging time points in WT (left) and R6/2 (right) animals. *p<0.05.

Figure 4. Downregulation of synaptic proteins in R6/2 cortex. **A**, PCA projections of soluble cortical samples from 5- and 8-week old R6/2 mice and WT littermates. **B**, Main PCA drivers of the separation that are downregulated (yellow frame) and upregulated (green frame) in 8-week-old R6/2 mice. Synapse-related proteins are highlighted in red. Main drivers were defined as the top 25 proteins accounting for the separation of samples in the PCA. **C**, Functional groups of the main PCA drivers downregulated in 8-week-old R6/2 mice (indicated by the yellow frame in B). See also Table 4-1. **D**, Fraction of proteins significantly up- or downregulated in the soluble fraction of the R6/2 cortex at the indicated ages. See also Table 4-2. **E-F**, Volcano plots showing proteins significantly up- or downregulated in the soluble fraction of 5-week-old (E) and 8-week-old (F) R6/2 cortex. Empty black circles, all significantly regulated proteins; empty red circles, significantly regulated synaptic proteins. **G**, Volcano plot of the cortical insoluble fraction at 8 weeks, showing only proteins significantly downregulated in the soluble proteome at this age (see F). See also Table 4-3. Significantly downregulated PV cell markers are shown as filled yellow circles and labelled on the plots in F and G. **H-I**, Representative images (left) and quantification (right) of excitatory (H) and inhibitory (I) synapses in the L2/3 of the M1 area at 8 weeks. Synapses were identified by the overlap or close apposition (arrows) of a presynaptic (red) and postsynaptic (green) marker. **K**, M1 cortex width in 8-week-old R6/2 and WT mice. *p<0.05; ***p<0.001. Scale bar in I, 3 μm.

Figure 5. Reduction in inhibitory inputs from PV INs in R6/2 and HD patient cortex. **A-B**, Representative images (A) and quantification (B) of PV synaptic terminals (red) on NeuN-labeled PC cell bodies (green) in L2/3 of M1 cortex from R6/2 and WT controls. **C-D**, Representative images (C) and quantification (D) of PV synaptic terminals (red) on Neurotrace-labeled PC cell bodies (green) in L2/3 of M1 cortex from HD autopsy cases and controls. Scale bars in A and C, 10 μm.

Table

Table 1. Demographic data of HD patients and controls.

Case no.	Sex	Age at death
HD 1	Male	70
HD 2	Male	60
HD 3	Male	56
Ctrl 1	Male	62
Ctrl 2	Male	70
Ctrl 3	Female	60

Extended data

Extended Data Table 4-1. Main PCA drivers for the soluble cortical proteome.

Extended Data Table 4-2. Soluble cortical proteome of R6/2 mice at 5 and 8 weeks.

Extended Data Table 4-3. Insoluble fraction of R6/2 cortical samples at 5 and 8 weeks.

Figure 1

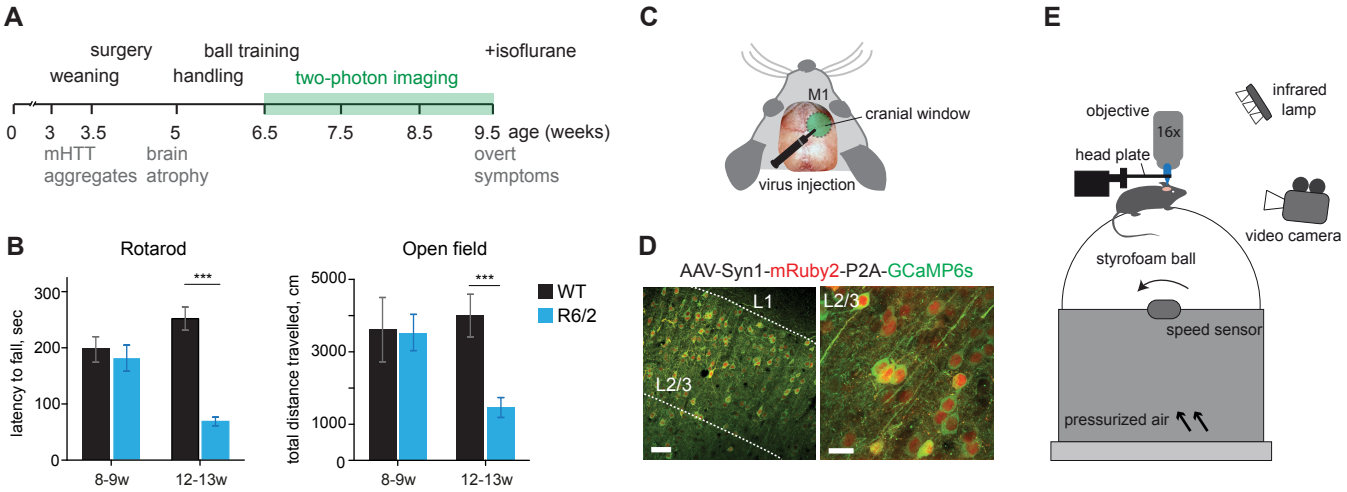

Figure 2

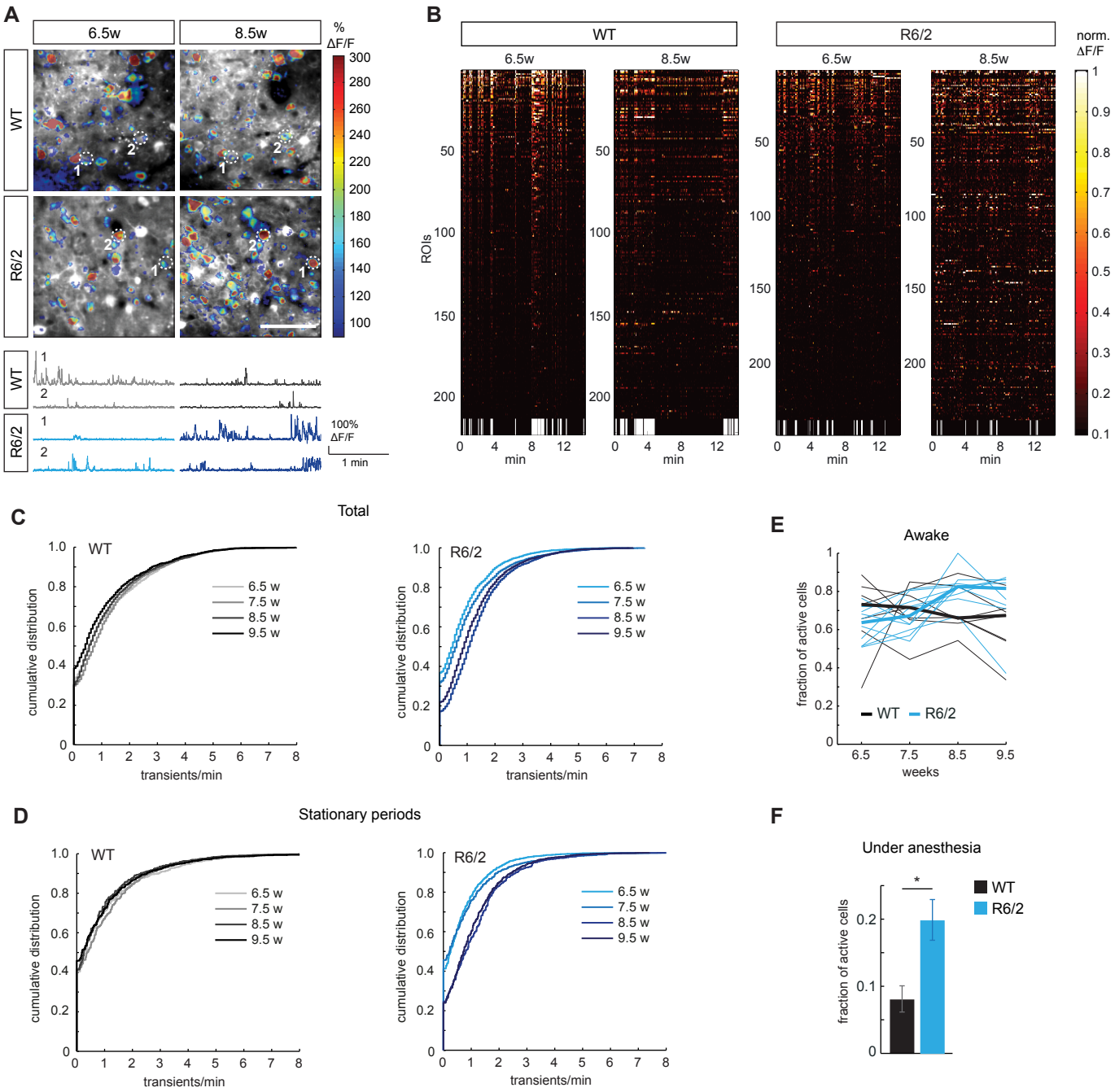

Figure 3

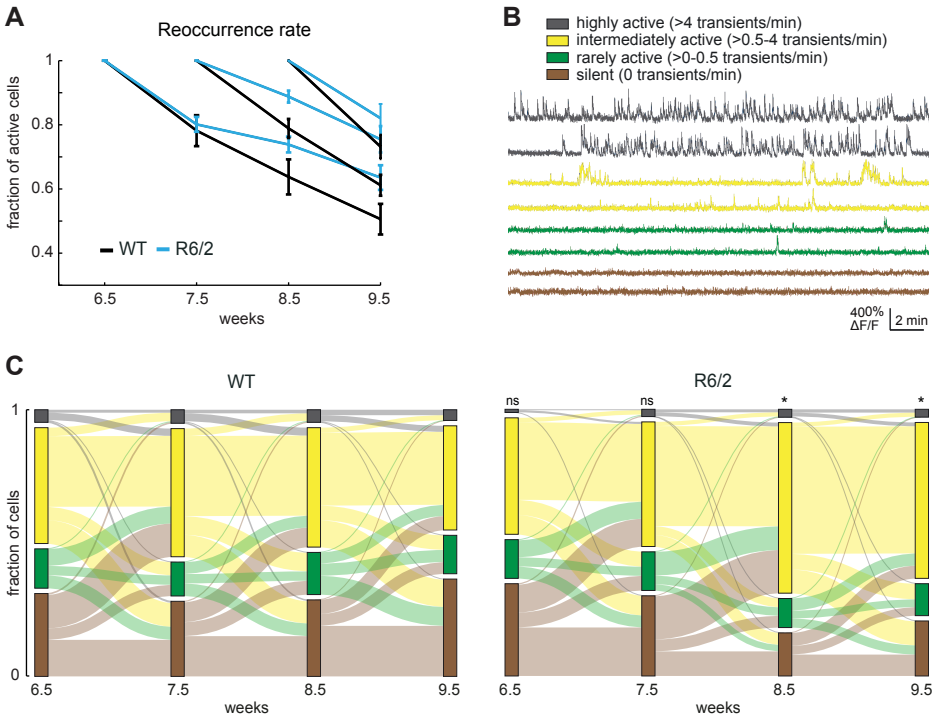

Figure 4

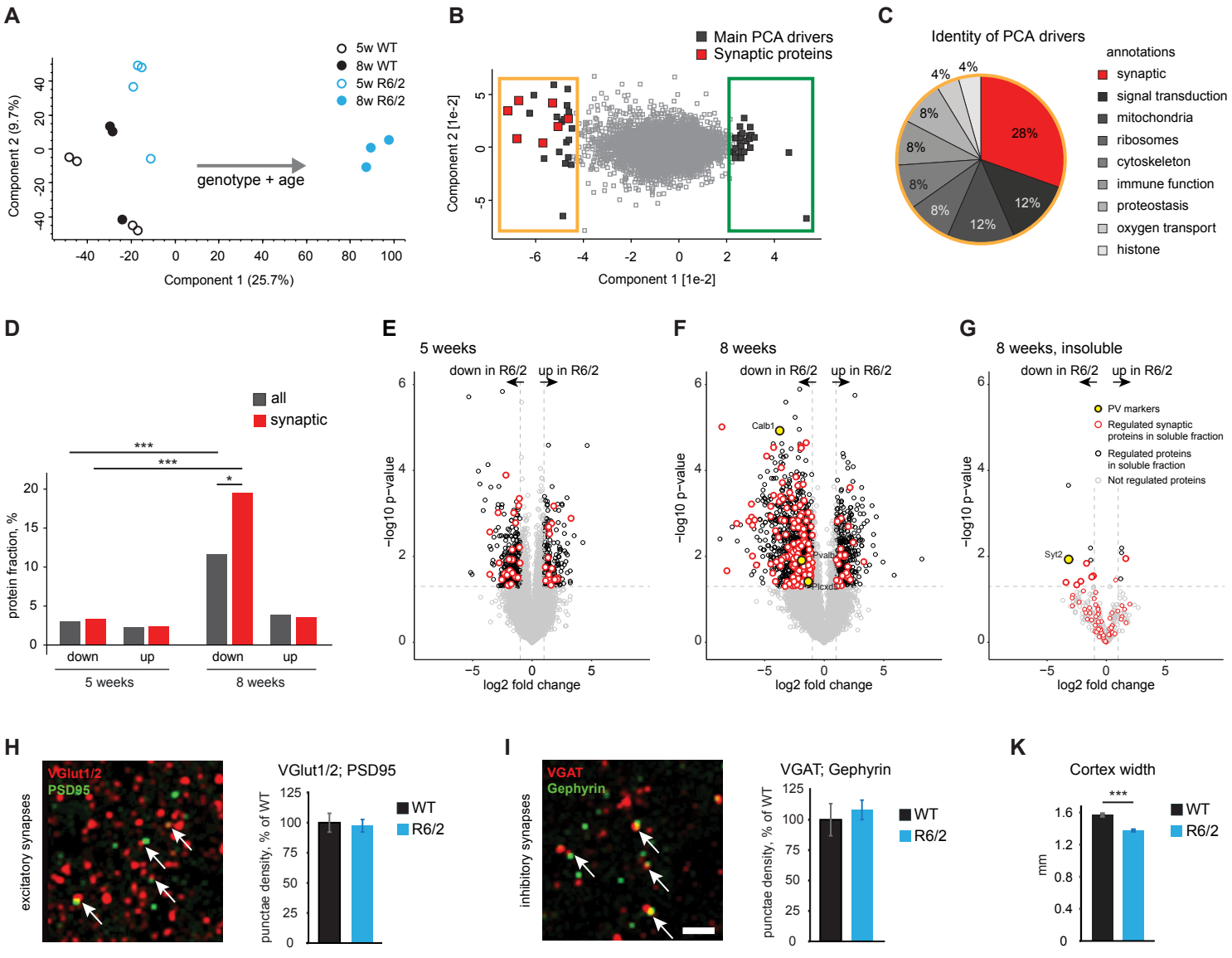

Figure 5

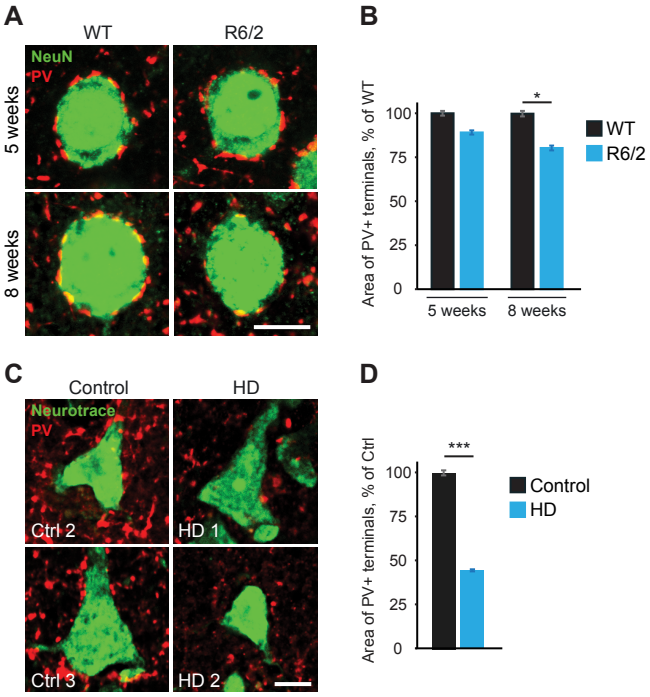

APPENDIX C

AUTHOR CONTRIBUTIONS

In the present project the following people contributed to the work:

Dr. Fabian Hosp contributed to Figure 2.3, Figure 2.4, Figure 2.5 A, Figure 2.6, Figure 2.7 and Figure 2.11 D. He also had an equal contribution in the publication *Spatiotemporal Proteomic Profiling of Huntington's Disease Inclusions Reveals Widespread Loss of Protein Function*, displayed in Appendix B.

Dr. Irina Dudanova contributed to generate proteomic samples, Figure 2.3 and supervised the full project.

APPENDIX D

ACKNOWLEDGEMENTS

I would like to thank Rüdiger for the given opportunity of working in such an international environment. There was never other pressure than my own while working on the project and I was always able to take my own decisions. This is essential for the development of a scientist and I like to think that I evolved into one.

I am profoundly grateful to Irina for the opportunity she gave me back in the day. My research background was everything but neuroscientific and yet, I was determined on getting into the field. She saw through it and recognized the genuine passion that still drives me today. Thank you very much for the trust and the independence you gave me to carry out science in general.

My research would have been impossible without the aid and support of Irene, which not only was my daily work college, but also my friend. I am thankful for her sharp scientific mind which put logic in many crazy ideas or shed light into just plain ignorance. However, I am even more grateful for the endless discussion hours and coffees we had and the daily laughs that made all this time beyond enjoyable.

Heartfelt thanks to all my lab mates and collaborators who helped my at some point through the project, either with a macro for analysis or a beer for refreshing the mind. Also many thanks to all my friends who where there, no matter the contribution, for a healthy work-life balance.

Finally, invaluable thanks to my parents and Diego. To them, because they always respected and supported my personal decisions, even if those meant to go abroad for

more years than what they would prefer. To him, because when the path is long and long-lasting, sometimes you need a cane to support yourself. I did not have a cane, but wings to fly over the path. Thank you.